Growth Study and Characterization of Single Layer Graphene Structures Deposited on Copper Substrate by Chemical Vapor Deposition

Stefanos Chaitoglou

Departament de Física Aplicada

Universitat de Barcelona

Growth Study and Characterization of Single Layer Graphene Structures
Deposited on Copper Substrate by Chemical Vapor Deposition

Presented by Stefanos Chaitoglou

Directors: Prof. Enric Bertran Serra (UB)

Prof. Jose Luis Andujar (UB)

PhD Program: Nanosciences,

Barcelona, July 2016

Cover design by Laura Alvarez

´´A graphene domain´´

Contents

Acknowledgment

I would like to seize the opportunity to acknowledge all the people that offered me their support during the realization of this Thesis.

First of all, Prof. Dr. Enric Bertran, tutor and director of my thesis during all this time, for his support as a scientific mentor. His encouragement and devotion to research was a true inspiration and a matter of fundamental importance for the succesfull realization of this work. Thank you, Enric.

I would like to thank the rest of the proffesors of the FEMAN group, Prof. Dr. Jose Luis Andujar and Prof. Dr. Esther Pascual, as well as Dr. Roger Amade. All of them are excellent scientists who are contributing to the continuous development of the group.

I acknowledge the help of the scientific stuff from Centres Científics i Tecnològics of the Universitat de Barcelona (CCIT-UB), especially Tariq for his support during the Raman spectroscopy measurements as well as the stuff of the microscopy laboratory.

My thanks to all the students of FEMAN group (most of them already doctors today) for being good partners and good company: Noemi, Victor, Shahzad, Reza and Edgar. I also send all my encouradgment to the ones that are following after me in this ´trip´, Arevic, Joan, Islam and Fernando. I would also like to thank all the academic stuff and all students of the Department of Applied Physics. I am also very thankfull to the secretery team of the Department, Ms. Maria Teresa Fraile Sanchez, Ms. Mireia Ortiz Ferrer, Ms.Teresa Torrejon Alabau, Mr. Jordi Sola Antolin, they were always organizing everything in the best possible way.

Of course, I would like to express my thanks to the people of the LTFN group in the Aristotle Univeristy of Thessaloniki. First of all, Prof. Dr. S. Logothetidis for giving me the opportunity to stay and work in his group. Moreover, all the people that I collaborate with during my stay in the group. Dr. A. Laskarakis, Dr. R. Pechlivani, Mr. Dimitris Papas and Mr. A. Zachariadis. Thank you all for welcoming me in your group.

I would like to recall all my colleagues from the degree years in Thessaloniki. We did this journey together during a long time and we share some of the most pleasant memories that stay for ever. Also, I would like to thank all my friends from University and else here, in Barcelona. It's nothing but pleasure (and big luck!) to feel like home while you study in a foreign country and all of them contribute to this day after day.

Finally, of course my deepest gratefulness is dedicated to my beloved family. To my Parents, Kostas and Kaiti, who were always providing me with all necessary and always

had the right piece of advice for me. I know that the termination of this work gives them a lot of joy and happiness. I only wish that in the future I will have the chance to offer them a lot more. To my younger sister, Iro, who is also following this path, even from a different field, this of Biology.

Next to them, ofcourse I would like to thank Laura for all her support and company. In her case the words are not enough to explain how much she has helped me during all this time.

Once again thank you all,

Stefanos,

Barcelona, July, 2016

Preface

Graphene, noun [U] (ˈɡræf.iːn): a form of carbon consisting of sheets that have the thickness of one atom. The atoms are arranged in a honeycomb pattern (= a pattern of shapes with six sides).

http://dictionary.cambridge.org/dictionary/british/graphene

Graphene overwhelmed the international research community by it's discovery in 2003. It is the last to be discovered in the family of carbon materials but in the same time the structural element of the rest of the allotropes including graphite, charcoal, carbon nanotubes and fullerenes. Although scientists have been theorizing about its existence for decades, providing the theoretical descriptions of its composition, structure and properties it was by then that was first managed to get isolated with the use of the famous 'scotch tape method'. For this work, scientists Andre Geim and Konstantin Novoselov at the University of Manchester won the Nobel Prize in Physics in 2010 "for groundbreaking experiments regarding the two-dimensional material graphene."

The discovery and wide interest that graphene attached gave a boost to the research around other 2D materials like Graphyne, Borophene, Germanene, Silicene, Stanene, Phosphorene due to their unusual characteristics and for use in applications such as photovoltaics, semiconductors, electrodes etc.

The work described here was carried out since October 2012 when I officially started my PhD Thesis. It took place in the Department of Applied Physics and Optics (FAO) of the University of Barcelona (UB).

Before this, the academic year 2011-2012, I carried out my Master studies in the University of Barcelona in the field of Nanoscience and Nanotechnology. My collaboration with FEMAN group and Prof. E. Bertran started since then, in the framework of my master thesis research. My Master thesis was entitled ''Arc-Discharge Synthesis of Fe@C Nanoparticles for General Applications''. This work was founded by the 'Nanotechnologies in Biomedicine (NANOBIOMED)' project, part of the 'CONSOLIDER-INGENIO 2010. MEC. Programa Nacional de Materiales'.

After finishing this work I moved to the research considering the graphene synthesis and characterization. My first year was founded by the project entitled ''Estudio de nanotubos de carbono para la mejora de láseres de alta potencia. Monocrom, S.L. Ref.: 304186''.

Resumen en castellano

La Nanotecnología es, por definición, la manipulación de la materia en la escala atómica, molecular y supramolecular. La Nanociencia estudia los fenómenos a escala nanométrica e incluye diferentes campos como son la ciencia de superficies, la química orgánica, la biología molecular o la física de estado sólido , entre otros. Además de entender el comportamiento del material en la nanoescala (1-100nm), donde los efectos de la mecánica cuántica son relevantes, en nanotecnología se estudia la síntesis de los nuevos materiales y el desarrollo de sus aplicaciones en los ámbitos emergentes como el de la nanomedicina, la nanoelectrónica o la producción de energía biomaterial.

El carbono es uno de los elementos más explorados a escala nanométrica. El carbono es el cuarto elemento más abundante en el universo y el segundo en el cuerpo humano. Este hecho, sumado a la gran diversidad de componentes orgánicos y su singular capacidad para formar polímeros, convierte al carbono en la base química de la vida.

En función de los lazos que van formando los átomos de carbono, se generan diferentes alótropos. Entre ellos, los más destacados son el grafito, el diamante y el carbono amorfo. Tras el establecimiento de la nanotecnología, aparecieron los fulerenos y los nanotubos. En los nanotubos –aparecidos a principios de los 90-, los átomos de carbono forman enlaces con hibridaje sp^2 entre ellos, únicamente similares a los del grafito. En aquel momento parecía que sólo faltaba un alótropo de carbono en las dos dimensiones para completar el puzzle. La ciencia, finalmente, logra aislar este material al comienzo del nuevo milenio, verificando los modelos teóricos que habían predicho su existencia décadas atrás. Se le dio el nombre de grafeno, muy similar al grafito, ya que comparten la misma estructura, una red en forma de panal de miel en el que cada vértice está ocupado por un átomo de carbono, variando en el hecho de que el grafeno tiene un grosor de un solo átomo.

El grafeno presenta excelentes características electrónicas, ópticas y mecánicas, convirtiéndose en un excelente candidato para aplicaciones tanto en electrónica como en almacenamiento de energía, ingeniería biológica, filtración, materiales ligeros, ultraduros, materiales compuestos, fotovoltaicos, materiales bidimensionales…

El grafeno fue aislado por primera vez a partir del grafito mediante el llamado método de la cinta adhesiva por científicos de la Universidad de Manchester (Andre Geim, Konstantin Novoselov); dicho trabajo fue posteriormente reconocido con el Premio Nobel en Física (2010) destacando su aportación innovadora. Aún así, el método de la cinta adhesiva o exfoliación mecánica no puede proporcionar dominios de grafeno mayores

que algunos cientos de micrómetros. Eran necesarias diferentes tecnologías que pudieran promover la síntesis de capas de grafeno continuas de area grande con el fin de impulsar el potencial para aplicaciones a gran escala. Para ello, se estudiaron diferentes enfoques, top-down y bottom-up, así como tambien la aplicación de iones, la reducción de dióxido de carbono, el corte de nanotubos de carbono y la síntesis electroquímica entre otras. La síntesis de deposición química en fase vapor (CVD) sobre diferentes sustratos metálicos es probablemente el método que cumple con los requisitos anteriores.

En la técnica CVD, se introduce un gas precursor de carbono en un horno donde se coloca el sustrato metálico. La molécula de gas se descompone y los átomos de carbono se depositan sobre la superficie metálica. El sustrato metálico cataliza la unión de los átomos de carbono para formar el grafeno. Por lo general, el proceso anterior se lleva a cabo a baja presión, en presencia de hidrógeno y argón. Existen diferentes factores que afectan el crecimiento del grafeno: la selección del sustrato del metal y el espesor de la misma; la temperatura de crecimiento, que debe ser mayor que la temperatura de descomposición del gas precursor del carbono seleccionado; la presión, así como las presiones parciales del gas precursor del carbono / hidrógeno / argón; y, por último, el tiempo de crecimiento.

Todos los experimentos de crecimiento de grafeno presentados en esta tesis fueron ejecutados en el reactor GRAPHMAN, ubicado en la sala limpia de la Facultad de Física de la UB. El reactor fue diseñado en primer lugar con el fin de permitir la inyección de gas precursor de carbono en la cámara en forma de impulsos, basado en el concepto del tiempo de formación de una monocapa, el cual se relaciona directamente con la presión del reactor. Más tarde, el reactor se modificó para permitir la introducción de los diversos gases en flujo continuo. Los resultados presentados en la tesis se han hecho teniendo en cuenta ambas técnicas.

Como gas precursor de carbono fue seleccionado el metano. Algunos experimentos adicionales se han realizado y presentado en esta tesis con benceno y tolueno. Como sustrato se utilizó una película de cobre metálico policristalino de espesor 75μm y 99% de pureza. Todos los experimentos se realizaron a 1040 °C. También se presenta a lo largo de la Tesis algunos experimentos adicionales realizados a temperaturas inferiores.

Teniendo en cuenta la síntesis de grafeno, el objetivo de la tesis recae en presentar nuevos experimentos y resultados que evidencien el efecto de la presión parcial de H_2, a través de la relación ϕ_{CH4}/ϕ_{H2} entre los flujos de gas, sobre el crecimiento de cristales

bidimensionales de grafeno y en su morfología. Para ello, hemos diseñado una metodología experimental que consiste en tres experimentos:

1) La aplicación de un plasma de hidrógeno para reducir el sustrato de cobre, en lugar del proceso regular en presencia de hidrógeno.

2) En relación con el crecimiento de grafeno, proponemos un experimento de optimización que determinen los factores de control para obtener una sola capa continua de grafeno y grandes dominios monocristalinos de grafeno.

3) Con la intención de identificar el papel de la relación de presiones parciales, $<P_{H2}> / <P_{CH4}>$, y el flujo de gas de hidrógeno y metano hemos llevado a cabo experimentos de la variación de estos parámetros.

Para la caracterización del pre-tratamiento con plasma de hidrógeno se ha utilizado la espectroscopia de emisión óptica y difracción de electrones retrodispersados. La caracterización del grafeno se ha hecho básicamente mediante microscopía (AFM y SEM) y espectroscopia (Raman). Para obtener información sobre la presencia de presión parcial de los gases diferentes, se utilizó un analizador de gas residual.

En el continuo, se presentan resultados teniendo en cuenta diferentes procesos de transferencia. Transferir el grafeno en diferentes sustratos es de vital importancia, ya que es un paso en el que se pueden introducir fácilmente las discontinuidades y las impurezas en la película de grafeno. Aparte del método habitual en el que se utiliza polimetacrilato de metilo (PMMA) que se utiliza como medio de transferencia; nosotros hemos experimentado con una técnica basada en la delaminación electroquímica de la película de grafeno por el sustrato metálico. La película delaminada está soportada por una cinta de desprendimiento térmico que facilita su transferencia sobre diferentes sustratos.

Por último, se han estudiado dos posibles aplicaciones diferentes. En primer lugar, el grafeno se ha utilizado para la fabricación de un transistor de efecto de campo. El objetivo es la caracterización eléctrica del grafeno a través de la determinación de la movilidad, la conductividad, la densidad de portadores y el tipo de portador. Los contactos son depositados por deposición física de vapor con el uso de una máscara de evaporación proporcionada por Ossila. El canal tiene una longitud L= 0,02mm y una anchura W = 4mm. Los contactos se depositan sobre una capa de 200 nm de SiO_2 térmico crecido sobre una oblea de Si (en este caso, <100> de p-Si dopado con boro, resistividad ρ = 0.001-0.005 $\Omega \cdot$cm, y 525 µm de espesor).

Conclusiones

- Se ha estudiado la posibilidad de un control más eficiente en el crecimiento del grafeno. El flujo de hidrógeno aparece para llevar a cabo un ataque quimico en los dominios de grafeno durante su crecimiento que afecta a su morfología y a su uniformidad. Los resultados revelan que un crecimiento eficiente de grafeno es posible cuando se optimiza la relación de flujo de precursor de carbono / flujo de hidrógeno durante el proceso. Esto reduce el efecto de ataque que el hidrógeno está llevando a cabo, lo que permite el crecimiento del grafeno en las condiciones adecuadas para obtener una capa continua de grafeno que cubre completamente el sustrato.

- Además, se ha investigado el importante papel que juega el tratamiento previo del sustrato. La aplicación de un plasma de hidrógeno antes del crecimiento reduce la capa de óxido de cobre eficientemente y con mayor rapidez que con otros métodos químicos (aplicación de baños ácidos), de modo que favorece el crecimiento de grandes cristales de grafeno.

- Se han estudiado dos parámetros: la presión total y el flujo del hidrógeno. Nosotros hemos estudiado los dos parámetros de forma independiente con el fin de conocer el efecto real que cada uno tiene en el crecimiento del grafeno. La caracterización SEM indica que pequeñas variaciones en dichos parámetros puede afectar la morfología, la densidad de nucleacion y el tamaño de los cristales de grafeno.

- Concretamente, el flujo del hidrógeno parece tener un rol importante en la morfología de los cristales, pero no en su tamaño. Una cantidad concreta de hidrógeno puede provocar un fuerte ataque en el grafeno. En los resultados obtenidos, el efecto del ataque se muestra inversamente proporcional al flujo del hidrógeno. En las partes del sustrato en las que el grafeno no esta atacado, podemos apreciar que los dominios mantienen su tamaño independientemente del flujo del hidrógeno.

- El area total cubierta por grafeno varía ampliamente dependiendo de la densidad de nucleacion y el efecto del ataque quimico en el grafeno. Aumentando el flujo del hidrógeno en una presión constante de la cámara resulta en el crecimiento de una película continua. Con flujos de hidrógeno ligeramente inferiores, la película fue atacada de forma anisótropa y se mostró seriamente dañada.

- La presión de la cámara parece afectar la densidad de nucleacion, así como el tamaño de los cristales de grafeno, en flujos de gas estables. Un gran aumento en la relación de presiones parciales ΔP_{H2} / ΔP_{CH4} durante el crecimiento, a

presión constante, parece disminuir la densidad de nucleacion. Una densidad de nucleación inferior genera más superficie libre para el crecimiento de cada cristal, cosa que resulta en la formación de películas de grafeno con menos fronteras de grano. La densidad de nucleacion parece seguir una dependencia lineal en relación con el porcentaje de la cobertura total, cuando el segundo se normaliza con la longitud del lóbulo.

- Por otro lado, hemos observado que la densidad de nucleacion es destacablemente mayor, siendo del doble o más, en la faceta (310) en comparación con la (221). Esta conclusión es fundamental en el sentido de que un ataque selectivo de las facetas de cobre podría permitir aumentar la abundancia de la faceta (221) en la superficie de la hoja de cobre que permitiría el crecimiento del grafeno a partir de una menor densidad de nucleación.

- Más allá de la gama de presiones que hemos estudiado aquí, entre 10 y 25 Pa, la nucleación grafeno no se ha realizado o bien la película obtenida aparece seriamente dañada, como resultado del ataque anisotrópico. La información anterior puede ser útil en el diseño de experimentos que se dirigen a hacer crecer cristales con una baja densidad de nucleación de grafeno.

- Subrayamos la importancia del aumento exponencial de la concentración de hidrógeno, que no se suele tener en cuenta cuando el flujo de hidrógeno es constante. Además, destacamos que la relación de las presiones parciales $<P_{H2}>$ / $<P_{CH4}>$ sigue la misma variación que el porcentaje de cobertura, lo que demuestra que la presión parcial parece ser el parámetro primario y no el flujo de hidrógeno, cuando queremos evidenciar el efecto del hidrógeno, ya que toma en consideración la eficiencia de evacuación del sistema de bombeo.

- La espectroscopia Raman confirma que toda la superficie de la lámina se cubre con una monocapa de grafeno. La presencia del pico D puede ser debido a la presencia de defectos en la capa de grafeno. Después de la transferencia de la película sobre el SiO_2 notamos una contracción significativa del pico 2D. Por otra parte, el ratio I_G / I_{2D} se muestra independiente del sustrato sobre el que se realiza la medida

- El proceso de transferencia de grafeno es tan crítica como el crecimiento del propio material. Casi en toda la variedad de aplicaciones, es un paso necesario para depositar la película de grafeno sobre el sustrato deseado. El proceso debe realizarse de forma que no introduzca defectos en la película de grafeno. Esta tarea parece ser complicada en la mayoría de los casos. Los diferentes materiales utilizados para la transferencia (polímeros, transferencia por cinta de

desprendimiento térmico, TRT, sustratos de soporte) introducen impurezas en la superficie de la película difíciles de evitar totalmente. Para solucionar esto, se han experimentado métodos que no necesitan de un medio de transferencia adicional. Aunque, con estos métodos se introducen tensiones superficiales que causan arrugas y huecos en la superficie de la película de grafeno. En otros casos, el método debe ser diseñado para transferir el grafeno sobre un sustrato específico, ya que no existe una única solución para todas las aplicaciones.

- A partir de nuestra experiencia, consideramos que la idea de usar el PMMA como un medio de transferencia y el TRT como una película de apoyo adicional en un proceso de delaminacion electroquímico es la solución ideal para la transferencia efectiva de grafeno. El método debe ser diseñado para aprovechar las características de cada medio. El PMMA es ideal para la transferencia de películas continuas de grafeno. Con el uso de la TRT como una capa de soporte, la película está protegida de la flexión que puede provocar arrugas. La delaminación electroquímica del catalizador de metal protege el grafeno de las impurezas que impone el grabador de metales. La observación mediante microscopio óptico o electrónico nos confirma la uniformidad de la capa transferida.

- El grafeno CVD puede presentar un menor calidad en comparación con otros, como por ejemplo el grafeno exfoliado. Ésto es debido a la presencia de fronteras de grano, así como de otros defectos en su estructura atómica; aunque el grafeno CVD presenta la ventaja de poder realizar la síntesis a gran escala y de obtener una gran homogeneidad en sus cualidades. Otra fuente de defectos pueden ser las impurezas ionizadas cargadas en la interfase con el óxido de grafeno. En otros trabajos se ha demostrado cómo estas impurezas pueden limitar las propiedades eléctricas del dispositivo [Hwang, 2007].

- La evaluación de electrodos de grafeno combinado con partículas dediferentes óxidos de metales se realiza con la intención de explorar la posibilidad de usar aplicaciones supercondensadoras. Los resultados muestran que todos los dispositivos presentan una mayor capacidad en la velocidad de exploración más pequeña (smallest scan rate) (10mV/s).

- La oxidación de la película de grafeno aumenta su capacitancia; lo mismo sucede al añadir más capas de Gr/óxido de metal sobre la primera capa. Los dispositivos en los que GR está combinado con CeO_2 presentan una capacitancia mejor de aquellos en los que Gr está combinado con WO_3.

- Teniendo en cuenta su estabilidad, todos los dispositivos mantienen su rendimiento inicial durante más de 800 ciclos. El período de carga-descarga aumenta al añadir más capas. La deposición de partículas de óxido de metal por pulverización catódica provoca la oxidazion de la película de grafeno.

- Deberían ser consideradas diferentes técnicas de deposición. Por otro lado, también, se debería realizar una caracterización estructural de los electrodos tanto antes como después de realizar las medidas para obtener información sobre la deposición de las partículas.

- El grafeno CVD se usa para la fabricación of a field effect transistor. El objetivo del cual es la caracterización eléctrica del grafeno en relación a características como la conductividad, la densidad de portadores y la movilidad de portadores.

- Más allá del campo del efecto de las medidas mediciones de efecto de campo, se ha medido una conductividad parecida en las películas de grafeno midiendo las características IDS-VDS en una configuración con dos contactos. La conicidencia de los resultados en las medidas (hechas con diferentes APARATOS), nos confirma su precisión. Grafeno CVD puede presentar un menor comportamiento cualitativo si se compara con otros, como grafeno exfoliado. Esto es debido a la presencia de los límites de granoasíc como también otros defectos en la estructura atómica. Aun y así, el grafeno CVD presenta la ventaja de síntesis de escala larga y una alta homogeneidad en su calidad.

Chapter 1: Introduction

1.1 Fundamentals of Carbon materials

Carbon is one of the most fundamental elements in the world. It is the 15th most abundant element in Earth's crust and the 4th most abundant element in the whole Universe, following hydrogen, helium and oxygen. It is the key element of all known forms of life on Earth, including the human. In our bodies is contained in a percentage of 18.5%, being the second most abundant element after oxygen. It has an atomic number 6, it is non-metallic and tetravalent. It has 4 electrons in the outer shell available to form covalent bonds. It's electron configuration is $1s^2\ 2s^2\ 2p^2$. It exists in 3 natural isotopes, the stable ^{12}C and ^{13}C and the radioactive ^{14}C.

The atoms of carbon bond together forming different allotropes, the best known of which are the graphite, the diamond and the amorphous carbon. The properties of the material present a wide variation depending on the allotropic form. For example graphite is one of the softest known materials meanwhile diamond is the hardest one. Graphite is a conductor of electricity while diamond is an insulator. Graphite is opaque while diamond is transparent.

Nowadays the research is focused in fullerenes, molecules of carbon in different configurations. The family of fullerenes includes buckyballs, carbon nanotubes, carbon nanobuds, nanofibers and fullerite (Figure 1.1-1).
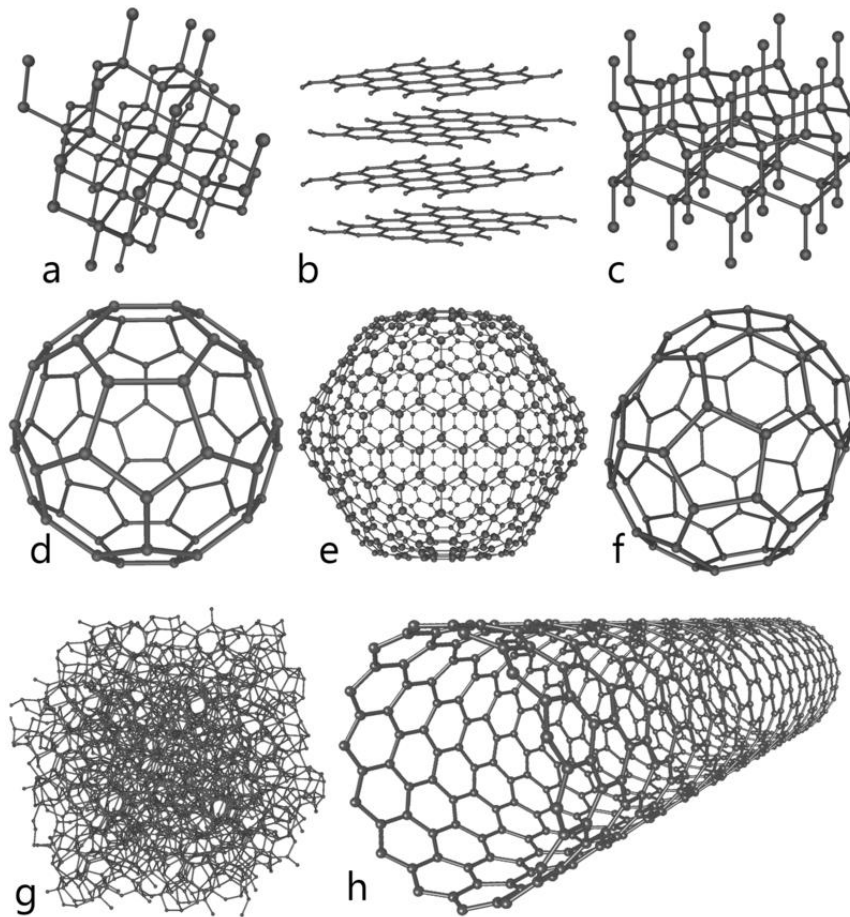
Figure 1.1-1: Eight allotropes of carbon: a) diamond, b) graphite, c) lonsdaleite, d) C60 buckminsterfullerene, e) C540, Fullerite f) C70, g) amorphous carbon, and h) single-walled carbon nanotube. [Michael Ströck, Wikipedia]

1.1-1 Amorphous Carbon

Amorphous is the carbon without any crystalline structure (also known as diamond-like carbon) [Robertson, 1986]. Its synthesis occurs by the development of the thin film deposition techniques (sputter deposition and cathodic arc deposition) as well as the thin film growth by chemical vapor deposition. It has localized π electrons that form bonds which are inconsistent to any other carbon allotrope in terms of length and distance [McNaught, 1987]. The properties of the material depend on its deposition parameters. It is characterized by its ratio between sp_2 to sp_3 hybridized bonds present. The more sp_3 bonds are present (the bonds from which the diamond consists) the more tetrahedral the shape of the amorphous carbon appears. In this case the material is called diamond-like carbon. It combines many different attractive properties like high mechanical hardness, high optical transparency in the visible and near infrared, high thermal conductivity, low

friction coefficient, and chemical inertness to some corrosive agents, which make it a strong candidate for applications in protective tribological coatings, radiation protection, electron field emitters, in biomedicine and as reflective coating [Da Silva, 2011].

1.1-2 Graphite

Graphite is the most stable form of carbon under standard conditions. It can be found in different forms. Crystalline flake graphite, lump graphite, highly ordered pyrolytic graphite and *amorphous* (in the case of very fine flake graphite) [Anthony, 1990].

Graphite has a layered planar structure. Its atoms are organized in a honeycomb lattice with a distance of 0.142nm between them (plane distance 0.335nm).
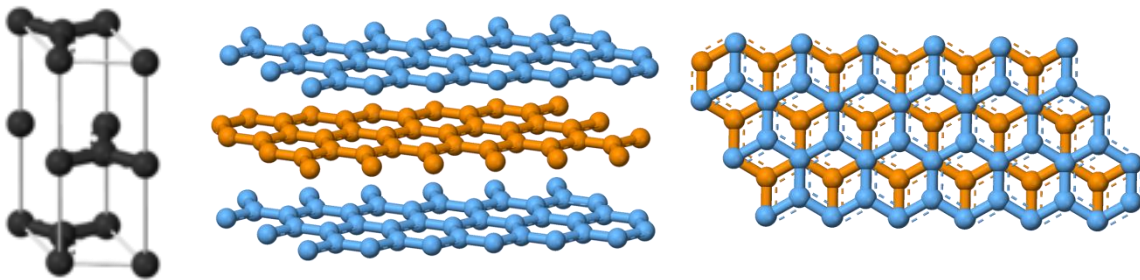
Figure 1.1-2: a) A graphite unit cell, b) a side and c) a plane view of layer stacking. [https://en.wikipedia.org/wiki/Graphite]

The 3 of the four electrons are forming covalent bonds. The 4th is free to move in the plane, making graphite electrically conductive. Between layers are formed weak Van der Waals bond, allowing the easy separation between them [Delhaes, 2001]. Its lattice system can be hexagonal (alpha) or rhombohedral (beta). The one system can transform into the other by mechanical or thermal treatment [Compendium of Chemical Terminology,1997].

Graphite has various uses. In the past (before 20th century) it was used in refractories to hold molten metals ["Graphite Statistics and Information, 2009]. In batteries it is used to construct the anode in both ion lithium and lithium carbonate technology

[galaxycapitalcorp.com, 2011]. Other uses meets in pencils, steelmaking, brake linings, foundry facings and lubricants.

1.1-3 Diamond

Diamond is the hardest known natural mineral. Due to its hardness and light dispersion is widely used in industrial applications and jewelry. It can not be cut by any other substance except another diamond thanks to the strong covalent bonding between its atoms. Each carbon atom in a diamond is covalently bonded to four other carbons in a tetrahedron. These tetrahedrons together form a 3-dimensional network of six-membered carbon rings (similar to cyclohexane), in the chair conformation, allowing a zero bond angle strain. This stable network of covalent bonds and hexagonal rings is the reason that diamond is so strong. It has a face centered cubic crystal structure. Its natural formation occurred in high temperatures and pressures at depths of 140 to 190 kilometers in the Earth's mantle [Mindat, 2009].

In the industry is mainly used for cutting, drilling, grinding and polishing. The synthesis of diamond is taking place under High Pressure High Temperature processes. Other synthesis routes are the chemical vapor deposition, the detonation of explosives and the ultrasound cavitation. Thanks to the continuous advance in the synthesis of diamonds, a lot of interest attracts today the research for further reclamation of it. It is expected to find applicability in semiconductors industry and as heat sink in electronics [Coutsoukis, 2009].

With the advance in the research and the technological evolution during the last decades, a new area of research, *nanotechnology*, has appeared with the aim to fully understand the material's behavior in the nanoscale and give a boost in the synthesis of new, high performance ones. Different fullerenes have resultant the last years as a result of this. We mention some of them here briefly.

1.1-4 Buckyballs

The spherical fullerenes are called buckyballs. They are carbon molecules containing pentagonal and hexagonal rings where no two pentagons are sharing an edge. Buckminsterfullerene is the smallest fullerene molecule containing pentagonal and hexagonal rings and the first to be discovered, in 1985, just 30 years ago! It contains 60 carbon atoms. It consists of twenty hexagons and twelve pentagons, with a carbon atom at the vertices of each polygon and a bond along each polygon edge [Qiao, 2007].

Other buckyballs contain 70, 72, 76, 84 until up to 100 carbon atoms. In general, they follow the Euler's polyhedron formula, $V - E + F = 2$ (where V, E, F are the numbers of

vertices, edges, and faces). The smallest fullerene is the dodecahedral C20. There are no fullerenes with 22 vertices. The number of fullerenes C2n grows with increasing n = 12, 13, 14, ...,[Meiza, 2006].The most usual fullerenes contain 60 carbon atoms.
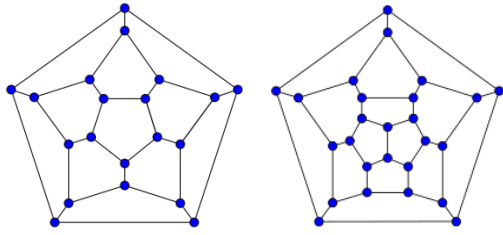
20-fullerene (dodecahedral graph)	26-fullerene graph	60-fullerene (truncated icosahedral graph)	70-fullerene graph

Figure 1.1-3: Examples of the configurations of different buckyballs. [https://en.wikipedia.org/wiki/Fullerene]

Buckyballs have also been made by boron and silicon, although no applications have emerged yet. Its optical absorption properties make it in candidate for use in photovoltaics through the synthesis of C60 based films. Thanks to its high electronic affinity it is used as an electron acceptor in donor/acceptor based solar cells.

1.1-5 Carbon Nanotubes

Nanotubes are allotropes of carbon with a cylindrical nanostructure. It is the material with the biggest length:diameter ratio ever constructed (up to 132,000,000:1). They have a hollow structure with walls formed by a one-atom thick carbon sheet (called *graphene*). These sheets are rolled in concrete angles (chiral angles). This angle in combination with the radius of the cylinder decides the properties of the material. The nanotubes can be either single or multi wall. They naturally align themselves into ropes held together by van der Waals forces [Wang, 2009]. All the chemical bonds between the atoms consist of sp_2 bonds. Usually the nanotubes have a diameter of about 1nm.
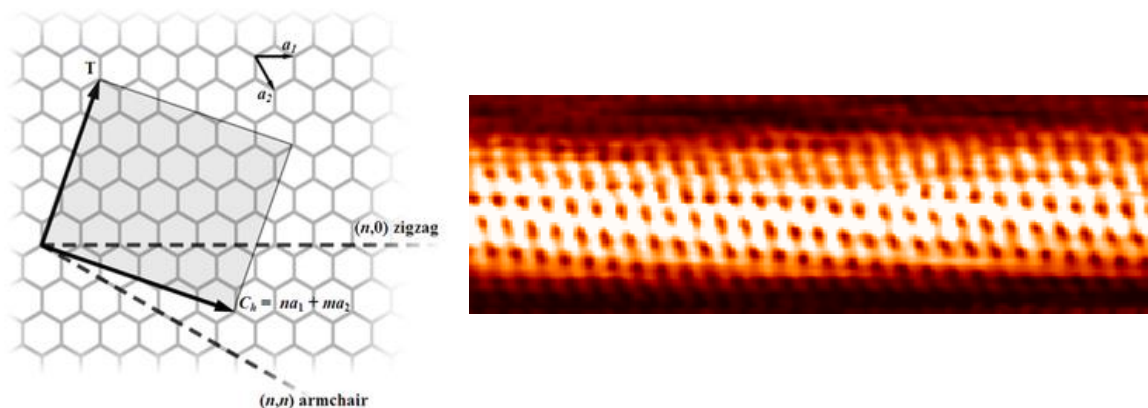
Figure 1.1-4: a) The (n,m) nanotube naming scheme can be thought of as a vector in an infinite graphene sheet that describes how to "roll up" the graphene sheet to make the nanotube. T denotes the tube axis, and a_1 and a_2 are the unit vectors of graphene in real space. b) STM image of single wall carbon nanotube [http://www.ncnr.nist.gov/staff/taner/nanotube/types.html]

The way the graphene sheet is wrapped is described by two indices, n and m, which denote the number of unit vectors along two directions in the honeycomb crystal lattice of graphene. They can be armchair (m=n), zigzag (m=0) or chiral for the rest of the cases. The diameter of the nanotube is calculated by the equation

$$d = \frac{a}{\pi}\sqrt{(n^2 + nm + m^2)}$$

Where a= 0.246nm

The properties of the nanotubes depends strongly on the n and m values. This dependance is described by a Kataura plot. For example, their band gap can take values from 0 to 2eV and their electical behaviour can be metallic or superconductive.

Carbon nanotubes are the strongest and stiffest materials yet discovered in terms of tensile strength and elastic modulus respectively thanks to the sp_2 bond between the carbon atoms. They have been reported nanotubes with tensile strength up to 100 gigapascals. In terms of hardness, they can withstand up to 25 GPa (standart single wall CNT). They have even synthesized nanotubes that resist up to 55 GPa but they were not so stable (collapse in higher pressures) [Peng, 2008].

As synthesized CNT are very hydrophobic (they have a contact angle of 160°). They can switch to hydrophilic by applying a low voltage. Concerning their thermal properties, they are very good conductors along the tube axe (following a ballistic conduction) and very good insulators in the lateral axe. As it occurs with all the nanomaterials, the presence of defects in the structure of the nanotubes is usual and it drastically affects their properties.

There are various different synthetic routes to obtain the CNT. Most of them take place in vacuum and require different gases as precursor and catalytic agents. CNT were observed for first time in 1991 after an arc discharge process between two graphite electrodes in a fullerenes synthesis experiment [Iijima, 1991]. Other synthesis methods use laser ablation, plasma torch, and chemical vapor deposition. It has even been reported their natural growth as a product of burning carbon included gases like methane, ethylene and benzene.

In actual applications carbon nanotubes are being used as bicycle components and as structural component to invigorate other structural materials. Potentially are expected to be used in a variety of applications in biomedicine, electrical circuits and wires, solar cells, batteries, supercapacitors, detectors and more. To occur this, the synthesis, transfer and storage of them has to get more standardised, ensuring the maintenance of their quality.

1.1-6 Fullerites

Fullerite is used to name the solid state fullerenes in general. Sometimes it can also be found by the name 'ultrahard fullerite' to describe materials synthesized in high pressure, high temperature conditions [Blank, 1998].
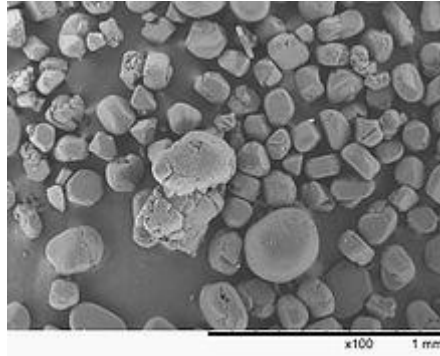
Figure 1.1-5: Scanning electron microscopy image of fullerites.

[https://en.wikipedia.org/wiki/Fullerene]

1.1-7 Toxicity Risks of Nanomaterials

Several toxic effects have been found in nanomaterials by different groups. Although, the causes for this behavior still remain not fully understandable. Still it is not very clear which aspect of the materials should be measured e.g. number, surface area or mass concentration, a combination of these, the possible agglomerations they form, their size or something else entirely. It is also very difficult to determine if these effects appear because of impurities in the materials, because of the material behavior themselves or as a combination of both and in what ratio. In the area of biomedicine, more sufficient analytical techniques have to be developed for the in vivo imaging in the case of biomedical applications in cells.

Another parameter to be considered is the effect of the surfactants used to control the shape and size of the various nanomaterials. Surfactants used today are often toxic, therefore should be replaced by new ones in order to incorporate new functionality on the material´s surface [Paresh, 2009].

To manage to use the nanomaterials in real applications and bring them closer to the population, there should be developed models capable of predicting the release, transport, transformation, accumulation, and uptake of engineered nanomaterials in the environment. They should be able to relate physical and chemical characteristics of

nanomaterials to their behavior, allow an integrated approach to predict potential impact of engineered nanomaterials and nanoproducts, as well as estimate the impacts they can have once they are within the populations.

Until now, the research studying the effect of the nanomaterials is always very focused and specific, both in the type of the material as well as in the effect examined. For example, back in 2008 researchers from Edinburg CIR reported that carbon nanotubes can be as harmful as asbestos for breathing as they can accumulate in the lungs forming scarlike tissue, provoking the reaction of the body to build new cells over them and thickening the walls of the lungs. Although, this behavior was occurred for a very specific type of thin and long CNT. They study CNTs that were emulated fiber behavior and their potential to cause a certain type of cancer [Greenemeier, 2008].

Concerning *graphene*, it has been reported that microsheets of the material can spontaneously penetrate the cell membrane and enter inside. The process begins with localized piercing sharp corners or at protrusions along graphene edges followed by propagation along the edge to achieve full penetration. This can lead to cytoskeletal disruption, impaired cell motility, compromised epithelial barrier function, or other geometric and steric effects [Li, 2013]. Graphene oxide has been also found to be toxic in case of exposure to water, in concentrations much higher than other toxic materials although (GO considered toxic in the range of 50 to 300 mg/L when arsenic does so for concentrations of 0.01 mg/L!).

To sum up, it is quite difficult to make extrapolation of results from one molecule to another for all kind of different nanomaterials and fullerenes in concrete. Any extrapolation must take into account considerations based on a quantitative structural analysis relationship study. To the above we must mention the necessity to follow process transparent for the public. Usually the scientific community meets a difficulty to communicate the results of their work to the society, even from fear to be misunderstood or because of difficulties to find the audience. Public involvement in discourse about technologies, the ethics and concerns related to them, is important to build up trust between the scientific community and public.

1.2 Graphene

Graphene is the name given to a flat monolayer of carbon atoms tightly packed into a two-dimensional (2D) honeycomb lattice. It is recognized as the basic building block for graphitic materials of all other dimensionalities. In the same time, it is considered as the first of a series of 2D materials to be discovered (some estimate 500 more remain to be explored) and it became very fast the star in the nanomaterial science community thanks to its outstanding properties [Gibney, 2015].

It can be considered as an aromatic molecule, being part of the family of flat polycyclic aromatic hydrocarbons. It can be wrapped into a fullerene, rolled into a nanotube or stacked into graphite. Theoretically is investigated since the late 1940's [Wallace, 1947]. Because of this, it was used to describe the properties of different carbon based materials. For many years it was believed to be an 'academic' material', not possible to exist in free state as it was expected to be thermodynamically unstable with respect to form curved structures like nanotubes, fullerenes etc [GEIM/NOVOSELOV, 2007] (Figure 1.2-1). According to the theory developed by Landau and Peierls, in such low dimensional crystal lattices materials, the thermal fluctuations could lead to displacements of the atoms comparable to their interatomic distances at any finite temperature. To put it forward more simple, the melting temperature of such thin films decreases rapidly with the decrease of their thickness leading to decompose or segregation of them (in thicknesses lower than dozens of layers). This was confirmed by observation stating that atomic monolayers were always present as an integral part of larger 3D structures, usually grown epitaxially on top of monocrystals with matching crystal lattice [Venables, 1984].
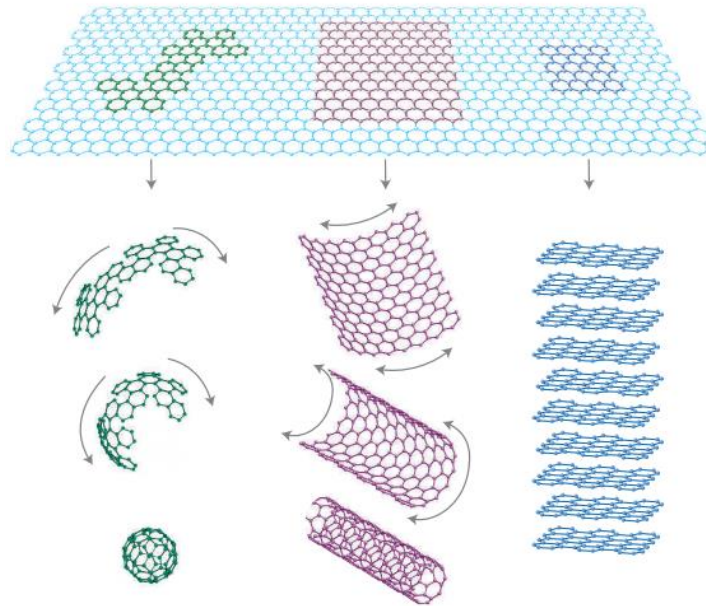
Figure 1.2-1: Graphene is a 2D building material supporting the formation of different 3D carbon based materials like buckyballs, nanotubes and graphite. http://www.springer.com/cda/content/document/cda_downloaddocument/97836423048 97-c1.pdf?SGWID=0-0-45-1344827-p174508169

1.2-1 History

The discovery of graphene did not occur out of nowhere. A lot of investigation had been made before, considering both the theoretical properties as well as synthetic routes of graphite thin films. The study of the graphite and graphite oxide structures has been carried out since the early 20th century. The graphite structure was first solved in 1916 by powder diffraction. The structure of graphite oxide, together with a study of its properties, was presented in 1924 from single crystal diffraction. P.R. Wallace started to explore the theoretical properties of graphene as a tool for the further studies in the electric properties of the graphite in 1947. G.W. Semenoff described the massless Dirac equation in 1984. By electron microscopy means, thin graphitic flakes have also been observed since 1962. The exfoliation method is used since the 1990's in order to isolate thin graphite films, although it had not been possible to isolate stacks of less than 50 layers before 2004. Without doubt, it was by this year that the graphene outburst took place. Andre Geim and Kostya Novoselov from the University of Manchester, UK, presented their work entitled '' Electric Field Effect in Atomically Thin Carbon Films'', in which they explain the extraction

and isolation of atomic thin graphene crystallites from bulk graphite using a scotch tape. The graphene layers were pulled from the graphite with the scotch tape and were transferred to SiO_2. The method was described as micromechanical cleavage or as more widely known, scotch tape technique [www.graphene.manchester.ac.uk]. The technique had been previously reported, even patented back to 2002, to describe how to process commercially available flexible expanded graphite to achieve a graphite thickness of 0.01 thousandth of an inch. The key factor here was the high-throughput visual recognition of graphene on the proper substrate, silicon, which provides a small but noticeable optical contrast, necessary to distinguish the graphene.

Geim and Novoselov received the Nobel Prize in Physics the year 2010 for this pioneering work ''in groundbreaking experiments regarding the two-dimensional material graphene'' [Geim, 2011]. In that point is when it finishes the 'preface' and starts the 'era of graphene'. The last decade graphene is the dominant player in the material science research in an excessive amount.

Figure 1.2-2: A lump of graphite, a graphene transistor and a tape dispenser. Donated to the Nobel Museum in Stockholm by Andre Geim and Konstantin Novoselov in 2010.[https://en.wikipedia.org/wiki/Graphene]

1.2-2 Properties

Graphene attracted very fast the interest of the scientific community thanks to its various outstanding properties. We will refer here to all of them but not in an extensive level· the principal target of this thesis is the exploration of the graphene growth.

1.2-2.1 Structural properties

Graphene is a crystalline allotrope of carbon with 2D properties. Its atoms form a hexagonal atomic scale pattern. Its carbon atom forms 3 σ bonds with its neighbouring carbon atoms and one π bond oriented out of plane, in the z direction. The structure can be seen as a triangular lattice with a basis of two atoms per unit cell. The lattice vectors can be written as

$$a_1 = \frac{a}{2}(3, \sqrt{3}) \quad, \quad a_2 = \frac{a}{2}(3, -\sqrt{3})$$

where a=1.42 Å is the carbon-carbon distance. The reciprocal-lattice vectors are given by

$$b_1 = \frac{2\pi}{3a}(1, \sqrt{3}), \quad b_2 = \frac{2\pi}{3a}(1, -\sqrt{3})$$

The theoretical specific surface area (SSA) of graphene is 2630m^2/g, much larger from that of black carbon and carbon nanotubes.
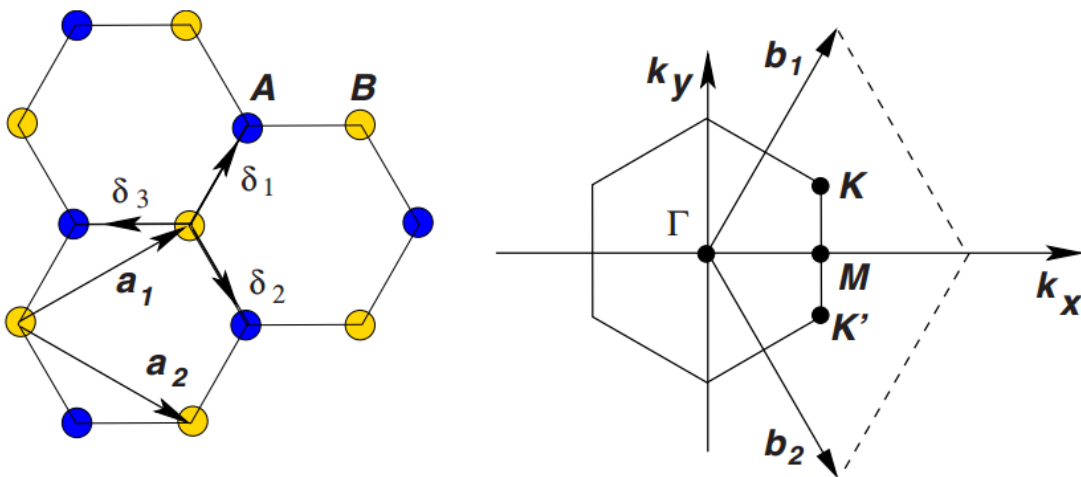
Figure 1.2-3: Right: Honeycomb lattice made out of two interpenetrating triangular lattices. Left: Corresponding Brillouin zone.

Of special importance regarding the graphene properties are the two points K and K' in the corners of the graphene Brillouin zone. These so called Dirac points are positioned at

$$K = (\frac{2\pi}{3a}, \frac{2\pi}{3\sqrt{3}a}), \quad K' = (\frac{2\pi}{3a}, -\frac{2\pi}{3\sqrt{3}a})$$

Their major contribution will be discussed later. Finally the three nearest-neighbouring vectors in real space as seen in Figure 1.2-3 are given by

$$\delta_1 = \frac{\alpha}{2}(1,\sqrt{3}), \;\; \delta_2 = \frac{\alpha}{2}(1,-\sqrt{3}), \;\; \delta_3 = -\alpha(1,0)$$

To visualize the π orbitals we can think of them as symmetric lobes oriented in the z axes and centered in the nucleus. Each carbon atom has one of these bonds. When they are hybridized together they form the π and π* bands which are responsible for the outstanding electronic properties of graphene [Cooper, 2012]. The atomic structure of graphene can be observed by transmission electron microscopy. The electron diffraction pattern reveals the honeycomb lattice. Some rippling can appear because of a partial instability usually present in 2D crystals or might has its origin in the dirtiness [Carlsson, 2007].
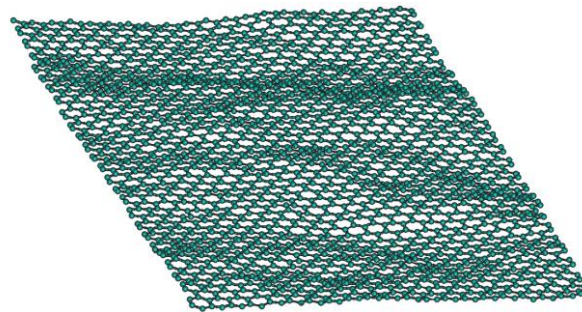
Figure 1.2-4: Section of a graphene sheet showing ripples of a finite size as obtained by Monte Carlo simulations. [Carlsson, 2007]

A matter of special importance in the graphene structure is the edges of the material. The various possible structures of the edges present unique electronic, magnetic and chemical properties. Single layer Graphene used in real applications will usually have the form of a ribbon. These ribbons usually present disordered edges that make the bandgap poorly defined, decreasing a lot the carrier mobility. After Joule heating, the ribbons can present two different kinds of edges, the armchair and the zig-zag, which depends on the orientation of the hexagons relative to the ribbon length (Figure 1.2-5). Hydrogenated or oxygenated group passivation during the heating treatment is commonly used to deter the spontaneous reconfiguration and stabilize the edges in air [Xiaoting, 2011].
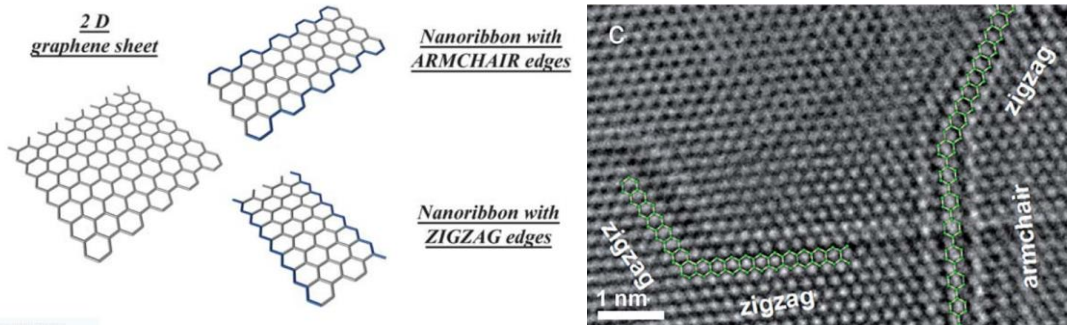
Figure 1.2-5: a) Scheme of the different possible edges and b) high resolution TEM image showing the well-defined zigzag and armchair edges (as illustrated by green hexagons). [Xiaoting, 2015]

Different methods to obtain the graphene ribbons include the CVD synthesis of them, the unzipping of carbon nanotubes, cutting by means of STM lithography and more.

Except from the edges, another key factor is the boundaries between grains, phase domains and layers regarding the graphene properties [Lin, 2013]. When it comes to more than one layer, the stacking between the different layers is crucial. The Bernal stacking presents a tunable bandgap, making it promising for nanoelectronic applications. Domains with the same crystal orientation can present two different kinds of Bernal stacking, AB and AC. This term refers to the shifting of the one of the graphene layers in opposite directions along one-third of the [1,1] crystallographic vector (Figure 1.2-6).
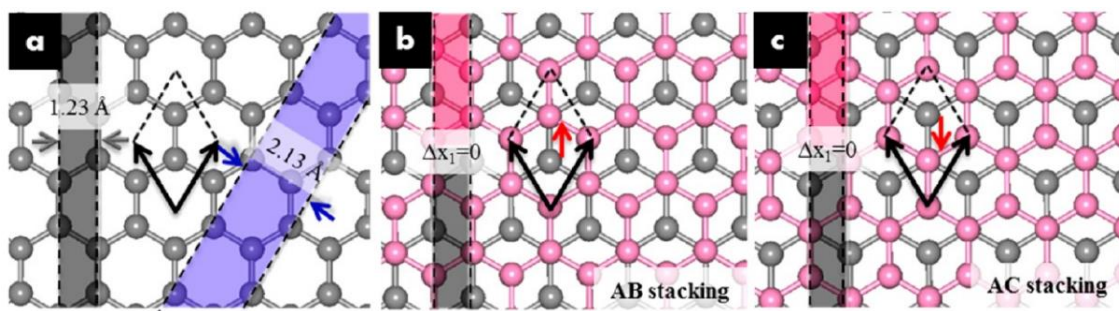
Figure 1.2-6: Schematic of AB and AC stackings in BLG. (a) Schematic of different lattice periodicities in monolayer graphene. (b,c) Schematics of AB stacking and AC stacking, respectively. The second layers are colored in pink. The dashed diamonds indicate the unit cells and black arrows are the unit cell vectors. The red arrow indicates the geometrical shift of the second layer with respect to the first layer. The pink strips in panels b and c indicate the lattice periodicity of 1.23 Å for the second layer, which is overlapped with the gray strip (lattice periodicity of 1.23 Å for first layer).[Lin, 2013]

By HRTEM means combined with molecular dynamics simulations it has been shown that these stacking are not atomically sharp but instead are forming nanometer-wide strained channels, most likely in the form of ripples, with diverse profiles of strain and morphologies. The strain engineering of the graphene bilayer stacking has been found to influence its electronic properties, thus it should be considered in the design of device applications.

1.2-2.2 Electronic Properties

Probably the electronic properties are the ones that graphene owns its fame and hype. As we commented above, the unusual semi-metallic behavior of graphene was first demonstrated by Wallace back to 1947. He calculated the band structure for a single graphite layer using a tight-binding approximation [Wallace, 1947]. Graphene is a zero-gap semiconductor as the conduction and valence bands meet at the Dirac point. To study the band structure we take the relationship between the energy and momentum of electrons within a given material. As graphene is a 2D material, its momentum space is also constrained to two dimensions. The tight-binding Hamiltonian for electrons in graphene considering that electrons can hop to both nearest- and next-nearest-neighbouring atoms is given by the equation

$$H = -t \sum_{(i,j),\sigma} (\alpha_{\sigma,i}^{\dagger} b_{\sigma,j} = H.C.) - t' \sum_{((i,j)),\sigma} (\alpha_{\sigma,i}^{\dagger} a_{\sigma,j} + b_{\sigma,i}^{\dagger} b_{\sigma,j} + H.C.) \quad (1)$$

where $a_{i,\sigma}$ ($a^{\dagger}_{i,\sigma}$) annihilates (creates)an electron with spin $\sigma = (\sigma=\uparrow , \downarrow)$ on site R_i on sublattice A (an equivalent definition is used for sublattice B), t(=2.8 eV) is the nearest-neighbouring hopping energy (hopping between different sublattices), and it´s the next nearest-neighbouring hopping energy (hopping in the same sublattice). The energy bands derived from this Hamiltonian have the form

$$E_{\pm}(k) = \pm t\sqrt{3 + f(k)} - t'f(k)$$

$$F(k) = 2\cos(\sqrt{3}k_y a) + 4\cos\left(\frac{\sqrt{3}}{2}k_y a\right)\cos(\frac{3}{2}k_x a) \quad (2)$$

where the plus sign applies to the upper (π*) and the minus sign the lower (π) band. We see that the spectrum is symmetric for t'=0. For the rest of the t' values the electron-whole symmetry breaks and the two bands become assymetric [Castro Neto, 2009]. The full band structure of graphene is given in Figure 1.2-7 with a zoom in of the band structure close to one of the Dirac points (at the K or K' point in the BZ). We can obtain this dispersion if we expand the full band structure of Eq. 2 close to the vector K or K'. As k=K+q and

$$E_{\pm}(q) = \pm u_F |q| + O[\left(\frac{q}{K}\right)^2] \quad (3)$$

In this equation q is the relative momentum in the Dirac point and u_F is the Fermi velocity calculated by u_F=3ta/2=10⁶m/s. The particularity here is that the Fermi velocity does not

depend on the energy or the momentum. The spectrum is expanding around the Dirac point including the t' which shifts in energy the position of the Dirac point breaking the electron-hole symmetry. The carriers behave like relativistic particles with a velocity very close to this of light (1/300th of the speed of light in vacuum).
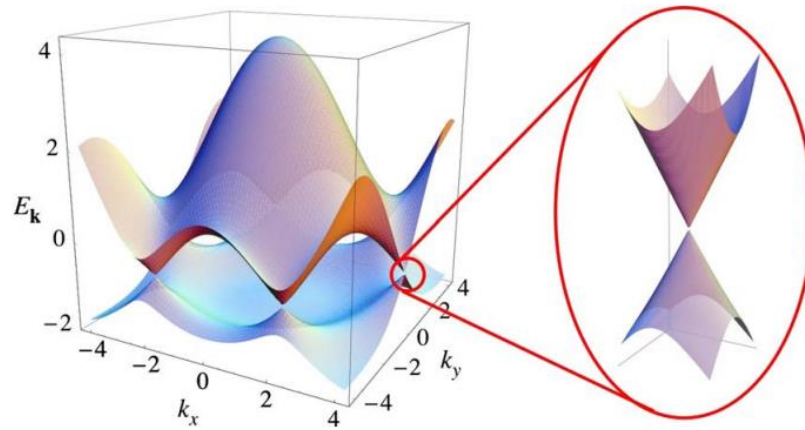
Figure 1.2-7: Electronic dispersion in the honeycomb lattice. Left: energy spectrum (in units of t) for finite values of t and t', with t= 2.7 eV and t'=−0.2t. Right: zoom in of the energy bands close to one of the Dirac points. [Castro Neto, 2009]

Graphene presents a special kind of chirality. Each sublattice is responsible for one branch of the dispersion and the distinct branches interact very weakly between each other. This effect points out that there is a pseudospin quantum number for the carriers. This number is analogous but independent of the real spin. Because of the pseudospin we can differentiate the contribution of each sublattice. This inability to transform one type of dispersion into another is what gives to graphene this chiral characteristic [Das Sarma, 2011].

Another original property is that the charge carriers can not be finite by electrostatic potential. As the particles are following the Dirac equation, the probability of their transmission is following the increase of the height barrier. When an electron hits a tall barrier will turn into a hole and propagate through the barrier until it reaches the other side, where it will turn back into an electron. This is called Klein tunneling phenomenon. By increasing the barrier height, is increased the degree of mode matching between the wave functions of the holes within the barrier and the electrons outside of it. When the modes are perfectly matched (in the case of an infinitely tall barrier) it occurs a perfect transmission through the barrier. In the case of graphene, the chirality discussed above

leads to a varying transmission probability depending on the angle of incidence to the barrier [Katsnelson, 2006].

To resume we appose briefly a comparison between graphene and other traditional semiconductors.

Traditional semiconductors have a finite bandgap while graphene has a zero bandgap. Usually we have to study differently doped semiconductors to study the motion of an electron and a whole in them. In graphene the charge carrier changes from an electron to a whole and vice versa in the Dirac point.

Graphene has a chiral and linear dispersion while most semiconductors have a quadratic one.

Graphene is much thinner that the other 2D electron gases that tend to have a thickness between 5-50 nm. Due to this, the electrons conducting through graphene are constrained in the z-axis to a greater stretch.

Graphene presents a finite minimum conductivity, even in the case of vanishing charge carriers. This is a question regarding the construction of field effect transistors as it leads to a low on/off ratio [Tan, 2007].

1.2-2.3 Field effect

The unusual electric behavior of graphene can be captured in electronic devices, the most common of which is the field effect transistor. In a device like this, graphene is deposited in a substrate, usually SiO_2. Electrical contacts, usually made of gold, are then patterned in a 4-lead or a Hall bar configuration (Figure 1.2-8). After cleaning the impurities by applying an annealing, the device is ready to work. A gate voltage is applied between the doped silicon substrate and the graphene domain. A surface charge density is being induced, calculated by n $=\varepsilon_0\varepsilon V_g/te$, where $\varepsilon_0\varepsilon$ is the permittivity of SiO_2, e is the electron charge, and t is the thickness of the SiO_2 layer. The charge density is shifting according to the Fermi level position and is expected to vanish in the Dirac point, although this does not happen due to thermally generated carriers (n_{th}) and electrostatic spatial inhomogeneity (n^*) that limit the minimum charge density. Away from the Dirac point the charge density is controlled by the gate voltage, following a linear relation. We do not deep more in how values like the conductivity, the carrier mobility and resistivity are being obtained but we mentioned them for bibliographic purpose.
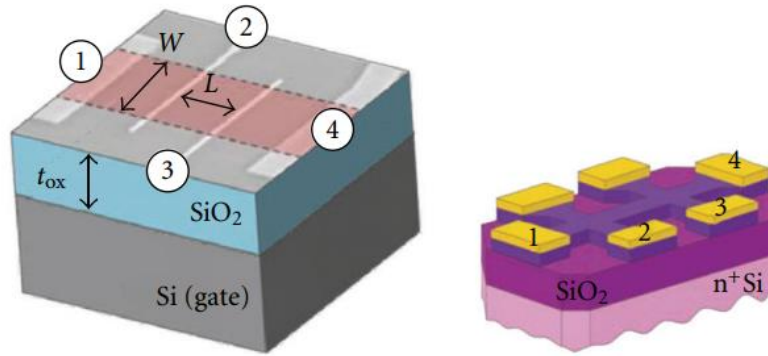
Figure 1.2-8: Schematic of field effect devices of different configurations :a) 4-lead, b) Hall bar. [Dorgan, 2010]

The minimum conductivity is calculated to be $\sigma_{min}=4e^2/\pi h=4,92*10^{-5}\Omega^{-1}$. This conductivity is expected to occur in the Dirac point. The carrier mobility typical value is on the range between 10000 to 15000 $cm^2V^{-1}s^{-1}$ for graphene on top of silicon oxide. This value increases a lot in the case of suspended graphene [Du, 2008]. It has been reported devices that presented mobility up to 200,000 $cm^2V^{-1}s^{-1}$. The resistivity of the graphene is in the order of $10^{-6}\Omega$ cm, a resistivity much smaller of this of silver which used to present the lowest known resistivity before [Chen, 2008].

1.2-2.4 Vibrational properties

The vibrational properties of the graphene present high interest as well. Thanks to them we can understand the record thermal conductivity that graphene presents and its optical properties through the phonon-phonon scattering. We start from obtaining the phonon dispersion relation. First we consider the vibrational modes of the crystal when it is in thermal equilibrium. The atoms are coupled between each other by torsional and longitudinal force constants which depend on the relative position of the atoms. If we consider the displacement of an atom n from each equilibrium position with the vector $\bar{u}_n$, we use the coupled equation of motion in frequency space

$$-\sum_m \Phi_{m,n}\bar{u}_n = \omega^2\bar{u}_n$$

the sum over m is typically over the second or the fourth nearest neighbors, with the corresponding coefficients $\Phi_{m,n}$. The atoms in graphene can vibrate in all 3 dimensions so the dynamic matrix has to be written in terms that include the sublattices A and B as well as the 3 spatial dimensions. We have 6 eigenvalues. The two correspond to the out of plane vibration ZO (optical) and ZA (acoustic) and the other 4 to the in plane vibrations

TA (transverse acoustic), TO (transverse optical), LA (longitudinal acoustic), and LO (longitudinal optical). The experimental data show that the dispersion is quadratic [Popov, 2004] and in the K and K' points we have a cone structure similar to this of the Dirac cones in the electronic structure. The in planes modes show an acoustic dispersion in the Γ point. The transverse modes follow the longitudinal modes with a bit reduced frequency, for both the acoustic and optical modes.

From the Raman scattering we can determine the phonon spectrum close to special symmetry points. The Raman peaks can determine the phonon energies for specific momentum values.

The high thermal conductivity of graphene is a result of the phonon dispersion relation. It presents an in plane sound velocity close to c_{ph} =20 km/s [Adamyan, 2011].

1.2-2.5 Thermal conductivity
From the kinetic gas theory we know that the thermal conductivity thanks to phonons is calculated by the relation

κ $\sim c_{ph}C_V(T)\lambda$

where $C_v(T)$ is the specific heat/unite volume and λ is the phonon mean free path. In the case of graphene thanks to the large c_{ph}, the thermal conductivity is very large as well. Experiments at room temperature have revealed a thermal conductivity κ=3080–5150 W/mK and a phonon mean free path of λ=775 nm [Balandin, 2008]. These values although decrease seriously in the case of nanoribbons or suspended graphene.

Thanks to its thermal conductivity graphene can be very useful in electronic devices. The high thermal conductivity facilitates the diffusion of heat to the contacts and allows the fabrication of more compact circuits.

1.2-2.6 Optical properties

Graphene presents a unique high opacity for an atomic monolayer in vacuum, of about 2.3% of visible light. Its absorption can be described in terms of its fine structure constant α. In free standing graphene the light transmittance T is calculated by the Fresnel equation considering a thin film with a universal optical conductance of $G_0=e^2/4h$

$$T = (1 + 0.5\pi\alpha)^{-2} = 1 - \pi\alpha = 0.977$$

As the graphene films behave as a 2 dimensional electron gas, they are non-interacting in superposition and present an absorbance proportional to the number of layers. It's

reflectance on the other hand increases from 0.1 to about 2% with the increase of the number of layers from 1 to 10 [Casiraghi, 2007]. Thanks to these properties graphene can be used in a variation of applications in optoelectronic and photonic devices, photodetectors, touch screens, smart windows, saturable absorbers, and optical limiters [Bonaccorso, 2010].
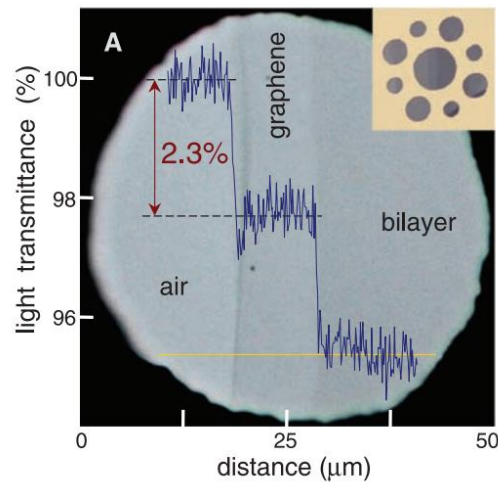
Figure 1.2-9: Photograph of a 50-mm aperture partially covered by graphene and its bilayer. The line scan profile shows the intensity of transmitted white light along the yellow line. On the inset the metal support with several appertures for the graphene placement [Nair, 2008].

1.2-2.7 Mechanical properties

Graphene is the strongest material, it presents a Tensile strength of 130 GPa and a Young's modulus (stiffness) of 1 TPa (150000000 psi) [Li, 2008]. As described in a pretty picturesque paradigm during the Nobel announcement, a 1 square meter graphene hammock would support a 4 kg cat but would weigh only as much as one of the cat's whiskers, at 0.77 mg (about 0.001% of the weight of 1 m^2 of paper) [nobelprize.org].

To measure its mechanical properties, suspended graphene was deposited over SiO_2 cavities and with the use of an AFM stress was applied in the sheet. By performing these measurements it has been possible to obtain graphene's spring constant in the range 1–5 N/m and the stiffness at 0.5 TPa [Frank, 2007]. To calculate the spring constant is applied a static force for a double champed beam. Knowing the fundamental resonance $f_0 = 1/2\pi \sqrt{\frac{\kappa_s}{m}}$, the resulting effective spring constant is

$$k_s = 16.23Ew\left(\frac{t}{L}\right)^3 + 4.93T/L$$

where E is Young's modulus, w is the width of the sheet, t and L are the thickness and length of the suspended graphene sheet, and T the tension of the beam.
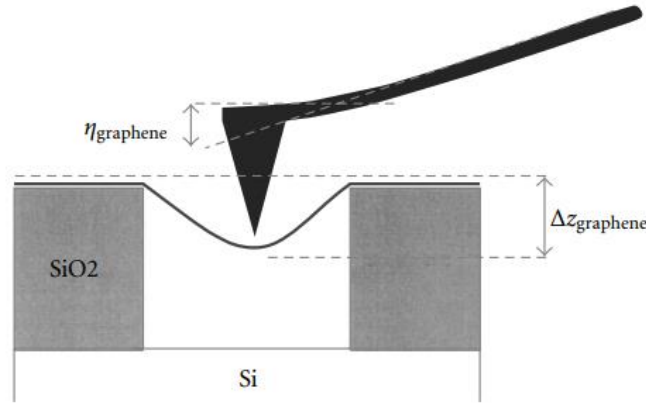
Figure 1.2-10: Scheme of the AFM tip while pushing the suspended graphene sheet. $\eta_{graphene}$ is the height that the tip is deflected by the graphene and $\Delta z_{graphene}$ is the height pushed by the tip. [Frank, 2007]

The tip used has a spring constant 2N/m which enables the deflection of the graphene. As the tip comes in contact with the graphene and the cantilever is pulled down onto the surface resulting in a dip in the deflection. As we see in Figure 1.2-10, $Z_{piezo}=n_{graphene}+\Delta z_{graphene}$ where n graphene is the deflection of the tip, z piezo is the location of the piezo moving the tip, and Δz graphene is the deflection of the graphene sheet. As the spring is following Hooke's law can be obtained the effective spring constant of the suspended graphene sheet.

1.2-3 Production techniques

There are two different types of approaches considering the graphene synthesis. These approaches are applied in most of the nanomaterials. They are the bottom-up and the top-down approaches. The top-down approach includes the breaking of the stacked graphite layers to obtain single graphene layers. To do so, it is necessary to overcome the van der Waals forces that hold the layers together. Key factor in this approach is the effective separation without damaging the individual layers and the prevention of re-agglomeration of the sheets once the layers have been exfoliated. The bottom-up methods involve synthesizing graphene from alternative carbon containing sources (Figure 1.2-11). The important factor here is the requirement for high temperature in order to promote high levels of graphitization. This kind of methods are more possible to present defects in the graphene in compare to the top-down approach but they offer the advantage of direct growth in certain substrates suitable for applications. In general, it is considered that all approaches present advantages and disadvantages. The most suitable method depends each time on the final application that the graphene is aimed to be used. Therefore, it is more possible that multiple methods of graphene synthesis will be needed to realize the full potential of graphene [Rebecca,2013].
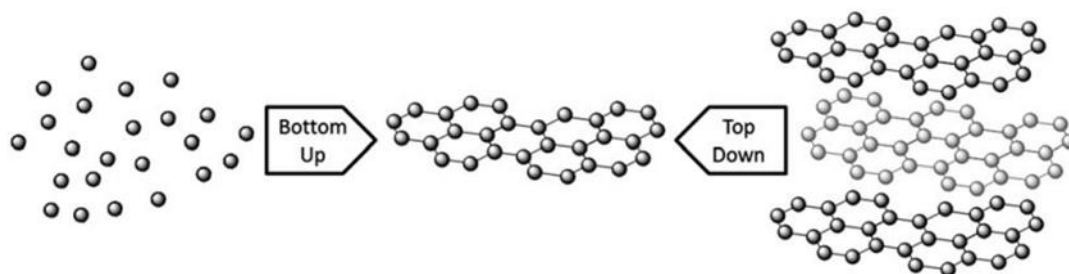
Figure 1.2-11: Scheme of the top-down and bottom-up approach in graphene synthesis. [Rebecca, 2013

1.2-3.1 Top-Down methods
Micromechanical cleavage

Micro mechanical cleavage or as more commonly known, the scotch tape method, performs the exfoliation of the graphene with the use of an adhesive tape to cleave apart the layers. Repeating the cleavage more times permits as obtain few layer or even single layer graphene. The graphene is easy to be spotted by means of optical microscopy if deposited on top of Si/SiO$_2$ (300nm) thanks to the change in refractive index between it

and the substrate. The material obtained by this method is of high quality but the technique is time consuming and the yield is low. It is preferred therefore for laboratory use and fundamental study and not for applications where large scale synthesis and re-productivity are necessary.

Electrochemical exfoliation

In this technique the graphite is used as a sacrificial electrode and the exfoliated material is being collected from the electrolyte material. Electrolytes used to date, include surfactants and H_2SO_4–KOH solutions. The surfactants prevent the re-agglomeration of the graphene as the hydrophobic groups interact with the p-orbitals of graphene, and the hydrophilic groups stabilize the sheets in water [Englert, 2009]. Usually the final product consists of a mixture of graphene flakes of various thicknesses. Extra centrifugation is needed to be performed to obtain few layer graphene.

In another version of this technique, the graphite electrode is being expanded in situ and after is being exfoliated by sonication. Lithium salts are intercalated to form graphite intercalation compounds [Wang, 2011]. Sonication separates the layers by injecting thermal shock into the material through ultrasonic cavitation. By this technique yields of ≥70% few layer graphene are being reported.

Exfoliation of graphite intercalation compounds (GICs)

Various approaches have been reported including solvent-assisted and thermal exfoliation. In solvent-assisted exfoliation GICs are sonicated in solution to aid the exfoliation. In addition to the intercalation of solvent molecules expanding the layers, interaction with the solvent can cause gas to be expelled that aids exfoliation, as observed in the case of lithium GICs in water.

The thermal expansion effect on GICs has been reported since the 1910's and attracted a marked interest in the 1960's [Chung, 1987]. By heating the GICs is caused thermal decomposition of them into gaseous species that push the layers apart. Expanded graphite is formed through its exposure to strong acids to yield a GIC which is later being exfoliated by rapid thermal heating.

Following repeated circles of intercalation–exfoliation followed by sonication yields single and bilayer graphene.

Exfoliation of graphite oxide

Another very popular method is this of the exfoliation and reduction of graphite oxide. First the graphite is being oxidized following different methods like one of the Straudenmaier, Brodie or Hummers. Various models describe the structure of the graphite oxide. The widely accepted Lerf–Klinowski model explains   the existence of a layered structure with hydroxyl and epoxy groups on the basal planes and carboxylic and carbonyl groups at the sheet edges. Thanks to these groups graphite oxide is hydrophilic and moreover presents a larger interlayer spacing (6–12 Å, depending on the amount of intercalated water) than graphite (3.4 Å) [Buchsteiner, 2006].

Graphite oxide is being exfoliated to graphene oxide, followed by a reduction to obtain the final product, graphene. Usually we refer to it as reduced graphene oxide (rGO) to indicate its origin and that probably it has not been performed a full reduction of it. Different thermal or chemical methods can be followed for the reduction process [Pei, 2012]. Unlikely to graphene, rGO is an electrical insulator due to the functional groups disrupting the sp_2 hybridization of the graphene layers. An efficient reduction is necessary in order the material to present its unique electrical properties.

Unzipping carbon nanotubes

By the use of wet chemistry methods with strong oxidizing agents is possible to unzip single or multi-layer carbon nanotubes and obtain graphene. Another possible way is the use of physical methods such as laser irradiation and plasma etching. The result is graphene nanoribbons with widths dictated by the diameter of the tubes. The properties of the ribbons depend on the width as well as the edge type. The unzipping starts with the fission of the C-C bond which usually occurs at defects sites, leading to irregular cutting [Cho, 2011]. To overcome this problem, it has been proposed the unzipping of flattened carbon nanotubes, attacking preferentially along the bent edges. By this means it is possible to obtain well-regulated nanoribbons (Figure 1.2-12).
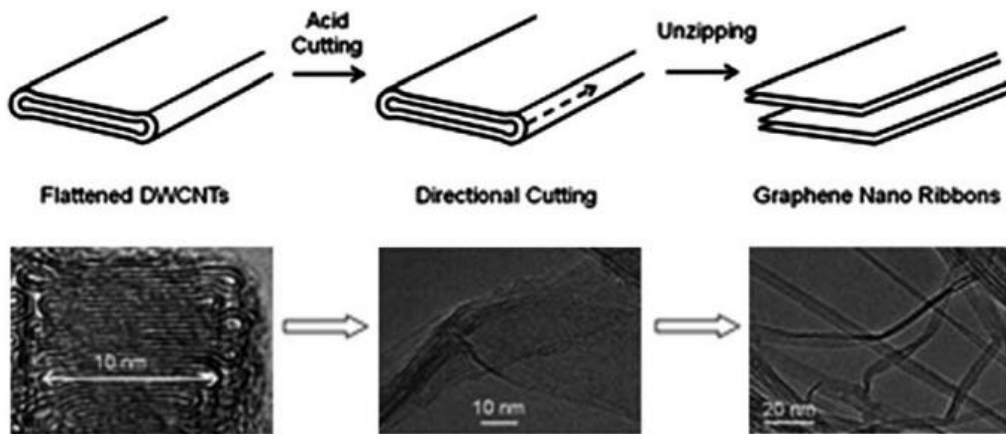
Figure 1.2-12: A schematic of directional unzipping of flattened carbon nanotubes (top) and corresponding TEM images (bottom) [Kang, 2012]

1.2-3.2 Bottom up methods
Epitaxial growth on silicon carbide

This method is based on the sublimation of silicon from the silicon carbide surface and the further graphitization of the carbon atoms that remain on it. In general high temperatures, above 1000 °C and ultra-high vacuum are necessary for the process. Although, the growth in argon atmosphere has presented the advantage of decreasing the silicon sublimation rate so that higher growth temperatures can be used. The higher temperatures have shown to increase the quality of the graphene [Emtsev, 2009]. Another method promotes the use of pulsed electron irradiation to induce the silicon sublimation.
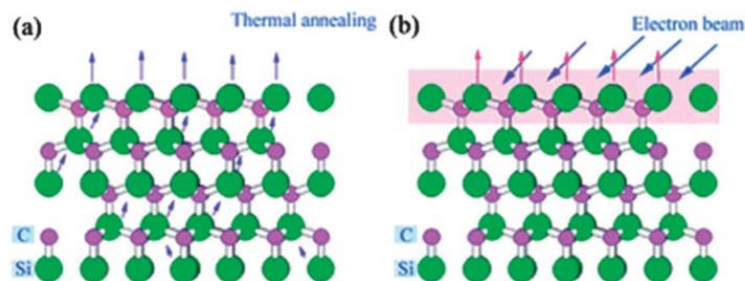
Figure 1.2-13: Schematic description of Si atom sublimation in Si-terminated 4H-SiC under thermal annealing process (a) and pulsed electron beam irradiation process (b) [Huang, 2010]

Graphene has been grown both in cubic phase and hexagonal phase SiC, in both its silicon rich and carbon rich faces. In the silicon rich face the graphene grown in a single orientation, rotated 30° with respect to the SiC, and exhibits the regular Bernal stacking [Riedl, 2010]. The SiC surface presents steps due to its structure. As a result, pits are present on it that affect the uniformity of the graphene film. On the other hand, when graphene is grown in the C rich face exhibits rotational stacking. In this case, each of the rotations forms a structure with either SiC or the underlying graphene layer. It is considered that because of this rotational misalignment, graphene grown on the carbon rich face presents higher electrical conductivity, as the electronic decoupling of the layers results in monolayer-like properties for the stacked multilayer [Mele, 2012]. The growth temperatures in this case are lower but this affects the growth rate resulting in restricted graphene grain sizes [Srivastava, 2012].

In order to decrease more the growth temperature, it has been promoted the idea of depositing a nickel thin film on top of the SiC. The nickel catalyzes the growth in temperatures about 700-800°C. The graphene is grown on top of it. The disadvantages are the introduction of the extra step of the deposition of the transition metal and the necessity to transfer the graphene to insulating substrates for use in electronic applications [Juang, 2009].

Graphene growth on SiC is appropriate for wafer based applications and presents the advantage of the lack of necessity of transfer. For different use transfer can be performed although is hindered by the strong interactions between the graphene and the substrate. Another important point considering the large scale use of the technique is the high cost of this substrate. Cubic SiC is cheaper so it can be an alternative substrate for the graphene growth.

Chemical vapor deposition growth

In the chemical vapor deposition growth graphene is formed by the high temperature pyrolysis of carbon containing gases. The method is used for the growth of graphene on top of transition metal substrates and it probably represents the most active and promising area of research concerning the graphene large scale synthesis.

During the process, gas species are being introduced into the reactor and pass through a hot zone were the hydrocarbon precursor is being decomposed into carbon radicals which form

the graphene on the metal surface. During the growth, the metal substrate has two roles. First it works as a catalyst that lowers the energy barrier of the reaction. Second, it determines the deposition mechanism of the carbon radicals to form the graphene. The process can be described as self-limited to form monolayer graphene as the surface is being pacified once fully covered. In the case of segregation, the carbon first dissolves in the bulk metal and later is being diffused in the surface to form the graphene. This occurs during the cooling when the solubility of carbon in the metal is lower in lower temperatures.

The most important step is the optimization of the growth conditions. Factors like the pressure, the temperature and the exposure time affect the quality and size of the graphene grown. Also, the strength of the interaction between the graphene and the substrates differs depending on the metal used and can impact the degree of graphene rippling, the sensitivity of graphene to defects in the metal surface and the ease of graphene transfer to arbitrary substrates. There are a number of factors that can affect the suitability of a metal for use in the graphene growth but finally the two most important ones are the cost and the availability of it, especially since the point that usually it is being etched away during the transfer process.

The first CVD graphene growths were reported in 2008 and 2009 using copper and nickel which until today are the two most explored substrates regarding the graphene synthesis. Later on a lot more research activity has been done using a variety of different transition metal substrates, Fe, Ru, Co, Rh, Ir, Pd, Pt, Au, as well as different alloys like Co-Ni, Mo-Ni, Au-Ni and stainless steel [Zhang, 2013].

Graphene grown on copper foil follows the surface catalyzed mechanisms whereas growth on nickel proceeds via segregation. The growth on copper results in the growth of monolayer graphene as it is self-limited at ultra-high vacuum conditions. It has been reported the growth of up to 30 inches graphene films in polycrystalline copper foils [Bae, 2010]. The growth on nickel is more difficult to control but presents the advantage of not requiring ultra-high vacuum conditions.

By studying the growth over single crystal metals it provides useful information concerning the growth mechanism but in reality it is very complicate and expensive to grow large area single crystal metals. It is more convenient to study the growth over polycrystalline metal films, in the form of polycrystalline metal foils or thin films deposited by sputter coating or electron beam evaporation. These substrates seem to be the future

for the large scale CVD growth. The continuous graphene is being grown in the metal grain boundaries of polycrystalline films, both in the case of copper and nickel.
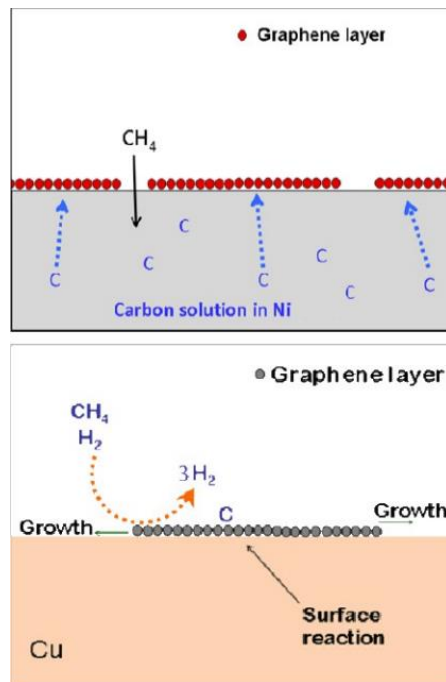
Figure 1.2-14: Schematic diagrams of graphene growth mechanism on Ni and Cu [Zhang, 2013].

It is a challenge to study the growth over these areas as, even in the case that the graphene grown is continuous, the sites have been shown to lead to defects such as nucleation of multi-layer graphene, which degrade the properties of the graphene films [Reina, 2009]. The thickness of the foil on the other hand does not appear to play an important role. Same quality graphene films have been observed to grown in different thickness foils varying from 12,5 to 50 μm [Edwards, 2013].

Other important factors concerning the synthesis over copper are the purity of the copper and its pretreatment. Sonication prior to annealing as well as different reduction processes have been found to be important concerning the uniformity of the film. The hydrocarbon concentration also impacts the uniformity due to its effect on the graphene nucleation density. In general is observed that lower hydrocarbon concentration hence the growth of more uniform graphene. A strategy followed includes keeping the concentration low at the beginning of the process to achieve a low nucleation density and increase it later during the process to achieve the complete growth [Li X., 2010].

Except hydrocarbon gases, different sources can contribute the carbon needed for the graphene synthesis. An alternative method includes the deposition of an amorphous carbon coating on top of the copper. Then an annealing is performed in high temperatures under hydrogen and argon flows which lead to the growth of the graphene. In other works have been used as carbon sources PMMA and even food, insects and wastes that can provide the necessary amount of carbon [Edwards, 2013].

In the case of nickel the growth conditions have to be explored even with greater care if single layer graphene needs to be grown as the process here is not self-limited like in the case of copper. High temperature, high hydrogen concentration, and short growth time are important factors for the few layer graphene growth. For the further reduction in the number of layers the optimization of the cooling rate is crucial as well as the growth on nickel surfaces has also been demonstrated based on diffusion and segregation of carbon from underlying amorphous carbon [Kim K., 2009].
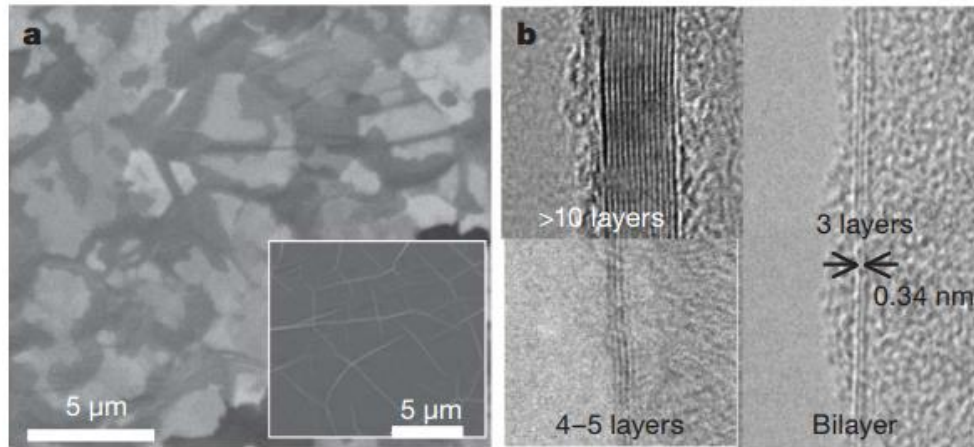
Figure 1.2-15: a) SEM images of as-grown graphene films on thin (300-nm) nickel layers and thick (1-mm) Ni foils (inset). b) TEM images of graphene films of different thicknesses [Kim K., 2009].

It has even been reported the growth of graphene by cvd techniques that do not involve the use of specific metal substrates. An example is the work of Dato et al were graphene is grown via microwave enhanced CVD of ethanol [Dato, 2008]. Liquid ethanol droplets are passing through argon plasma. The synthesized graphene is being collected from a membrane filter inside the reaction chamber. Another work proposed a route of growth via the thermal decomposition of sodium ethoxide in ethanol [Herron, 2011].

Miscellaneous methods

Graphene of different thickness and morphologies has been synthesized via a number of distinct methods. Through the flash pyrolysis of the solvothermal product of sodium and ethanol has been produced graphene with a foam-like structure of sheets held into a porous structure. With further sonication the sheets are getting separated [Choucair, 2009]. Other reported methods include the reduction of carbon containing species in different means such as igniting magnesium in dry ice, calcining calcium carbonate with magnesium powder and calcining aluminium sulphide (Al_2S_3) in carbon monoxide [Edwards, 2013].

By the use of polyaromatic hydrocarbons different graphene structures have been synthesized. In the work of Wang et al [Wang X., 2008] they are being dissolved into chloroform and spin coated over electrically insulating substrates like glass or SiO_2 which are then being heated to cause fusion of the molecules, resulting in graphene films of different thickness.

	Electrical conductivity	Strength	Elasticity	Surface area	Transparency	Thermal conductivity	Chemical inertness	Gas impermeability
Transistors	✓	✗	✗	✗	✗	✗	✓	✗
Energy storage devices	✓	✗	✗	✓	✗	✗	✓	✗
Electrodes	✓	☐	☐	☐	☐	✗	✓	✗
Electrically conductive inks	✓	✗	✓	✗	☐	✗	✓	✗
Polymer composites	✓	✓	✓	✓	☐	✓	✓	☐
Sensors	✓	✗	☐	✗	✗	✗	✓	☐

Table 1.2-1: Graphene properties and their importance to applications. A tick indicates importance, a cross indicates relative unimportance and a square indicates that the property is sometime important.

To sum up, it seems difficult to choose which is the 'best' technique regarding the graphene synthesis as all present advantages and disadvantages. The growth process affects the properties of the final material and therefore the range of applications it can be used to (Table 1.2-1). To choose the appropriate process we must be guided by the end-application that the material is aimed to be used to.

1.2-4 Things you could do with graphene-Potential Applications

Graphene and its derivatives are very versatile materials. Its special electrical, optical and mechanical properties results in being proposed for a wide range of different applications. As it has attracted the attention, and founding, of the research community worldwide, academics and technology manufacturers constantly try to introduce the material to new applications or to improve existing ones. Until today some areas are more developed, like flexible electronics and conductive inks and other are still in a more conceptual stage, like biomedical and aerospace technologies. This has to do with the fact that in the graphene research had in principle got involved physicist and chemist, not biologist and engineers, so applications based on these sciences got developed first. Here we refer to some indicative applications from different fields, in order to highlight the pluralism in possible uses of the material [''Things you could do with graphene'', Nature Nanotechnology, 2014]

1.2-4.1 Graphene in flexible electronics

Flexible and stretchable electronic components are more versatile than the obdurate ones and are being developed for use in different optoelectronic devices. An important component of these devises is the electrode that moreover needs to be transparent. Until today the main material used in this kind of devices is the indium tin oxide (ITO) as it is transparent and it presents a good conductivity. Its disadvantage is the fact that it cracks when bent or get stretched and this degrades its electrical properties. Graphene is a potential candidate to replace ITO and overcome this problem. It presents a superior optical transmission than ITO when it is single or bilayer and a similar sheet resistance thanks to its high carrier mobility and carrier density. Graphene can be transferred into flexible substrates and remain mechanically robust. In addition it has the smallest bending radius among all flexible transparent conductors. So far, graphene has been used as a transparent electrode in a variety of flexible optoelectronic devices, including touch-screen sensors, organic light-emitting diodes, and organic photovoltaic devices (Figure 1.2-16).
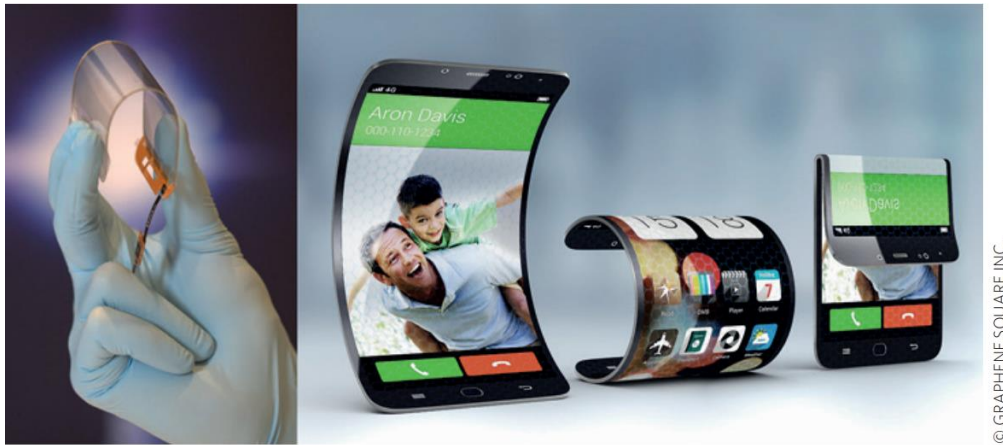
Figure 1.2-16: Graphene-based multi-touch screen showing excellent flexibility (left) and possible applications in bendable or foldable mobile devices (right). [''Things you could do with graphene'', Nature Nanotechnology]

Large scale graphene synthesis is being realized via roll-to-roll process. The possibility to integrate the transfer over the flexible substrate into this process makes the use of graphene even more appealing. The reason that for the moment we can not proceed in a total replacement of the ITO by graphene is the architecture of the device itself. This kind of devices have an interconnected, multilayered structure where is complicate for the moment to deposit the graphene on. This problem does not occur for ITO as it can easily be sputtered over irregular surfaces. Resolving this challenge considering the graphene will get us closer to flexible electronics.

1.2-4.2 Conductive inks for electronic circuits printing

Graphene and other 2D materials have the potential to make an impact on printed electronics as they are solution-processable and fulfill most of the requirements for this technology like high carrier mobility, mechanical robustness, environmental stability and potentiality for low-cost production.

To produce an ink like this, graphene nanosheets have to get dispersed in a liquid by liquid-phase exfoliation in solvents to give few-layer nanosheets. The same method can produce suspensions of a range of other 2D nanosheets, including WS_2, MoO_3 and BN, materials that have diverse properties, being suitable for a wide range of applications in printed electronics. Graphene can be used in flexible interconnects or as an active material in printed supercapacitors or composite devices. It cannot replace conjugated polymers as the semiconducting material in printed electronic devices due to its lack of bandgap though. The most exciting applications will come from devices that integrate two or more different nanomaterials in well-defined structures. All-ink jet printed heterostructure photodetectors and transistors have already been produced by sequential printing of graphene and WS_2, MoS_2 or BN.

Some hurdles that still remain to get overcome have to do with the yield of monolayer graphene when the nanosheets are made by liquid-phase exfoliation. For the moment the yield is low, between 5-25% and the flakes size difficult to be controlled. Moreover, the concentration of these suspensions is usually low (0.01-1 wt%) due to the high aspect ratio of the nanosheets and this can be a problem for some applications. Another issue is the electrical performance of these devices. As they consist of networks of either graphene or inorganic nanosheets, the charge mobility will be limited by junctions between the sheets, resulting in mobilities typically two orders of magnitude lower than in individual nanosheets. This limits the conductivity of graphene interconnects and therefore the performance of the device. In general it is expected that as new combinations of materials are demonstrated and the production scales up, the cost will reduce and new devices will emerge.

1.2-4.3 Graphene in energy storage

Graphene is a strong candidate for energy storage applications thanks to its high surface area (theoretical value of 2.630 m^2g^{-1}), excellent electrical conductivity, high mechanical strength and potential for low-cost manufacturing. For the moment, graphene sheets for energy storage are made by oxidation and reduction of graphite. Despite the structural

defects and oxidized functional groups these multiple stacked graphene sheets are better than single layer graphene as they can be made in larger quantities. Two devices have been investigated until now, batteries and electrochemical capacitors. In the batteries we have high energy density but slow charge and discharge. In the capacitors appear the contrary phenomenon, rapid charge and discharge but low energy density. An ideal device should be able to combine both high energy and high power.
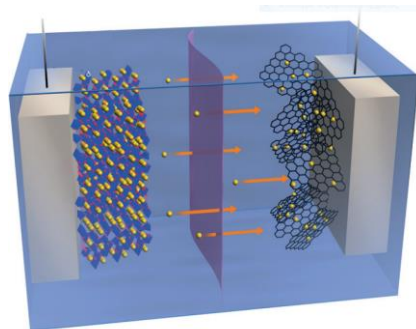
Figure 1.2-17: Scheme of a hybrid battery–capacitor device. On the left there is an intercalation material used as cathode and on the right graphene used as anode. Lithium ions (yellow) are inserted and de-inserted during charge and discharge cycles. [''Things you could do with graphene'', Nature Nanotechnology]

The theoretical capacitance of graphene is as high as 550 Fg^{-1} when all the surface is used. Until now this value has not been achieved but values up to 200-300Fg^{-1} have been reported. This is still much higher than the commercial capacitors made of activated carbon which present capacitance of about 100 Fg^{-1}.

In Li-ion batteries graphene can be used as an anode or cathode material. Its specific capacity is greater than 500 mA h g^{-1}, when this of graphite, which is the commercially used material today in these batteries, is 372 mA h g^{-1}. The practical problem though is that in order the graphene to achieve a high capacity, it should be charge in more than 3V which is a non-realistic value. The anode material should be charged and discharged at less than 1 V and for this potential graphite has higher specific capacity. An all graphene battery has been fabricated where reduced graphene sheets are used as the cathode, which can be charged to a high voltage, and graphene oxide is used as the anode. The battery presented high energy density (225 W h kg^{-1}) and high power density (6,450 W kg^{-1}).

Looking for alternative ways to take profit of graphene, it has been promoted the idea to use it as a coating material to enable the direct use of Li-metal anodes, which despite the high capacity that lithium presents, it can not be used because of the dentritic morphology

that it forms and can cause internal shortage. In addition, graphene is being added to low conductivity materials such as TiO_2, $LiFePO_4$ and organic materials can aid charge transfer and promote high-rate charge–discharge cycles.

Graphene has very low packing density, as low as 0.015 g cm^{-3} (, typical graphite anode materials have a packing density of about 1 g cm^{-3}), which translates in a very low volumetric energy density in a device. Graphene sheets also use to restack and this reduces their effective surface area and even may change their structure. It is important to make electrode materials thick enough to obtain meaningful capacitance or capacity per unit area.

1.2-4.4 Graphene against metal corrosion

Metallic corrosion in infrastructures costs hundreds of billions per year both in United States as in EU. Until now chromium and zinc based coatings are used to prevent it but because of the adverse effects of them on human health and the environment, its supply and use in Europe are restricted. Graphene has attracted the attention as a candidate for coatings as in addition to all its other attractive properties, it presents impermeability to all gases and salts.

The anticorrosion mechanism provided by graphene can be explained by 3 different processes. First, graphene coatings can make the path of permeating water more turbinal. Second, pristine graphene acts as an excellent barrier to water, oxygen and other corrosive materials. Because of its electrical conductivity, when used as a coating it can offer an alternative path to the electrons so that they never reach to the cathodic site. Electrons need to reach there in order to complete the corrosion reaction. If this happens, it is difficult for the corrosion to stop. Finally, graphene and graphene hybrid nanocomposites can be used as inhibitors in protective coatings to prevent oxidation of underlying metals in oxidizing chemicals, water or air. A recent approach for the use of graphene in industrial production proposed graphene based coatings made from liquid exfoliation of graphite and incorporation into organic coatings. These structures were used as coatings in bipolar plates in fuel cells, which are stainless steel components that separate individual cells in a stack and help in the distribution of fuel and oxidant, water management and current collection [Kirkland, 2011].

1.2-4.5 Graphene in biomedical applications

Graphene is the archetypal structure in the family of carbon nanostructures, between fullerenes, carbon nanotubes, nanohorns, graphene quantum dots and others. Its 2 dimensional flat surface can be modified to change its character from highly hydrophobic to patchy amphiphilic to highly hydrophilic. Graphene can be used in different areas of biomedicine, including transport (delivery) systems, sensors, tissue engineering and biological agent. In Figure 18 is presented a table where we see the possibilities offered by graphene and the rest of the various nanocarbon forms in terms of their biomedical applicability and potential, compared with challenges in implementation and clinical adoption.

Table 1 | Opportunities and challenges in biomedical applications for different forms of nanocarbon.

	Fullerenes	Carbon nanotubes	Graphene materials	2D heterostructures
Unique properties used in biomedical and life science	Free radical scavenging	Cylindrical shape Photothermal capability Inner space (for filling)	2D flat shape Large available surface area Flexibility Electrical conductivity Absence of bandgap Aqueous solubility (in the case of graphene oxide) Versatility of chemical functionalization	Similar to graphene materials in shape and structure More variability in the 'mix' of physical properties from different single layers
Biomedical application (most mature or intensively explored)	Antimicrobials	Molecular transporters (drug delivery) Near-infrared imaging agents	Highly sensitive biosensors Molecular transporters Coatings/substrates for tissue engineering and implants	Almost no such applications reported Biosensing and biodetection will be prime candidates
Opportunity	Interaction with double-stranded nucleic acids (for example mitochondrial DNA)	Translocation of biological membranes and barriers	Responsive to a wide range of parameters High sensitivity Multiple read-out routes Ease and speed of degradation	'Fabricate-by-design' based on the selection of layers
Challenge	Aqueous dispersibility Non-specific DNA binding leading to cytotoxicity	Controlled manufacturing and surface functionalization Aqueous dispersibility Adverse (inflammatory) responses related to fibre shape Slow kinetics of biodegradation	Unknown cytotoxic limitations Controllable dimensions Determination of *in vivo* biodegradability kinetics	Interaction with biological matter is currently unknown

Figure 1.2-18: Opportunities and challenges in biomedical applications for the various nanocarbon forms [Kostarelos. 2009].

Scientists are taking advantage of the very large surface to volume ratio of graphene and its facile chemical modification. The easy tuning of its hydrophobic/ hydrophilic surface character allows control of their capacity to translocate or interact with different biological barriers. The razor-like shape of the graphene sheets helps to slide through membranes and become internalized in a cell.

Another use is this of graphene flakes as therapeutic agents for hyperthermia treatment. As it lacks of bandgap, graphene is sensitive in a wide spectral range of laser irradiation,

so agents can be designed to get locally heated and serve for this kind of treatment. Graphene materials can potentially be used in antimicrobial applications as well but various fundamental pharmacological parameters (for example, blood circulation kinetics, immune cell interactions and responses, and tissue distribution) have to get clearer before graphene gets transported to any specific location of the body.

In addition graphene seems ideal for various sensor applications. As most of its properties are interlinked, it can be used to sense a wide range of parameters and also provide a large choice of read-out methods (for instance, chemical doping can be easily detected by transport, optical or Raman measurements). For the moment most promising seems to be the fabrication of sensors with biological or optical read-outs. Other interesting approaches include devices for DNA sequencing through nanopores or even the use of graphene as a photodetector or in plasmonic chemical sensors. In addition, graphene has been proposed for coatings and fabricating matrices and substrates for the engineering of various artificial tissue components and implants, including artificial skin and orthopedic implants. Finally, graphene and graphene oxide membranes have been proposed to get engineered and chemically functionalized to allow controllable permeation of different molecules.

As always when it comes to biomedical applications, how graphene materials will be finally incorporated in devices will be mainly determined by the risk–benefit ratio that each particular medical need and application allow.

1.2-4.6 Graphene products

Despite the intense efforts to incorporate graphene in new applications, for the moment the list of graphene products launched in the market remains very poor. We present them next.

GRAPHENE INFUSED 3D PRINTER POWDER. The Noble 3D printers company has introduced Graphenite, which consists of Graphene infused Binders and Composite Powder. The company claims that by adding a 0.03% of graphene to their cementitious composites resulted in a 32%-51% increase in cured material's elongation and compression strength [noble3dprinters.com].

Siren Technology security smart packaging. Vorbeck Materials launched a graphene ink based product where a fully integrated conductive circuit consists of graphene. The advantage is that the product can be flexed and wrinkled without damage to the circuit [http://www.graphene-info.com/].

Flexible touch panels for mobile devices. By Shanghai's Powerbooster Technology. No more technical information is provided to their web page though.

Tennis Rackets and Skis. By HEAD company. Graphene is used to make these products stronger and lighter.

Graphene-Oxide based Thermene Graphene Thermal Paste which is aimed towards CPU cooling. By the Thermene Company. They are using graphene oxide flakes.

Graphene enhanced helmets and cycling shoes. By the company Catlike [http://www.graphene-info.com/].

1.2-5 Scientific output

Graphene is an example of merging translational nanotechnology, where discoveries in laboratories are transferred to applications. A look in the rise of the patenting activity around the material can assure us about this.
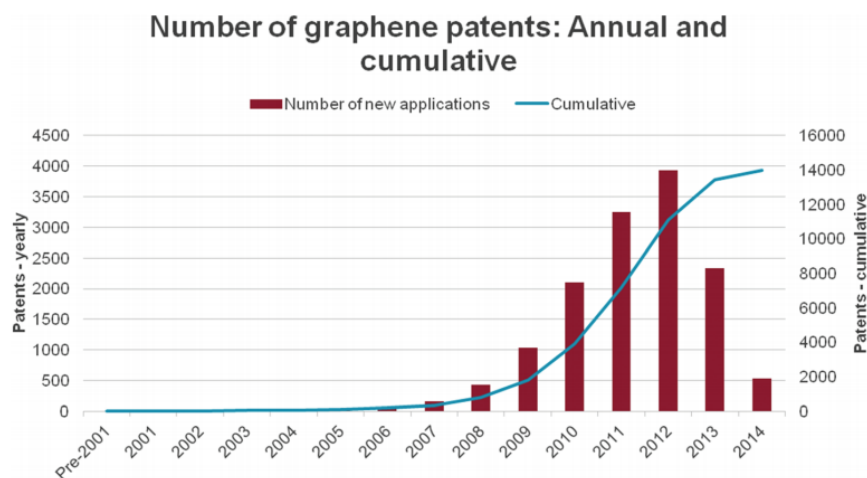
Figure 1.2-19: Patent applications on graphene as a function of application year. Note: Years 2013 and 2014 are under-represented us the patents remain unpublished for the first 18 months from their filing. [Ferrari, 2015].

Graphene materials have the potential to make an impact in the same way that carbon based plastics revolutionized the manufacturing industry in the 20th century. This is supported by the increasing number in publications, indicating the growing interest around the topic. There are various reasons for this increase. Graphene has unique properties, either alone or in combination with other materials. This makes it a topic of interest in many different fields and applications. In addition, all the science and technology around graphene is based in one of the most abundant materials on earth, carbon, making it an inherently sustainable and economical technology. Third, as graphene is a planar material, is compatible with the established production technologies in information and communication technologies and integrable with conventional materials like silicon. These clues give promises for expectations of a more powerful and versatile, sustainable and economically viable technology platform. Graphene is today the number one topic of research in material science. Due to its unique properties, many of its possibilities remain not fully understandable and its analysis requires highly sophisticated methods. As it has been quoted by Frank Wilczek: «graphene is probably the only system where ideas from quantum field theory can lead to patentable innovations»
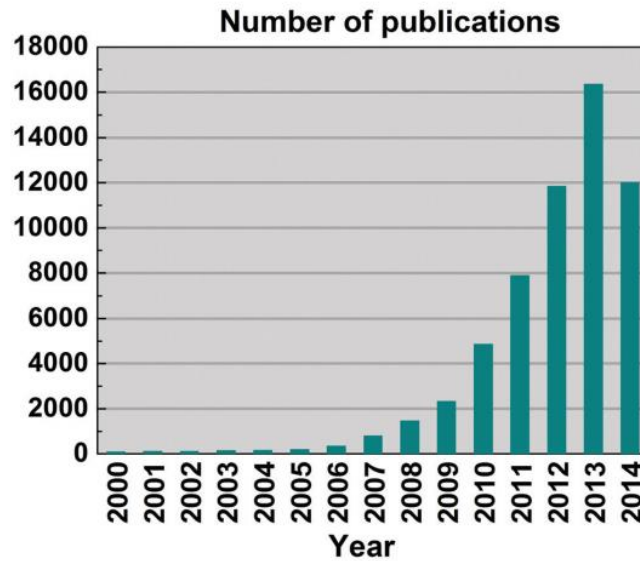
Figure 1.2-20: Publications on graphene from 2000 to Aug. 2014 (thus, well over 18000 are expected by end 2014). Source ISI Web of Science (search: Topic = Graphene). [Ferrari, 2015].

The patent activity around graphene has been rapidly increased since 2007, leaded especialy by major corporations and universities in South Korea and USA firstly, with China following. Giving a look in the top graphene patent owners reveals the broad spectrum of graphene to diverse industry sectors, such as automotive, computing and industrial chemicals. It is important to understand how the patent landscape is growing as this kind of activity gives important datas concerning business models and business practices observed in many of the technology sectors in where graphene research is ,and will be, deployed. In addition, in Figure 21 we see the geographical distribution of the research paper activity. Europe is leading by 34%, a number that does not match with the patent activity taking place in the continent, giving an extra evidence of the need to take action to bring closer leading players in academia (who are, broadly, responsible for scientific production) and industrial leaders (who are, broadly, responsible for patent applications).
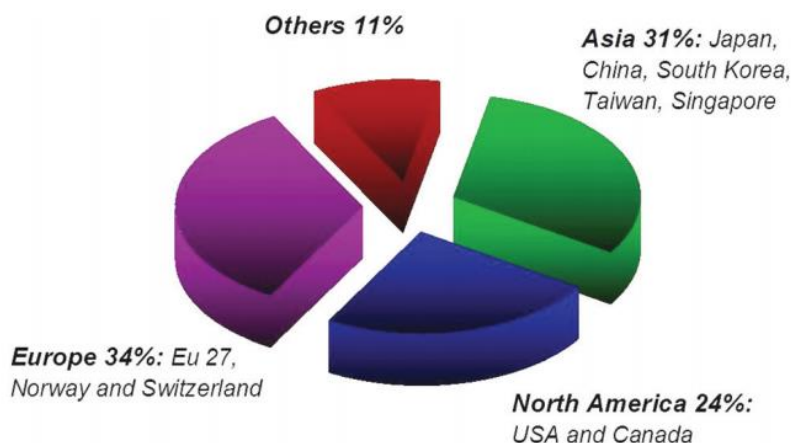
Figure 1.2-21: Geographical distribution of scientific papers on graphene as of December 2013. [Ferrari, 2015].

Reviewing the patent dataset we see a very diverse range of applications including characterization, polymer composites, transparent displays, transistors, capacitors, solar cells, biosensors, conductive inks, windows, saturable absorbers, photodetectors, tennis rackets. Although, the biggest part of these pattenets refer to sythesis techniques and electronics, covering a 30% of the total space each (Figure 1.2-22). This happens because of the fact that the graphene pattenting activity is still in an early stage,with plenty of space for development, especially if we think of all the crossing vertical technologies and cross-disciplinary research taking place. As the patent space evolves, the most probable is that there will be a re-distribution of the pattenting activity towards end-use applications in the next years.
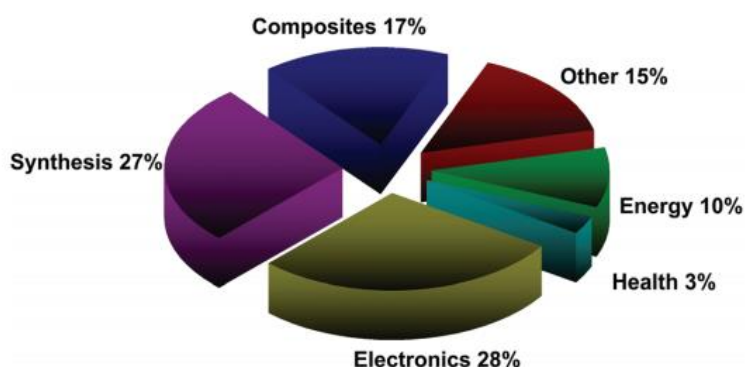
Figure 1.2-22: Proportion of overall graphene patents, by sector as of July 2014. [Ferrari, 2015].

On Figure 1.2-23 we see how the geographical breakdown of graphene patent filings by filing jurisdiction for different time periods. Companies tend to file first in their home jurisdiction and then to the key market or key manufactoring location. In these plots we can notice the increased activity in China within the years and the counter tendency in Europe. The importance of US, China and South Korea is emphasised when we give a look in the top assignees in Figure 1.2-24. The Korean multinational Samsung is dominating the field of patented applications with over three times as many filings as its nearest rival. Its activity is spread in a wide range of graphene applications, including
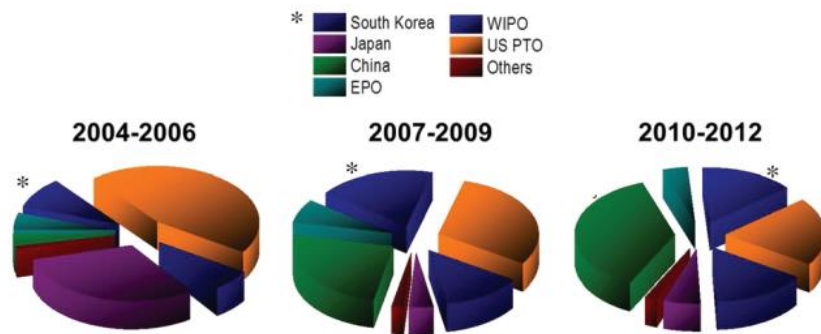
Figure 1.2-23: Graphene patentfiling authorities. EPO, European patents office; WIPO, World Intellectual Property Organization; US PTO United States Patent and Trademark Office. [Ferrari, 2015].

synthesis procedures, transparent display devices, composite materials, transistors, batteries and solar cells while in the same time they maintain collaboration (co-assignment of patents) with a wide range of academic institutions. In the European area, Finland's Nokia is the biggest patent holder primarily around incorporation of graphene into electrical devices, including resonators and electrodes. Noticeable is the high contribution of the universities and research institutions as well, as they occupy about 50% of the total patent filling.
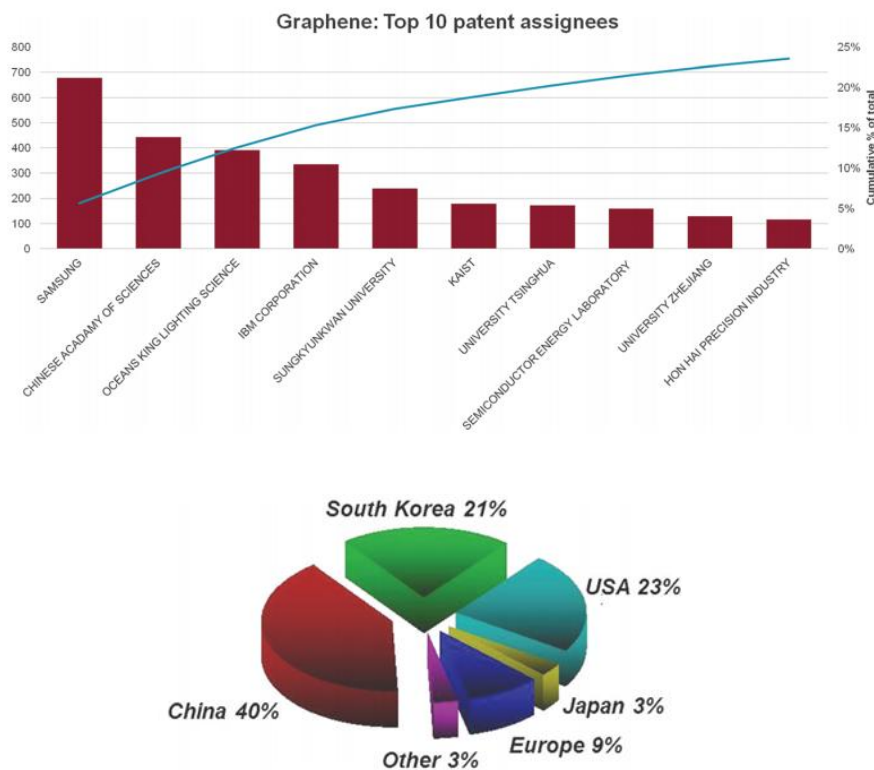
Figure 1.2-24: a) Top 10 graphene patent assignees by number and cumulative over all time as of end-July 2014. Number of patents are indicated in the red histograms referred to the left Y axis, while the cumulative percentage is the blue line, referred to the right Y axis.b) Geographical breakdown of academic patent holders as of July 2014. [Ferrari, 2015].

To close this patent short review we can refer to some features than can function as sidetracked factors considering the patenting process. Because of the high volume of patent activity is possible the 'multiple overlapping granted patents' around aspects of graphene technology systems. Also, is often the phenomenon to claim carbon nanostructures other than graphene in graphene patent landscapes. As the field is still relatively new and the graphene patent nomenclature is not entirely settled, is possible that different patent examiners might grant patents over the same components which the different experts and industry players call by different names [Ferrari, 2015].

In order to promote the graphene research and innovation, the European Commission is coordinating the Graphene Flagship. Its task is to bring together academics and industrial researchers with the aim to bring graphene into the European society in a space of 10 years. The project was first launched in 2013 and today are participating on it 142 academic and industrial research groups in 23 countries, organized in 16 specific work packages. With a budget of €1 billion, is Europe's biggest ever research initiative.

Together with the Human Brain Project flagship, the Graphene flagship form the first two Future and Emerging Technology (FET) Flagships in Europe, with the aim to provide a sustained support for a period of 10 years to promote ambitious large-scale, science-driven, research initiatives that aim to achieve visionary goals that can have a transformational impact on science, technology and society overall [http://graphene-flagship.eu].

1.2-6 Graphene and other 2D crystals

Graphene was the first 2D material ever obtained as it has been extracted from 3D graphite. Today we know that there is a big family of 2D crystals waiting to be studied. Most of them have unique properties and are expected to provide breakthroughs that can extend the limits and boundaries of various applications. Many times 2D crystals present exciting properties, often unique and quite different from their 3D counterparts. Although, it is the combination of these 2D crystals in different 3D stacks that can provide heterostructures with especially designed functionalities. Today is possible the combination of conductive, insulating, probably superconducting and magnetic 2d crystals in one stack with atomic precision which fine-tunes the performance of the resulting material. The functionality of heterostructures like these is not given only by the combination of the properties of the individual 2D crystals. Interactions and transport between the crystals promote improvements in performance and create a truly "quantum leap" in functionality. With a careful choose of the components we can tune the parameters and create superstructures with properties that do not exist in nature. Today there are 3 methods for the synthesis of atomically thin heterostrucures. A) growth by CVD, b) layer by layer stacking via mechanical transfer [Ponomarenko, 2009] and c) layer by layer deposition of chemically exfoliated 2d crystals. An example of a CVD growth of an heterostructure can be seen in Figure 25 where H-BN is grown on top of graphene [Liu Z., 2011].
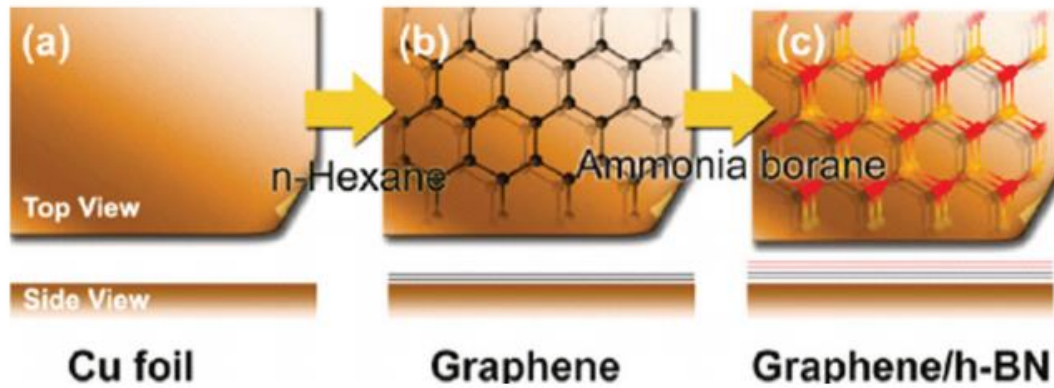
Figure 1.2-25: Schematic of Graphene/BN stacked film. (a) The Cu foil is cleaned and prepared as the growth substrate. (b) High-quality and large-are graphene film is grown viaCVD withn-hexane as a liquid carbon source at 950°C. (c) The as-grown graphene is then loaded into another furnace for the growth of h-BN film on top [Liu Z., 2011].

Next, we present the rest of the members of the family of 2D crystals

Silicene

Silicene is the silicon equivalent of graphene. It has a honeycomb atomic structure with a Si-Si distance of 0.23nm and with a long range epitaxial order confirmed by sharp LEED patterns. It has a conical band dispersions at the corners of the silicene Brillouin zone and a Fermi velocity of $1.3 \times 10\ 6\ ms^{-1}$, as theoretically predicted. It is predicted to have non-trivial topological properties. This structure can have an important impact in new devices thanks to its compatibility with existing Si technologies. A key to realize this, is the transfer or even grow over insulating substrates. Until now silicone has been reported to grow over silver (111) surfaces. (Figure 1.2-26a)

Germanene

Germanene is the equivalent of graphene for Ge. It also has a nontrivial band topology, and a gap induced by effective spin orbit coupling for the π orbitals at the K point. It has been synthesized by molecular beam epitaxy over gold (111) surface. The Ge-Ge distance is 0,25nm [Bampoulis, 2014]. (Figure 1.2-26b)
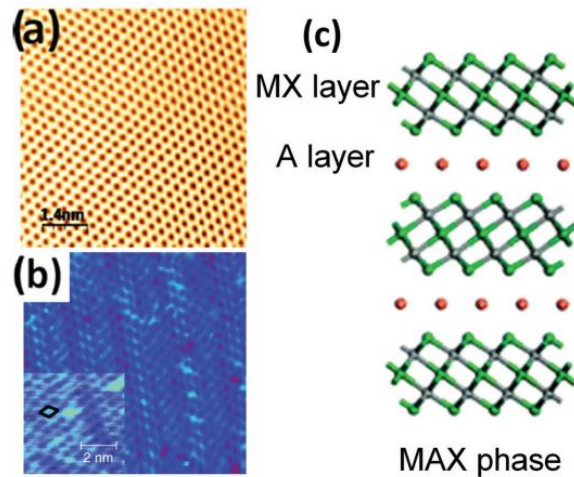
Figure 1.2-26: STM image showing the graphene-like structure of one monolayer of silicon deposited on a close packed silver surface, Ag (111). (b) 16.2 nm × 16.2 nm STM image of the modulated honeycomb of germanene √7×√7 superstructure with a zoom in at the bottom left corner (the √7×√7 unit cell is drawn in black). (c) Side view of MXene, where M (green dot) is an early transition metal, X is either carbon and/or nitrogen (grey dots) and A is an A-group (mostly IIIA and IVA, or groups 13 and 14) element.[Bamboulis, 2014]

Stanene

Stanene is a monolayer of tin atoms. It has an arrange manner similar to this of graphene and when deposited on a substrate it has a gap of 0.3 eV with quantum spin Hall states able to be tuned by chemical functionalization. Theorists have predicted that in room temperature electrons should be able to travel along the edges of the mesh without colliding with other electrons and atoms, permitting the film to conduct electricity without losing energy as waste heat [Xu, 2013].

Phosphorene

Phosphorene is the stable 2D material coming from bulk black phosphorus. Black phosphorus has a layered structure, held together by van der Waals forces. It is superconductive at high pressures with T_c above 10 K and T-dependent resistivity and magnetoresistivity. It has a honeycomb lattice structure but the shape of its structural ridges is non-planar. Its lattice parameters are: a_1 = 3.36 Å, a_2= 4.53 Å, and a_3= 11.17 Å. a_3 has a very large value as a result of the nonplanar layer structure and the presence of two AB stacked layers in the bulk unit cell. In contrast to graphene, it has a nonzero fundamental band gap.

MXenes

MXenes is a family of 2D crystals including transition metal carbides and nitrides where the Al has been removed from layered ternary carbides known as MAX phases. This process is separating the carbide layers into two MXene sheets where various ions and molecules can be placed in between by intercalation. A variety of cations, including Na^+, K^+, NH_4^+, Mg_2^+, and Al_3^+, can also be intercalated electrochemically, offering capacitance in excess of 300 F cm^{-3}, making these structures suitable in applications as electrochemical capacitors, batteries, hydrogen storage.

It is important to mention here the widening in the properties that the chemical modification offers when applied to 2D crystals. Methods for the chemical modification of the two sides of the crystals are desirable. Thanks to it we can have a control over the distance between neighbouring planes in the 2D heterostructures.

Finally, we present a timeline as presented in the Graphene Science and Technology Roadmap (GRM),2015, showing how is expected to proceed the various growth process in the next 10 years and the expected output in the materials library. Timescales: 2–3 years: Formulation of GRM inks. CVD growth high μ (6×10^4 cm^2 V^{-1} s^{-1}) graphene films. Homogeneous (mm^2) graphene films on SiC. 3–5 years: Production of heterostructures with on-demand (opto)electronic properties via LPE and CVD.5–7 years: Production of 2d crystal by MBE and ALD. Formulation of high concentration inks (10 g L^{-1}) with tuneable morphological (>80% 1-L) and controlled rheological properties (v=1–1000 mPas).7–10 years: Production of large area (mm size) 2d crystals via LPE. Large area single crystals. Surface roughness <0.2 nm. Engineered band gap NRs and QDs [http://graphene-flagship.eu]
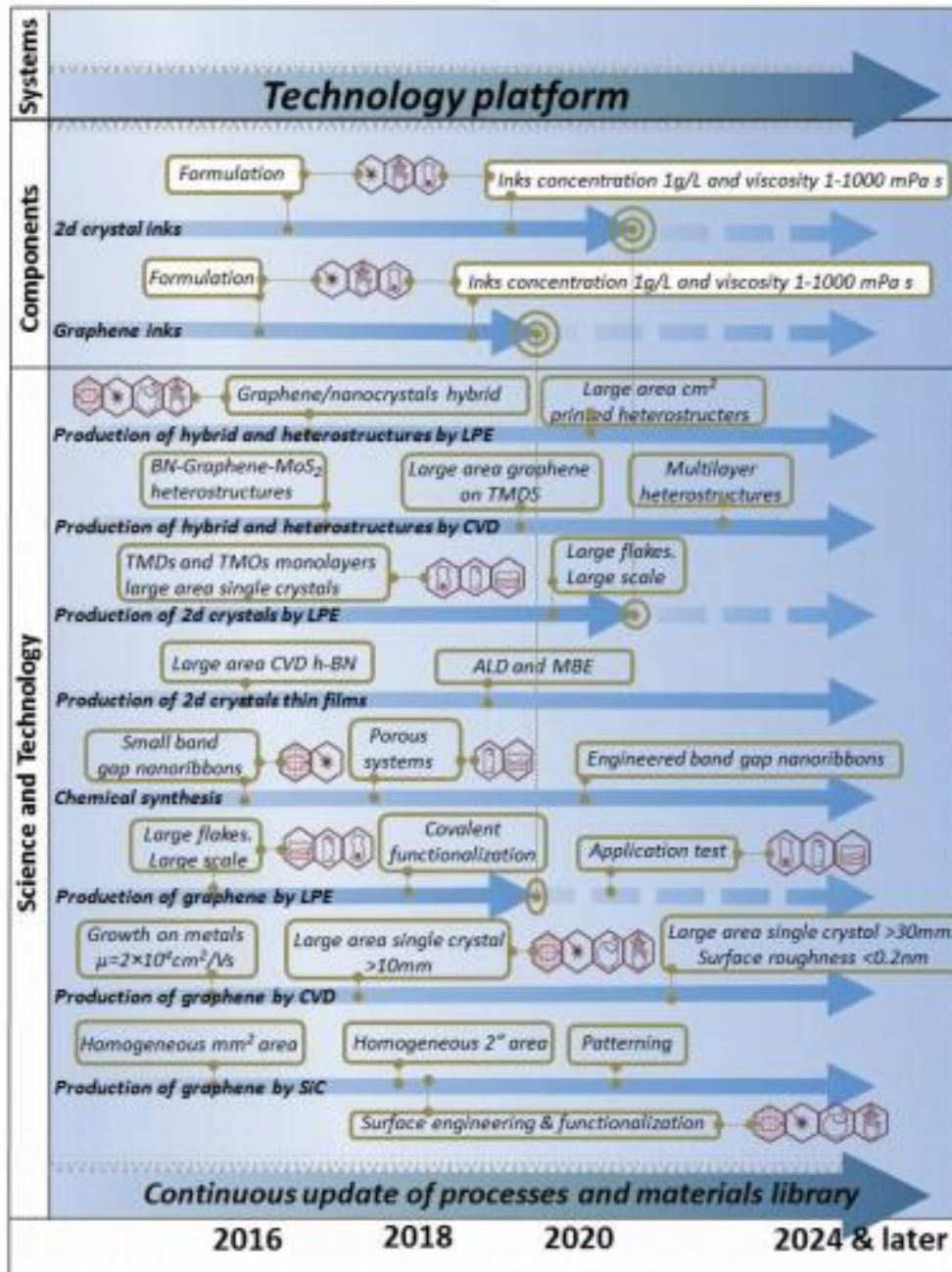
Figure 1.2-27: GRM production timeline. [Ferrari, 2015].

1.3 Graphene Transfer

Chemical Vapor Deposition is till today the method that mostly facilitates the growth of large area graphene films. The excellent tuning in the growth conditions has made possible the growth of graphene films of 30 inches diameter, growing the expectations for industrial scale synthesis that will boost the develop of applications. [Bae, 2010] Although, for most of the applications the film must be transferred after the synthesis from the metal catalyst to different substrates. The transfer process should therefore secure that the film will remain undamaged, maintaining its unique properties. [graphene-supermarket] Although this step is as challenging and demanding as the growth process, it does not usually attracts the same attention. [Kang, 2012] The degradation in the quality of the film occurs during the transfer process due to tearing and ripping of the film. [Li, 2009; Liang, 2011]

1.3-1 Transfer Techniques

1.3-1.1 Mechanical exfoliation

Graphene was firstly isolated and obtained by exfoliating thin films of graphite from a highly oriented pyrolytic graphite [HOPG] piece. The technique of exfoliation can be technically considered as a transfer technique itself. The exfoliation is carried out with a usual scotch tape. In order to reach to isolate few layers and even single layer graphene films the process of peeling has to be repeated many times.

Another version of this method includes the attachment of the HOPG at the tip of an AFM silicon cantilever and its operation in contact mode. By dragging it across the Si wafer, graphene flakes are yielded [Zhang, 2005].

The obtained graphene by the above methods is of high quality and the crystal structure is well ordered. [Novoselov, 2005; Meyer, 2007] The flakes obtained usually can not overcome in lateral size a few μm. Their thickness also varies from some to hundreds of nanometers. In Figure 1.3-1 we see a collection of optical images of graphene obtained by mechanical exfoliation of HOPG. After every exfoliation the result is a mix of flakes of different thickness, from single to few layer graphene. It is extremely rare (if not impossible) to obtain homogeneous number of layers after an exfoliation. The size of the flakes in these images reaches up to hundreds of micrometers. These images were selected as representatives of various in the doctoral thesis of V.M Freire [Freire, 2014].
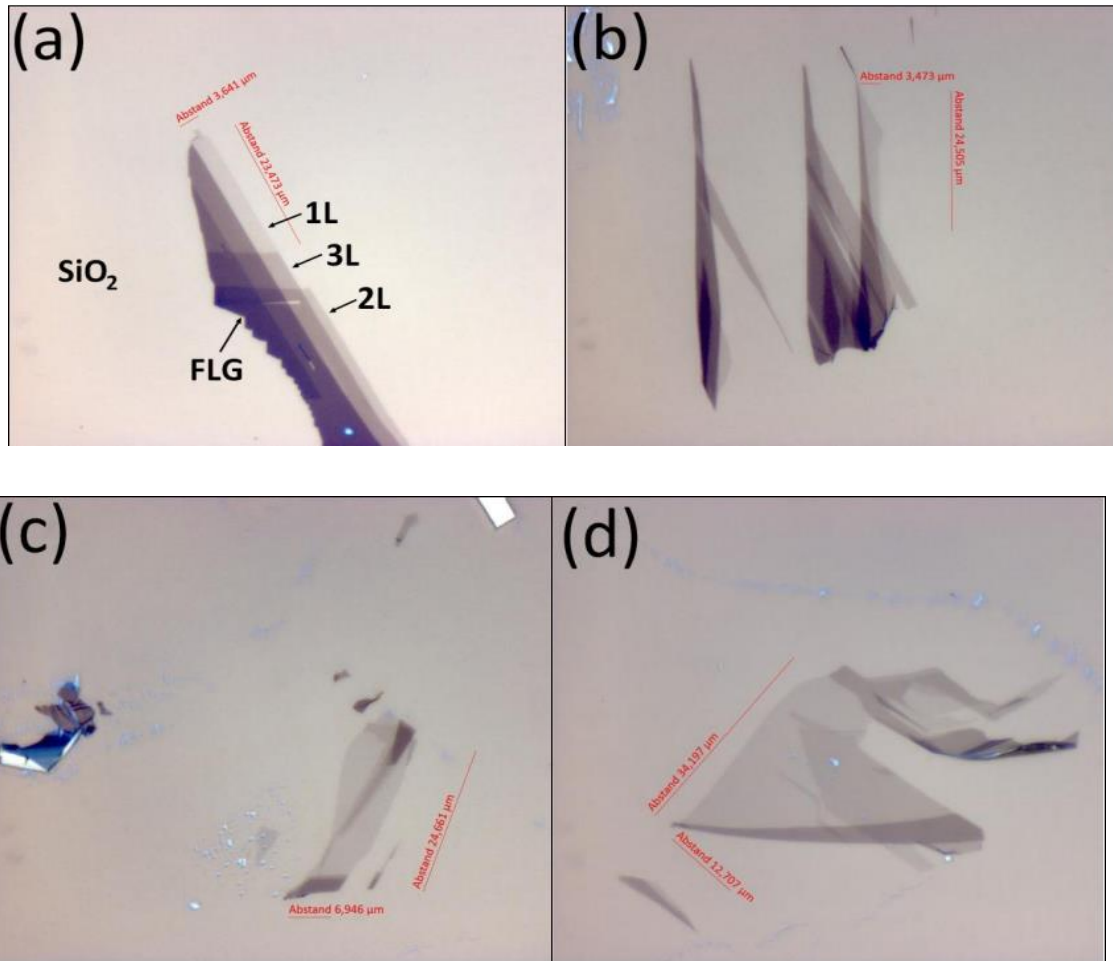
Figure 1.3-1: Optical Images of graphene flakes obtained by mechanical exfoliation from HOPG. The lateral size of the flakes reaches up to hundreds of micrometers. After each exfoliation the obtain graphene is a mixture of flakes of different thickness which is difficult to be controlled. [Freire PhD Thesis, 2014]

1.3-1.2 Lift-off from SiC with metal support

The epitaxial growth of graphene on SiC permits the growth of large graphene domains. To perform the transfer to another target substrate, in the work of *S. Unarunotai et al* [*Unarunotai, 2009*] they deposit a bilayer film of gold and polyimide. The polyimide functions as a mechanical support for the Au/graphene stacking. Performing Raman spectrometry in the transferred graphene film revealed a D defect peak. To reduce the degrading effect of the holes and tears that appear in the film they stack several graphene

layers together.

1.3-1.3 Lift-off with thermal release tape

In the work of *Caldwell et al* [Caldwell, 2010] is performed a lift off with the use of a thermal release tape. In this technique, the tape is adhered on the top of the graphene layer. Peeling the tape off, the graphene remains attached to it. Then, in order to transfer to the preferable substrate, the tape/graphene stacking should be pressed to it and then heated to about 100°C. At this temperature the tape loses its adhesion and graphene is ablated and deposited on substrate. Probably due to the mechanical stresses applied during the peeling, many holes of about 10 μm appear. The effect of these holes in the quality of the film is decisive as the carrier mobility drops from 1485 $cm^2V^{-1}s^{-1}$ to 201 $cm^2V^{-1}s^{-1}$ after the transfer. Moreover, as the catalyst is sputtered on top of the Si wafer, during the peeling it remains attached on the tape/graphene stacking. Then, an etching step is required to dissolve the metal. As the most common metal catalyst regarding the graphene chemical deposition synthesis are copper and nickel, the most usual etchants being used are iron nitrate, iron chloride, and ammonium persulfate [Kim, 2009]. Here it appears the problem of introducing chemical doping effects [Hong, 2012]. In the work of Hong et al the generation of a damaged O=C–OH carbon bond during the etching step is explored by means of XPS analysis. The comparison of the carrier mobility of the graphene sheet before and after removing that bond indicates that the boundary is responsible for 30% of degradation.

Searching ways to skip this etching step, *Lock et al* [Lock, 2012] used an acide-based linker molecule, deposited on a polystyrene substrate. When attached and applied with heat and pressure, it forms strong covalent carbine bonds, favoring the clean removal of the graphene sheet from the catalyst. [Lock, 2012] Under the same motivation, Yoon et al. used a thin layer of epoxy to peel off the graphene sheet [Yoon, 2012].

In both above methods we have a substance acting as a glue to attach to the graphene sheet. Although, it still exists the issue of the efficient removing of these substances after.

1.3-1.4 Transfer with the support of polymers

The transfer of the graphene with the support of different kind of polymers usually consists of 3 steps. 1) The polymer is deposited on top of the graphene sheet. 2) The metal catalyst used for graphene synthesis by CVD is etched away. 3) The polymer/graphene stack is deposited in the favorable substrate. The polymer is removed.

There have been works demonstrating the direct etching of the metal catalyst without a polymer support. In the work of *Kim et al* the graphene grown by CVD on top of Ni/SiO$_2$, is transferred by a wet technique and the nickel is etched away in a BOE/ FeCl$_3$ solution. In this case although the transferred film appears seriously damaged as it is extremely sensitive to ripping and tearing [Kim, 2009]. Figure 1.3-2, extracted from [Kim, 2009], shows a scheme describing the growth and transfer process. The transfer is performed both with and without the support of a PDMS (polydimethylsiloxane) film to compare how effective it is as a support layer.
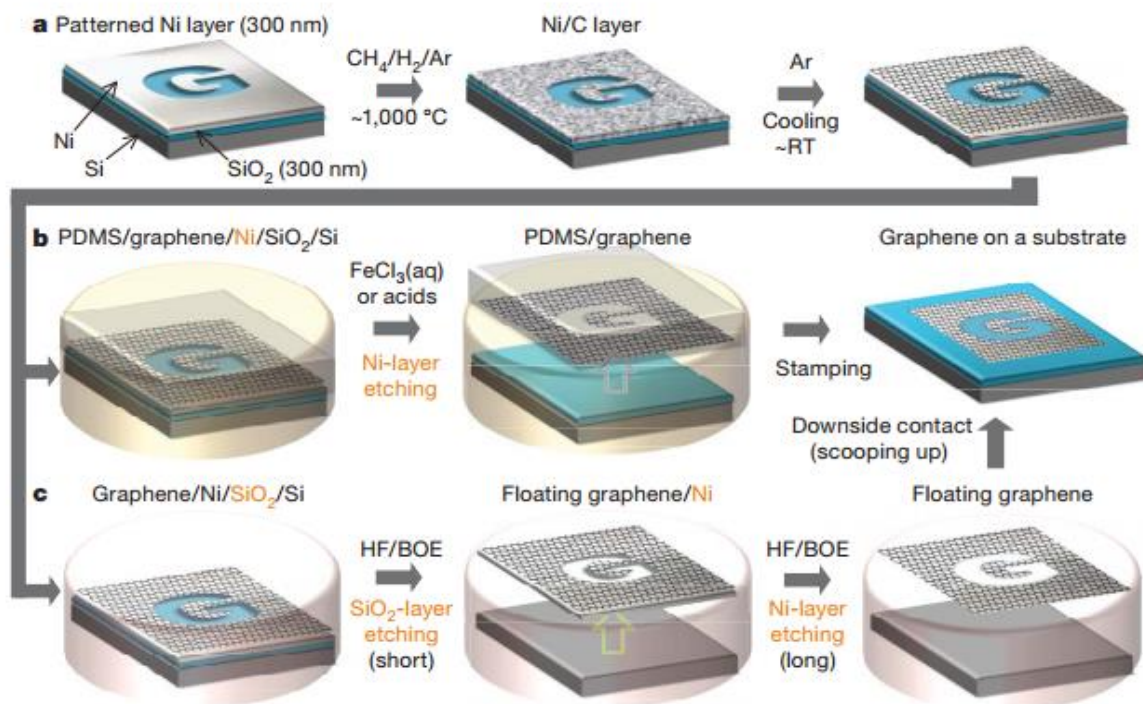
Figure 1.3-2: Synthesis, etching and transfer processes for the large scale and patterned graphene films. [Hong, 2012]

In the growth step on patterned structure, graphene is obtained on top of a 300nm/300 nm Ni/SiO$_2$ layer structure at 1000°C in a CH$_4$/H$_2$/Ar gas mixture. The cooling down is taking place in an Ar atmosphere. After the etching of the SiO$_2$/Ni, the graphene layer or the graphene/PDMS stays floating inside the aqueous etchant solution. The favorable substrate (SiO$_2$/Si) for transferring the graphene layer is used to scoop it up (Figure 2b, last image on the right). On Figure 3, extracted from the work of Hong et al., we can see: a SEM image of the as grown graphene on top of the nickel film sputtered on SiO$_2$ (Figure 1.3-3a) (in the inset, image of graphene grown on nickel foil), a TEM image of graphene films of different number of layers (Figure 1.3-3b), an optical image of the transferred

graphene film on top of a 300 nm SiO_2 layer (Figure 1.3-3c) (on the inset of Figure 3c, an AFM image where rippled structures are visible), a confocal scanning Raman image (Figure 1.3-3d) corresponding to image of Figure 1.3-3c and finally, the acquired Raman spectra (Figure 1.3-3e) corresponding to the colored spots of image of Figure 1.3-3c.

PDMS is one of the most suitable polymers used for the graphene transfer as it is not reactive, it resists in various solvents and it is as well preferable for soft lithography [Lee, 2003]. Thanks to its low surface free energy, PDMS is ideal for the graphene transfer. After the etching of the metal catalyst the graphene/PDMS is brought into the substrate of our choice, usually SiO_2 or PET. The graphene then is released from the PDMS to the substrate with the higher surface free energy. Moreover, it is very useful for device fabrication. Grown patterned graphene on a pre patterned metal catalyst is really difficult to be transferred avoiding to be damaged. Instead of this, it is easier to mold the PDMS with the desired pattern and stamp it in the graphene film. After the transfer, the desired graphene pattern will remain. Figure 1.3-4 shows an example of this technique used to fabricate an organic field effect transistor [Kang, 2011].
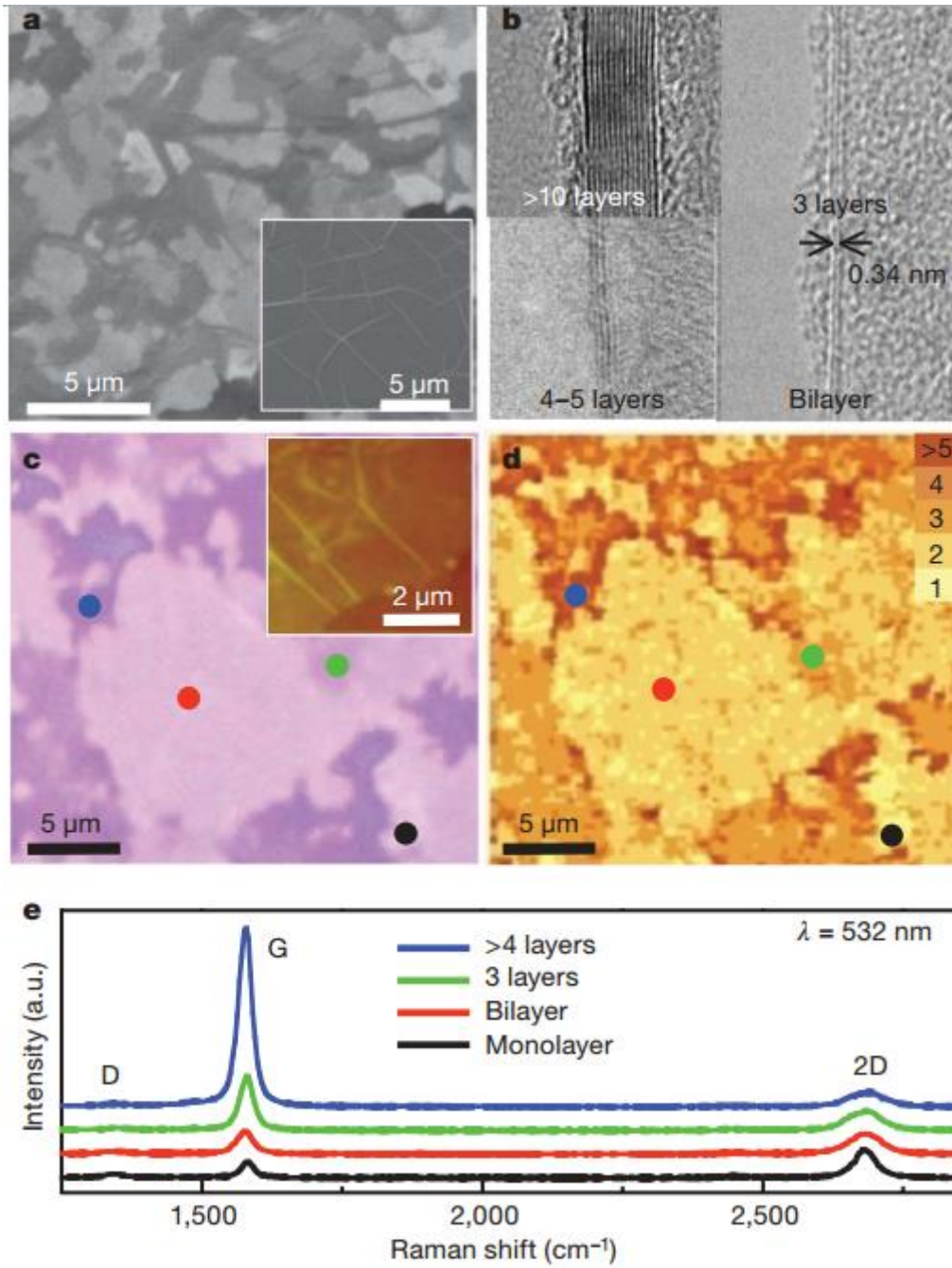
Figure 1.3-3: Various images of CVD grown graphene film as presented in the work of Kim et al, [Kim, 2009]. a) and b) are SEM images of graphene film; c) is an optical image and d) is a Raman mapping image; e) finally, these are the Raman spectra of different thickness of graphene films.
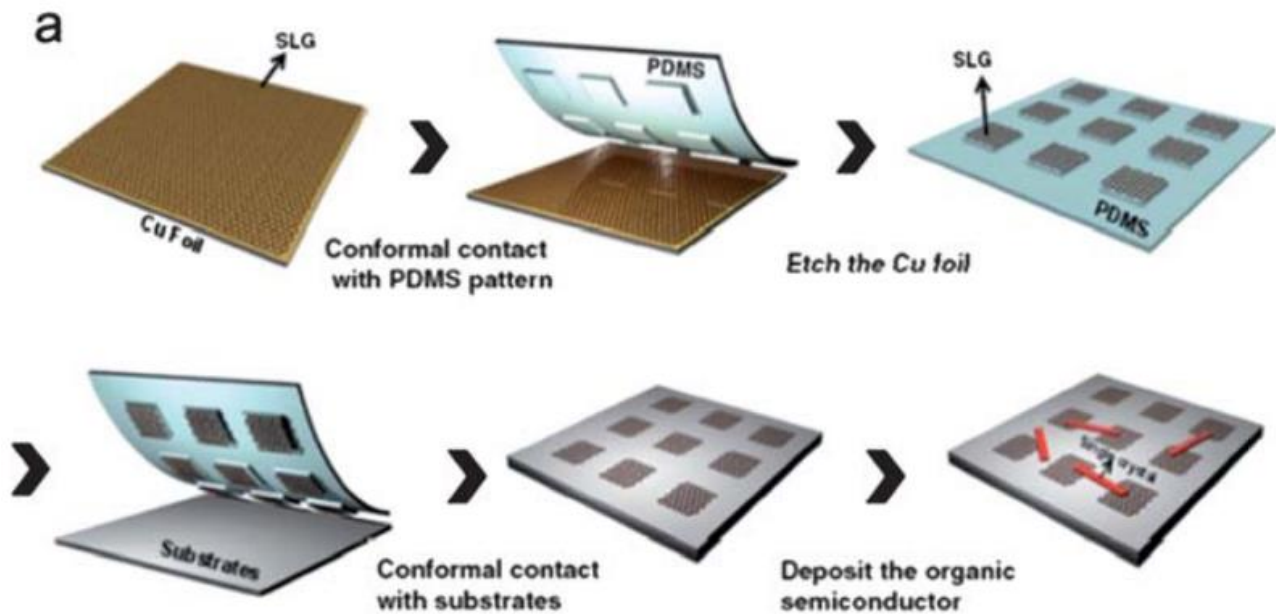
Figure 1.3-4: Schematic illustration of the patterning and transferring of CVD grown graphene using a patterned elastomeric stamp. An OFET was fabricated using rubrene as single crystal semiconductor. [Kang, 2011]

Another very usual polymer in graphene transfer (and the one we used in all the transfer processes we followed) is PMMA (polymethyl methacrylate). In contrast to PDMS, PMMA forms strong covalent bonds with graphene. In principle, the PMMA transfer method is pretty similar to that using PDMS. The PMMA is spin coated in top of the graphene, the metal catalyst is etched away and the graphene/ PMMA stacking is scooped up to the desired substrate. PMMA can be easily removed then by acetone. Although, most of the times cracks are introduced during the transfer. The explanation for this was given by the work of *Li et al*. [Li, 2009] The PMMA coating keeps the graphene sheet rigid. The ripples usually formed during the growth remain there, preventing the good contact between the sheet and the transfer substrate. The graphene in this case tears off during the PMMA wash. [Li, 2009] To solve this, the authors propose the deposition of a second PMMA film which redissolves the first coat. Thus, the graphene sheet relaxes as well and rests more gently in the substrate.

Another issue introduced by the PMMA use is this of the residues usually left after its wash. These residues usually result in a p-type doping effect on the graphene film, degrading its electrical performance. To effectively remove all these residues, is usual a thermal annealing treatment under argon-hydrogen atmosphere at temperatures around

300-400°C. The AFM image of Figure 1.3-5 shows the smoothing effect on surface roughness characteristic of graphene. After 3 hours at 300 °C under UHV, graphene appears much smoother and the main parts of residues have disappeared. The electrical results reaffirmed that the p-type doping was significantly reduced [Pirkle, 2011].

To strengthen the electrical behavior of devices is usual the multiple stacking of some graphene sheets (3-4). Using this technique, the PMMA coating, graphene transfer, and PMMA removing (wash) should be done for each layer [Kasry, 2010].
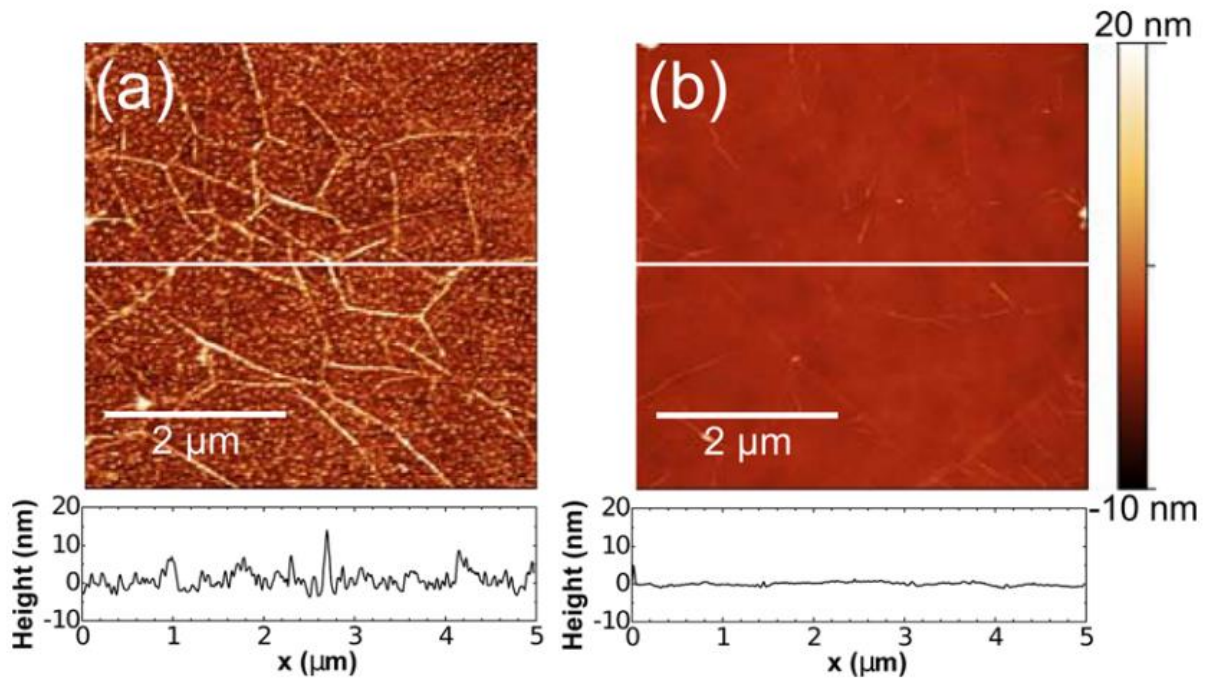
Figure 1.3-5: AFM image of graphene sheet before (a) and after (b) the thermal annealing in 300 °C. The PMMA residues have been removed and the sheet is much smoother. Extracted from [Pirkle, 2011].

1.3-1.5 Transfer by Thermal Release Tape (TRT)

TRT is an usual alternative method to the ones including polymers. Its main advantage is that allows the large scale transfer of graphene. The tape is applied by pressure, manually or by other means to achieve a better adhesion, on top of the grown graphene layer. The greatest adhesion force between graphene and tape causes it to separate of the substrate and remains on the tape and stays on tape. Placing the tape on the desired substrate and applying heat to about 100°C, the tape releases, letting the graphene relax on the substrate [Caldwell, 2010].

TRT is ideal for roll to roll transfer of graphene. The multi mentioned 30 inch diagonal size graphene grown by *Bae et al* [Bae, 2010] was transferred by this method. The whole process is described in Figure 1.3-6. First, the graphene is grown on rounded copper foil. After attaching the polymer support or TRT, the stacking is left on etchant to remove the metal catalyst (Figure 1.3-6a). Then the TRT/graphene is transferred on a flexible PET. In the last step, the stacking is passed through rollers heated in the desired temperature so that the TRT becomes released. This work permitted the fabrication of the first graphene made touch panel (Figure 1.3-6c).

To overcome the shear stress introduced by the rollers, the team of *Kang et al* used a thermal press technique to place the TRT on top of the graphene. This eliminates the ripping on the obtained sheet, decreasing a lot the resistance of it [Kang, 2012].
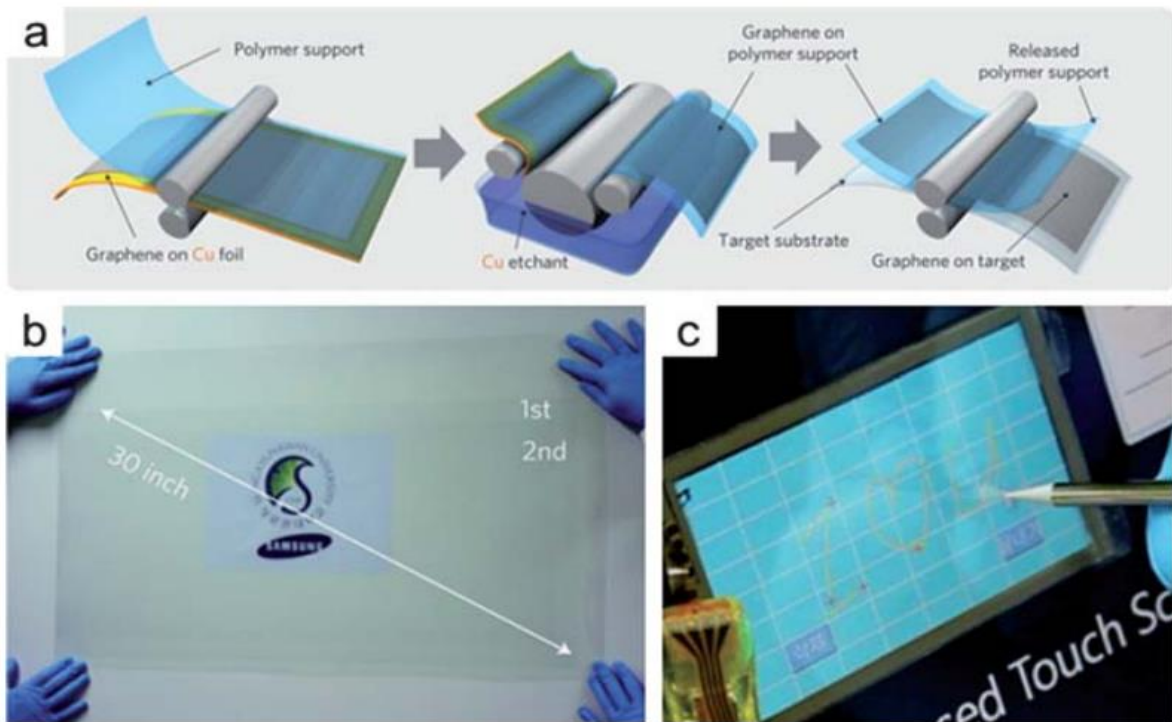
Figure 1.3-6: a) Step by step of the roll to roll graphene transfer. The grown graphene on copper foil is passing by two rollers so that the TRT is being placed on it. Then, it is deeped into etchant to remove the catalyst. After its transfer on flexible PET, it passes through two heated rollers to release the tape. b) Image of the graphene film obtained. c)First graphene based touch panel had been fabricated under the same framework. Extracted from [Bae, 2010].

1.3-1.6Transfer free synthesis

Despite the efforts and the originality that the scientists show in continuously improving the transfer methods, it seems that all of them finally introduce some kind of factor that degrades the quality of the film.

Oriented by this idea, it has been also performed the effort to grow the graphene on ways that can skip the transfer step. The only disadvantage here is that this synthesis can only be performed in specific substrates, setting a limit in the large area synthesis that is more favorable in foil use methods. The two basic methods are based on the idea that the thin metal catalyst can be removed after the graphene growth, allowing the film to stay on top of the base substrate.

In the work of *Ismach et al.* [Ismach, 2010] graphene is grown on top of a thin copper film

previously deposited on top of a quartz substrate. Annealing the graphene/copper/quartz structure at high temperatures up to 7 hours leads to evaporation and dewetting of the copper film. Then, graphene remains on top of the quartz substrate. Although, Raman spectroscopy revealed that with the pass of the time the quality of the film was degrading (D peak became larger with the time). The problem is that the copper did not get completely removed before this degrading started. [Ismach, 2010]

In a different approach, *Shin et al.* [Shin, 2011] introduced carbon source materials (like PMMA, polystyrene) between Si/SiO$_2$ and the metal catalyst. The stacking was introduced into a high temperature pyrolysis reaction. The carbon precursor materials show a self-assembling behavior during this reaction, forming a high quality graphene film. Later, the metal catalyst was simply etched away. The etching process remains but the graphene is not affected that much by it as it is already below the catalyst. [Shin, 2011]

Another interesting observation regarding the graphene growth was made by *Su et al.* [Su, 2011] permitting as well the skipping of the etching step. It was observed that the carbon atoms can travel through the copper grain boundaries during the CVD synthesis. In the case of copper deposited on Si/SiO$_2$, the diffused carbon atoms formed a graphene layer below the copper film, on top of the SiO$_2$. Then the copper layer has to be etched away. [Su, 2011]

1.3-1.7 Electrochemical delamination transfer

In another effort to skip the etching step, scientists performed an electrochemical delamination to de-attach the graphene from the metal catalyst. In this way there are two main benefits. 1) The graphene does not come in contact with the etchant, usually responsible for doping the graphene and 2) the metal catalyst is re-usable for further growths.

In a typical delamination process like this described in the work of *Wang et al.* [Wang, 2011] PMMA is spin coated on top of the CVD grown graphene previously grown on top of copper foil. The role of the PMMA here is to protect/support the layer of graphene during the delamination. Then, the stacking is introduced in an aqueous solution of potassium persulfate (K$_2$S$_2$O$_8$) and the electrochemical process can be performed. In other works, they use NaCl [Cherian, 2015] or NaOH [Zhan, 2015] instead, although the state of the art remains the same. The copper/graphene/PMMA is the cathode and glassy carbon is used as the anode. As the graphene/copper electrode is cathodically polarized, hydrogen bubbles are emerging in the copper-graphene interface due to the water

reduction. These bubbles are applying a small but continuous force to the graphene until the moment it detaches from the catalyst foil. The role of PMMA here is crucial. The bubbles apply forces that tend to scroll the graphene sheet instantly once it is released. The PMMA coat acts as a support for the graphene sheet preventing it from shearing and scrolling.

1.4 Raman Sprectroscopy in Graphene

Raman spectroscopy was one of the main characterisation tools used during the execution of this thesis. Therefore, is considered important by the author to provide a brief analysis of the principles behind the graphene spectrum. All the Raman spectrum were obtained with a Jobin-Yvon LabRam HR 800 system, provided by the Centres Científics i Tecnològics of the University of Barcelona. The lens has a 800mm focal length. It has been used a green laser at 532 nm and a x100 objective lens. Generally the incident power used was 3.3 mW at most, and the size of the spot is 2 µm; the diffraction grating used was 600-1800 lines/mm. The results are presented in the relative chapter in the Results section.

Raman spectroscopy is an undivided tool of the graphene research. It borrows its name by Sir C. V. Raman, who was the first to experimentally observe the inelastic scattering of monochromatic light [Raman, 1928]. The Raman effect takes place when electromagnetic radiation strikes on a molecule and interacts with the polarized electron density and the bonds of the molecule. During the spontaneous Raman effect, the photon excites the molecule in either the ground rovibronic state or in an excited rovibronic state. Therefore, the molecule remains in a virtual energy state for a short period of time before an inelastically scattered photon results. The resulting inelastically scattered photon can be of either lower (Stokes) or higher (anti-Stokes) energy than the incoming photon. The difference in energy between the original rovibronic state and this resulting rovibronic state leads to a shift in the emitted photon's frequency away from the excitation wavelength, the so-called Rayleigh line. In the case of a Stokes shift, the final vibrational state of the molecule is more energetic than the initial state, therefore the inelastically scattered photon will be shifted to a lower frequency for the total energy of the system to remain balanced. For the anti-Stokes shift it occurs the opposite, the final vibrational state is less energetic than the initial state, then the inelastically scattered photon will be shifted to a higher frequency [Gardiner, 1989].

Thanks to Raman technique, we can determine the number and orientation of layers, the quality and types of edge, and the effects of perturbations, such as electric and magnetic fields, strain doping, disorder and functional groups. It presents technical characteristics that make it an ideal tool. It is fast and non-destructive, offers high resolution, gives structural and electronic information, and is applicable at both laboratory and mass-production scales. Today, Raman spectroscopy is one of the most popular characterization techniques for the whole sp^2 -bonded carbon allotropes family, including disordered and amorphous carbons, fullerenes, nanotubes, diamonds, carbon chains and polyconjugated molecules [Ferrari, 2004]. The Raman spectrum of graphite has been recorded since the 1970's [Tuinstra, 1970]. Especially in the case of graphene Raman can be used to provide information about both atomic structure and electronic properties. The absence of a bandgap makes all wavelengths of incident radiation resonant [Ferrari, 2007].

To provide an interpretation of the Raman spectrum of graphene we have to understand its phonon dispersion. It contains 3 acoustic (A) and 3 optical (O) branches. The modes with out-of-plane (Z) motion are considerably softer than the in-plane longitudinal (L) and transverse (T) ones. Graphene has two atoms per unit cell, thus six normal modes (two being doubly degenerate) at the Brillouin zone centre Γ: $A_{2u} + B_{2g} + E_{1u} + E_{2g}$. There is one degenerate in-plane optical mode, E_{2g}, which is Raman active and one out-of-plane optical mode, B_{2g}, which is not [Nemanich, 1977].

The distinct bands of single layer graphene can be seen in Figure 1.4-1a [Ferrari, 2006].
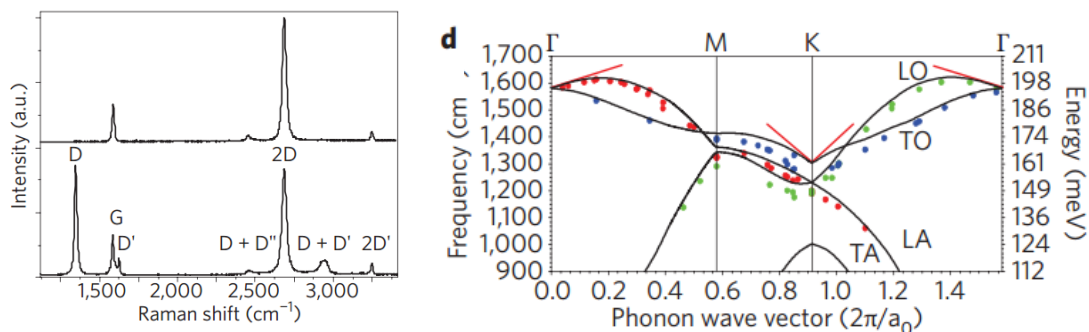
Figure 1.4-1: Raman spectra of pristine (top) and defected (bottom) graphene. The main peaks are labelled. b) The black curves represent the dispersion of in-plane phonon modes in graphene in the energy and frequency range relevant for Raman scattering. The red lines represent Kohn anomalies. [Ferrari, 2013]

In Figure 1.4-1b is plotted the optical phonon dispersions of SLG, relevant for the interpretation of the Raman spectra. The G peak corresponds to the high-frequency E2g

phonon at Γ. The D peak corresponds to the breathing modes of six-atom rings and requires a defect for its activation. It originates from the transverse optical phonons around the Brillouin zone corner K and is active by double resonance [Thomsen, 2000]. D' peak is a result of the double resonance between 2 connected points belonging to the same cone around K (or K´). 2D and 2D' are the overtone of D and D'. As they originate from a process where momentum conservation is satisfied by two phonons with opposite wave vectors, no defects are required for their activation, and are thus always present [Basko, 2009]. The D+D'' peak, at 2450 cm^{-1}, is assigned a combination of a D phonon and a phonon belonging to the LA branch, seen at ~1,100 cm^{-1} in defected samples when measured with visible light.

Except the above peaks that are present both in single layer graphene as in graphite, there are also peaks that have their origin to relative motions of the planes themselves, either perpendicular or parallel to their normal, like the shear (C) modes [Tan, 2012] and the layer-breathing modes (LBMs) [Lui, 2012]. Peak C is a result of the low frequency E_{2g}
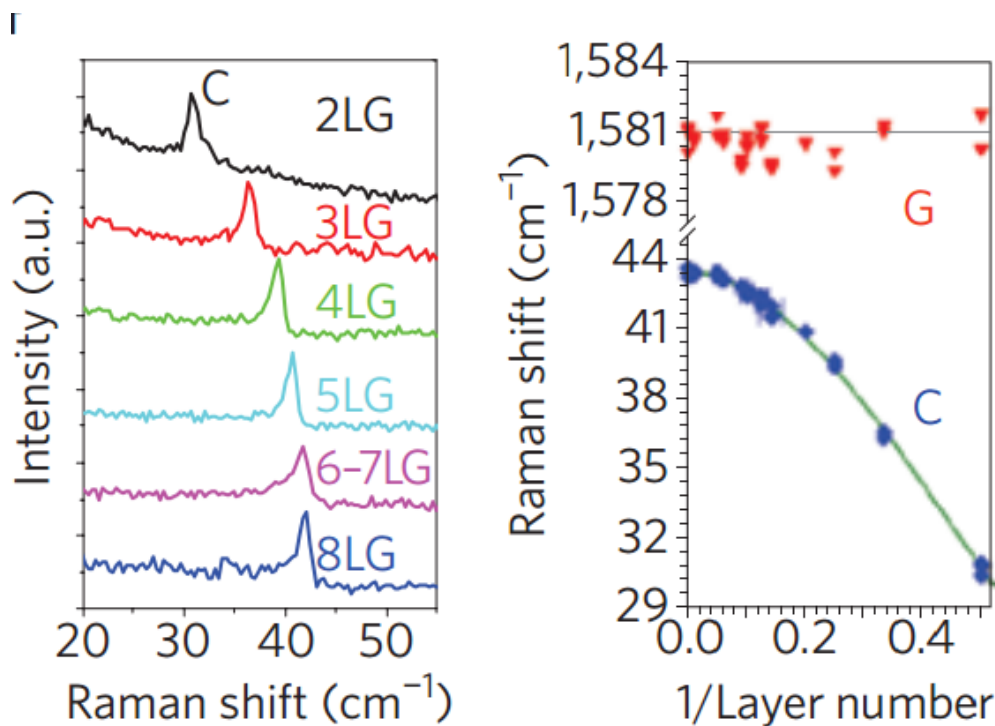
Figure 1.4-2: C peak as a function of number of layers (left). Fitted C- and G-peak position as a function of inverse number of layers (right). The line passing through the C-peak data is from equation (1). Flakes with N layers are indicated by NLG. Thus, for example, 2LG is BLG (bilayer graphene), and 8LG is 8-layer graphene [Tan, 2012].

mode in graphite. It is very sensitive to interlayer coupling, therefore its absence can be an evidence of the single layer character of the graphene. In Figure 1.4-2 we see the

shifting of the C peak as a dependence of the number of layers. Starting from 42cm⁻¹ in the case of graphite, It scales until 31cm⁻¹ for bilayer graphene.

For Bernal stacked graphene, the position of the C peak varies with the number of layers N according to the equation

$$Pos\ [C] = \sqrt{\frac{2\alpha}{\mu}} \sqrt{1 + cos\frac{\pi}{N}} \qquad [1]$$

where α = 12.8 × 10¹⁸ N m⁻³ is the interlayer coupling, and μ = 7.6 × 10⁻²⁷ kg Å⁻² is the graphene mass per unit área. The layer breathing modes can be observed in the range 80-300 cm⁻¹. Considering the 2D peak, despite the factthat it is an in-plane mode, it is sensitive to N because the resonant Raman mechanism that gives rise to it is closely linked to the details of the electronic band structure, , the latter changing with N, and the layers relative orientation [Ferrari, 2006].

The change in the shape and intensity of the 2D and G peak according to the number of layers can be found in Figure 1.4-3.
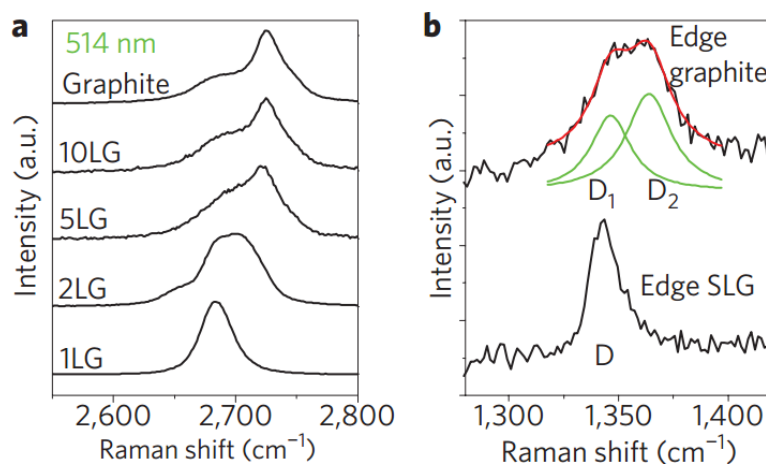
Figure 1.4-3: a, 2D peak as a function of N for 514 nm excitation. b, D peak at the edge of graphite and SLG [Ferrari, 2006].

In graphite the 2D peak consists of twocomponents, $2D_1$ and $2D_2$ with intensities roughly at ¼ and ½ of I(G). In Figure 4a we see the 2D peak in the case of bilayer graphene. It has four components, $2D_{1B}$, $2D_{1A}$, $2D_{2A}$, $2D_{2B}$, two of which, $2D_{1A}$ and $2D_{2A}$, have higher intensities. When we have more tan 5 layers is difficult to distinguish the spectrum from this of graphite.

The evolution in 2D peak is explained with the evolution of the electronic bands according to the number of layers. In the case of bilayer graphene the interaction of the graphene planes causes the π and π* bands to divide in four, with a different splitting for e and h. The incident light couples only two pairs of the four bands. On the other hand, the two almost degenerate transverse optical phonons can couple all bands. The resulting four processes involve phonons with momenta q_{1B}, q_{1A}, q_{2A}, q_{2B} (Fig. 1.4-4b). q_{1A}, q_{2A} link bands of the same type and are associated with processes more intense than q_{1B}, q_{2B}, because the portion of the phase space where triple resonance is satisfied is larger. These correspond to different frequencies, due to the phonon dispersión around K. This gives four peaks in BLG. Their excitation-energy dependence is determined by both electron and phonon dispersions. Measuring it probes the interlayer coupling for both [Mafra, 2007].
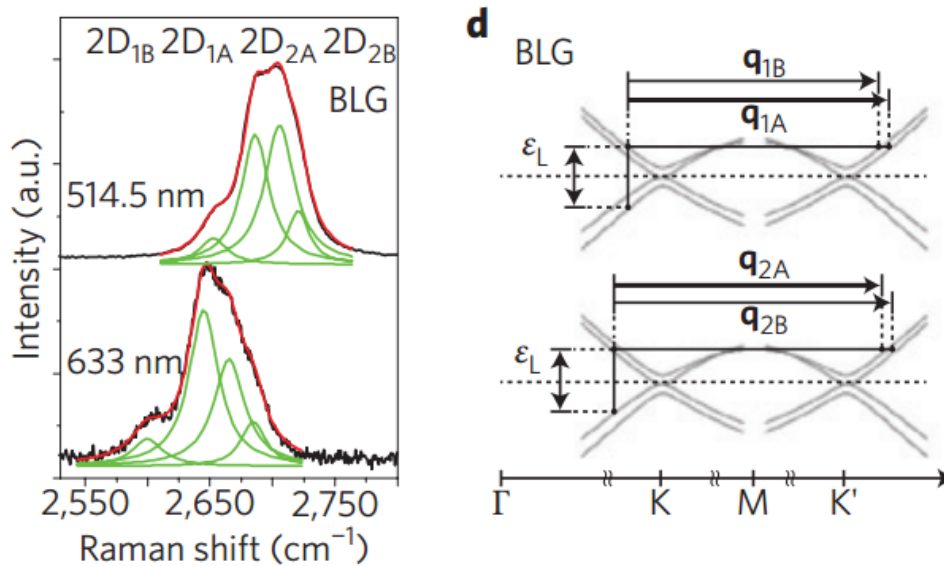
Figure 1.4-4: a) 2D peak of BLG measured at 514.5 nm and 633 nm. The red curves show multiple Lorentzian fits, and the green curves show the individual Lorentzian components. b) Phonon wave vectors corresponding to the 2D peak in BLG [Ferrari, 2012].

Additional information about the number of layers can be obtained if we carefully look at the area close to G peak (Figure 1.4-5a). Especially, there is one peak in ~1730 cm^{-1}, assigned to the Stokes combination of the E_{2g} Longitudinal optical (LO) phonon and the B_{2g} layer breathing mode (ZO´) phonon. It corresponds on a double resonance process and its frequency depends on the excitation energy of the laser. Its anti-Stokes combination is also visible, just below the G peak. When we have more than 1 layer, the

C peak splits into several components, the frequencies of whom depend on the number of layers and stacking order [Maultzsch, 2004].

Raman characterization is also a valuable tool in order to detect the defects in graphene. This permits us to understand the limits in the mobility of the material [Ni, 2010]. Robertson and Ferrari have introduced a classification of the amount of disorder, which leads from graphite to amorphous carbon [Ferrari, 2000]. It consists of 3 stages and allows all Raman spectra of carbons to be assessed simply: (1) Graphite to nanocrystalline graphite; (2) nanocrystalline graphite to low sp^3 amorphous carbon; (3) low sp^3 amorphous carbon to high sp^3 amorphous carbon.
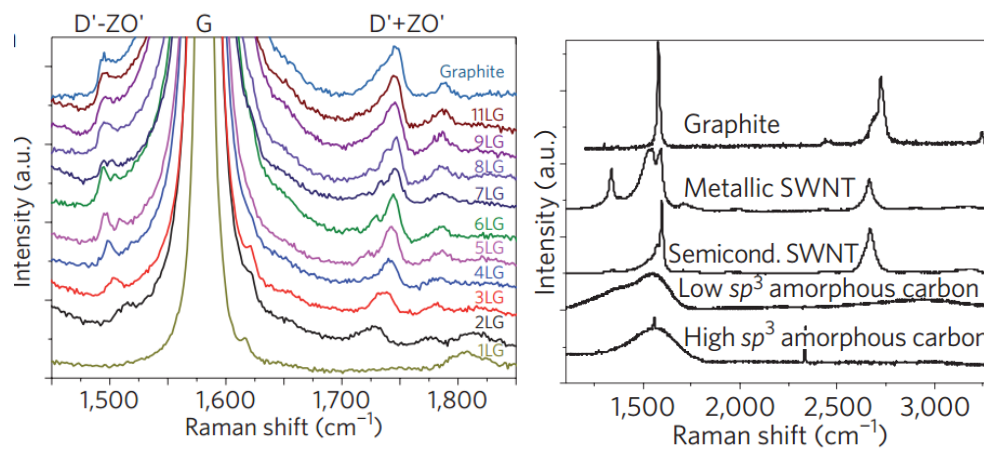
Figure 1.4-5: a) , Combination modes close to the G peak as a function of N. . The peaks at ~1,500 cm⁻¹ and between ~1,700 cm⁻¹ and ~1,840 cm⁻¹ are assigned as the anti-Stokes and Stokes combinations of the E2g LO phonon and the B2g ZO' phonon (layer-breathing mode), respectively. [Maultzsch, 2004] b) Raman spectra of graphite, metallic and semiconducting nanotubes, low and high sp^3 amorphous carbons. [Ferrari, 2000]

In stage 1 the D peak appears and the I(D)/I(G) ratio increases. The D´ appears and all the peaks are getting broader. Then the D+D´ peak appears. In the end of this stage the D´ and G are so wide that is more convenient to consider them as a single wide upshifted G peak. During this stage the ration between the D and G peak is calculated by the Tuinstra and Koenig relation, I(D)/I(G) = C(λ)/ La, where the coefficient C(514 nm) ~4.4 nm and La is the crystal size. λ is the excitation wavelength.

The I(D)/I(G) ratio varies inversely with the size of the crystal. The D peak is produced in a small area of the crystal, close to a defect or an edge. It´s intensity is proportional to the overall length of the edge. In the case that the sample has rare defects, the intensity of the D peak is proportional to the total number of defects probed by the laser spot. The intensity of the G peak is proportional to the area of the sample [Basko, 2009].

During the 2nd stage the spectra evolves as follows : The position of the G peak decreases from ~1,600 cm^{-1} towards ~1,510 cm$^{-1;}$ (b) the Tuinstra and Koenig relation fails; I(D)/I(G) → 0; (c) the position of the G peak acquires a dispersion as a function of excitation energy, the bigger the stronger the disorder; (d) there are no more well-defined second order peaks, but a small modulated bump between 2,300 and ~3,200 cm^{-1} (Figure 1.4-5b) [Ferrari, 2000]. The dispersion of the G peak increases with the disorder. If the material contains only sp^2 rings, the peak saturates at 1600 cm^{-1}.In case that it contains sp^2 chains (such as in amorphous and diamondlike carbons) the position of the peak continues to rise past 1,600 cm^{-1} and can reach 1,690 cm^{-1} for 229 nm excitation [Ferrari, 2001]. The D peak presents a lower dispersion for higher disorder, opposite to the behavior of the G peak. The FWHM of the G peak increase always with the disorder. I(D)/I(G) and FWHM(G) information should be combined in order to discriminate stage 1 from stage 2 [Ferrari, 2013].

In addition to the above, the edges of the graphene crystals can be considered as defects as well. If the translational symmetry breaks, the D, D´ peak is actiaved immediately. The D´ peak specifically is activated both by zigzag and armchair edges, as it does not involve any intervalley scattering [Ferrari, 2013]. The G peak is also modified near the edges. This is because there the electronic state is different and affects (i) the EPC correction to the phonon frequency, and (ii) electron–phonon and electron–photon matrix elements, responsible for the Raman process [Saaki, 2009]. In the case of a displacement or light polarization, one of the two modes, the electron–phonon or the electron–photon matrix element, does not demonstrate a Kohn anomaly and do not contribute to the Raman spectrum. This causes dependence of both the position and the intensity of the G peak near the edge.

1.4-1 Raman Mapping

In addition to single Raman spectrums, we performed Raman mapping to observe the graphene crystals. The Raman mapping results have been performed partially by the Jobin-Yvon LabRam HR 800. Althought, this system is not relatively fast for this kind of measurements. In addition, mapping has been performed by the DXRxi system of ThermoScientific, while it was in the facilities of the Centres Científics i Tecnològics as a demonstration apparatus.

Raman mapping can generate chemical images of graphene samples with submicron spatial resolution. It permits the characterization in regards to whether the sample is

composed entirely of one layer across the whole sample or whether it contains areas of differing thicknesses [Wall, Thermo Fisher Scientific]. It can serve as an imaging tool providing maps regarding the relative intense of the various graphene peaks as well as their position shifting and shape (through extraction of information considering peak´s FWHM). Knowing this, we can extract information considering the mechanical strain and charge doping in graphene films [Lee, 2012]. An example of Raman mapping is presented in Figure 1.4-6 from the relative work of Lee et al where the native strain in graphene samples is determined by Raman spectroscopic analysis notwithstanding the interference from the coexisting charge-doping effects. It is proven that it can serve as a fast and reliable characterization technique for this kind of materials and devices.
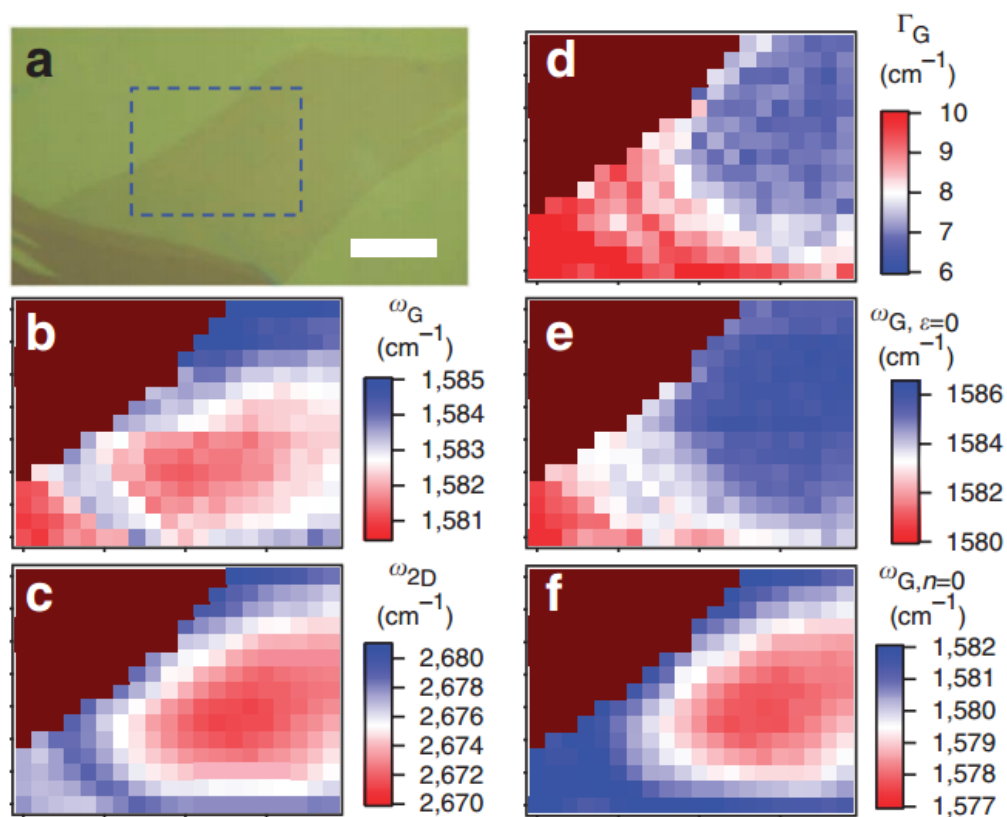
Figure 1.4-6: Decomposition of the effects of strain concurrent with spatially varying charge doping in pristine graphene. (a) Optical micrograph of a graphene sample (K5) under tensile stress concurrent with charge doping. Scale bar, 10μm. (b) Raman map of ωG. (c) Raman map of ω2D. (d) Raman map for ΓG. (e) Raman map of ωG, ε=0. (f) Raman map of ωG, n=0. [Lee, 2012]

Chapter 2: GRAPHMAN reactor

2.1 Description of the reactor

All the experiments carried out during this Thesis concerning the Graphene CVD growth were performed in the GRAPHMAN reactor based in the Clean Room of the Physics Faculty of the University of Barcelona.

The Clean Room consists of two spaces. The main space, where the GRAPHMAN reactor is installed, is classified as ISO 7 (10000 particles maximum/ft^3) (200m^2). In addition, it exists a photolithography room of 50 m^2, classified as ISO 6 (1000 particles maximum/ft^3) [FED-STD-209 E, 2001]

The reactor was installed in the Clean Room with the aim to secure the less possible contamination of all the materials and samples during their storage and preparation. Moreover, we secure the most stable conditions regarding the temperature and humidity of the storage area. In previous work it has been shown how the airborne contaminants can affect the wettability of graphene during its storage [Li, 2013]

The GRAPHMAN reactor was designed and developed by the FEMAN group of the University of Barcelona under the framework of the Doctoral Thesis of V.M Freire [Bertran, 2013]. Initially, the reactor was built in order to serve for the growth of graphene by the introduction of low pressure pulses of the carbon precursor gas. The sequence of the valves in the CH$_4$ line (see Figure 2.3) are set to serve to this concept. Small modifications were carried out later in the geometry of the system regarding the sample deposition arm and the order of the CVD oven and Sputtering Chamber to facilitate the whole process. Regarding the influx of gases, lines were added to allow the continuous inflow of the gases into the chamber.

Figure 2.11 shows a scheme (a) of the GRAPHMAN reactor and a view of the assembly (b).
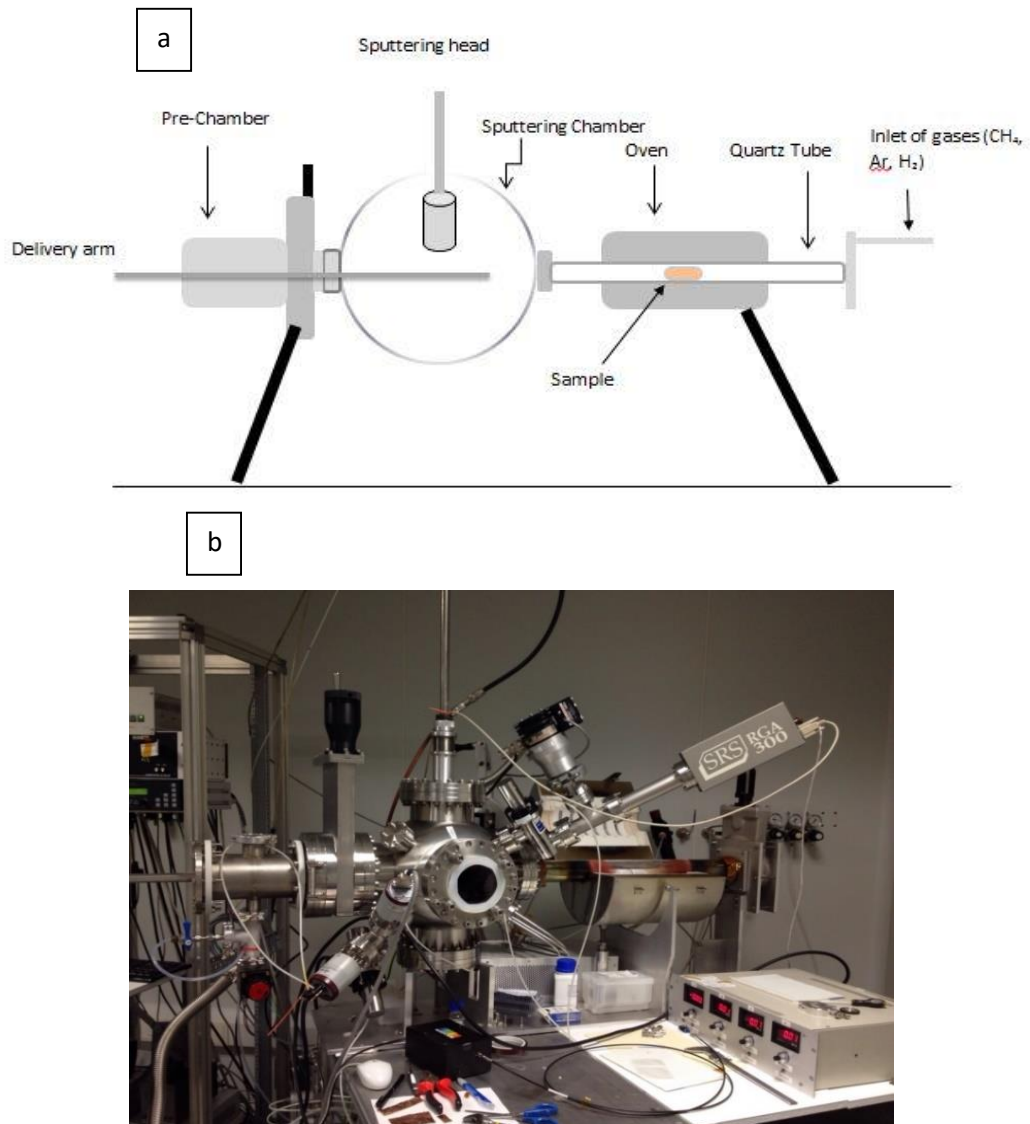
Figure 2.1: a) Schematic illustration and b) image of the GRAPHMAN CVD reactor installed in the Clean Room of the Physics Faculty, UB.

The Reactor consists of the following parts:

• *The magnetic arm*. The sample is loaded into the reactor by a magnetic manipulator arm. The arm can rotate and move back and forward. A quartz substrate-holder is mounted at the end of arm. The sample is positioned on this holder and inserted inside the reactor (Figure 2.2). Thanks to the quartz holder geometry the sample can be fixed vertically or horizontally on it (regarding the gases influx orientation).
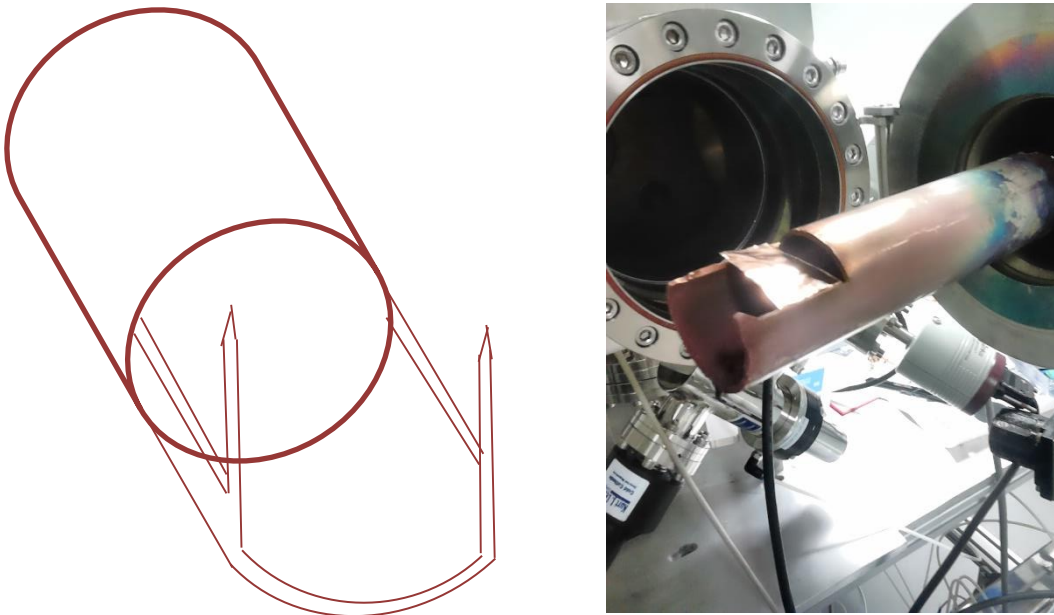
Figure 2.2: Quartz sample holder. Thanks to its geometry both foils as well as wafers can be deposited on it and inserted in the reactor.

• *The pre-chamber*. First the sample is loaded in the pre-vacuum chamber. There, the pressure is controlled by a mechanical pump which functions in the range between atmospheric pressure to ~5 Pa. This first pre-vacuum is necessary as the turbomolecular pump which is in the main chamber is not recommended to function at pressures higher than this. Moreover, thanks to the pre-chamber, the pressure in the main chamber and quartz tube never exceeds the 5 Pa, avoiding contamination of the reactor.

• *The main chamber*. In the main spherical chamber is installed the magnetron sputtering header, the turbomolecular pump as well as pressure controllers and the residual gas analyzer (RGA). The distance between the sputtering target and the sample is fixed to 8 cm. The RGA can measure the time evolution of up to 10 different masses in real time. It is especially effective in order to monitor the pulsed injection of various gases. The pressure inside the chamber can be controlled by an automatic conductance valve. In the main chamber are being sputtered various catalyst metals on top of the Si/SiO_2

wafers. Moreover, in the main chamber is performed the hydrogen plasma used to chemically reduce the copper foils.

•   *The chemical vapor deposition oven*. The oven can reach temperatures up to 1040 °C, temperature close to the melting point of copper (1083 ºC). The chemical vapor deposition takes place inside a cylindrical quartz tube. The tube is surrounded by a cylindrical furnace of two leaflets, heated by resistors. The gas inlet is placed inthe right side (as seen in Figure 2.1).The gases (carbon precursor gas, hydrogen, argon) flow through the quartz tube where graphene growth takes place by CVD . The evacuation of the gases from the main chamber is made by the turbomolecular pump. The main chamber and the quartz tube are connected by an open tube. This allows the turbomolecular pump to evacuate the entire chamber volume at a time.

•   *The pneumatic valves*. They allow the introduction of distinct pulses of various gases. Each gas line consists of two valves and one mass flow controller with a bypass line to purge (Figure 2.3). The pulse lines consist of a tandem of two valves with a sequential aperture. We have the possibility to choose between pulsed or continuous flow introduction of the gases. The range of the mass flow controllers is 10, 50 and 100 sccm (standard cubic centimeters per minute) depending of the kind of gas and gas flow needed.

•   *The vacuum system* consists of two vacuum lines. The first one evacuates the inert gases and hydrides (CH_4, H_2, Ar, C_6H_6) and is connected to a mechanical and a turbomolecular pump. The second line evacuates only air and oxygen (oxidizer). The base pressure of the system is close to 10^{-5} Pa.

•   *The monitoring system*. The monitoring system has been designed by FEMAN Group using the LabView 7.1 language. Through the monitoring system we have access and control to the main part of elements needed for processing graphene in the reactor. The opening/closing of the pneumatic valves, the mass flow controllers, the monitoring of the residual gas analyzer, the oven temperature and pressure of the chamber. Figure 2.3 shows one of the screen shot of the program. On the left part of the screen we have the gas management system with a diagram of the connections of the chamber with the different gas sources. On the right part we have the valves connecting the chamber with the different pumps as well as the pressure controller and the residual gas analyzer. On the right down part of the figure we can see the chart for monitoring the oven temperature, in the image, during the cooling down step. The monitoring system also provides information about the pressure in the interior of the chamber and allows the handling of the conductance valve, the control of the gases flow and the automatic introduction of

various pulses in pre-selected pressure.
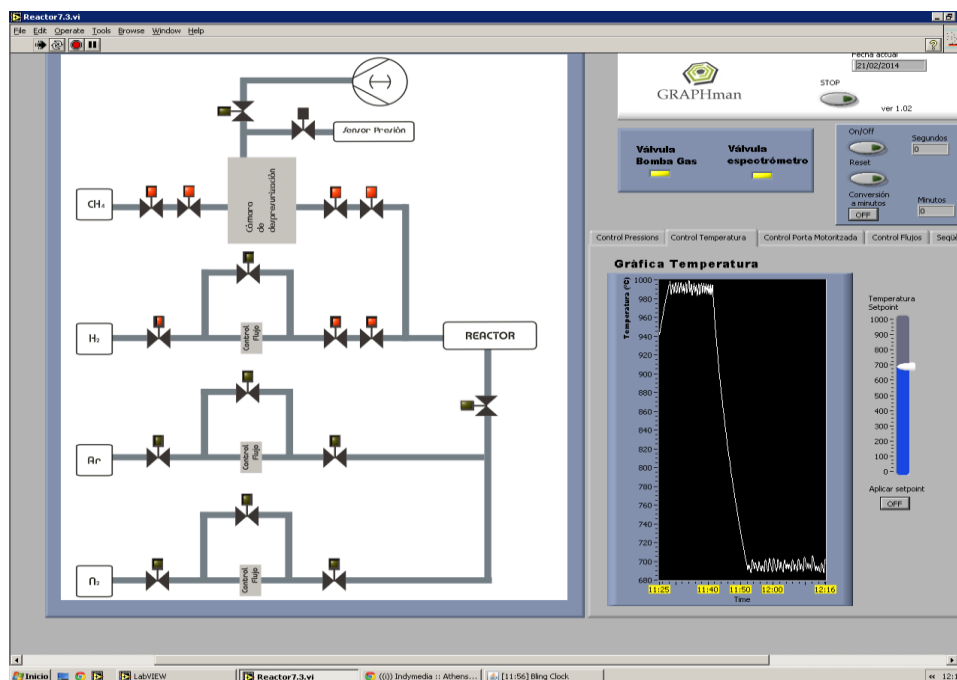
Figure 2.3: Screen shot of the LabView 7.1 interface.

Chapter 3: Experimental Part

3.1 Copper pre-treatment

Copper is the most explored and used metal as catalyzer during the graphene synthesis up to today (Zheng Yan, 2012). In various publications is presented the capacity to grow graphene crystals of various sizes, from few μm [Yu, 2011; Wu, 2013], hundreds of μm [Wu, 2012; Geng, 2012] until up to mm scale [Wang, 2012], on top of it. Polycrystalline copper foil of various thicknesses is being used. The most common are 25, 75 and 125 μm thick. The thickness of the foil in principle has been found to affect the lateral dimension of the copper grain boundaries [Mattevi, 2011] but it has not been demonstrated any relation between it and the graphene film quality. The atoms of carbon present a very low solubility into the copper. So its thickness can not affect the stock of carbon atoms that participate in the synthesis of the graphene.

The as bought copper foil is usually polycrystalline. Single orientation foils are also available but their cost is much higher, which makes it prohibitive to use on a large scale. . The orientation of the copper substrate is significant for the graphene growth, regarding the shape and morphology of the graphene domains as well as their growth rate. A phase field model developed by Meca et al. has managed to explain this dependence and reaffirm it with experimental results [Meca, 2013]. To be able to develop recipes which permit to obtain a significant growth rate of graphene films is important to know which are the most appropriate orientations of the copper crystals. It has been demonstrated that the surface of common copper foil appears strongly (100)-textured after the annealing [Wofford, 2010].

In a common growth process the first step taking place inside the reactor is the annealing of the copper substrate. This process contributes in different ways the graphene growth that follows by 'preparing' the copper surface. It is necessary in order to reduce the native copper oxide layer which is formed on the surface of the foil. It cleans the catalyst surfaces and modifies the surface morphology including crystalline orientation, roughness (smoothing) and grain size of the metal catalyst. It is important to have the lowest possible evaporation of metal. The annealing temperature and annealing time and how they affect the formation of the copper grains have been studied in various publications. In the work of Wood et al [Wood, 2011] they demonstrated that the (111) crystallographic facets of copper enable the growth of higher quality graphene than on (100). To achieve this orientation it was needed longer annealing at 900°C in an argon/hydrogen ambient [Zhang, 2011].

In our case we use a hydrogen plasma to clean and etch the copper foil at room temperature. The process lasts only a few minutes. Not need for an extra heating source is the great advantage of this method. The exploration of it has showcased the potential to grow graphene in a mixture of methane/hydrogen in a plasma enhanced chemical vapor deposition process without any extra heating source apart from the one generated by the plasma itself [Boyd, 2015].

3.2: Graphene Growth

In this section we present the experimental conditions of the graphene growth and the reasons to choice the parameters and their ranges. The results of these experiments are presented in the next chapter 4.

All the samples have been prepared in the GRAPHMAN CVD reactor installed in the Clean Room of the Physics Faculty, in the University of Barcelona.

We divide the work in two parts. First are presented the processes where the gas introduction is occurring in the form of continuous flows. Then we present the approach where the gas introduction is occurring in the form of pulsed injection.

3.2-1 Experimental growth control on the edge of graphene monolayer crystals

Graphene growth on copper foil by chemical vapor deposition is currently one of the most promising synthetic routes to achieve large scale graphene [Li, 2009]. Current works demonstrate the possibility to move to industrial scale synthesis [Bae, 2010; Han, 2011]. To achieve this, the growth of large monocrystalline domains is of high importance [Miseikis, 2015]. Up today the full cover of the metallic substrate by graphene takes place by the join of the various graphene crystals that are being grown during the process. The grain boundaries between the crystals are one of the main reasons that affects the quality of the graphene layer, both concerning mechanical and electrical properties [Kim; 2012; Gran Table, 2010; Kumar, 2010; Yazyev, 2010; Li, 2010]. Therefore, in relation to the initial nucleation, it is important to have graphene islands formed from the smallest possible number of nuclei.. Here we have the necessity to find synthetic routes that can ensure the low nucleation density of the crystals. In this way the crystals have more free surface area to grow before they join to each other. Important parameters in the CVD synthesis on copper foil are known to be the gas flow, the pressure and the growth time. It is of crucial importance to have a clear understanding of the effect of these parameters [Vlassiouk, 2013]. Between them, the role of the hydrogen flow appears to be critical. Various works have studied the hydrogen function. It reduces the copper oxide, activates the graphene growth and performs etching in the grown domains [Wu, 2012; Zhang, 2011; Gang, 2013; Kim, 2012]. Understanding these multiple effects of hydrogen is fundamental to have a full control of the graphene growth mechanisms. In other works, it is revealed how hydrogen presence can affect the thickness, shape, size, edge configuration, and crystallinity quality of graphene islands/domains [Vlassiouk, 2011; Zhang, 2013; Ma, 2013; Mohsin, 2013]. A careful design is required to ensure that the

flow of the gases is suitable to facilitate the growth of graphene. If the process is too aggressive, the formed graphene layer can easily be taken away by the etching activity of hydrogen flow. Up today various works have been reported, proposing ways to control the nucleation density on copper, which presents a low carbon solubility [Yan, 2012; Wu, 2012; Geng, 2012; Wang, 2012]. Some of them propose physical polishing [Brown, 2014] and Cu re-solidifying [Mohsin, 2013]. Another interesting approach is the enclosure of the copper in a 'pocket' during the growth. In this medium the nucleation density is reduced [Li, 2011]. The growth under high temperatures, close to the melting point of copper, results in the synthesis of high quality graphene, as a result of the more effective recrystallization of the catalyst [Faggio, 2013]. The option of growing the graphene at low pressure ensures that the whole process is taking place in high purity conditions. The copper oxide also is an important factor that can control the nucleation density of the graphene. In various recent works it has been demonstrated that the oxidation of the copper substrate is an efficient method to reduce the graphene nucleation [Hao, 2013; Gan, 2013]. Based on this idea, it has been managed to synthesize up to one centimeter single graphene crystals [Li J., 2015]. Various annealing processes are proposed in order to chemically reduce the copper foil. They usually require long baking of the foil at high temperature [Wang, 2011]. Here, we apply a hydrogen plasma that can sufficiently and quickly reduce the copper surface, which is ready for the following growth step. Concerning the graphene growth, we report the controllable growth both of continuous graphene film as well as of large graphene single domains. To identify the role of the pressure and the hydrogen flow we run experiments varying these two parameters. The characterization by scanning electron microscopy (SEM, model JEOL JSM 7100F) reveals that keeping the methane/hydrogen ratio stable and varying the total pressure of the chamber during the growth affects the nucleation density of the graphene crystals and therefore their size. Maintaining a stable total pressure and methane flow, while the hydrogen flow varies, affects the morphology of the individual crystals and performs an anisotropical etching while keeping stable their size. Finally, based on these results, we have used the conditions that appear the most efficient in terms of crystal size and morphology to control the growth time necessary to obtain substrates full covered with single layer graphene films.

Polycrystalline copper foil of 99% purity and 75 μm thickness was used for all the experiments. A typical processing of copper foil involves the following steps: a)the copper foil is being cut in pieces of 2x2cm^2; b) first the foil is introduced in an ultrasound bath of acetone and isopropanol, 10 minutes each, for removal of the impurities; c) then the piece is loaded into the CVD reactor GRAPHMAN; d) a DC hydrogen plasma is then applied to

remove the native oxide layer, e) finally, the copper substrate is internally transferred from the plasma chamber to the oven and annealed, under a low pressure H$_2$ atmosphere, at 1040 °Cvery close to the melting point of copper (1080 °C), to obtain a texturing of the copper foil. This methodology is very effective and reproducible to prepare copper substrates before the graphene growth, as previous studies from our group have revealed [Hussain, 2014; Chaitoglou, 2015].

The choice of the temperature of 1040 °C was based on the results reported by Wang et al. [Wang H., 2012] on the growth of graphene layers. Although, it has been reported the successful growth of graphene at much lower temperatures [Zhang, 2012], in our case we could not obtain any high quality graphene at temperatures below 950 °C (under the studied conditions of pressure and gas flow).

 Considering the texturing of the copper foil, the author has presented in previous recent publication [Chaitoglou, 2016] the evolution of the copper grain size. Electron back scattered diffraction (EBSD) analysis has revealed an increase of the copper grain size from 30 μm^2 (for the as received foil) to more than 2000 μm^2 (grain size after annealing). In the same work, results have been presented considering the effect of the orientation of the copper grains over the shape evolution of the graphene crystals. In the present work, various experiments have been executed in order to control the effect of the total pressure as well as the hydrogen flow on the graphene growth. First, the experiments were executed to control the pressure effect. The observations considering the shape of the graphene crystals, size and density evolution are extracted from analysis of a large collection of SEM images by *Image J* software. Here we present the average results that have been derived from the analysis of measurements as well as histograms with the size distribution of the lobe lengths of the flat graphene dendritic crystals.

In this analysis, we were interested to find the most suitable pressure to perform the graphene growth. Even though in previous works the effect of the pressure on the nucleation density and size of the graphene crystals have been already reported [Vlassiouk, 2011], we have explored different pressure ranges and introduced new variables in order to evidence the role of hydrogen on the growth of graphene. Thus, we have studied the effects of pressure keeping stable the methane/hydrogen rate (5 sccm/20 sccm) and controlling the total pressure byrotating the automatic conductance valve of the turbomolecular pump. The SEM images of this series of samples appear in Figure 2. In these results, the growth time was always 20 min and time cooling of the sample to 500 °C is as fast as the time it takes to be removed from the hot zone of the tubular oven. The pressure was varying from 12.5 Pa (sample

15a2601) to 15 Pa (sample 15a2202), 17.5 Pa (sample 15a2602), up to 20 Pa (sample 15a1502).

In the continuous we run a series of experiments to control the effect of hydrogen flow in the graphene growth. The values we used are similar to the previous graphene growth experiments. The CH_4 flow was always 5 sccm and the pressure stable at 15 Pa. This pressure was selected after checking that hydrogen over methane ratio of their partial pressure remained stable at constant flows (Figure 3.2-1e) and resulted in complete cover of the copper substrate by graphene.In Figures 3.2-1a-3.2-1d we see the evolution of the methane and atomic hydrogen partial pressures. These Figures served in obtaining Figure 3.2-1.
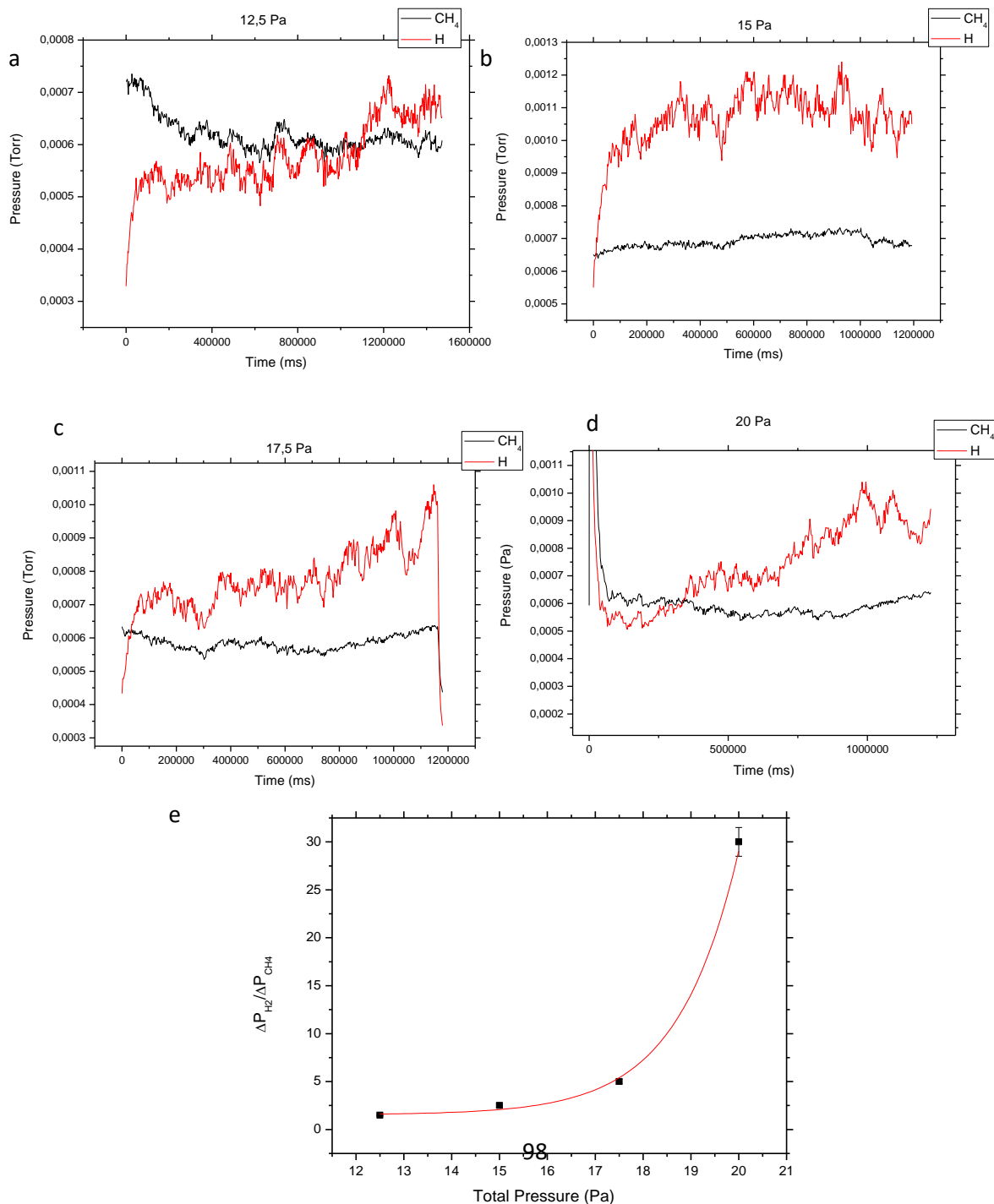
Figure 3.2-1: a)-d) Evolution of the methane and atomic hydrogen partial pressures as measured by the residual gas analyzer for total pressure 12,5-20Pa. e) In this plot is presented the ratio of the partial pressures ΔP$_{H2}$/ΔP$_{CH4}$ for the different total pressures in which have performed graphene growth. We can distinguish the exponential evolution of the graph, as a result of the higher concentration of hydrogen in higher total pressures.

The growth time of samples of figure 3.2-1 was 20 min. The temperature was always 1040 °C. The growth processes were performed at 10 sccm hydrogen flow (sample 15b1101), 15 sccm (sample 15b1602) and 20 sccm (sample 15b0401).

Table 3.1 shows the conditions used in the experiments designed to control the effect of total pressure and hydrogen flow. From the microscopy results is being evaluated the effect on the graphene crystals size and nucleation density. Finally, after optimizing the parameters that result in larger and better shaped graphene crystals, we run longer growing experiments to control the quality of the obtained graphene layer.

Sample (corresponding figure)	Total Pressure (Pa)	Hydrogen flow (sccm)	Crystal's lobe Length (µm)	Nucleation density (nucleus/1000µm^2)	% surface cover
Figure 4.2-1a	12.5	20	13	1.6	15
Figure 4.2-1b	15	20	27	3 (Full cover)	100
Figure 4.2-1	17.5	20	14	7.2	82
Figure 4.2-1d	20	20	32	2.4	40
Figure 4.2-7a	15	10	30.5	2.6	55
Figure 4.2-7b	15	15	30.1	0.8	82
Figure 4.2-7c	15	20	27	1.3	95

Table 3.1: Growth conditions of the graphene crystals presented in Figures 4.of the Results chapter2-1 and 4.2-7. The methane flow in all the experiments is 5 sccm. The growth time was always 20 min and the growth temperature was always 1040 °C. In the table are presented the effect of growth total pressure and hydrogen flow to the crystal size as well as the nucleation density.

3.2-2 Experimental conditions to study the effect of a balanced concentration of hydrogen on graphene CVD growth

In this work we pursue to grow graphene without voids or defects forming large domains, by means of a modified method. A continuous graphene film without defects is desired in order the material to maintain its exceptional properties and to be useful for applications. The carbon-precursor/hydrogen flow ratio and its modification during the growth are significant in order to obtain large area graphene crystals with few defects.

For the evaluation of the obtained graphene we used Raman spectroscopy and mapping as well as scanning electron microscopy (SEM). The SEM images where taken with a JEOL JSM 7100F microscope working at 5 keV. The Raman spectroscopy was performed with a Jobin-Yvon LabRam HR 800 system. It has been used a green laser with a 2 μm spot diameter. AFM images have been obtained with an AFM Multimode 8, electronica Nanoscope V (Bruker) and operated by the NOVA software.

CVD synthesis was performed, after the plasma etching and the reduction of copper foil, inside a quartz tube surrounded by an oven, as it has been described in the last section. All the processes have been performed in the GRAPHMAN Reactor.

All the steps of the process have been performed by a computer program, moreover, in order to secure the high purity conditions under which the graphene growth was carried out, the reactor was pumped to high vacuum (down to 6×10^{-4} Pa) with a turbomolecular pump. In "continuous flow mode", the tubular furnace was heated to 1040°C.

Various publications have reported the crucial impact of this temperature concerning the CVD synthesis of graphene on copper using methane as a carbon precursor [Eres, 2014]. In our case, after exploring in a wide range of experimental conditions, we conclude that the best quality graphene is obtained at this temperature. Other studies reveal the possibility of CVD graphene growth at lower temperatures. However, it requires working at higher pressures (8-15 Torr), outside of the range that our system can reach [Choi, 2013]. The pressure was stabilized at 20 Pa through an automatic variable conductance valve. Flows of 20 sccm of hydrogen and 5 sccm of methane were introduced in the chamber and, in order to compare the characteristics of the obtained graphene crystals, we kept running the deposition process during 20 min (sample14k1302) and 40 min (sample 14k1401), according the running times proposed by Wang et al. [Wang H., 2012]. After these running times, the flows of methane and hydrogen were stopped and the system was cooled down to room temperature at high vacuum (10^{-4} Pa). This operation prevented the oxidation of the samples under atmosphere exposition [Michon, 2013].

3.2-3 Experimental conditions to study the graphene growth by pulsed injection of methane

A different approach considering the introduction of the carbon precursor is "pulsed injection mode" instead of a "continuous flow mode". The growth of graphene by the pulsed injection of acetylene on top of nickel films was proposed by Puretzky et al. (Puretzky, 2013). Before that, our group (FEMAN-UB extensively studied the growth of monolayer graphene on top of copper films and copper foils. This work is described in the doctoral thesis of VM Freire (Freire, 2014). The method is based on the concept of monolayer formation time which assumes that in the case that the sticking coefficient is one for the molecules of the gas reaching the surface, the formation time of a monolayer is only dependent by the pressure [Bertran, 2013]. This is expressed by the equation

$$t(s) = \frac{3 \cdot 10^{-4}}{P(Pa)}$$

Where *t* is the time and *P* the pressure. According to this equation, it takes about one second to cover a surface at a pressure of 300 μPa. In our case, we could not know the value of the sticking coefficient. It is something that needs further theoretical calculations to be investigated.

The injection system in the GRAPHMAN reactor was designed in order to permit the pulsed injection of methane. Each pulse is introduced in a period of approximately one second, through an automated controlled valve system. In the experiments presented in this thesis, we grow graphene with the injection of various amounts of pulses on the same type of copper foil as described before. The pre-treatment of the foil was the same. The sample was inserted in the quartz and heated to 1040 ˚C. The background pressure was always in the order of 10^{-4} Pa during the pulses injection. The injection of the methane pulses was taking place in the absence of any additional hydrogen flow. We carried out growths delivering 1, 5, 10, 30, 50, 70 and 100 methane pulses. As before, after the injection of the methane, the sample was cooled down in the same high vacuum before being removed from the reactor.

Chapter 4: Results

4.1-1: Native copper oxide reduction

RF plasma of hydrogen is commonly used to reduce the native copper oxide layer formed on top of the copper foil. Moreover, the microcrystal copper surface becomes smoother, favoring the graphene growth, which continues after [Boyd, 2015]. Plasma pre-treatment is preferred in front the thermal annealing as it is much faster and does not require heating to high temperatures. In only a few minutes the metal oxide can be removed. In order to know the presence of copper oxide, we have monitored the plasma composition by optical emission spectroscopy (OES). The spectra of emission of a plasma is composed by the set lines corresponding to the radiative transitions of the excited species present in the plasma. The radiative species are some of the excited elements, ions, radicals or molecules of the plasma. OES is an analysis technology offering a partial vision of the chemical composition of the plasma. In order to have a more complete information of the chemical composition, OES information can be completed by other analysis technologies like, mass spectrometry (quadrupolar spectrometry, residual gas analysis, RGA) and/or infrared spectroscopy.

A continued electrical excitation of a neutral gas, at relatively low pressure, can produce gas ionization because the collision of free electrons with neutral species (radicals, atoms and molecules) present in the gas. This phenomenon can produce a self-sustained gas discharge or plasma, which is composed by neutrals, ions and free electrons. The electrical excitation used in our work has been obtained from a radiofrequency (RF) power applied through a capacitively coupled electrode.

In particular, the reduction of the copper oxide has been achieved by means a plasma of hydrogen excited by a 3" cathode with a magnetron, which increases the hydrogen plasma density with a very low level of sputtering of the metallic electrode (cathode) due to the low mass of hydrogen ions. In order to chemically reduce the copper substrates, usually they are positioned at 4-5 cm in front of the cathode-magnetron that is surrounded by the hydrogen plasma.

The excited species of the plasma generate a unique emission spectra which consists the fingerprint of each radiative element, radical or excited molecule present in the plasma. The intensity of each emission line depends on the concentration of the corresponding species. Special photodetectors can measure the presence and intensity of each spectrum, providing a qualitative and quantitative measurements of the elements [shimadzu.com].

Here, we present the performance of hydrogen plasma for the same purpose. From previous studies made in our group [Hussain, 2014], we have been able to optimize the parameters necessary to use in order to reduce the native copper oxide layer. According to these results, first, a background pressure of 7×10^{-4} Pa is achieved with a turbomolecular pump to secure that the whole process is taking place under high purity conditions.   RF hydrogen plasma was then applied to chemically reduce the copper substrate. The conditions of hydrogen plasma were 20 sccm of hydrogen flow at 20 Pa and 100 W of RF power. The hydrogen radicals reacts with the copper oxide according to the following reaction:

$$CuO + 2H \rightarrow Cu + H_2O \qquad\qquad (Eq.1)$$

During the plasma treatment, the hydrogen radicals react with the copper oxide reducing it to metallic copper [Getty, 2002]. We use optical emission spectroscopy to determine and evaluate the reduction of the copper surface. The out coming light from the discharge was collected by a spectrophotometer (Stellarnet EPP2000C), which operated in the range (300-850 nm). The integral spectral intensity evolution of the OH radical emission in the spectral range of 305-330 nm is a sufficient tool to evaluate the removal of the oxide [Raskova, 2002]. Results show that the intensity of the peaks corresponding to OH radicals decrease after 5 min of plasma treatment. In particular, the first peak at 305 nm decreases from 22.6 to 5.9 a.u., as we can see in Figure 4.1-1. The reduction in the OH concentration reveals the decrease of the oxygen radicals (as a result of the oxide reduction). Nevertheless, as the copper oxide cannot be completely removed, the peak does not decrease more with further treatment [Chang, 2013]. Graphene protects copper from oxidation, which explains that even after the pass of days the reflected color of the substrate does not change [Chen, 2011]. Copper foil before etching appears with a higher pitch of red because of the copper oxide layer on the top. After the treatment, it appears brighter and large crystalline domains can be distinguished at naked eyes. This treatment is much faster if compared to the usual pre-annealing required for the Cu substrates taking up to several hours [Wang, 2011].

The X-ray diffraction pattern of the copper foil after the plasma pretreatment indicates the absence of copper oxide peaks (Figure 4.1-2). The copper oxide has been sufficiently removed from the surface of the foil. The continuous graphene film protects the foil from further oxidation [Chen, 2011].
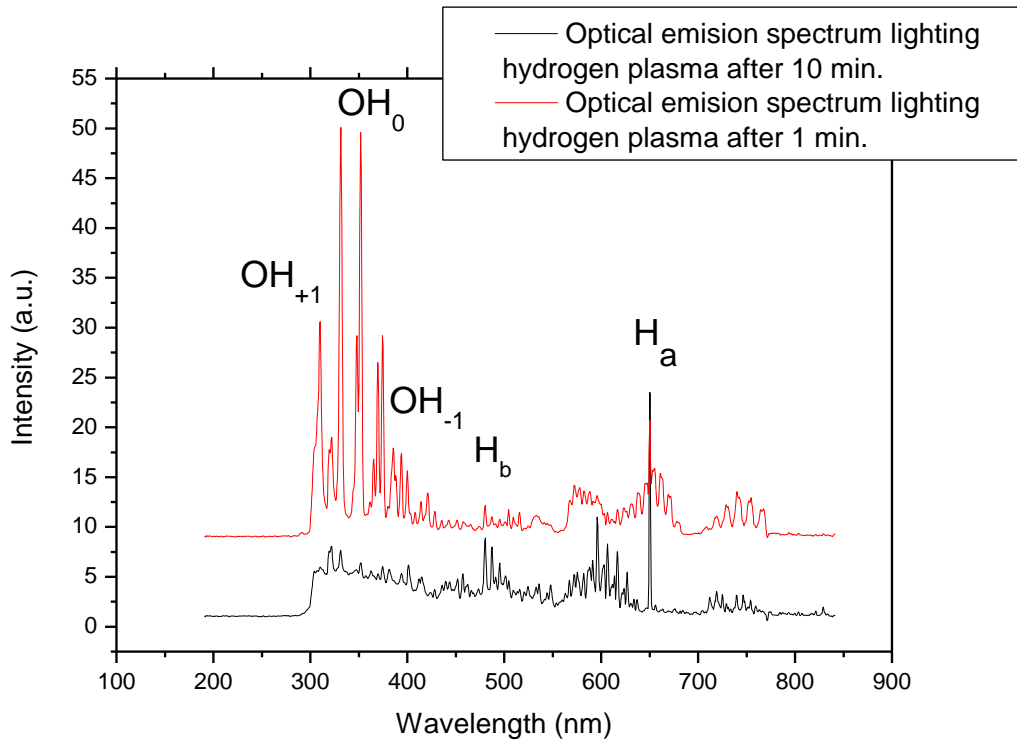
Figure 4.1-1: Optical emission spectroscopy of hydrogen plasma during reduction of copper: after 1 min (red line) and b) after 10 min (black line). The reduction of the OH radical peak intensity in the spectral range of 305–330 nm reveals the removal of the oxide layer.

To demonstrate the importance and efficiency of the plasma pre-treatement process we have compared both experiments of graphene growth with and without including this step In the experiment that plasma was not applied, we performed a pre cleaning of the copper foil in a HNO_3/distilled water solution (70% aq.) as described in the work of Kim et al. [S. Kim, 2013].
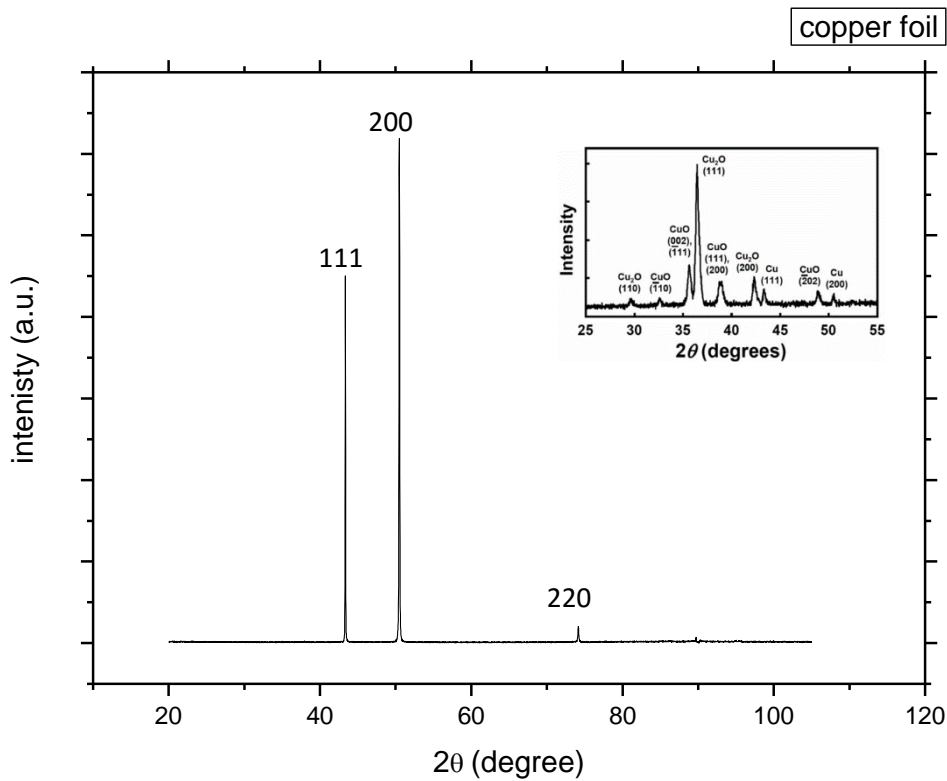
Figure 4.1-2: XRD pattern of the copper foil after annealing. Three peaks at 2θ values of 43.6, 50.8, and 74.4 deg. corresponding to (111), (200) and (220) planes of fcc copper were observed.Copper oxide and cuprous oxide peaks are visible in the internal image which serves as a reference [Cheng, 2012]

In these processes, after the pre-treatment step, the copper foil piece is inserted inside the quartz tube oven. A vacuum down to 5×10^{-4} Pa is applied and then the oven is heated to 1040°C. Once the temperature is reached, methane and hydrogen are introduced in the oven in a methane/hydrogen ratio of 5/20 sccm at a total pressure of 20 Pa. The total pressure is controlled by a butterfly valve to keep constant during all the experiment. The growth step lasts 20 min. Then, the foil is let inside the oven to cool down at high vacuum. We do not remove it before reaching the room temperature in order to avoid any possible oxidation.

As an additional tool to characterize the copper surface we used electron back scattered diffraction (EBSD). It is a large-area imaging method, which detects the different index facets of fcc copper. In combination with scanning electron microscopy (SEM) characterization we can match characteristic geometries of the graphene domains to their

corresponding copper facets. As explained in detail in the work of Meca et al [Meca, 2013], the geometry of each graphene domain depends on the copper facet index over which is being grown. In our case the EBSD is used to demonstrate the growth of the copper grains after the H_2 plasma and the growth process, with respect to the as-received copper foil. In Figure 4.1-3 we provide the EBSD mapping of untreated policrystalline copper foil 75 μm thick (Figure 4.1-3a), copper foil after 20 min of growth (Figure 4.1-3b) and copper foil after 50 min of growth (Figure 4.1-3c).
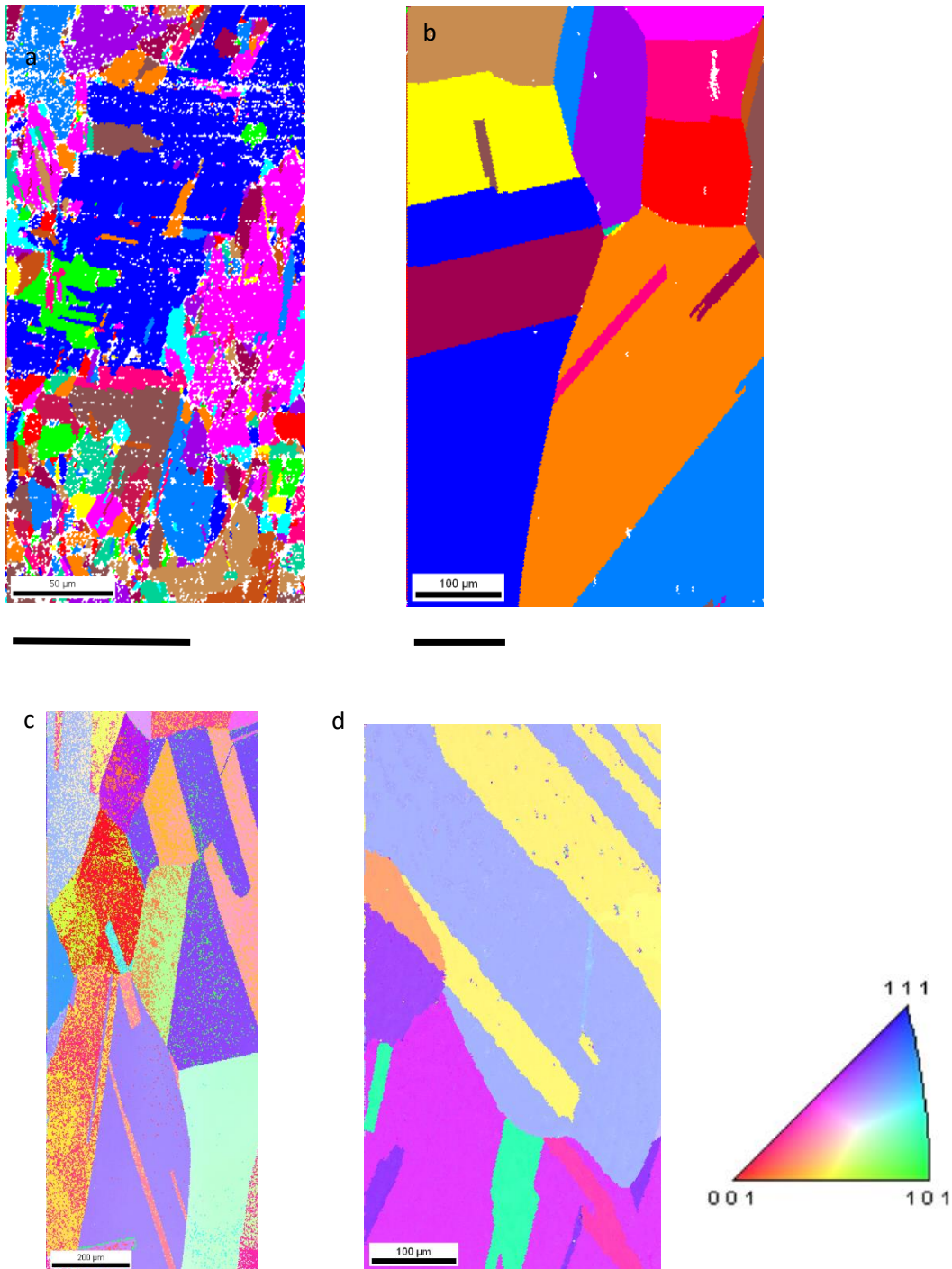
Figure 4.1-3: EBSD maps of a) the as-received polycrystalline copper foil (scale bar 50 µm), b) the foil after plasma annealing and 20 min graphene growth at 1040 ˚C, (scale bar 100 µm), c) the foil after plasma annealing and 50 min graphene growth (scale bar 200 µm), d) the foil after plasma annealin followed by 60 min thermal annealing at 1000 ˚C and 20 min of growth (scale bar 100 µm). The triangle palette matches the copper facets orientation with the relative color code for all four maps.

The crystalline grains of the untreated copper (Figure 4.1-3a) have various sizes with most of them not overcoming an area around ~1000 $µm^2$. The boundaries between the grains are randomly oriented. During the annealing process, copper atoms can difuse and relocate to the energetic favorable sites, therefore grain boundaries move and grains increase in size. In our experiments the annealing takes place under no presence of gas, at a high vacuum, in the order of 10^{-4} Pa. The growth takes place under the presence of hydrogen and methane, at a pressure of ~20 Pa and a temperature of ~1040˚C [Jin, 2014]. Figure 4.1-3 b and 4.1-3c show that with a longer growth the grains become larger. Grains of sizes up to ~8000$µm^2$ for the longer growth are usual. To test if the copper grains can grow further, we performed long annealing of 60 min and 20 min of growth, at the same temperature. At lower annealing temperature (around 1000ºC), the grain areas do not exceed few hundreds of $µm^2$ (Figure 4.1-3d). The edges between the grains now appear much straighter. These factors affect the quality of the graphene domains grown later. Graphene bidimensional crystals need smooth and large grains to grow over. Usually, the boundaries are defect sites for the graphene, so the fewer grain boundaries the fewer defects.

Figure 4.1-4 shows the SEM pictures of the graphene domains obtained with plasma pretreatment (4a) and without plasma pretreatment (4b). Figure 4.1-4a shows the formation of crystals with different morphologies. There are present crystals with a ''butterfly'' shape (blue circle) and others formed with four lobes and dendritic extensions (red circle). Shape and symmetry of graphene crystals depend on the orientation of the copper crystalline domain of the substrate. According to the model of Meca et al., the four lobes with dendritic extension crystals are being grown on Cu (100) planes, whereas the crystals with the ''butterfly like'' shape are being grown on Cu (221) planes. The pictures were taken directly in the copper substrate without any previous transfer. The lobes of the graphene crystals are about 30 µm long (growth velocity 1.5 µm/min). The results indicate that the growth ratio is independent of the crystal morphology. The growth of crystals with a morphology having the four lobes with dendritic extensions appears to be more favourable. As SEM pictures evidence (Figure 4.1-4), the crystals present a medium nucleation density in most parts of the substrate and large areas of the substrate

are not covered by graphene. Figure 4.1-4b shows the crystals formed on the copper foil without any plasma cleaning. The nucleation density seems to have increased, if compared to Figure 4.1-4a, as there is no areas of the surface without nucleation points. The crystals of Figure 4.1-4b have no as regular form as in the graphene obtained in the previous samples of Figure 4.1-4a. We have considered two possible explanations to this. The first is that with the chemical etching, the native copper oxide film was not completely removed. The other is that the oxidation of the sample takes place during its cooling, which takes place at high vacuum in absence of hydrogen or any other gas, resulting in the formation of copper oxide islands along with the graphene [Qi, 2012]. A recent study [Gottardi, 2015] reports the growth of graphene on copper oxide (111) and compares it with graphene grown on metallic copper (111). They explain that the vacancies present in the copper oxide can trap the CH_4 inside. The oxygen atoms present there catalyze the dehydrogenation to form –OH and $–CH_3$. Then the $–CH_3$ acts with other molecules to form the graphene. Therefore, the oxygen atoms play the role of nucleation centers for the growth of graphene. Moreover, according to Gottardi et al., and as evidenced by density functional theory (DFT) calculations, both surfaces copper oxide and metallic copper, have similar dehydrogenation energy barrier. In addition, the methane bonds slightly stronger to Cu_2O (111) than to Cu (111) by 0.10 eV. The relative ratio between methane dissociation and desorption (given by the Boltzmann factor) becomes very similar on both surfaces. These data explain why graphene can be grown under both surfaces.

Gottardi et al. revealed from their study that the oxide decouples the graphene from the metallic surface. Measurements obtained by angle-resolved photoemission spectroscopy (ARPES) show that there is no any kind of n-doping on the graphene grown on the oxidized copper. This kind of doping is expected when graphene is coupled to the metal surface. Its absence reveals that the graphene is weakly interacting with the metal surface.

We consider that this is the reason that the graphene domains in Figure 4.1-4b present this morphology. The weaker interaction facilitates the etching of the graphene from the surface of the copper. In addition to this, we should include the point that the increased nucleation density in the case of the copper oxide means an increased concentration in the amount of hydrogen atoms, which are the factors that perform the etching to the graphene. As explained in other chapter of this Thesis, the effect of hydrogen in the graphene grown is complicate to be completely predicted. It consists always of two antagonistic effects, etching and co-catalysis of the graphene growth. Although, it is difficult to describe its dominating effect in each case.
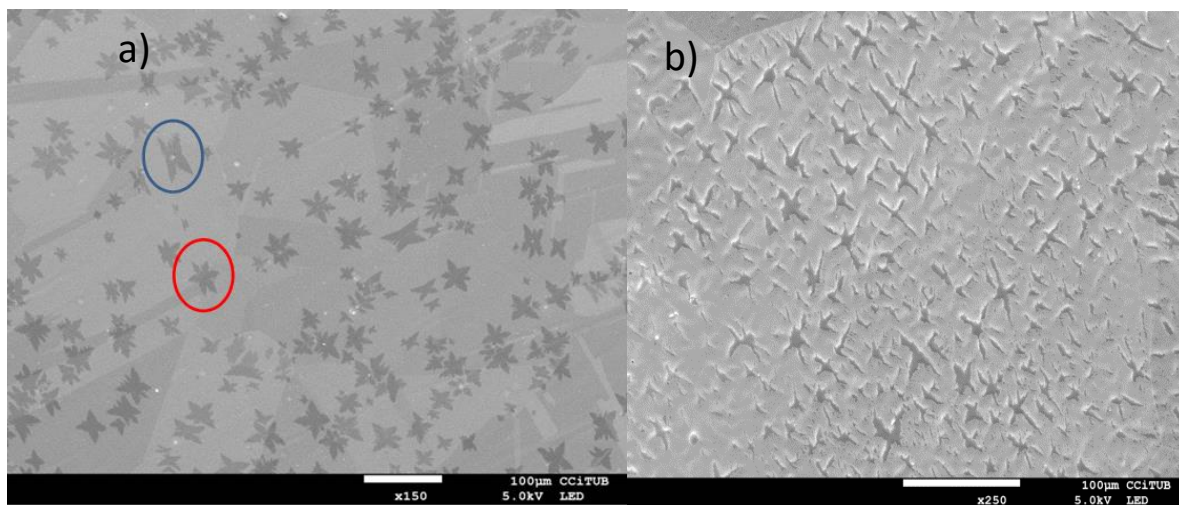
Figure 4.1-4: Graphene crystals obtained in copper foil, (a) with plasma pretreatment [sample 14I1901] and (b) without hydrogen plasma pre-cleaning [sample 14k1301]. The not sufficient removal of the copper oxide from the surface of the foil difficults the formation of well-shaped graphene domains.

4.1-2 Conclusions

The study reveals the sufficiency of hydrogen plasma to reduce the copper oxide layer that is formed on top of the copper foil. The technique is quite faster than the usual thermal annealing that is applied in this case. The optical emission spectroscopy is proved to be a very sufficient tool to obtain information about the reduction of the copper oxide. Electron back scattered diffraction provides useful information about the crystallinity of the copper surface. Longer thermal annealing or longer growth processes do not affect the results in further growth of the copper domains. The copper domains in all cases reached no more than 8000 μm^2.

4.2: Graphene growth
4.2-1: Experimental growth control on the edge of graphene monolayer crystals

4.2-1.1 Lobe's length and nucleation density
We have observed that graphene two dimensional crystals are formed on crystalline copper as a consequence of a planar dendritic growth, with an incorporation of the carbon species mainly on the borders of the graphene islands. From the SEM images presented in Figure 4.2-1, we can see that a small variation in the pressure leads to a significant effect in the nucleation density as well as the size of the graphene islands. For the growth taking place at 12.5 Pa the nucleation density of the graphene islands is 8 nuclei/10000 μm^2 and the average size of them is 26×26 μm^2 (Figure 4.2-1a). The different shapes shown by the graphene nuclei are associated to the copper facets. The graphene islands with a 6 cusps shape corresponds to a Cu (310) facets whereas the islands with 4 lobes corresponds to Cu (221) facets [Mea, 2013]. Later in the discussion we return to present some statistic data considering the growth on the different facets. Increasing the pressure to 15 Pa results in the complete cover with high quality monolayer graphene as we can confirm by the Raman spectroscopy (Figure 4.2-1b) [Hong, 2013]. The nucleation density in this case is 12 nuclei/10000 μm^2. At 17.5 Pa of pressure, the graphene islands cover the whole surface without joining to each other (pre-coalescence phase). Only some of them reachs to join (coalescence phase). These images offer indicative proofs of the process through which single layer graphene is grown on a substrate. The nucleation density is 37 nuclei/10000 μm^2 (Figure 4.2-1c). Finally, at 20 Pa we obtain a graphene cover similar to the case of 12.5 Pa (Figure 4.2-1d) but with a considerably lower nucleation density of 5 nuclei/10000 μm^2. In this last case, the islands have an average

area of 30×30 µm^2. This nucleation at first seems too high, considering Figure 4.2-1d and the size of the domains. We have to underline that the lobe´s length dimensions given above correspond to the largest graphene crystals. Although, there are many points in the surface where the nucleation takes place later so the graphene domains grow less. Small domains are the reason that increase the total nucleation density a lot more than what we see in Figure 4.2-1d. Figure 4.2-1e correspond to the same conditions as Figure 4.2-1d. In this figure we can see that the size distribution of the crystals varies a lot.
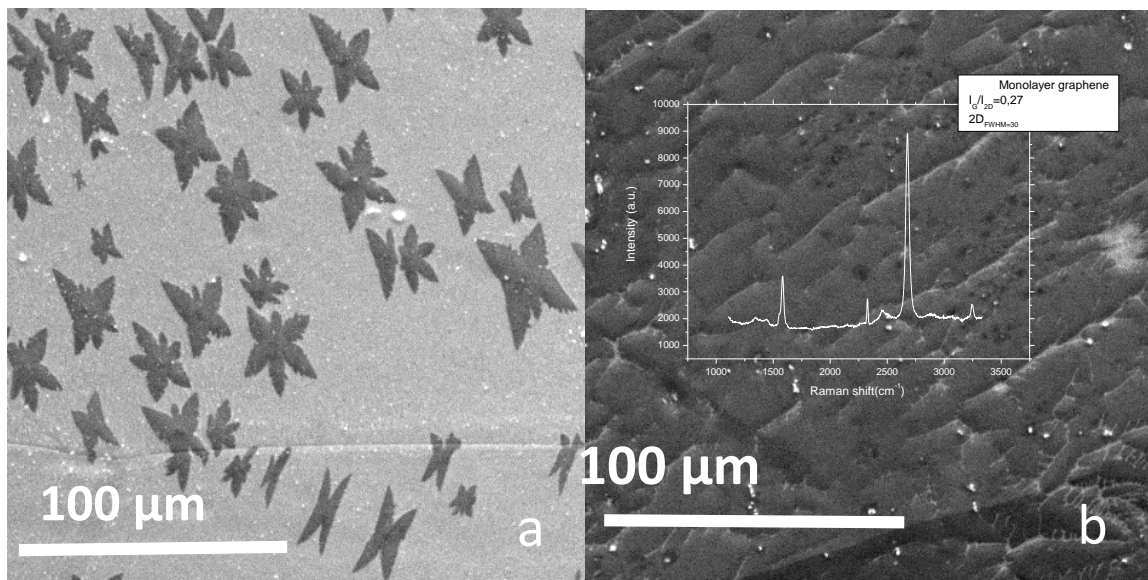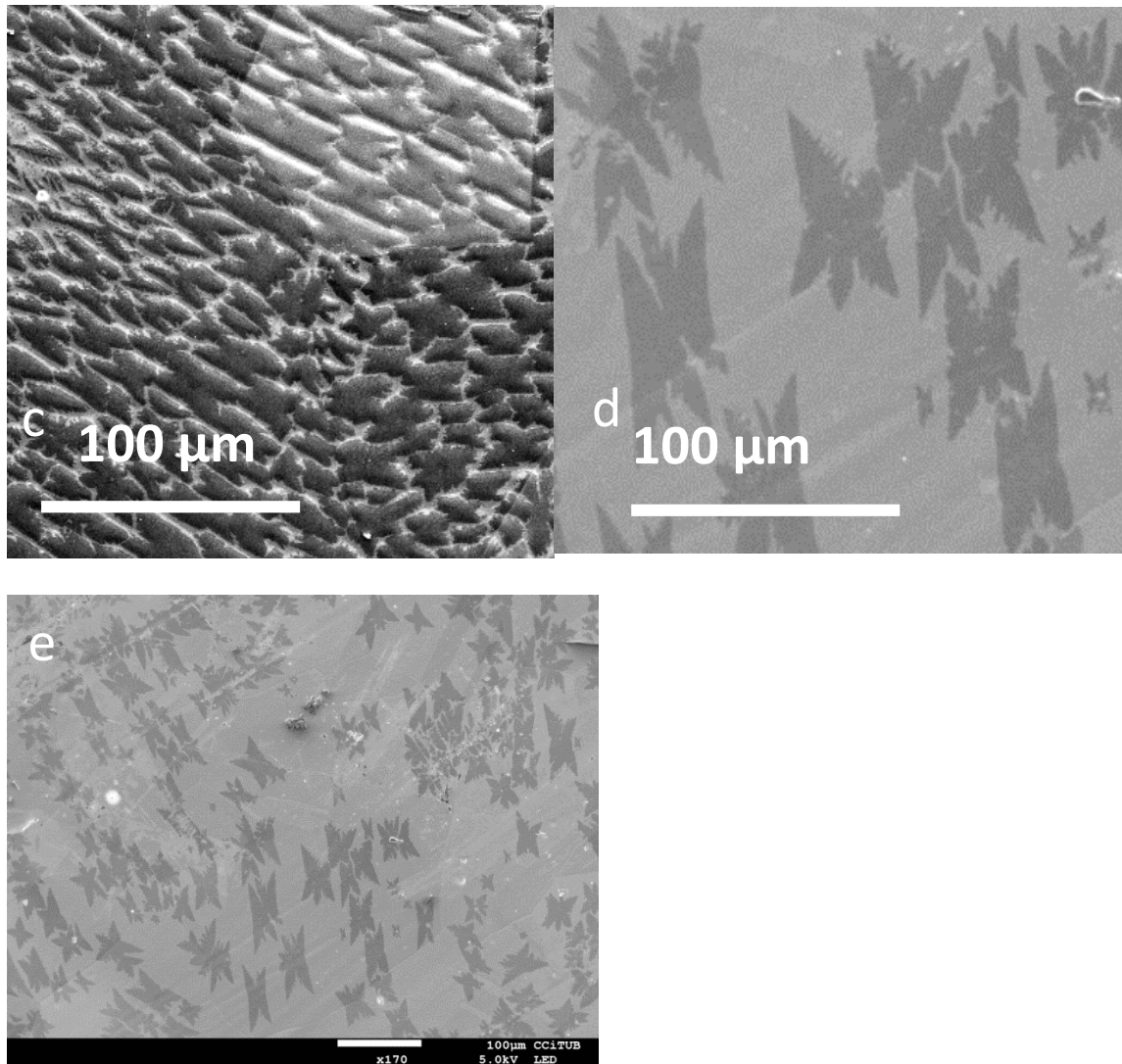
Figure 4.2-1: Scanning electron emission images of graphene grown in stable CH₄/H₂ (5/20 sccm) flows for various pressures. Image (a) corresponds to 12.5 Pa of total pressure [sample 15a1601], (b) to 15 Pa [sample 15a2202], (c) to 17.5 Pa [sample 15a2602], and (d) to 20 Pa [sample 15a1502].(e)same same sample as in Figure (d), in less magnification. The size of the crystals is dependent of the total pressure during the growth process in a not linear way. The plot on (b) provides a Raman spectrum of the continuous graphene film after its transfer on the SiO₂ substrate.

In very few spots of the graphene film a second layer nucleation is formed below the first layer. This is a result of the penetration of the carbon atoms through the graphene overlayer [Wu, 2014]. From the SEM images we can distinguish a favorable state considering the growth under 15 and 17.5 Pa. The nucleation density for these pressures

appears higher even though the flow ratio of CH_4/H_2 remains stable. We can see how the nucleation density affects the size of the graphene crystals. In the samples with high nucleation (at pressures of 15 and 17.5 Pa) the crystals maintain a small size or even they join together forming a large area graphene monolayer. In this case the grain boundaries usually affect the quality of the film. To avoid this it is necessary to achieve a low nucleation density followed by large crystals. This case appears more clearly in the sample grown at 20 Pa (Figure 4.2-1d).

At lower pressures the crystal growth presents a maximum in which they form a continuous film. A few increase of pressure leads to a higher nucleation density so every individual crystal has less surface to grow. As a result the crystalline islands achieve a lower maximum size before they join to the neighbouring crystals. At higher pressure (20 Pa), the low nucleation provides a larger espace to the crystals to grow. With the use of a quadrupolar mass spectrometer (QMS) we have monitored the partial pressure of methane and hydrogen inside the reactor during the growth.

QMS provides partial pressure values dependent of mass owing to different causes, such as, the ionization probability in the ionization chamber of QMS, which, for each mass, depends on the element or radical or molecule nature. Also, CH_4 has a molecular mass of 16 amu equal to monoatomic oxygen. Oxygen from residual gas (water) can contribute to this mass, therefore, we had to check other masses like 18 amu (H_2O) and 17 amu (-OH). Methane also appears craked in the form of $-CH3$, $>CH2$ or $\equiv CH$, giving place to the corresponding peaks in the mass spectrum. Hydrogen partial pressure also shows measurement problems. Hydrogen appears as monoatomic hydrogen, H, and as molecule, H_2. In addition, hydrogen sources are, in our case, from hydrogen inflow, methane inflow and water of the residual gas. These circumstances really make difficult to have an objective measurement of hydrogen and methane.

In the plot of Figure 4.2-2 we can see how the $\Delta P_{H2}/\Delta P_{CH4}$ ratio measured by QMS increases exponentially with the total pressure and does not remain constant as expected. The only change between these measurements was the adjustement of the conductance valve previous to the turbomolecular pump, which permits to reduce the pumping velocity. The effect of reducing the conductance of the valve is not balanced for all the gas species present in the reactor, such as the plots a, b, c and d of Figure 4.2-3 evidence. Hydrogen content increases several times compared to methane content when total pressure increases. This circumstance produces an enhancement of the effect of hydrogen during the growth of graphene.
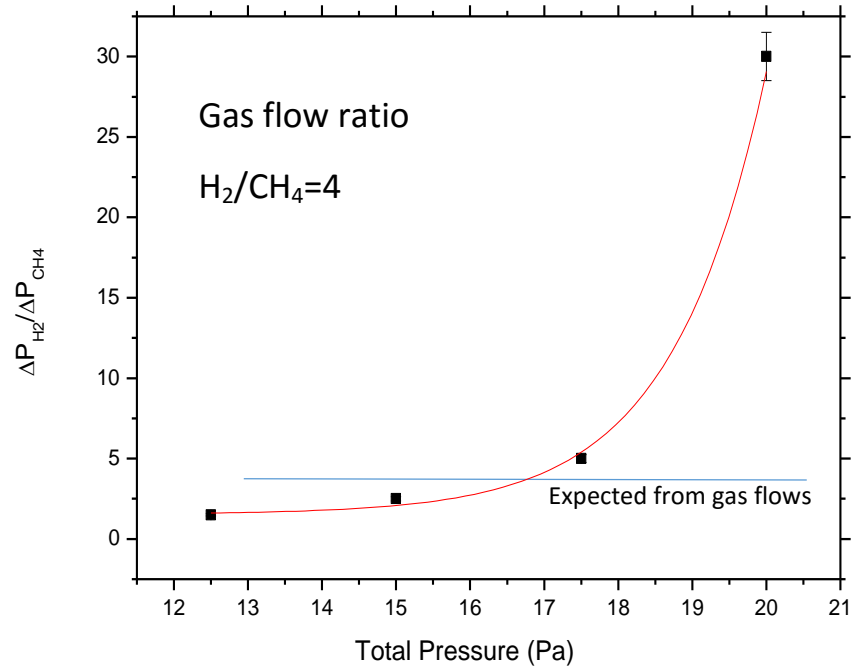
Figure 4.2-2: The plot shows the ratio of the partial pressures $\Delta P_{H2}/\Delta P_{CH4}$ for the different total pressures in which graphene growth was performed. The exponential evolution of the graph becomes evidenced as a result of the higher concentration of hydrogen at higher total pressures. Blue line corresponds to the gas flow ratio. Substrates were treated with hydrogen plasma during 10 min to reduce copper oxide.
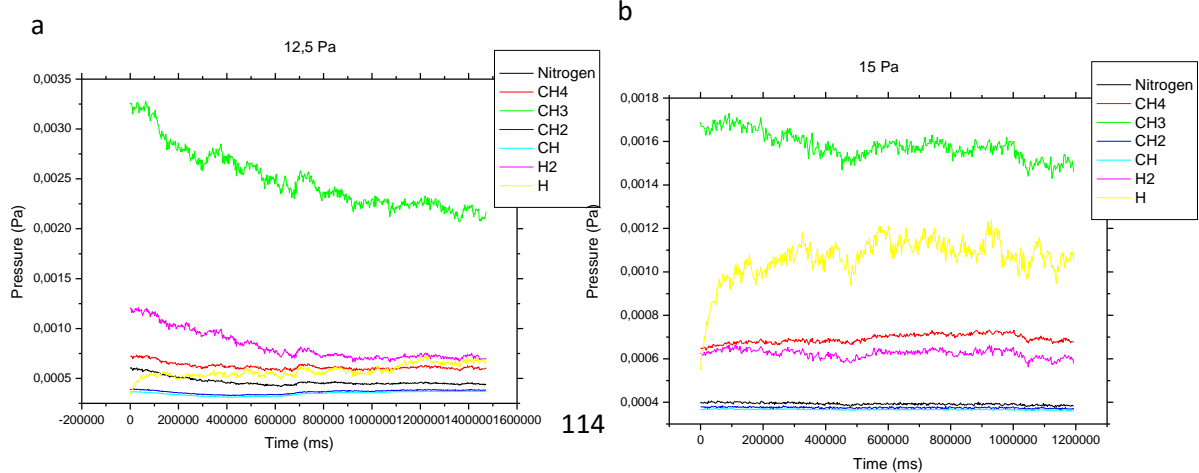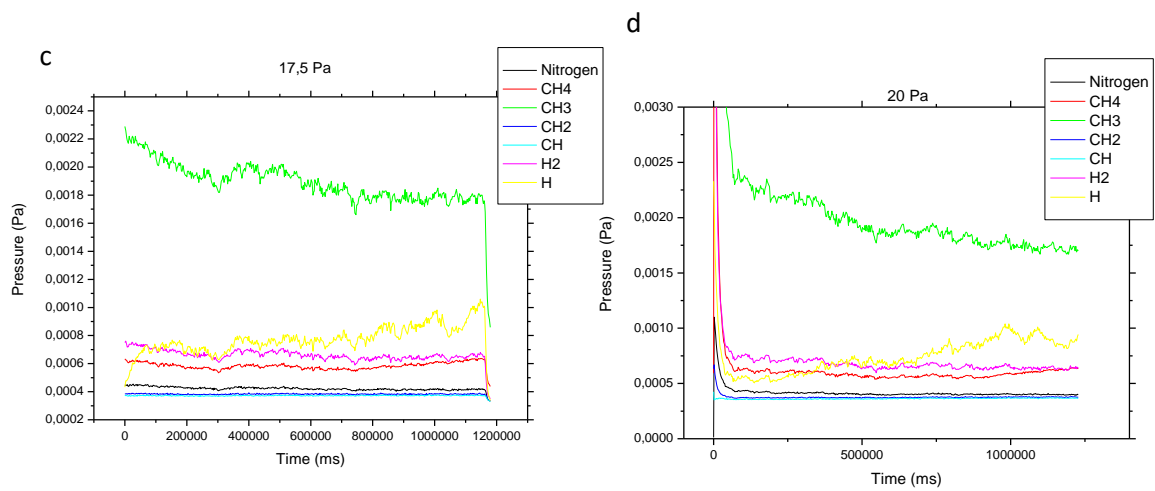
4.2-3: In the graphs we see the evolution of the partial pressure of all CH_x and H_x radicals and nitrogen for a) 12,5 Pa, b) 15 Pa, c) 17,5 Pa and d) 20 Pa of total pressure.

Table 4.2-1 Technological parameters of samples corresponding to the study of graphene growth at different total pressures

Sample	Substrate	Acid treatment	Total Pressure (Pa)	Time (min)	Temperature (°C)	H_2 flow (sccm)	CH_4 flow (sccm)
15a2202	Cu foil	yes	15	20	1040	20	5
15a2601	Cu foil	yes	12,5	20	1040	20	5
15a2602	Cu foil	yes	17,5	20	1040	20	5
15a1901	Cu foil	yes	20	20	1040	20	5

Results of Figure 4.2-2 shows the difficulty of the turbomolecular pump to evacuate the low mass atomic hydrogen because the increase of hydrogen backflow at higher chamber pressure, when the turbomolecular pump operates at lower pressures (due to the closure position of the variable conductance valve).

This is a result of the difficulty of the turbomolecular pump to evacuate the low mass atomic hydrogen. The increased concentration of hydrogen in the 20 Pa growth is responsible of the reduction of the nucleation density of the graphene crystals at this pressure and of its deviation from a linear behavior. When the % coverage is normalized with the lobe´s length^2, we can extract the linear dependence between it and the nucleation density (Figure 4.2-4). Check Annex III for calculations considering the linear dependence between the %coverage normalized with the lobe´s length^2 and the nucl. density.
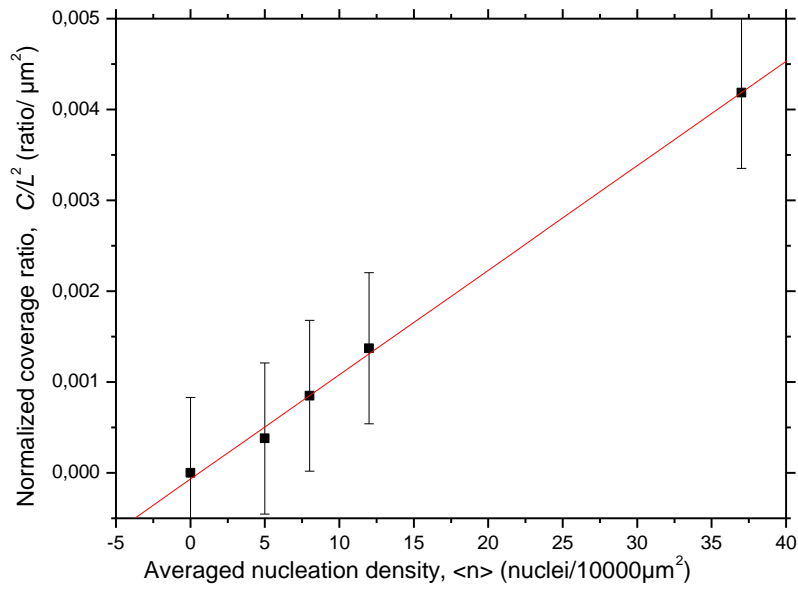
Figure 4.2-4: Diagram demonstrating that once the covered surface is normalized with the lobe´s length^2, it follows a linear dependence with respect to the nucleation density.

Finally in Figures 4.2-5a, 4.2-5b and 4.2-5c are presented the histograms of the lobe's length size distribution measurements (individually of the copper facet) for the growths taking place in 12.5 Pa, 17,5 Pa and 20 Pa.
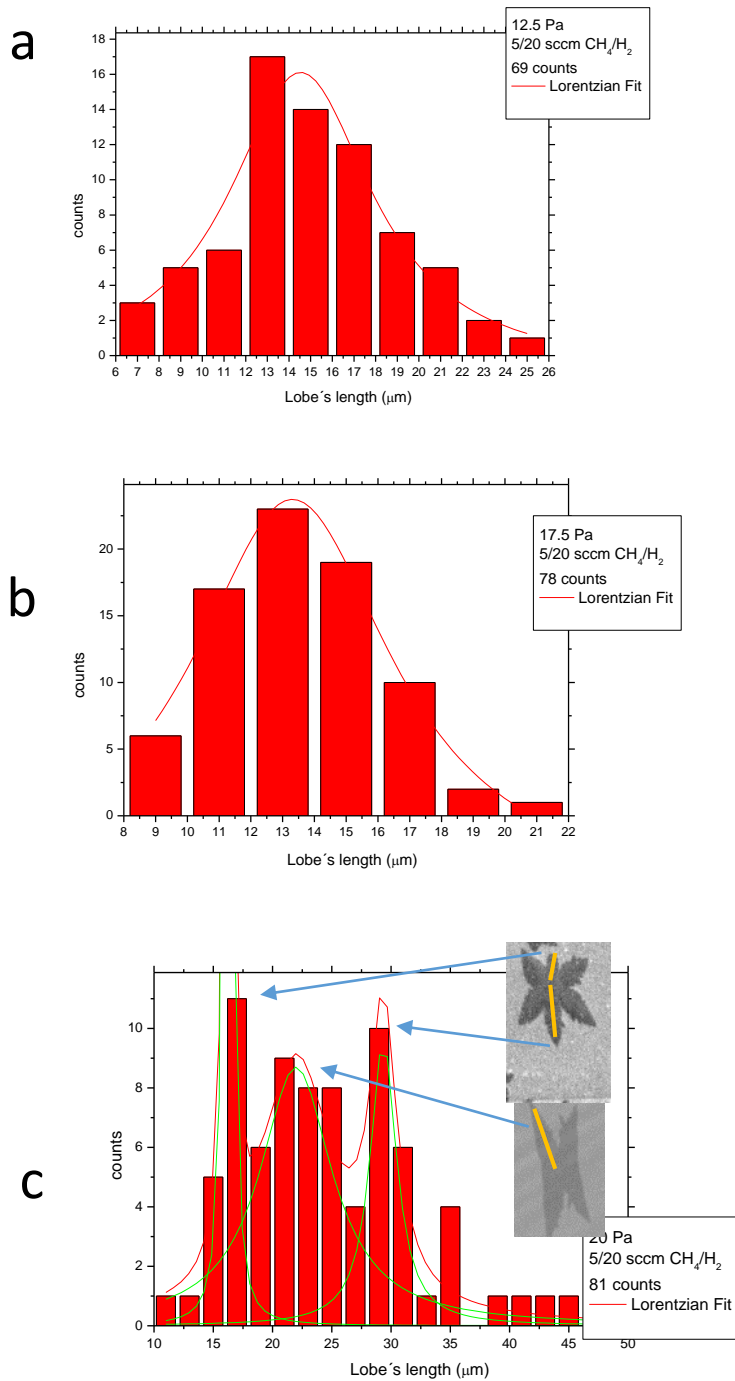
Figure 4.2-5: a) Histogram of the lobe´s length distribution measurements for the growth taking place in 12.5 Pa total pressure. b) Histogram for 17.5 Pa of total pressure. c) Histogram corresponding to the lobe's length distribution at 20 Pa total pressure.

The two-peak distribution in histogram 4.2-5c results of the different growth velocity for the different orientation graphene cusps on the (310) copper facet. At 15 Pa a complete cover of the substrate with graphene takes place, therefore it is not possible to distinguish between the different domains and to provide a histogram for this condition.

4.2-1.2 Nucleation density and copper facet
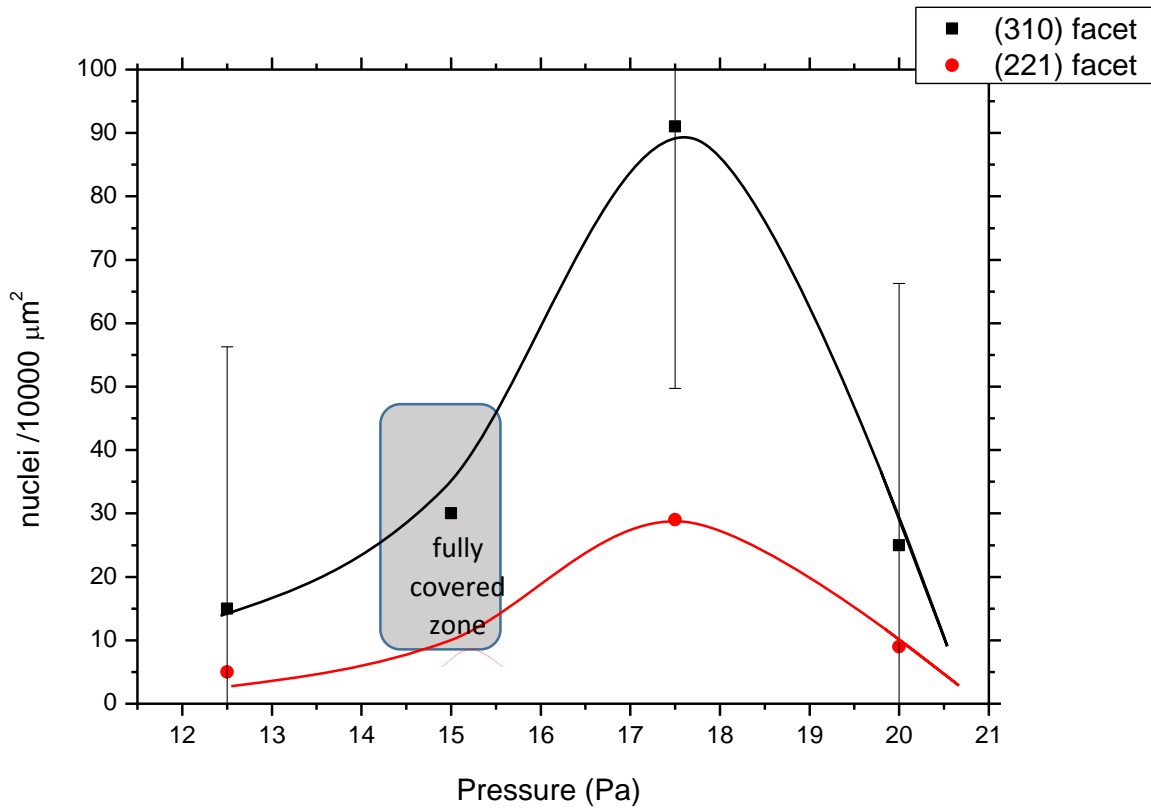
Figure 4.2-6: Diagram presenting the variation of the nucleation density with pressure and in relation to the copper facets (310) and (221). The graphene grown on the facet (310) always presents a bigger nucleation density than graphene grown on the facet (221).

SEM images (corresponding to samples of Figure 4.2-1) provide information about the dependence between the graphene nucleation density and the facets of the copper substrate foil. As the catalytic activity of the different facets varies, we observe a similar variation in the nucleation density. On previous works Wood et al. reported the difference in the nucleation densities on different crystallographic orientations of copper [Wood, 2011]. As we mention earlier, in all our images the dominant graphene crystals are those corresponding to copper facets (310) and (221). Identification is easy to do, following the model presented by Meca et al. [Meca, 2013] In particular, we observe that in all pressures studied in the growth process (corresponding to the images of Figure 4.2-1), the nucleation density of the graphene crystals grown on the copper facets (310) is

significantly higher than that grown on the copper facets (221). At 12.5 Pa, the nucleation density of crystals grown on the facets (310) is 15 nuclei/10000 μm^2. Crystals grown on the facets (221) present a nucleation density of 5 nuclei/10000 μm^2. Similar or even wider differences were observed for the other growth pressures. At 17.5 Pa the nucleation density is 91 nuclei/10000 μm^2 on the facets (310) and 29 nuclei/10000 μm^2 on the facets (221). Finally, at 20 Pa of pressure the nucleation density is 25 nuclei/10000 μm^2 on the facets (310) and 9 nuclei/10000 μm^2 on the facets (221). At 15 Pa is not possible to distinguish the morphology of the graphene crystals since they join to each other and fully cover the substrate, The nucleation at this pressure is about 30 nuclei/10000μm^2 as determined considering the density of boundaries from Figure 4.2-1b. It corresponds to nucleation without taking under consideration the copper orientation. The results are presented in Figure 4.2-6. They indicate that the facet (221) is preferable to grow graphene films with the lower possible number of grain boundaries.

4.2-1.3 Rate of coverage

In addition, we measure the graphene total rate of coverage of the surface for each case to obtain a more complete record of the growth process. We use the *ImageJ* program to extract this information from the SEM pictures. Figure 4.2-7 shows that the rate of coverage follows the same fluctuation as the partial pressure ratio, $<P_{H2}>/<P_{CH4}>$. The rate of coverage varies from low percentages for low nucleation densities (15% and 40% for 12.5 Pa and 20 Pa respectively) to very high ones for the higher densities (82% and 100% for 17.5 Pa and 15 Pa, respectively).

a

b
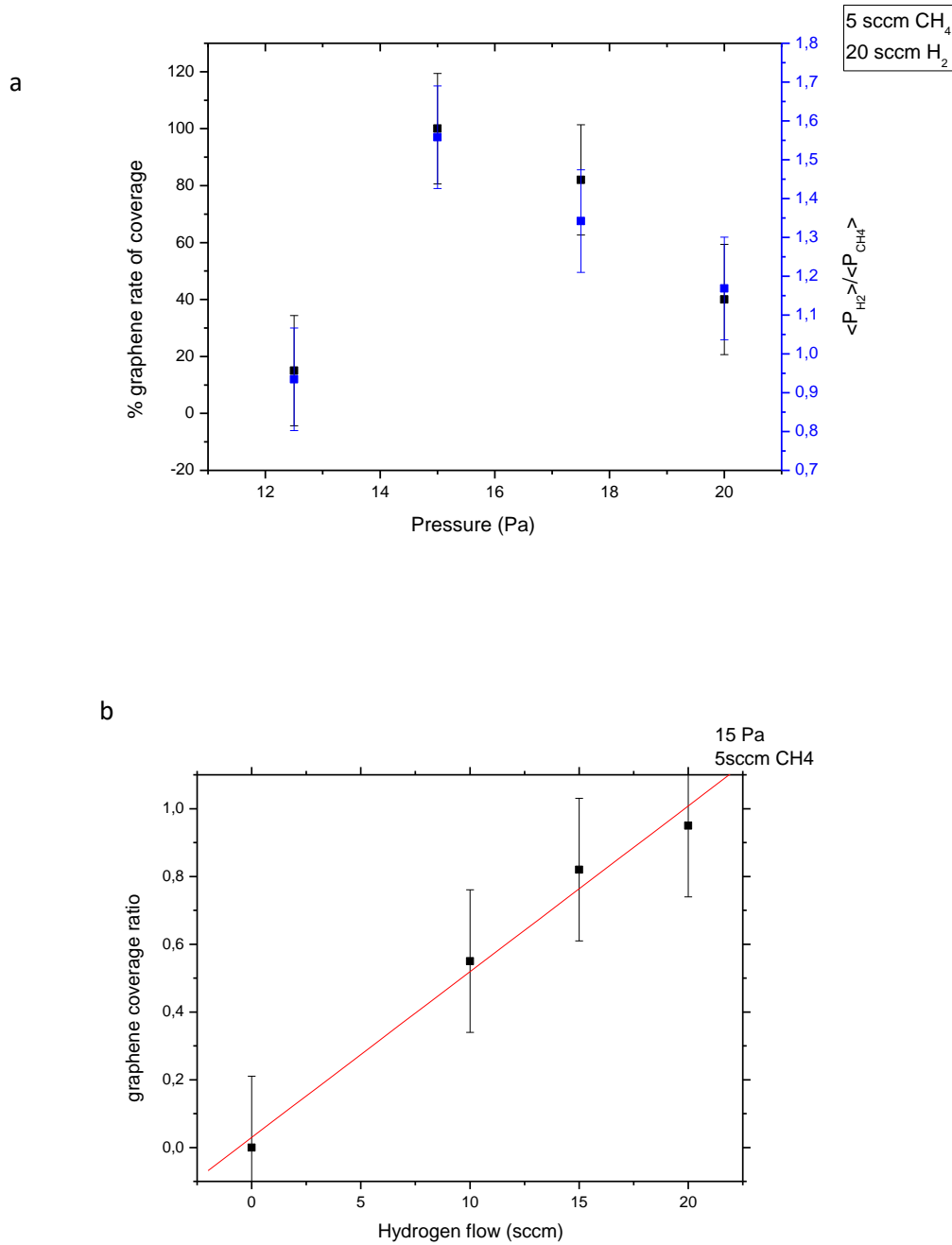
Figure 4.2-7: a)On the left Y axis we see the graphene rate of coverage of the surface as a function of the total pressure. The graph follows the fluctuation of the partial pressure ratio, <P_{H2}>/<P_{CH4}> and a similar fluctuation of the nucleation density. On the right Y axis we see the <P_{H2}>/<P_{CH4}> ratio of the average relative pressure values as a function of time, for the different total pressures. The match in the variation of the values between the two graphs is a clear evidence of the importance of hydrogen in the graphene growth. b) Plot demonstrating the relation between the <PH2>/<PCH4> and graphene coverage ratio.

 We can distinguish that the graph follows the fluctuation of the nucleation density and not this of the graphene crystal size (check also Figure 4.2-8).
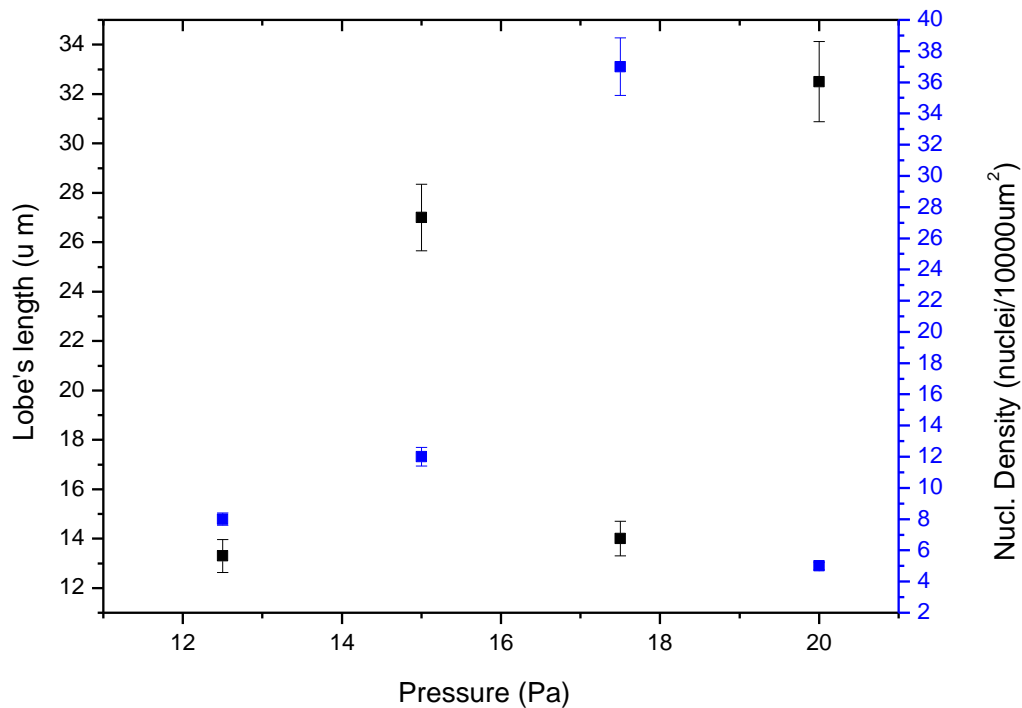
Figure 4.2-8: Diagram presenting the effect of the total pressure during the growth to the graphene lobe's length or bidimensional crystal size (black squares/left axe) and to the nucleation density (total values without considering the crystalline facets) of the graphene flakes in the copper substrate (blue dots/right axe).

 On the right axe of the same plot (Figure 4.2-8) we present the $<P_{H2}>/<P_{CH4}>$ ratio of the average relative pressure values as a function of time, for the different total pressures. The plot reveals that the desired low nucleation density (about 15-25 nuclei/10000 µm²) appears at 12.5 and 20 Pa of total pressure. Although only at 20 Pa this is followed by the growth of large graphene domains. In the intermediate pressures the nucleation density is much higher allowing the full cover of the substrate by graphene. At 15 Pa the crystal growth presents a maximum when they join to each other to form a continuous film. A low increase of the pressure leads to a higher nucleation density so, every individual crystal has less surface to grow. As a result, every individual crystal achieves a lower maximum size before it joins with the neighbouring crystals. At a higher pressure

(20 Pa) the low nucleation provides a larger area to the crystals to grow.The total match in the variation of the values between the two plots of Figure 4.2-7 reveals the important role of the hydrogen in the coverage of the surface with graphene. Moreover, it reveals that the partial pressure can be a more efficient evidence than the flow when we want to characterize the effect of the hydrogen. Outside this range of pressures, graphene crystals were not grown or were grown anisotropically etched. As we can see in Figure 4.2-9a, a growth in 10 Pa under same conditions of flow and temperature does not allow a successful nucleation of graphene domains. Only some domains of amorphous carbon are visible by the SEM images. When a higher growth pressure was used (30 Pa, Figure 4.2-9b), it resulted in the formation of a randomly etched, not continuous graphene film. The crystals are neither oriented nor ordered as a result of the increased etching effect. As explained by Vlassioul et al [2011], hydrogen can play a dual role in graphene growth. It acts as a cocatalyst in formation of active surface bound carbon species (CyHx)s required for graphene growth. In low pressure (10 Pa), the low presence of hydrogen is not sufficient to catalyze the graphene nucleation. On the same time, hydrogen controls the grains shape and dimension by etching away the "weak" carbon-carbon bonds. The high presence of hydrogen in higher pressures (30 Pa), results in a reinforced etching effect. Graphene nucleation, the growth rate, and the termination size of grains are affected by competition of these two processes."
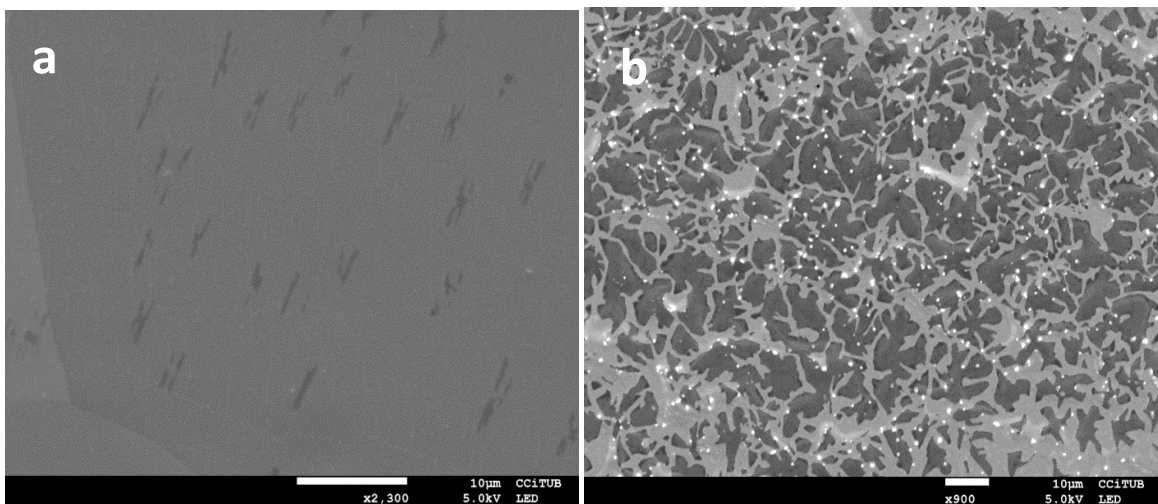
Figure 4.2-9: Scanning electron microscopy images of CVD growths run at:a) 10 Pa [sample 15a1401], not enabling the graphene nucleation and b) 30 Pa [sample 15a1402], leading in broken shaped crystals, result of the anisotropic etching. The scale in both images is 10 µm.

4.2-1.4 Hydrogen effect

Evaluating the hydrogen effect, we can see that in the growth performed with 10 sccm of hydrogen flow the graphene domains appear not homogeneous as a result of the anisotropic etching (Figure 4.2-10a). The lobe's length is 30.5 μm. By increasing the hydrogen flow to 15 sccm it results in the growth of symmetrical dentritic graphene domains with 30.1 μm of lobe's size (Figure 4.2-10b). The edges of the crystals here do not appear randomly etched as it happens in the case of figure 4.2-10a. At 20 sccm of hydrogen flow all the area of the substrate is covered by graphene crystals (Figure 4.2-10c). The grain boundaries allow us to distinguish that each crystal has 27 μm of lobe's size. In this case, as there are samples that appear randomly etched (Figure 4.2-10a), it is not reliable to compare only the crystal's or lobe's length. We measured the total graphene covered surface in relation with the hydrogen flow. As presented in Figure 4.2-10d, the graphene covered area appears to increase proportionally to the hydrogen flow, coming in agreement to other previous works that associate the graphene domains size growth analog at the hydrogen flow [Vlassiouk, 2011; Yin, 2014].
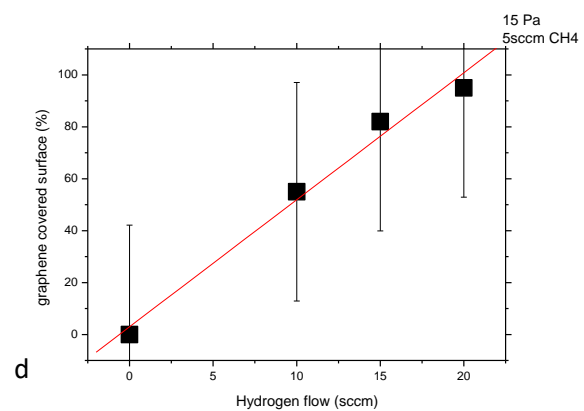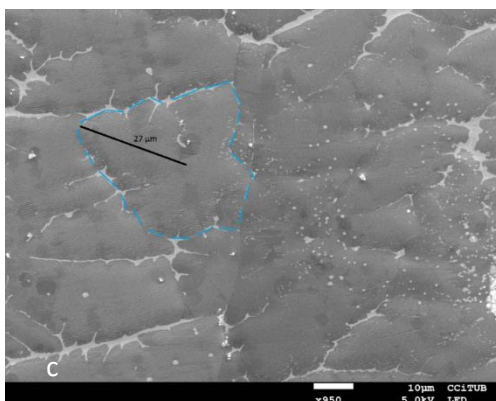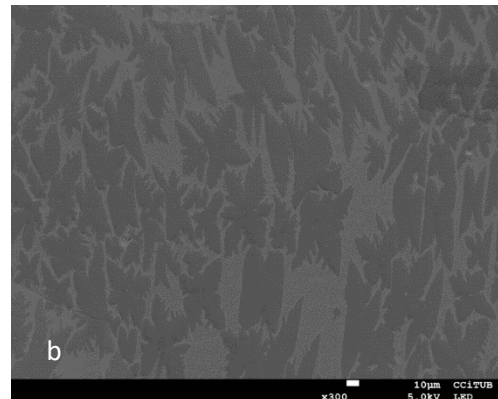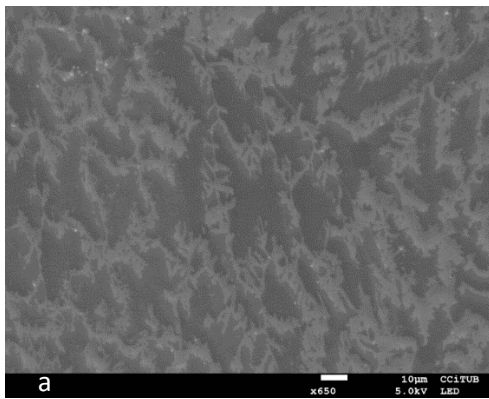
Figure 4.2-10: Scanning electron Microscopy images of graphene grown under 5 sccm of methane, at 15 Pa total pressure, in 1040 °C, during 20 min. Varying the hydrogen flow, at a) 10 sccm [sample 15b1101], b) 15 sccm [sample 15b1602], c) 20 sccm [sample 15c0502] affects the morphology of the film. In figure c) some parts where second nucleation has occurred are shown. The scale bar is in all the images 10 µm. In figure d) the plot demonstrates the % graphene covered area. The highest coverage, ~95% corresponds to the highest hydrogen flow.

The % covered area is 55 % for 10 sccm of H_2 flow, 82% for 15 sccm of H_2 flow and 95% for 20 sccm of H_2 flow. Hydrogen can control the graphene shape by etching away the weak carbon-carbon bonds. Because of this mechanism, a higher hydrogen flow is favoring the graphene growth, enabling the full coverage of the substrate as we see in Figure 4.2-10c [Vlassiouk, 2011]. In our work we differentiate the hydrogen flow from the total pressure and study them separately. This allows us to better understand the effect of the two parameters and to design more efficient growth processes. We see that the effect that each parameter performs is different. The hydrogen flow appears to have a strong etching effect that affects mostly the morphology of the domains because of the anisotropic etching it performs and secondary the size of them. This has been confirmed after the experiments executed to control the effect of time.

4.2-1.5 Growth time effect

The turbomolecular pump installed in our chamber can achieve a vacuum level down to the order of 10^{-5} Pa. This pump cannot sufficiently evacuate the hydrogen atoms due to their small mass and high thermal velocity. Result of this is that in a constant hydrogen flow, the partial concentration of hydrogen is increasing with the time, causing a strong etching effect on the grown graphene evidenced in the SEM images of Figure 4.2-11. These figures show the evolution of the graphene varying from single crystals of 20 µm lobe's length after 10 min of growth (Figure 4.2-11a), full cover of the substrate after 20 min of growth (Figure 4.2-11b), partially damaged graphene film after 30 min of growth due to the dominant etching effect of the hydrogen (Figure 4.2-11c) until the serious damage of the film after 40 min of growth (Figure 4.2-11d).
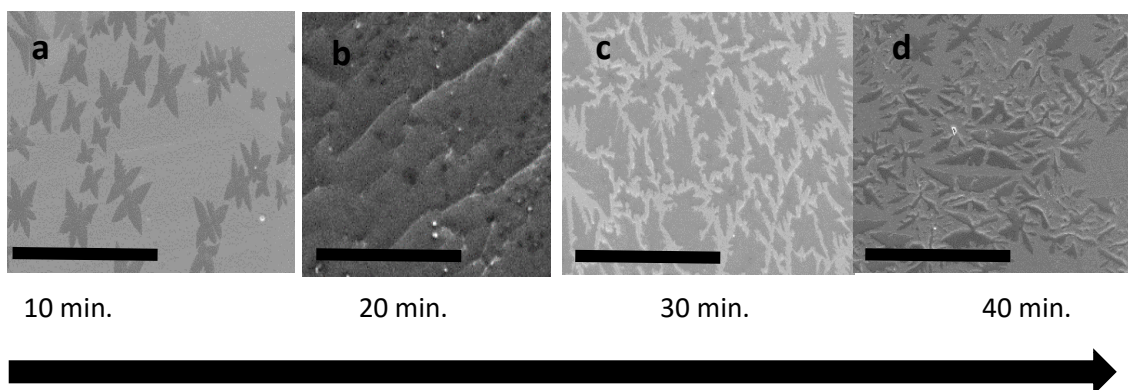
Figure 4.2-11: Scanning electron microscopy images of graphene grown under 15 Pa with a 5/20 sccm methane/hydrogen flow rate varying the time. a) After 10 min of growth [sample 15c2302], 20 μm lobe's length crystals are obtained. b) After 20 min of growth [sample 15c0502], copper substrate appears fully covered by graphene. c) After 30 min of growth [sample 15c1601] the film appears partially damaged. d) After 40 min of growth [sample 15c3001] most of the graphene have been etched away from the catalyst substrate, result of the hydrogen increased concentration inside the chamber. The scale bar is always of 100 μm.

Due to the hydrogen etching the graphene is removed from most parts of the catalyst copper substrate. In all the growth experiments 5/20 sccm methane/hydrogen flow rate at 15 Pa of total pressure and 1040°C of oven temperature were used. Previous works have demonstrated a two-step growth process for the full graphene coverage. At lower methane flow and low methane partial pressure a low nucleation density results. In the second step the methane flow and partial pressure is being increased, promoting a faster growth and filling of the gaps [Li, 2010]. Based on our observation we believe that a one-step growth can sufficiently results in a complete coverage of the surface with large area graphene crystals, followed by a low nucleation density. The correct pressure selection permits the total coverage with the lowest nucleation density. The careful evaluation of the hydrogen effect permits the gas to act as a co-catalyst favoring the growth, without applying a catastrophic etching.

4.2-1.6 Growth on larger copper surface

In all the previous experiments the copper foil piece loaded in the furnace was of 2x2 cm^2. To control if the same synthetic conditions are valid for larger pieces we used a piece of 4x3 cm^2 and run a synthetic route designed to grow a continuous graphene film.

The extended Raman measurements show that monolayer graphene was grown in all the area of the surface, both in the center as well as in the edges of the foil, in both faces of it (Figure 4.2-12a). A green laser was used for this characterization. The background noise owing to the copper photoluminescence was extracted. In the up side of the foil, the G position appears at 1578 ±3 cm^{-1} and the 2D at 2671 cm^{-1}. The I_G/I_{2D} is 0.27 ± 0.03 with a FWHM of 30 cm^{-1}. These data (Table 4.2-2) confirm the single layer nature and the high crystallinity of the grown graphene as they come in agreement with the known results concerning graphene grown on copper foil [Costa, 2012]. The spectra acquired from the back side of the foil reveal the growth of same quality graphene there as well (Table 4.2-2). Then the graphene was transferred on top of glass (with quartz on top) and SiO$_2$ (Figure 4.2-12b) with a variant of a technique that is based on the electrochemical delamination of the graphene from the copper foil [Wang, 2011]. This technique will be presented in a future work. After the transfer of the graphene film to glass, the G peak appears at 1575 cm^{-1} and the 2D peak appears blue shifted at 2679 cm^{-1} with a 67 cm^{-1} FWHM, about 5 cm^{-1} more than the measurements taken directly to the metal catalyst. The I_D/I_{2G} ratio appears increased as well. These shifts can have their origin to edges, dislocations, cracks or vacancies in the sample that cause the so called self-doping to the graphene [Das, 2008]. They can possibly be induced during the transfer process. After the transfer a D peak appears at 1350 cm^{-1}. In pristine graphene the D peak can appear because of some disordered structure.

Table 4.2-2: Table presenting the Raman results. The G and 2D position as well as the I_G/I_{2D} ratio are very close in all the area, in both faces of the foil. After the transfer to SiO_2 the 2D peak appears muche narrower (the FWHM reduces aprox. 20 cm^{-1})

Sample	2D position (1/cm)	G position (1/cm)	I_G/I_{2D}	2D FWHM (1/cm)
Cu foil	2671	1582	0.38	59
Cu foil	2668	1575	0.40	64
Cu foil	2674	1578	0.42	65
Cu foil	2671	1575	0.45	60
Cu foil	2668	1575	0.44	63
After transfer on glass	2679	1575	0.64	67
Back side	2663	1578	0.43	65
After transfer onSiO_2	2676	1582	0.40	35
After transfer on SiO_2	2676	1582	0.48	40
After transfer on SiO_2	2676	1582	0.03	37
After transfer on SiO_2	2671	1575	0.27	30
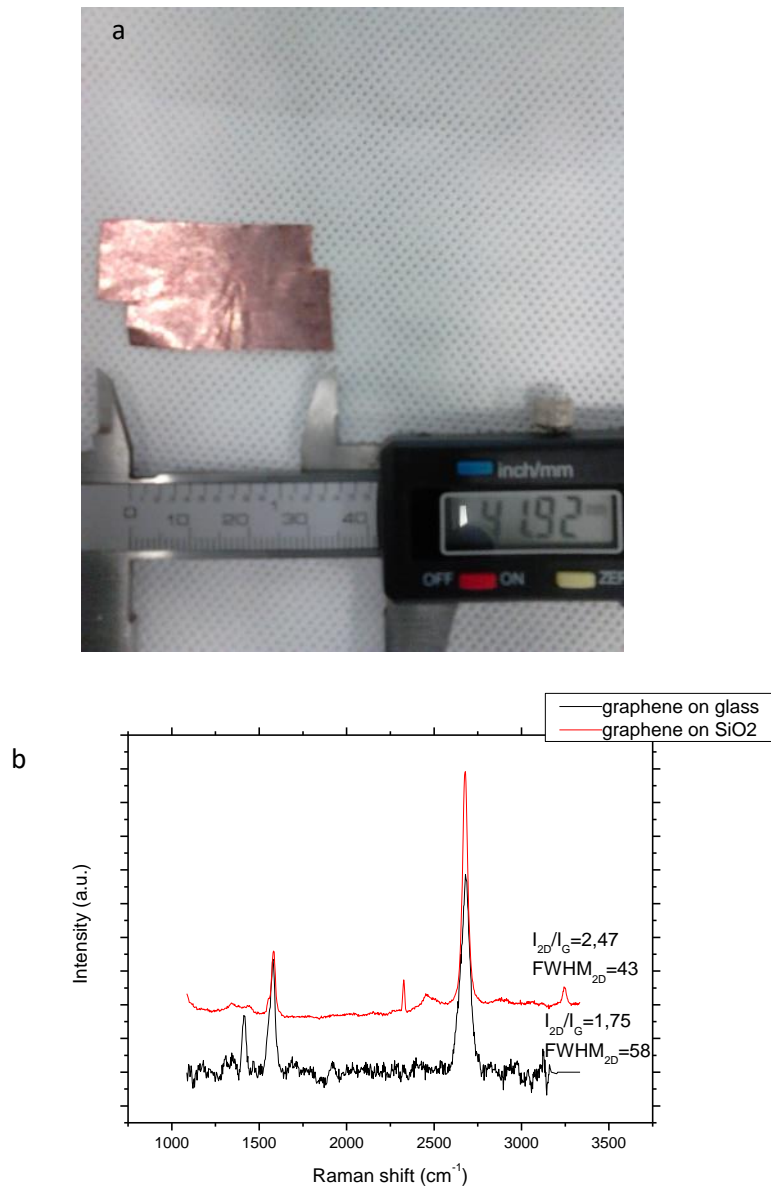
Figure 4.2-12: a) Image of the copper foil [sample 15d2101] piece loaded in the oven marked with the spots where the Raman measurements are taken. b) Raman spectra after the transfer of the graphene film to glass (with thermally grown quartz on top)(black line) and on SiO₂.(red line)

4.2-2 Effect of a balanced concentration of hydrogen on graphene CVD growth

Scanning Electron Microscopy (SEM) was used to evaluate the moprhology of the obtained graphene. The micrographs of Figures 4.2-13a, 13b and 13c where taken with a JEOL JSM 7100F microscope. The electron beam has an energy of 5keV. Figure 4.2-13a shows graphene crystals obtained in sample A, similarly to the obtained by Vlassiouk et al. [Vlassiouk, 2013]. These crystals show different morphologies. There are crystals with a ''butterfly'' shape (blue circle) and others formed with four lobes and dentritic extensions (red circle). Shape and symmetry of graphene crystals depend on the orientation of the copper crystalline domain of the substrate. According to the model of Meca et al., the four lobes with dendritic extension crystals are being grown on Cu (100) planes, whereas the crystals with the ''butterfly like'' shape are being grown on Cu (221) planes [Meca, 2013] . The pictures were taken directly on the copper substrate without any previous transfer. The lobes of the crystals have about 30 µm of length and a growth velocity of 1.5 µm/min. The growth ratio is independent of the crystal morphology. The growth of crystals with the four lobes with dentritic extensions appears to be the more favourable morphology. The crystals present a medium nucleation density in most parts of the substrate as SEM picture shows in Figure 4.2-13a. Large areas of the substrate are not covered by graphene. Therefore, longer growth time seems to be necessary.   We consider that a process provides a high-quality graphene when, on the substrate, only grows "monolayer graphene".

In sample B (Figure 4.2-13b), with double growth process time and same deposition conditions than sample A (in particular, gas flows), we have observed that the size of the graphene flakes does not change appreciably, but the nucleation density increases significantly. Although now, flakes do not appear with such regular shapes. This phenomenology seems a clear effect of the presence of hydrogen species bombarding the carbon adatoms with high mobility. Then, carbon adatoms would move along the hot surface and on the boundaries of the graphene islands. In this hypothesis, hydrogen bombardment would remove the carbon atoms which are not well positioned in the energetically favourable sites. Furthermore, this phenomenon seems to be associated with an effect of anisotropic etching of hydrogen along the crystal direction of polycrystalline copper substrate during the growth of graphene [Zhang Y., 2012; Zhang X., 2013] (Figure 4.2-13b).

The white spots observed in the images of Figure 4.2-13b correspond to oxides formed on the surface [Li, 2009]. Despite the plasma etching and the high pre-vacuum, in the

order of 10^{-4} Pa, to ensure the highest pure conditions, at high temperature (above 1000ºC) even the smallest amount of oxygen can be highly active. This may originate from impurities in the walls of the reactor and the inside of the oven. Even after a precise cleaning of the oven it was not possible to completely eliminate these oxides. Characterising the oxides by EDX analysis revealed that they are SiO_x (Figure 4.2-. Lately Kasap et al. has also mentioned this observation [Kasap, 2015]. These silicon particles are introduced to the copper foil from the quartz tube during the heating process. It has been studied in other works that they can function as nucleation center and catalyst for the graphene growth [Kim, 2013]. In our SEM images it does not appear any matching between the nucleation center of each graphene crystal and the SiO_2 particles, therefore we do not consider that they affect the process.

Taking into account these observations, we performed a graphene growth (sample C, figure 4.2-13c) during 40 min under the same pressure and growth rates, but pausing the hydrogen flow after the first 20 min had passed (Table 4.2-1). All the growths have been performed inside the same quartz tube. The methane flow remains open during the whole time (40 min). To conclude this growing process, in phases, we reduce the hydrogen concentration in the chamber during the last 20 min, not managing although to fully evacuate it. This is a result of the inability of the turbomolecular pump to sufficiently evacuate low mass atoms as hydrogen. In the range of pressures that we have used, the hydrogen concentration increase had been balanced by the reduction of the hydrogen flow in order to keep constant the hydrogen concentration.
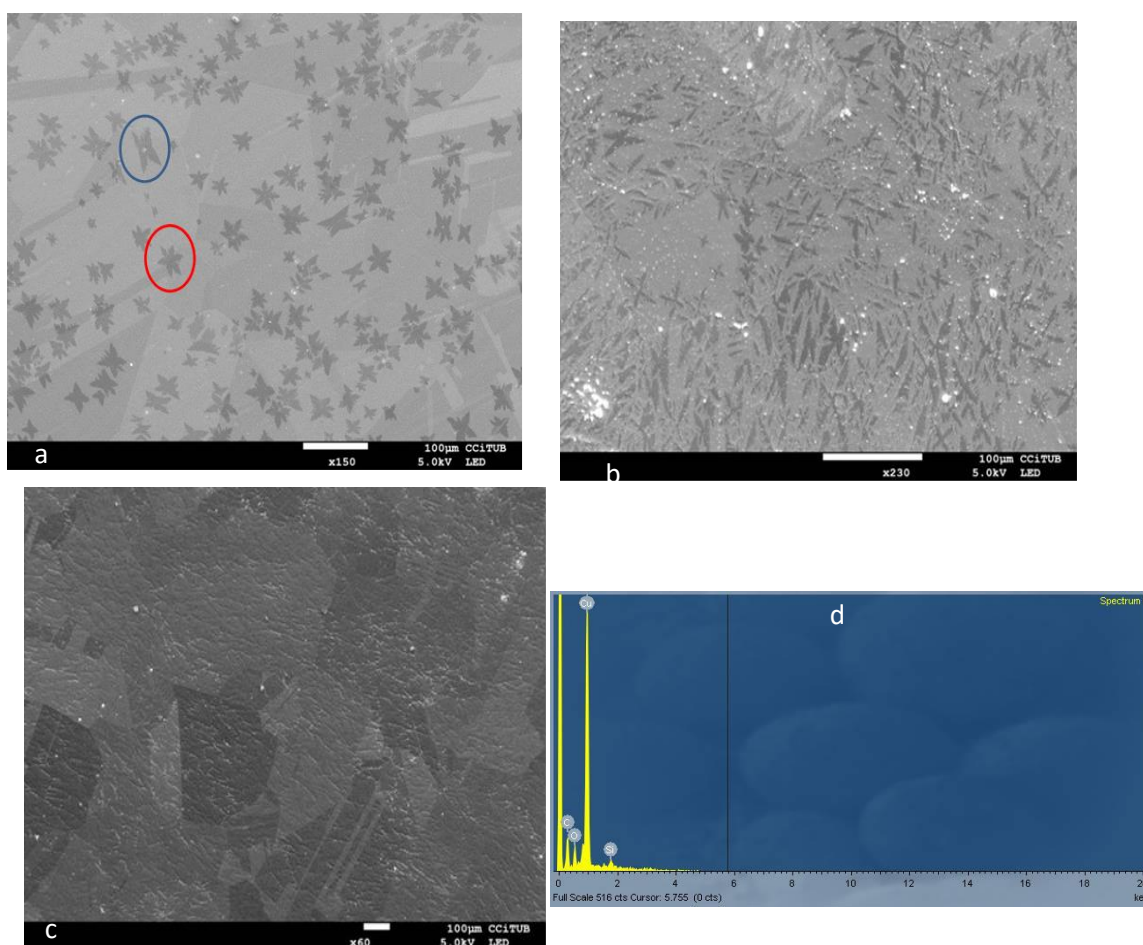
Figure 4.2-13: Scanning electron microscope pictures of graphene domains on copper foil after (a) 20' growth. 4 lobes with dentritic extension (blue circle) and butterfly like (red circle) graphene islands are grown with a size of 40 µm. (sample 15a2702), (b) 40 minutes growth. The nucleation density is higher but the domains are etched because of the high hydrogen concentration (sample 14k1401), (c) 40' growth with reduced hydrogen flow. During the first 20' of growth, the hydrogen flow was 20 sccm and in the rest of process H2 flow was stopped. This method avoids the etching observed in the previous sample. Most of the substrate appeared covered with graphene (sample 14k1301). The scale bar is always at 100 µm.(d)EDX analysis of white spots of Figure (b)

Table 4.2-1: Experimental conditions for growing graphene: of precursor flows, growth time, pressure and substrate pretreatment and resulting crystal size.

Sample	Methane flow (sccm)	Hydrogen flow (sccm)		Total time (min)	Pressure (Pa)	Pre-treatment	Crystal Size (µm^2)
A	5	20		20	20	Hydrogen plasma etching	~50
B	5	20		40	20	Hydrogen plasma etching	~60
C	5	First 20 min, 20sccm	Last 20 min, 0 sccm	40	20	Hydrogen plasma etching	~60 (Full cover)
D	5	20		20	20	Chemical etching	Bad shaped

The hydrogen amount that remains in the chamber is enough for smoothly performing the effects induced during the graphene growth. Hydrogen has a double role during the graphene growth. It activates the surface-bound carbon that leads to monolayer growth and function as an etching reagent that controls the size and morphology of the resulting graphene domains. A careful design should ensure that the flow and concentration of the gases is suitable to facilitate the growth of graphene. If the concentration of hydrogen is too high, as we see in Figure 4.2-13b, the formed graphene can easily be taken away by the etching activity of hydrogen flow. The reduced hydrogen concentration of the sample C avoids this, permitting the total coverage of the surface by graphene [Vlassiouk, 2011] SEM images show the complete coverage of the substrate with graphene (Figure 4.2-13c). Only in few parts, the grain boundaries are visible. The boundaries affect the quality of the film. In these parts we can distinguish that the graphene domains forming the continuous graphene film have the same average size as in the samples A and B. This observation comes in contrast to previous ones which suggests that the absence of hydrogen during the growth step leads to smaller graphene domains [Jin, 2014]. We consider that in a stable total pressure the graphene domains size remains stable and that the hydrogen variation affects the etching mechanism and therefore the domains shape. The inflows of methane and hydrogen to the reactor as a function of the growth time for samples B and C are plotted in Figure 4.2-14. The hydrogen flow is 0 for the second step of the growth of sample C. This moderates the hydrogen etching effect, resulting in an increase of the graphene surface coverage from 25% to 99% of the total surface. The graphene coverage was measured by the image processing program, ImageJ.
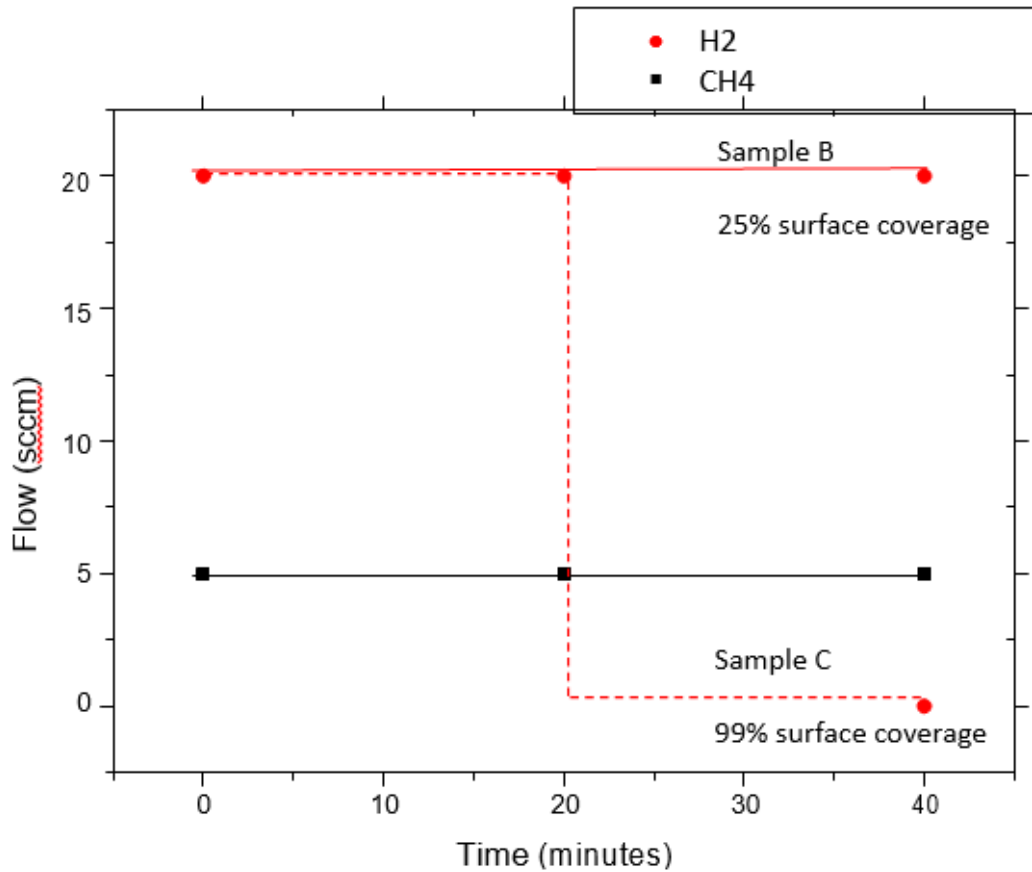
Figure 4.2-14: The flows of methane and hydrogen are plotted as a function of the growth time. Meanwhile methane flow remained stable at 5 sccm for samples B [sample 14k1401]and C [sample 14k1301], hydrogen flow keept stable only for sample B at 20 sccm. After 20 min of growth, hydrogen flow of sample C was stopped. This moderates the hydrogen etching effect, resulting in an increase of the graphene surface coverage from 25% to 99% of the total surface.

The results of Raman spectroscopy, performed with a Jobin-Yvon LabRam HR 800 system, are shown in Figure 4.2-15. The Raman spectrum in figure 4.2-15a shows G and 2D peaks with an intensity $I_{2D}/I_G{\sim}1.5$ (red and green colored spectra, corresponding to graphene grown in the two different faces of copper foil).This confirms the high quality, monolayer thickness of graphene [Ferrari, 2006] grown for the above conditions.

Although, as the spectrum is taken directly from graphene deposited on the copper without any transfer process, some background noise in the signal appears because of photoluminescence from the copper substrate. So, a background subtraction during the data analysis was performed to evidence the signal coming from graphene [Costa, 2012]. To obtain an enhanced Raman spectrum from graphene, a common transferring process was followed [Regan, 2010]. A polymer support, Poly(methyl methacrylate) (PMMA), was deposited via spin-coating on top of the graphene/copper substrate. Then, it was immersed into $FeCl_3$ to etch the copper and the graphene/PMMA was transferred onto a SiO_2(90 nm thick)/Si substrate (Figure 4.2-15b) and quartz substrate (Figure 4.2-15a, black colored spectra).   After transferring the graphene from the metal catalyst to SiO_2 substrate, the background noise disappeared and the characteristic peaks appeared sharperand highlighted on the background. The characteristic D+D´´ peak is also visible (Figure 4.2-15b) [Hong, 2013]. The 2D peak appears upshifted with respect to the spectra taken directly from the copper foil. The I_{2D}/I_G ratio now is 2.5. Similar upshifting and ratio increase appears in the spectra obtained from the quartz substrate. Although, a small D peak is visible, possible result of defects introduced in the graphene sheet during the transfer.
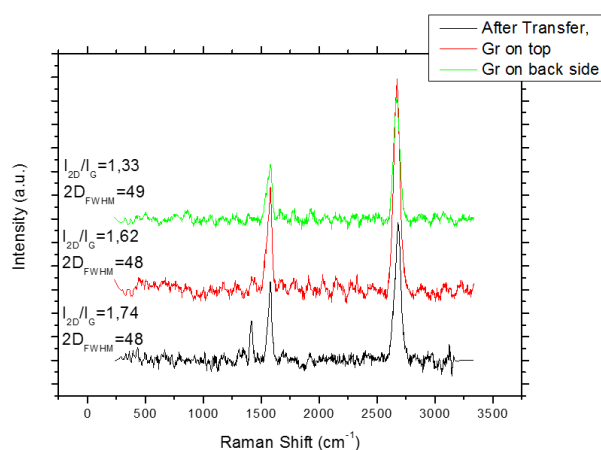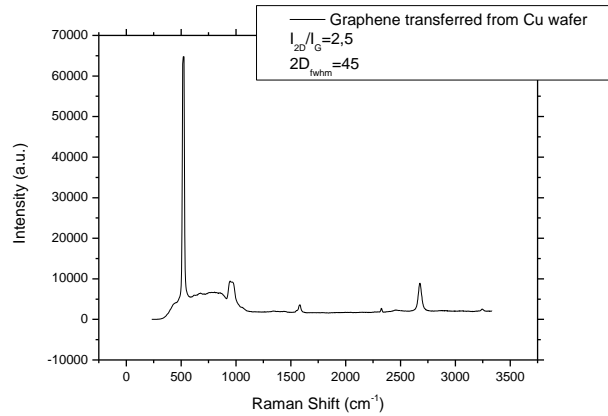
Figure 4.2-15: a) Raman spectra of graphene as growth on copper foil (red line), after transfer to glass (black line) (with thermally grown quartz on top of the glass) and in the back side of the foil (green line. After the transfer a small D peak appears in the spectra, probably a result of defects introduced during the transfer. In the spectra obtained directly in the copper foil the background noise of the copper has been removed. b) This spectra corresponds to graphene after the transfer on top of SiO$_2$/Si. The characteristic 2D´ (3240cm^{-1}) peak is also visible.

The upshifting of the 2D peak after the transfer is a result of the decrease in the stress, as it has been experimentally proved in the recent work of Androulidakis et al. [Androulidakis, 2015]. All the results considering Raman spectra, the G and 2D position, the intensity ratio between them and the 2D$_{FWHM}$, are presented in Table 4.2-2.

Table 4.2-2: The data of the Raman spectra regarding the G and 2D position, the intensity ratio between them and the 2D FWHM are presented.

Sample	G position (cm^{-1})	2D position (cm^{-1})	I$_{2D}$/I$_G$	2D$_{FWHM}$ (cm^{-1})
Graphene on copper	1578	2671	1.62	48
After transfer to SiO$_2$	1582	2679	2.5	45
After transfer to quartz	1587	2679	1.74	48

The transfer process should be done carefully to ensure that the graphene film obtained is uniform and without damage. The AFM image (Figure 4.2-16) confirms the morphology of the crystal. It has been analyzed with the NOVA software. The software includes tools which allows to obtain the root mean squared roughness of the surface. The lobes of the butterfly-like domains are visible at darker color, similar to the ones observed by SEM. From the color scale it seems that the graphene domains are dipped inside the surface. We suppose as an explanation that a thin PMMA layer remains on top of the SiO$_2$ + graphene despite the cleaning, affecting the AFM measurement. The

PMMA also affects the roughness measurement of the graphene domains. The root mean squared (RMS) roughness of the inside white box in figure 7 is 0.78 nm. In other works, CVD graphene presenting a RMS roughness of 4.6nm (after transfer to SiO_2) has been reported [Pirkle 2011]. With a careful PMMA cleaning by annealing at 300 °C, this value could decrease to 0.6 nm [Pirkle, 2011]. The value we obtained is close to this value. Some white spots have their origin in etching or PMMA residues and despite the careful cleaning they are difficult to be completely removed. The homogeneity in the crystal roughness indicates that no second layer of graphene is grown in any part. Some cracks are visible, probably introduced during the transfer process. The image is taken after the transfer of the graphene on top of SiO_2. The enlarged image of the figure shows the profile of a 1x1μm area that is within a domain of graphene.
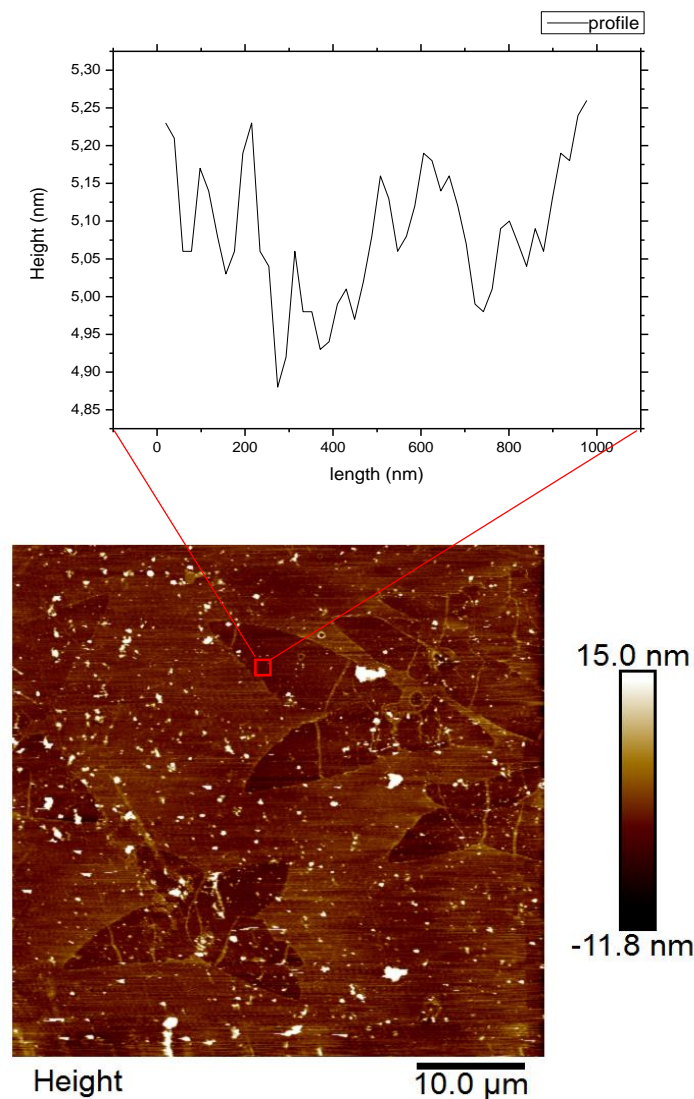
Figure 4.2-16: AFM image of the graphene transferred on top of Si/SiO₂ (sample 15a2702). The lobes of the crystal can be distinguished. The roughness reveals good homogeneity and absence of second layer growth. Some cracks are introduced by the transfer process. The white spots are impurities introduced by the PMMA, difficult to get completely cleaned. The enlarged image shows the profile of a 1x1µm area (the indicated square) with a RMS roughness of 0.78 nm.

The important role of hydrogen plasma, used for etching the copper foil, was revealed when the growth of graphene was carried out under the same conditions as described for Sample A, without any previous ion etching pretreatment on the copper foil (sample D). This time, a pre-cleaning process in a HNO₃/distilled water solution was performed as described in the work of Kim et al [S. Kim, 2013].

Figure 4.2-17 (sample 14k1902) shows the SEM pictures of the graphene domains obtained. The nucleation density remains high but the crystals are not well formed as in the graphene of previous samples. We considered two possible explanations to this. The first is that with the chemical etching, the native copper oxide film was not completely removed. The other is that the oxidation of the sample takes place during the cooling of it, which is taking place at high vacuum in absence of hydrogen or any other gas, a part of residual gas, resulting in the formation of copper oxide islands along with the graphene [Qi, 2012].
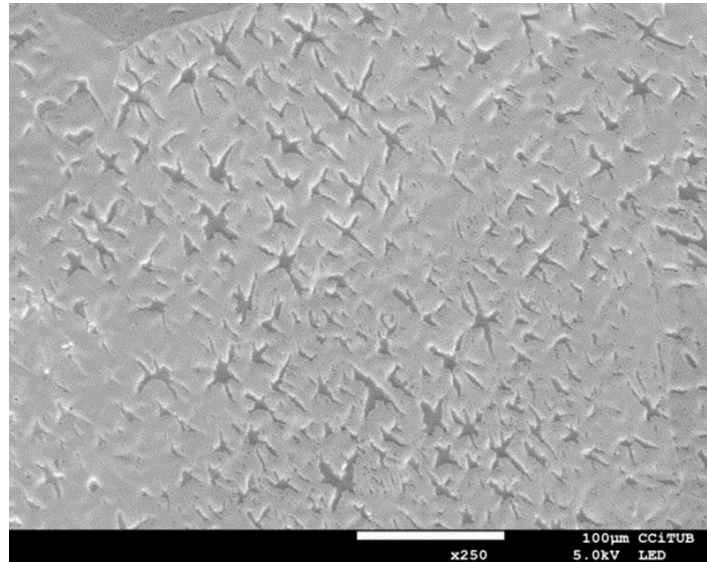
Figure 4.2-17: Scanning electron microscope picture of graphene grown on copper foil that has not been pre-treated by hydrogen plasma etching (sample D, code 14k1902). The growth time is 20 minutes. The scale bar has 100μm. The copper oxide presence does not allow the formation of large continuous domains.

4.2-3 Graphene growth by pulsed injection of methane

A QMS controller has been used to capture the injection of the pulses of methane. It monitors the partial pressure of the injected pulses and the time it takes to evacuate each pulse. The software monitors the partial pressure of upto ten different gases inside the chamber. A plot of example is presented in Figure 15 where we see the raise in the partial pressure of methane after that the gas pulse is injected. It takes a few seconds for the pressure of methane to return to its baseline value after the injection of the pulse. It is interesting to mention that in the same moment we see an increase in the partial pressure of the rest of the CH_x species. This reveals that during its decomposition, methane produces all the possible variety of different radicals, CH_3, CH_2 and CH. (Figure 4.2-15)
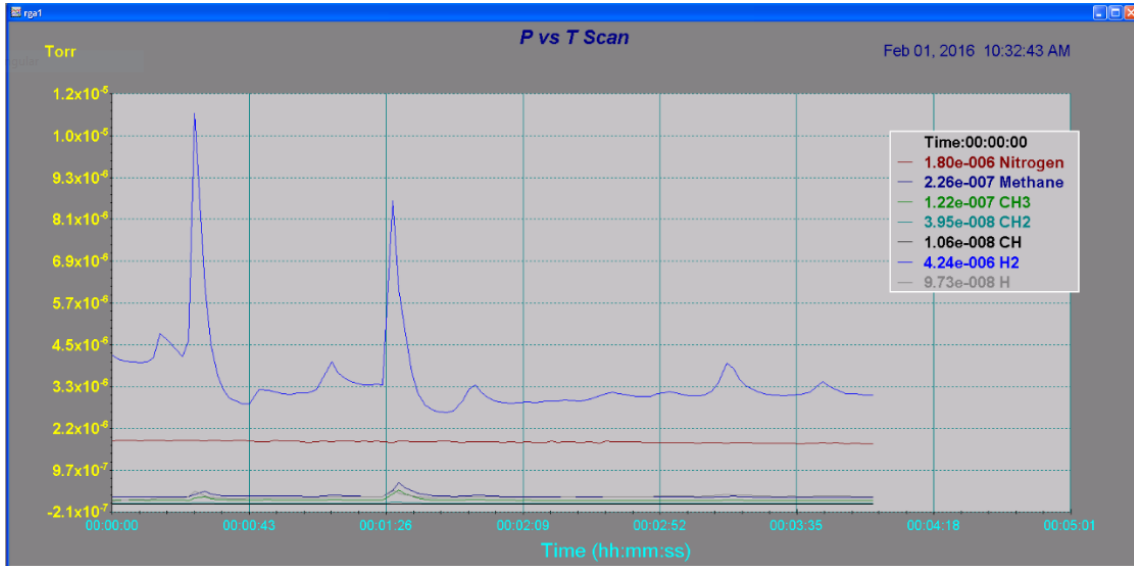
Figure 4.2-15: Screenshot from the Residual Gas Analyzer monitoring program. We can see the instantaneous increase of the partial pressure of methane, its radicals as well as molecular and monoatomic hydrogen, after that a methane pulse is introduced. Despite introducing a methane pulse, the increase of the partial pressure of hydrogen is much higher (blue line). This is a result of the insufficient evacuation of the low mass hydrogen from the pumping system of the reactor and to the decomposition of methane.

From the monolayer formation time model, described in the experimental part, it is expected that one pulse of methane is enough to form a monolayer of graphene. Although, this model supposes that the sticking coefficient is one. This needs to be further investigated. From the characterization of the grown graphene by means of scanning electron microscopy, we see that by the injection of one pulse of methane only some small domains of graphene of 1×1 μm^2 size are grown (Figure 4.2-16). Similar results are obtained by the injection of few pulses of methane, up to 5-10. It needs the injection of up to 30 pulses in order to obtain larger crystals.
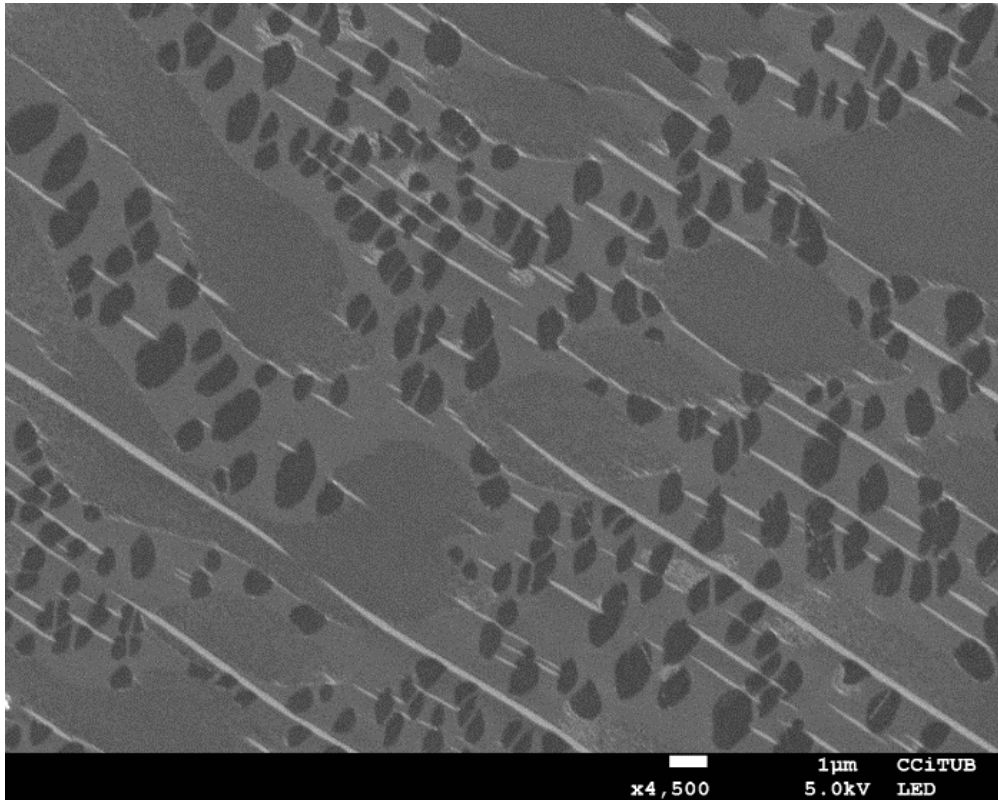
Figure 4.2-16: Domains of graphene grown after the injection of one pulse of methane (sample 14k2102). The domains have a size of approximately 1µm^2.

We perform growths injecting 50, 70 and 100 pulses of methane in order to see which is the amount needed to obtain a monolayer of graphene. Figure 4.2-17 presents the SEM images of the graphene grown with 50 pulses (sample15b1601).
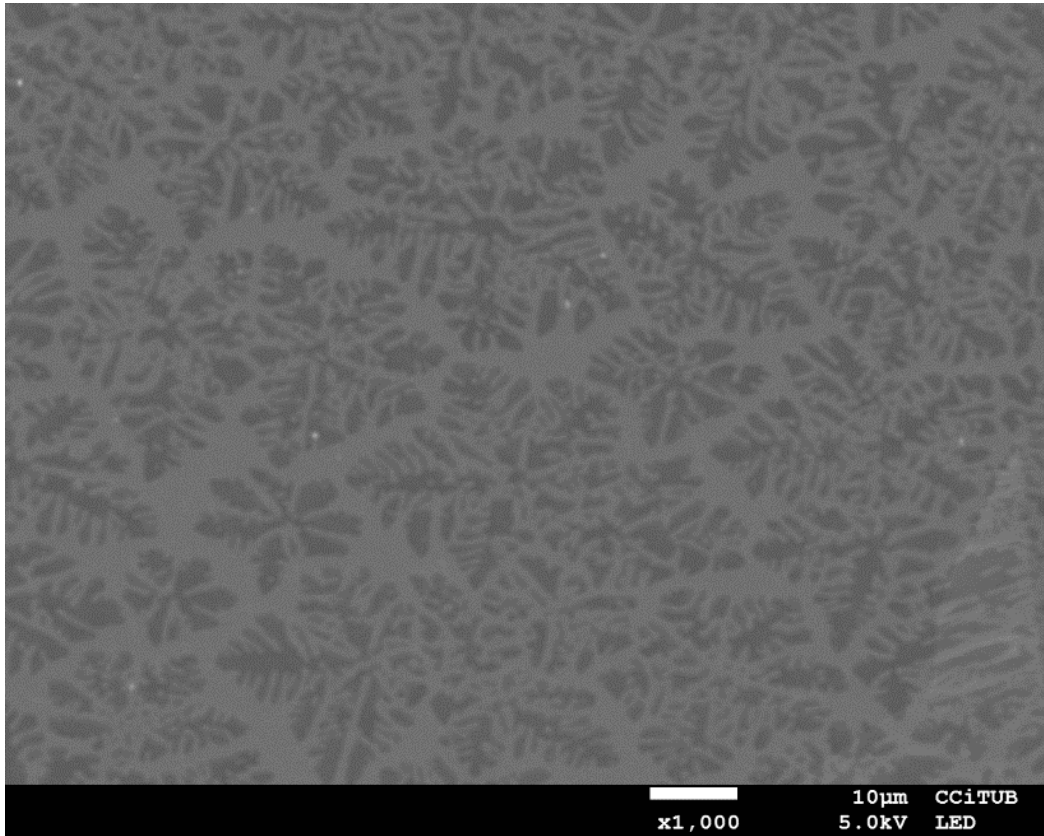
Figure 4.2-17: Domains of graphene after the injection of 50 pulses of methane. The domains have a size of approximately 20μm². Sample15b1601.

In Figure 4.2-17, the domains have a size of approximately 20 μm^2. Although, they appear seriously etched. As explained earlier, the turbomolecular pump used can not efficiently evacuate the monoatomic hydrogen produced by the methane decomposition. During the pulses injection, the increase in the concentration of hydrogen provokes an anisotropic etching to the grown graphene. This is confirmed when more pulses are inserted. Instead of resulting in larger domains that could form a single layer, the graphene appears more etched. Raman spectroscopy confirmed the single layer thickness of the graphene domains.

We propose that additional studies can be carried out to control the possible effect of additional flows of hydrogen/argon during the injection of the pulses or the possibility to perform the injection at a different total pressure.

4.2-4 Graphene growth at lower temperature by alternative carbon sources.

Apart from the use of methane, alternative carbon sources have been used. The graphene grows over the same metal catalyst as before, over polycrystaline copper foil. DFT calculations have previously predicted that graphene can grow more rapidly in lower temperatures when othe aromatic source molecules than methane are used as carbon sources. Toluene (or methylbenzene) is the one of them. Toluene is a liquid consisting of a CH_3 group attached to a phenyl group. Therefore, we used vapors of it for the growth of graphene. The use of toluene for the graphene growth in a lower temperature than this needed in the case of methane has been reported previously (B. Zhang, 2012). Here we report the growth of single layer graphene with the use of toluene vapors at 600°C. The sample was exposed to toluene vapors during 60 minutes in a pressure of 50 Pa. The graphene grown can be seen in Figure 4.2-18 (sample 14b2702). Small domains of single layer graphene with a size ~1µm^2 are gown, presenting a high nucleation density of ~7.5nucleus per 10µm^2.

In addition, graphene has been grown with the use of vapors of benzene (C6H6) as a
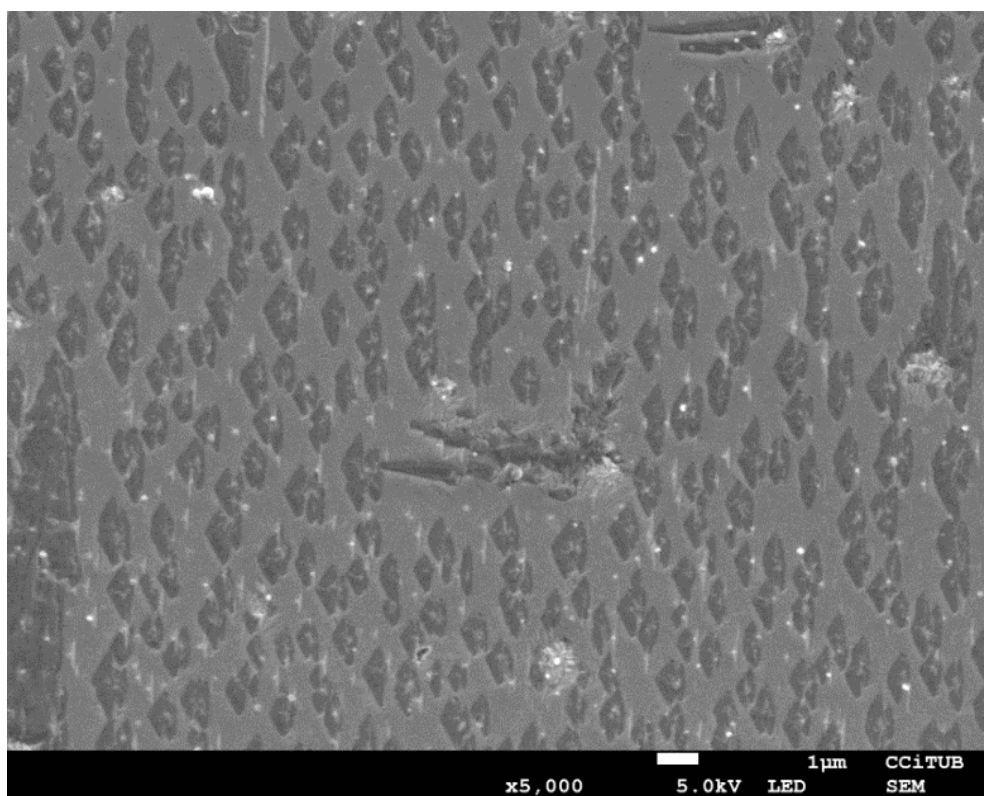
Figure 4.2-18: Single layer graphene grown by toluene vapors at low temperature of 600°C.

carbon source. Benzene is also promoted as a carbon stock as it can reduce the graphene growth temperature down to 300°C (Choi, 2013). Here we report the growth of monolayer graphene domains at a temperature of 500°C. The pressure is at 5 Pa and

the growth time is only 480 sec. At Figure 4.2-19 we see a sem image of the grown domains. The domains have a size of about 5µm^2 and the nucleation density here is about 3 nucleus per 10µm^2.sc
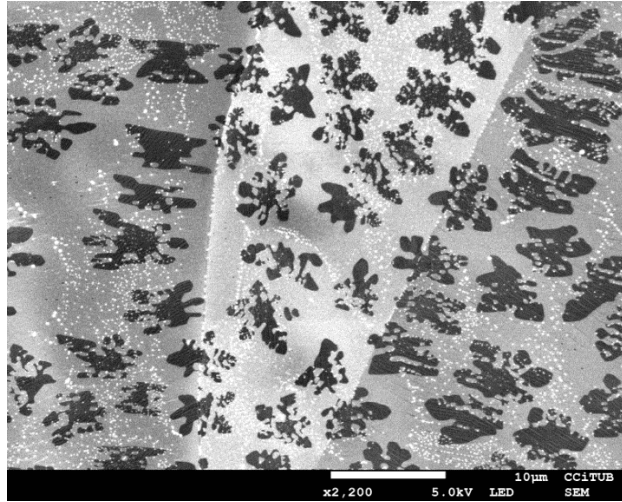
Figure 4.2-19: Single layer graphene grown by benzene vapors at low temperature of 500˚C [14b0603].

4.2-5 Energy-dispersive X-ray spectroscopy (EDX) analysis

EDX analysis was used for the elemental characterization of the samples. The set up is installed in the SEM that we use for all the microscopic characterization described before

(working at 5KeV of excitation energy). We detected the main components of our samples that in all cases were copper and carbon. An indicative spectrum can be seen in Figure 4.2-20a.
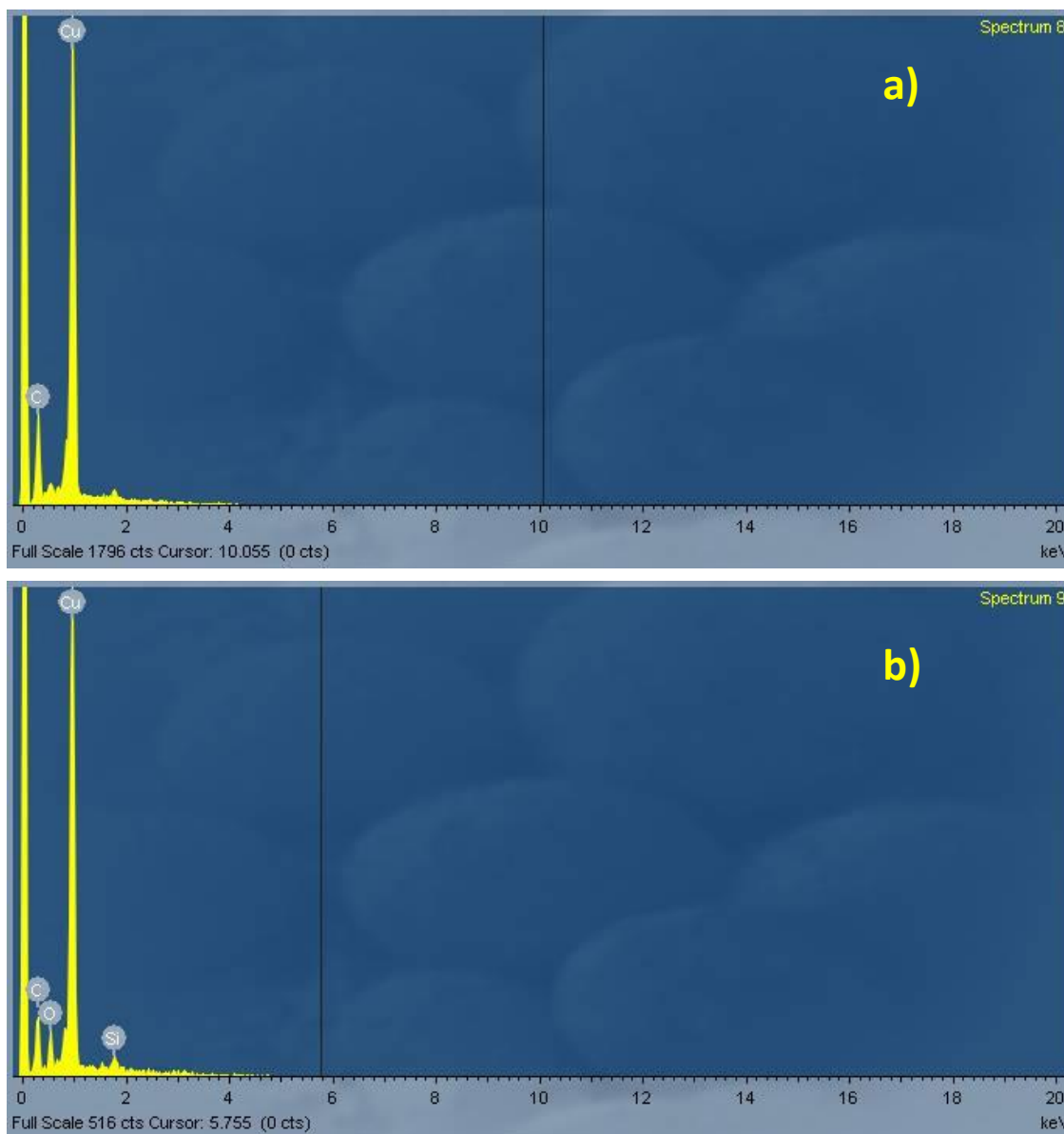
Figure 4.2-20: a) EDX spectrum where the carbon and copper elements are present (sample 14k1401). b) EDX spectrum where carbon, copper, silicon and oxygen elements are present (sample15j1401).

As the copper foil is much thicker than the graphene, the copper concentration is higher. This analysis helped us to determine the origin of the silicon oxide particles that we observed in the SEM images (Figure 4.2-20b, see also "*Effect of a balanced concentration of hydrogen on graphene CVD growth*" Chapter 4.2-2).

146

4.2-6 Conclusions

Graphene crystals were grown by CVD in both sides of copper foil at low pressure and at 1040°C. Two parameters are being explored, the total pressure and the hydrogen flow. We studied the two parameters individually to know the effect each one has on the graphene growth. The SEM characterization indicates that small variations in these parameters can affect the morphology, nucleation density and size of the graphene crystals. In concrete, the hydrogen flow appears to have an important role to the morphology of the crystals but not on their size. Specific amount of hydrogen can perform strong etching to the graphene. In our results the etching effect appears to be inversely proportional to the hydrogen flow rate. In the parts of the substrate that the graphene is not being etched away we see that the domains maintain the same size independently of the hydrogen flow. The total graphene covered area varies widely depending on the nucleation density and the hydrogen etching effect. Increasing the hydrogen flow rate at a stable chamber pressure resulted in the growth of a continuous film. At slightly lower hydrogen flow rate the film was being etched anisotropically and appeared seriously damaged. The chamber pressure appears to affect the nucleation density as well as the size of the graphene crystals at stable gas flow rates. A large increase in the $\Delta P_H/\Delta P_{ch4}$ ratio during the growth, at a stable pressure, brings on a decrease of the nucleation density. A smaller nucleation density provides more clearance for the 2D crystal growth, resulting in the formation of graphene films with less grain boundaries. The nucleation density appears to follow a linear dependence in relation to the % total coverage normalized to the lobe´s length. In addition, we observed that the nucleation density is remarkably higher, the double or more, on the facet (310) if compared to the crystalline facet (221). This is one of the main conclusions, because, the etching of selected zones of the copper facets could permit the abidance of the (221) facet in the foil surface, which would allow the growth of graphene from a small number of nucleus. Outside the range of pressures that we studied here, between 10 and 25 Pa, either the graphene nucleation is not being performed or the film obtained becomes seriously damaged as a result of the anisotropic etching of graphene crystalline islands. The above information can be useful in the design of experiments that target to grow graphene crystals from low nucleation density. We underline the importance of the exponential increase of the hydrogen concentration which is not usually taken into consideration when the hydrogen flow rate is constant. In addition, we highlight that the relative pressure $<P_{H2}>/<P_{CH4}>$ ratio diagram follows the same variation as the % coverage diagram, proving that the partial pressure can be a more efficient evidence than the flow rate when we want to evidence

the effect of the hydrogen, as it takes under consideration the evacuation efficiency of the pumping system. The Raman characterization ensures that all the surface of the foil is covered with monolayer graphene. The presence of the D peak can be due to defects on the film. After the transfer of the film to SiO_2 we notice a significant contraction of the 2D peak. On the other hand, the I_G/I_{2D} ratio appears unaffected by the substrate.

The experiments performed to achieve a balanced concentration of hydrogen were aimed at improving the control of growth of graphene.The hydrogen flow rate seems to perform an etching in the graphene domains, which affects their morphology and uniformity. The results reveal that a suitable graphene growth is possible when we optimize the switching of the carbon precursor/hydrogen flow ratio during the process. This reduces the etching effect that the hydrogen is performing, allowing the growth of graphene that fully covers the substrate. Large area graphene is necessary when it comes to large scale applications followed by a careful transfer, to avoid the damaging of the graphene film. Raman spectroscopy allows ensure when the graphene growth was in the form of an atomic monolayer. Performing the Raman measurements on top of different substrates, (copper foil, glass, SiO_2/c-Si) does not affect significantly the shape and ratio of the characteristic graphene peaks. In addition the important role of the substrate pre-treatment is being investigated. Performing hydrogen plasma before the growth reduces efficiently and faster the native copper oxide layer so that large graphene crystals can be grown.

Considering the pulsed injection of methane, the ability of growing graphene through a different synthetic route is explored. Based on the concept of the monolayer formation time, we propose the injection of pulses of methane instead of a continuous flow. By this way the growth becomes faster. The results reveal the growth of domains of single layer graphene of 20 μm^2.

Considering the use of different carbon precursors, alternative carbon sources were used, benzene and toluene, to promote the growth of graphene at lower temperatures, at 500 ˚C and 600˚C respectively. By this method, single atomic layer of graphene has been grown on copper foil obtaining domains with an area of 5 μm^2.

4.3 Raman Additional Results

In this chapter some additional results from the Raman spectroscopic measurements are presented. During the whole thesis, the Raman spectroscopy along with the scanning electron microscopy (SEM) were habitual methods of characterization of our samples.

Raman spectroscopy was performed with a Jobin-Yvon LabRam HR 800 system. The acquisition time for the collection of each spectrum was always between 30 and 60 s.

An optical microscope is coupled to the Raman apparatus, which permits us to locate the graphene domains in order to perform the measurement. This is very useful to examine small domains. A typical image where we can see the various graphene domains is shown in Figure 4.3-1. The light pink color of the image is a result of the PMMA residues

2D

Figure 4.3-1: Image of the optical microscope coupled to the Raman spectometer where we can see the 4-lobes and 6-lobes graphene domains. The image corresponds to domains that have been transferred over SiO₂. (Sample 15C2001)
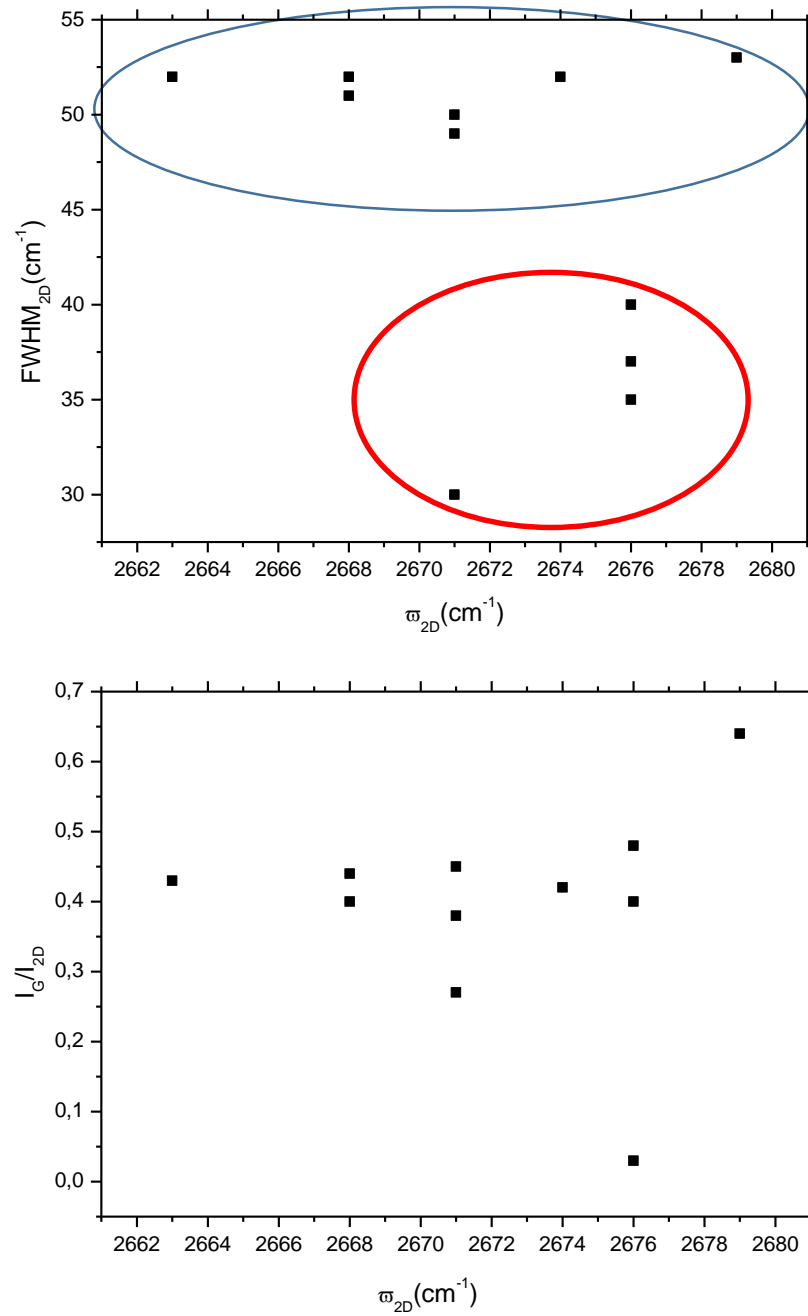
Figure 4.3-2: a) FWHM of the 2D peak as a function of Raman shift. The points in the red circle correspond to spectra acquired after the transference of graphene to SiO_2. The points to the blue circle correspond to spectra acquired directly from graphene on the copper foil. b) I_G/I_{2D} ratio as a function of the 2D peak Raman shift.

When transferred to SiO$_2$ (300nm thick) the 2D peak shape presents slight but notable differences [Das, 2008]. Figure 4.3-2a shows the FWHM of the peak as a function of its position. The points circled in red correspond to the spectra acquired from the SiO$_2$ substrate. The points circled in blue correspond to the spectra acquired directly on the copper foil [Da Costa, 2012]. The Raman shift, ω$_{2D}$, has a narrower distribution and the FWHM appears~15cm^{-1} lower. The fact that the substrate can substantially modify both the electronic and phonon structure of the overlaying graphene has been explained before [Frank, 2014]. On Figure 4.3-2b we see the I$_G$/I$_{2D}$ ratio as a function of the 2D peak position. The phonon frequency of the 2D peak appears on average at 2670 cm^{-1} when the graphene lies over copper and at 2675 cm^{-1} when it is transferred over SiO$_2$. After the finish of the cooling of the growth process and during the cooling, the copper foil is forming ripples. This corrugation rise the increase of the surface area of copper which results in the insertion of an amount of strain in the graphene. This manifests itself in a shift of the 2D phonon mode by ~5 cm^{-1}. Once the graphene is transferred in another substrate (here SiO$_2$), it relaxes (unstress). To measure the amount of strain we use the equation

$$\varepsilon = -\frac{\Delta v_{2D}}{2v_{2D}^0 \gamma_D}$$

Where γ_D = 3.55 has been calculated the Gruneisen parameter. Δv_{2D} denotes the shift of the frequency of the 2D phonon mode with respect to u^0_{2D} = 2680 cm^{-1}, the value of unstrained, pristine graphene.[Mohiuddin,2009] The strain is calculated ε = 0.052%, when graphene is grown on Cu by a CVD process. This value is much lower than other reported in recent literature that calculate the strain to be 0,158% [Troppenz, 2013]. Thus, we can assume that the origin of this stress is not the substrate deformation. Othe possible origin like the hydrogen bombardment or strain introduced by condamination should be investigated. When transferred over SiO$_2$, the strain relaxation is calculated ε = 0.026%. To avoid the introduction of this stress, it has been proposed the structural design of the growth substrate in order to modulate the density and even the structures of wrinkles and ripples [Liu, 2011].

Considering the I$_G$/I$_{2D}$ ratio (Figure 4.3-2b), except three of measurements carried out, the rest of them gather around the value 0.4% and it does not appear any dependence on the kind of the substrate where the measurement was taken. The variation in the ratio can be a result of the position of the laser. If the measurement is performed in the edge of the graphene domain the ratio can change, as we can see in the next chapter considering the acquisition of Raman maps in the edge of the crystal.

4.3-1 Raman Mapping

Raman mapping was performed to obtain information about the homogeneity of the grown graphene. We present here two different Raman mappings. The first has been performed with the Jobin-Yvon LabRam HR 800 system in graphene grown on top of copper (Sample 14J0201). This is a mapping of the relative intensity ratio I_{2D}/I_G. The Raman mapping was performed in an area of 1700 μm² (with a 2 μm step) which was almost fully covered with a monolayer graphene (Figure 4.3-3). The bright green and green areas of the map correspond to monolayer graphene with $I_{2D}/I_G > 2$. Only the dark green parts correspond to bilayer/few layer graphene. This can be because of small areas where second nucleation has occurred on top of the first graphene layer or because of defects that can affect peak´s intensity. Although, this system is not adequate for Raman mapping as the scan rate is very low. We performed another measurement with the system DXRxi of Thermo Fisher Raman Imaging Microscope (while the apparatus remained as an exhibition object in CCiT-UB). This system fast
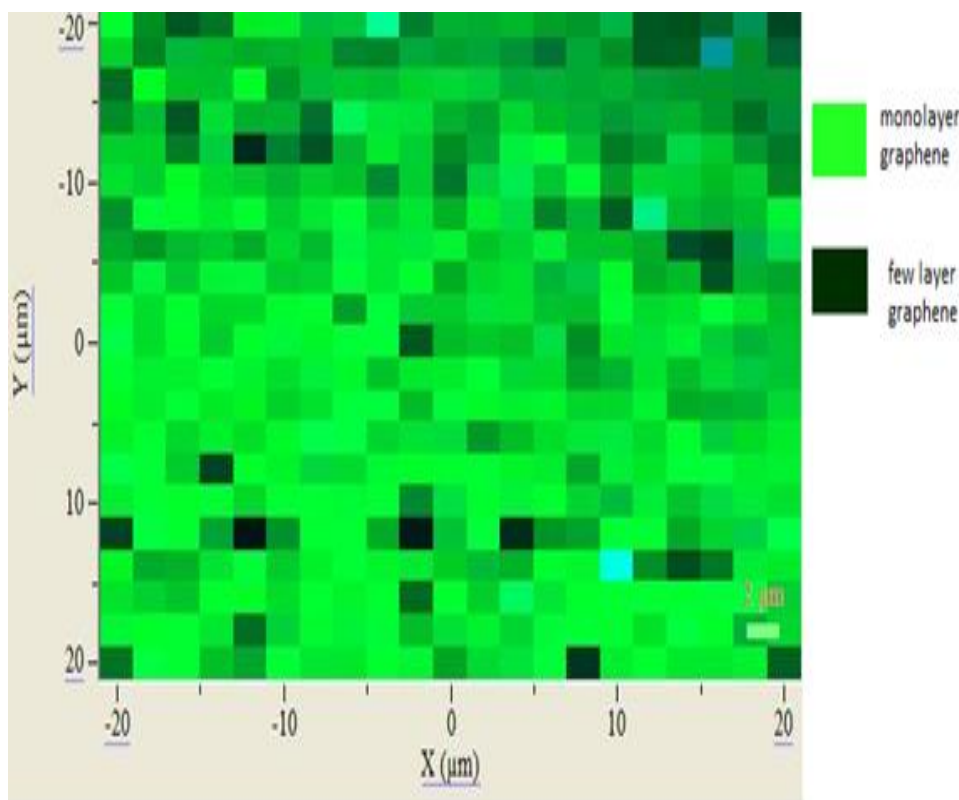
Figure 4.3-3: Mapping of a 1700 μm² area with a 2 μm measuring step revealing that most of the substrate is covered with monolayer graphene. The bright green parts correspond to a $I_{2D}/I_G > 2$ peaks intensity ratio. The dark green parts correspond to a $I_{2D}/I_G < 1$ peaks intensity ratio. Light blue parts correspond to non covered substrate,

trucks the spectrum collection. Unfortunately, we could not have access to the relative software further than the time we spend during the exhibition session so all the data had to be extracted in the form of images. We present them here as we believe that it is a good evidence of the potentialities of the Raman mapping.

The measurement was performed on the edge of a graphene domain lying over a 90nm thick SiO_2 substrate. Thus we can have a good contrast in the signal and which permits the clear identification of the graphene edge morphology. Some isolated red spots are result of the relative values that the intensity ratio can present even in zones not covered with graphene. In Figure 4.3-4 we can see the map that is being formed when we take the ratio between the area of the 2D and G peak. The square pattern of the map is a result of the square dimensions of each step during the measurement. The 2D peak occupies the area between 2683-2730 cm^{-1} and the G peak occupies the area between
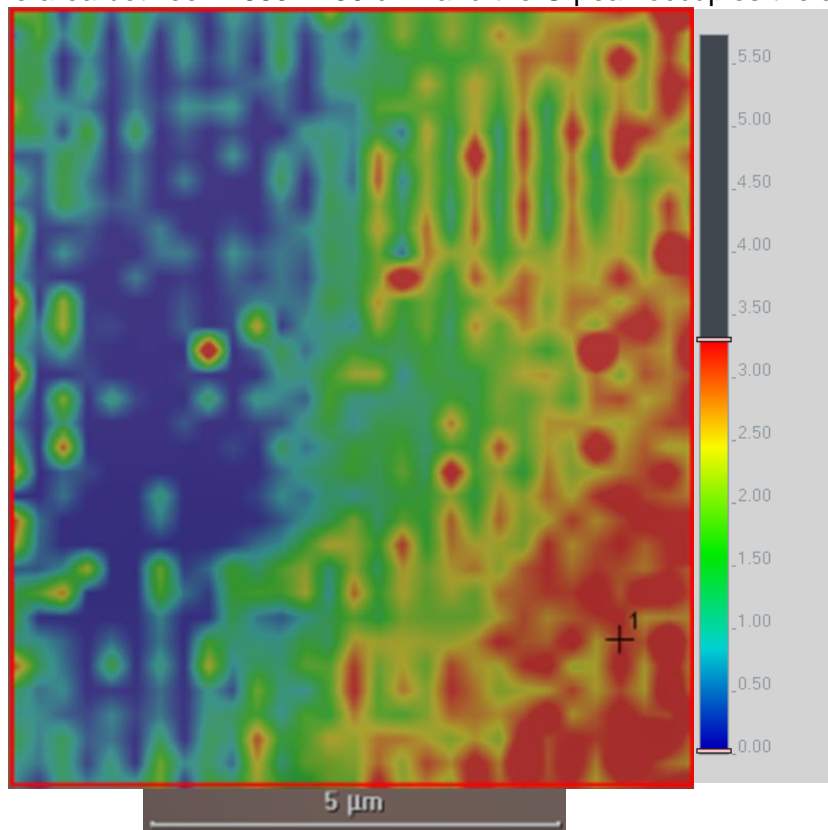
Figure 4.3-4: Raman mapping of the 2D/G area ratio of a monolayer graphene domain. The mapping has been performed in the edge of the domain. The blue zone corresponds to the SiO_2 substrate. On the right is provided the color/ ratio scale bar.

1558-1610 cm^{-1}. The intense red area corresponds to a I_{2D}/I_G ratio ~3.3 as we see in the scale bar. The blue area corresponds to I_{2D}/I_G ratio 0 (no existence of 2D peak), such as the signal coming from the SiO_2 substrate. The mapping corresponds to an area of 8×9 μm^2. In the extreme edge of the graphene crystal, the intensity of the areas of I_{2D}/I_G

ratio does not diminished sharply to 0 (Figure 4.3-4). This is a result of the fact that the Raman intensity of the allowed peak is proportional to the volume of the sample, both in the case of G and 2D peak but not in the case of D where its intensity is proportional to the amount of defects, which, neglecting structural disorder, can be assumed to be proportional to the edge length under the laser spot. Similar observations have been reported before [Casiraghi, 2009]. The green zone corresponds to I_{2D}/I_G ratio ~1.7. We also provide a representative Raman spectrum corresponding to the red zone of this map (Figure 4.3-5).
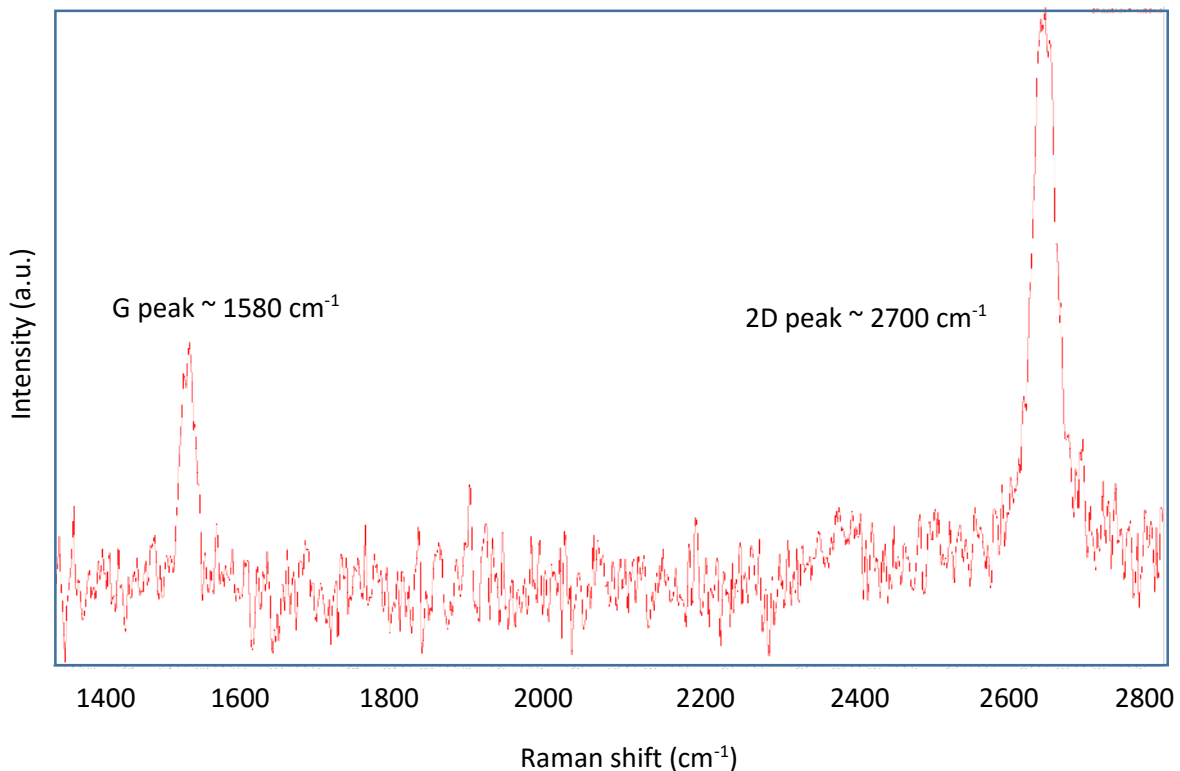
Figure 4.3-5: Raman spectrum of the monolayer graphene corresponding to the red zone of the map. (Sample 15C2001)

Other possible maps that we can obtain if we elaborate in the collected data are the I_{2D}/I_G peak intensity ratio as well as the individual peaks intensity. We provide an example of the 2D peak intensity map in Figure 4.3-6. As we see the map is similar to the one corresponding in the peaks intensity ratio. Finally both of them are extracted from the same data.
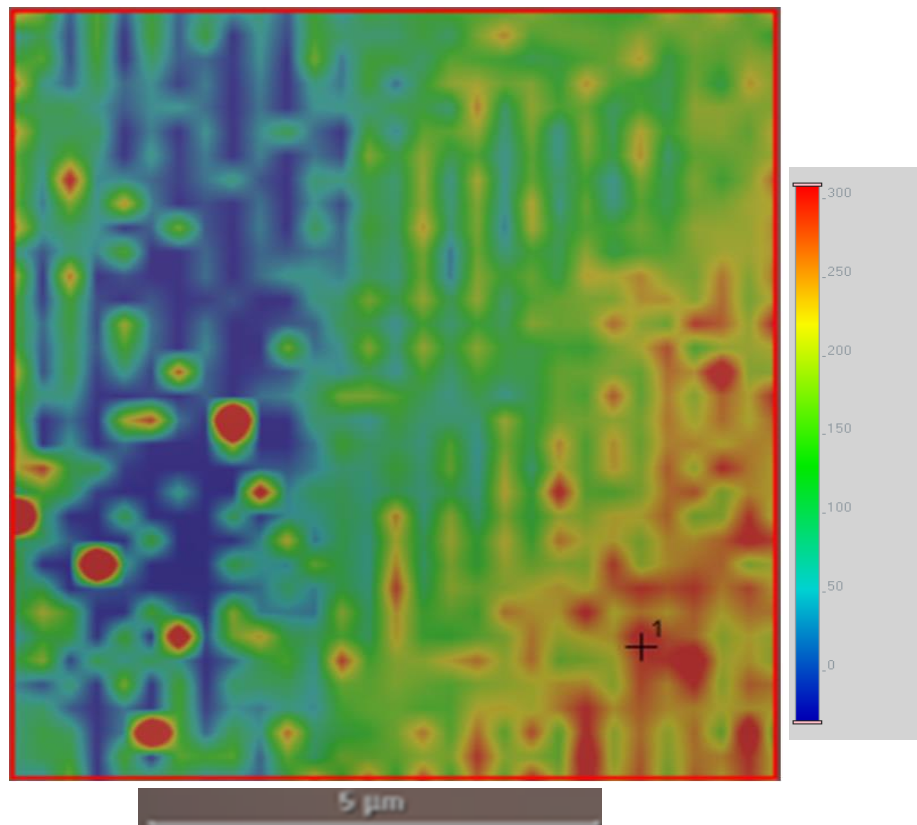
Figure 4.3-6: Raman mapping of the 2D peak intensity of a monolayer graphene domain. The red zone corresponds to the area where the graphene shows the highest 2D peak intensity. From the I_{2D}/I_G ratio we assume that the grown graphene is monolayer.

4.3-2 Control of the strain in CVD grown Graphene via the H2 flow.

The control of the strain offers the possibility to tune the electronic properties of graphene. In the present chapter we demonstrate that it is possible to tune the strain of graphene by varying the hydrogen flow in the chemical vapor deposition growth of graphene over copper foil. Based in experimental results, we propose a mechanism where the high bombardment of hydrogen results in the ablation of the graphene from the rippled surface of the copper foil. This results in the disappearance of the compressive stress that is present in lower hydrogen flows. The evaluation of the strain is done by analyzing the 2D peak shift by Raman spectroscopy and the ripples density by scanning electron microscopy.

The growth of the graphene samples was made in the same reactor and in same conditions as described in the previous chapter, varying the hydrogen flow. The growth temperature was always 1040 °C and the growth pressure 20 Pa. The methane flow was stable at 5 sccm and hydrogen flow was varying, in order to study its effect. We performed growths under 10 sccm, 15 sccm, 20 sccm, 25 sccm, 30 sccm and 35 sccm of Hydrogen (Table 1). The growth time was always 20 minutes. After its pass, the furnace was opened and the cooling down to 500 °C was taking about 10 seconds.

The characterization was made by scanning electron microscopy (SEM, model JEOL JSM 7100F) and Raman spectroscopy (Jobin-Yvon LabRam HR 800 with a green laser). By the SEM images we can measure the density of the ripples in each sample. In Figure 1 we present the SEM images for the different hydrogen flows. Figure 4.3-7a corresponds to graphene grown under 15 sccm of hydrogen flow, Figure 4.3-7b to 20 sccm, Figure 4.3-7c to 25 sccm, Figure 4.3-7d to 30 sccm and finally Figure 4.3-7e to 35 sccm of hydrogen flow.
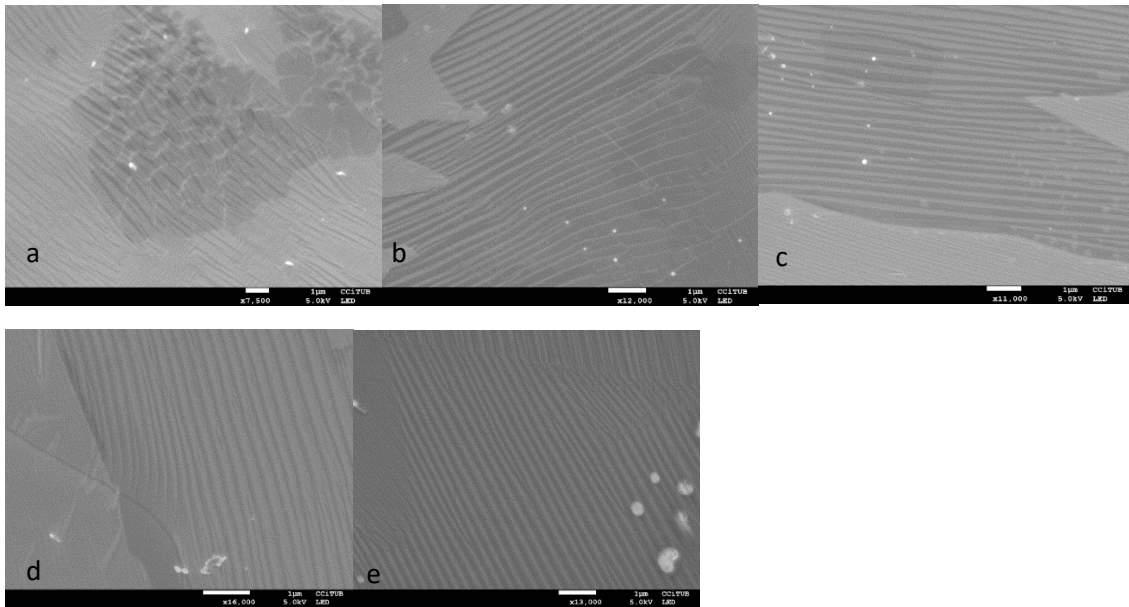
Figure 4.3-7: a-e) sem images of graphene growth in different hydrogen flows. a) 15 sccm, b)20sccm, c)25 sccm, d) 30 sccm, e) 35 sccm. Scale bar is always 1um.

In Figure 4.3-8a we provide Raman spectra corresponding to samples grown in the different hydrogen flows. In Figure 4.3-8b we can see an enlarge image where the shift in the 2D peak is visible when varying the hydrogen flow.
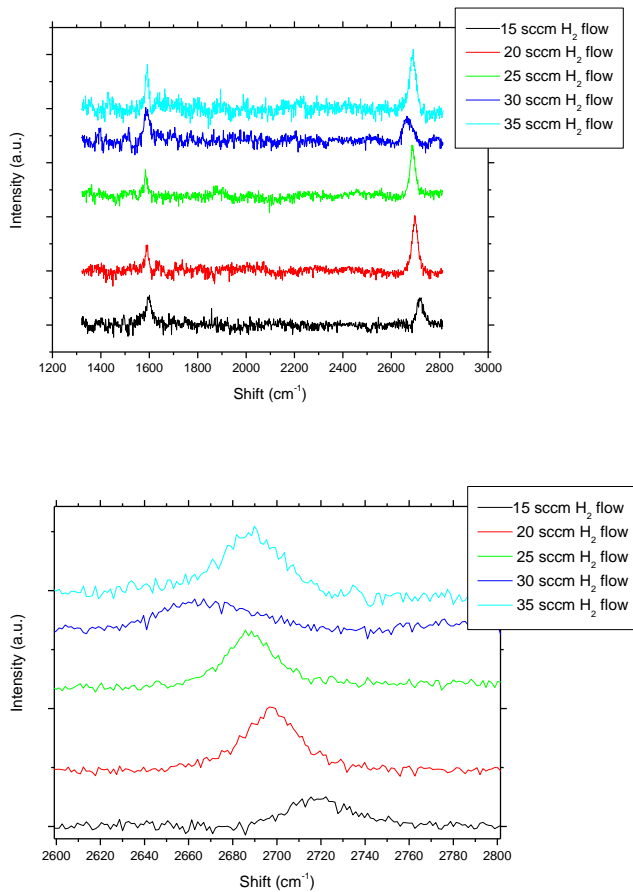
Figure 4.3-8: a) Raman spectra of the different samples. b) Enlarge figure of the 2D peak of the same samples.

In previous works [Paronyan, 2011] it has been studied the formation of ripples in graphene during cvd growth. In the case of cvd growth, graphene tends to replicate the morphology of the substrate. When graphene is grown over copper foil, the formation of these ripples is a common phenomenon. Although, when the copper foil is exposed in the same heating and cooling process (as when graphene is grown), but in the absence of any hydrocarbon, no ripples are formed. In this case, the formation of dendrite-like structures or ´´snowflakes´´ is observed. Therefore, the presence of hydrocarbon is a necessary condition for the formation of ripples.

The mechanism describing the ripple´s formation is the following. In high temperatures, above 1000 ˚C, a massive movement of the copper atoms takes place underneath the growing graphene. This gives rise to the surface reconstruction and the formation of the nano-ripples. While cooling down to room temperatures, the copper substrate contracts, whereas the graphene which is on top tries to expand according to its negative thermal expansion coefficient. In the areas where graphene is pinned to the copper, it is

displayed to a strong compressive stress, whereas in the areas where the graphene is suspended above the nano-ripples it is allowed to relax some amount of the compressive strain through out-of-plane deformation (rippling) [Tapasztó, 2012].

In the present work, when we measure the ripples in the samples corresponding in different hydrogen flows, we see a sigmoid increase in the density of ripples in the higher hydrogen flows (Figure 4.3-9). More in specific, the ripples density increases from 2,6ripples/um, 3,6 ripples/um, 3,8 ripples/um, 4,3 ripples/um while the hydrogen flow increases from 15 sccm to 30 sccm (with a step of 5 sccm). Finally, in 35 sccm hydrogen flow the ripple´s density is 4,3 ripples/um as well.
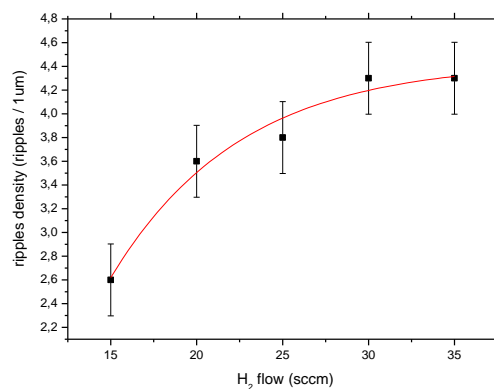
Figure 4.3-9: a) Ripples density in graphene for various hydrogen flows.

In all above described experiments the methane flow is stable, therefore the variation of the flowing hydrogen is the factor that affects the density of the formed ripples through the turbulences it generates in the substrate surface. In Figure 4.3-10 we present the Raman measurements for the different hydrogen flows. In Figure 4.3-10a we see the Full Width Half Maximum (FWHM) of the 2D peak with respect to the hydrogen flow. Despite some extreme values, mostly in the sample grown under 25 and 30 sccm of hydrogen flow, the majority of the spectra present a FWHM close to the value of 28cm^{-1} , which is the reference value of the 2D peak FWHM for single layer graphene [Lin, 2015]. In Figure 34.3-10b we plot the position of the 2D peak with respect to the hydrogen flow. The position of the 2D peak blue-shifts from 2719 cm^{-1} to 2680 cm^{-1} with the increase of the hydrogen flow from 15 sccm to 30 sccm (Table 4.3-1). The values presented in Table 1 regarding the 2D FWHM and the 2D position for the different hydrogen flows, are the average values resulting from those presented in the plots of Figures 4.3-10a and 4b.
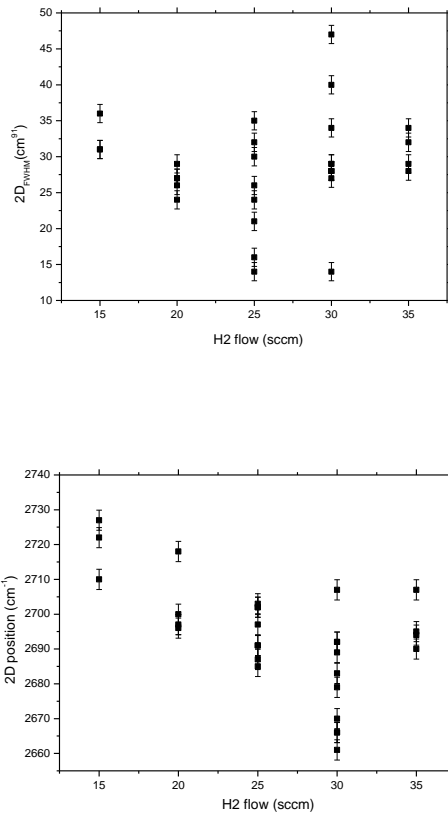
Figure 4.3-10: a) Plot of the 2D FWHM with respect to the different hydrogen flows. b) Plot of the 2D position with respect to the different hydrogen flows.

sample	Hydrogen flow (sccm)	Ripples density (number/um)	2D FWHM (cm⁻¹)	2D position (cm⁻¹)
A	15	2,6	32,6	2719
B	20	3,6	26,6	2701,6
C	25	3,8	24,75	2694,75
D	30	4,3	30,4	2680,5
E	35	4,3	30,75	2696

Table 4.3-1: Experimental data of the ripples density and the 2D peak characteristics (position and FWHM).

The results reveal an average blue-shift of the 2D peak following the hydrogen flow increase. We relate this observation with the strain introduced to the graphene as a result of the ripple´s formation. Specifically, we propose the decrease of the compressive strain effect as the reason for this shift. As mentioned earlier, the graphene replicates the

morphology of the copper substrate. As seen in the illustration displayed in Figure 4.3-11a, graphene remain relaxed in both concave and convex regions when grown. This is a result of the mismatch in the lattice parameters between graphene and copper.
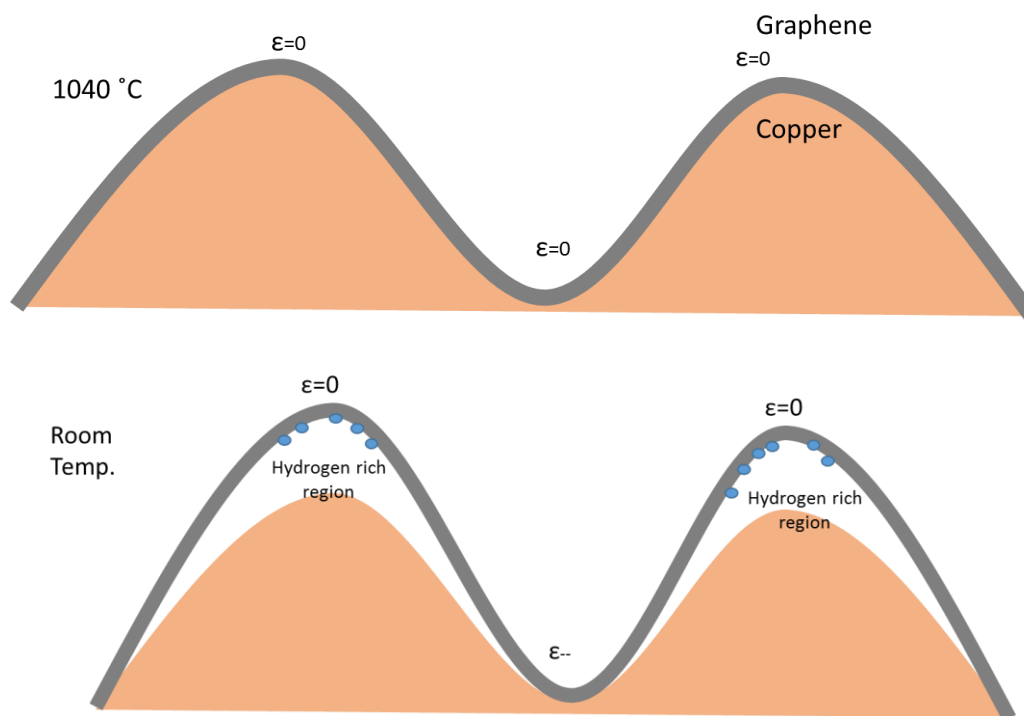
Figure 4.3-11: a) Illustration of the introduced strain in the graphene grown over copper foil. b) aspect of the graphene after its ablation from the concave regions

As explained above, while cooling, the copper foil contracts. This induces an increase in the compressive stress of the graphene in the concave region. In the convex region the graphene detached from the copper and remain suspended and relaxed. This detachment probably is the reason that graphene in the convex regions favors the hydrogen storage. As explained in previous works by experimental and density functional theory calculations [Goler, 2013], graphene chemisorption of atomic hydrogen is energetically favorable in the convex regions (Figure 4.3-11b). We consider that the blue-shift of the 2D peak is a result of the reduction/absence of the compressive strain with the increase in the hydrogen flow. With the increase in the ripples density, more regions where graphene is relaxed are contained in each spectrum, resulting in a reinforcing of the blue-shift of the 2D peak.

By the shift in the 2D peak we can calculate the strain of the graphene. This is calculated by equation

$$\varepsilon = -\frac{\Delta u_{2D}}{2u_{2D}^0 \gamma_D}$$

, where ε is the value of the strain, γ_D=3,55 is the Gruneisen parameter and Δu_{2D} denotes the shift of the frequency of the 2D phonon mode with respect to $u_{2D}^0 = 2680 \, cm^{-1}$ (which is the position of 2D peak for unstrained pristine graphene)[Troppenz, 2013]. The compressive strain is reduced with the increase of the hydrogen flow from ε= -0,2% for 15 sccm of hydrogen to ε=-0,026% for 30 sccm of hydrogen (Figure 4.3-12).
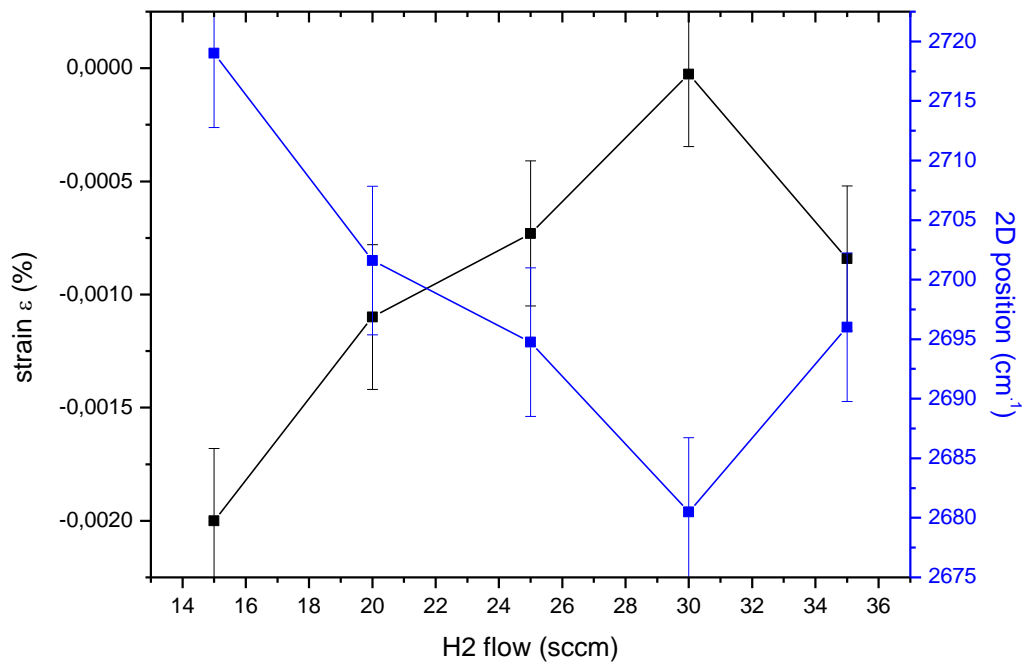
Figure 4.3-12: Left axe: Compressive strain for the different hydrogen flows. Position of the 2D peal (on average as extracted from the data in Figure 4.3-11b)

4.3-3 Conclusions

Raman spectroscopy is proved to be a direct, fast and trustworthy mean to characterize the graphene samples. The only ´disadvantage´ is the necessary post treatment of the data in order to remove the photoluminescence background signal. By a careful observation in the characteristic of the graphene peaks we confirm the monolayer thickness of the samples. In addition, we report the small but noticeable decrease in the FWHM of the 2D peak when the graphene is transferred over SiO_2. The shift of the 2D peak with respect to its position when it is relaxed, allows us to calculate the strain of the graphene. This is a result of the ripples that are formed in the copper foil during the cooling step. The ripples increase the surface area, introducing a strain $\varepsilon = 0.052\%$ in the graphene. When transferred over SiO_2, the graphene relaxes. This is translated in a decrease in the shift of the 2D peak and a strain relaxation of $\varepsilon = 0.0026\%$.

Finally, the Raman mapping performed in different samples can provide useful information about the homogeneity of the graphene domains. An interesting observation is the decrease in both the 2D peak intensity as well as in the 2D/G area ratio in the very edge of the crystal. The intensity of these peaks is proportional to the volume of the sample, which is higher in the inside part than the edges. Our results indicate the capability to control the strain in cvd single layer graphene by a careful control of the hydrogen flow. Through the control on the flow, the ripple´s density is regulated. An increase in the flow of hydrogen can reduce the compressive strain, as a result of the levitation of the graphene from copper substrate in the concave regions. Although, the introduced hydrogen flow should be selected with care, as high flows can lead to the anisotropic etching of the graphene film.

4.4 Graphene Transferring
4.4-1 Early Results of Graphene Delamination Transfer

Motivated by the promising electrochemical delamination transfer, we started some experimental trials with this method. Graphene was grown by CVD on top of polycrystalline copper foil of 99% purity and 75 µm thickness. PMMA was spin coated on top.

Figure 4.4-1 shows a scheme of the set up used for the transfer. The graphene used for

these experiments was grown up in the GRAPHMAN reactor of FEMAN group of UB. The aqueous solution used for the delamination was $K_2S_2O_8$ of 0.5 mM concentration. By varying the applied voltage is possible to control the delamination time. A higher voltage accelerates the reaction and more hydrogen bubbles are generated, accelerating the delamination time. (Figure 4.4-2)
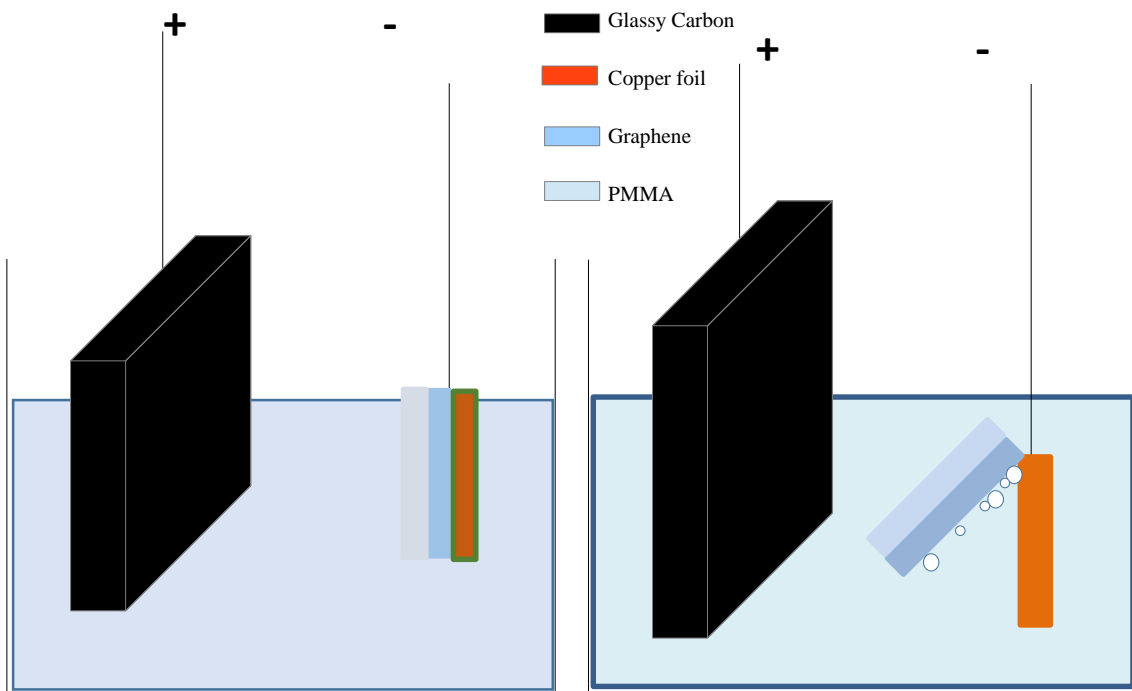
Figure 4.4-1: Set up of the cell for the electrochemical delamination transfer processes. In the left part we see the geometry of the system in the beginning of the process. In the right part we see the final stage of the process, when the graphene +PMMA have been completely delaminated from the copper foil.
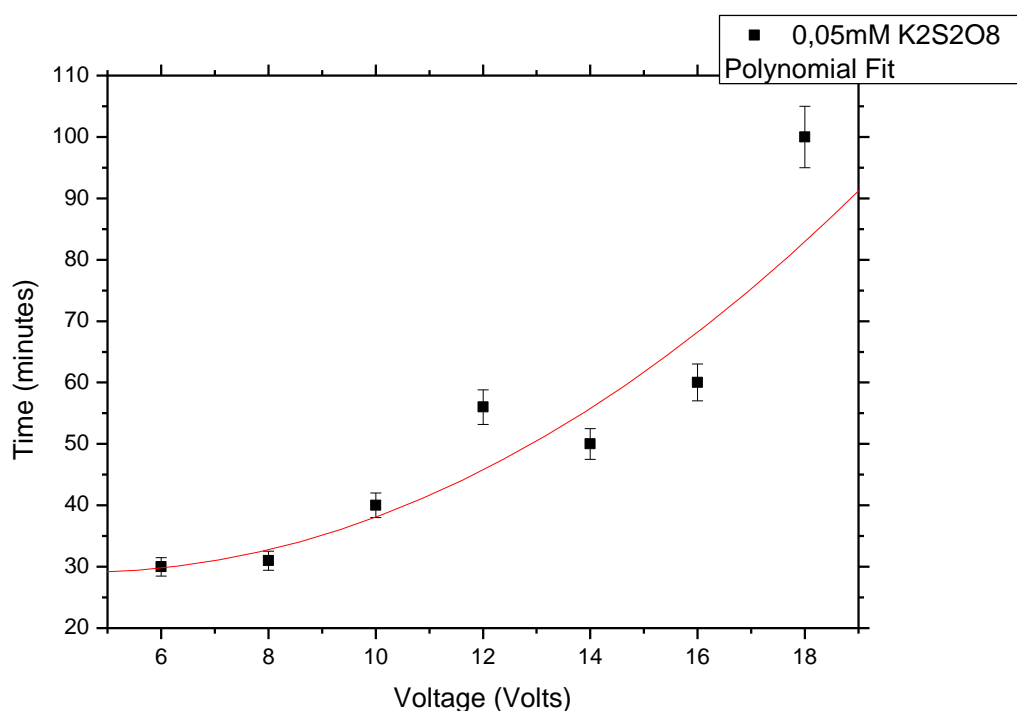
Figure 4.4-2: Period of time needed until the delamination is completed as a function of the applied voltage. For the delamination were used the samples 15C3002 and 15D0801

In these preliminary studies we transferred samples where the graphene crystals were still distinguished and had not reach to the point of forming a continuous sheet. In Figure 4.4-3a we have a scanning electron microscopy image of the grown graphene on top of
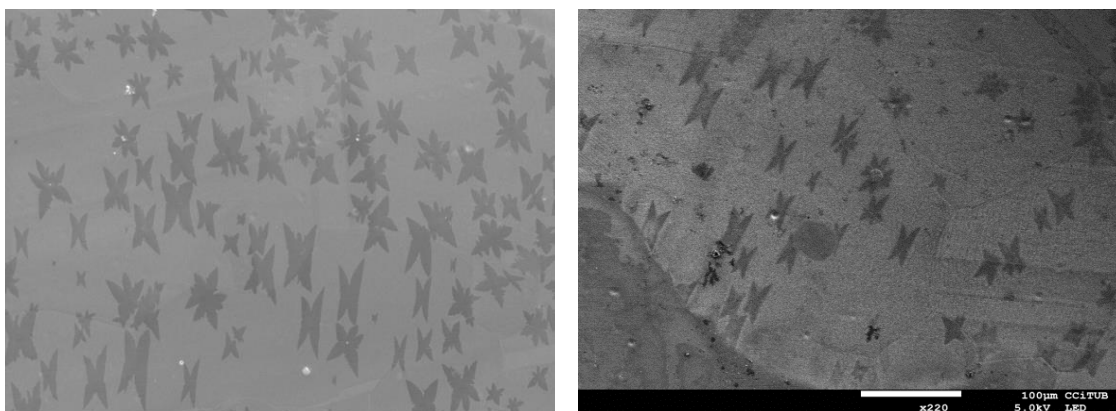
Figure 4.4-3: SEM images of a) of the grown graphene on top of the copper catalyst before the delamination process , b) the copper foil after the delamination, revealing that some crystals remain on top of it,

the copper foil, before the transfer. The crystal has a four-lobes morphology and each lobe has a length of approximately 30 μm. The growth of these samples was made in FEMAN group, UB. The growth conditions are described in detail in the chapter dedicated to it. After the transfer with the delamination technique, we return to observe the copper foil in the SEM. It seems that during the delamination not all the graphene crystals have been sufficiently transferred from the copper surface. In Figure 4.4-3b we see that in some parts of the foil the graphene has not been delaminated. In other parts the crystals appear seriously damaged. Some parts of the crystal remain in the foil while others have been delaminated (Figure 4.4-4a). Finally in some parts of the foil appears the 'fingerprint' of the delaminated graphene crystals (Figure 4.4-4b). These 'fingerprints' are most probably copper oxide (Cu_2O) layers. Their 'brighter' appearance could be due to a higher backscattering of electrons than from naked copper. As described at [Cherian,
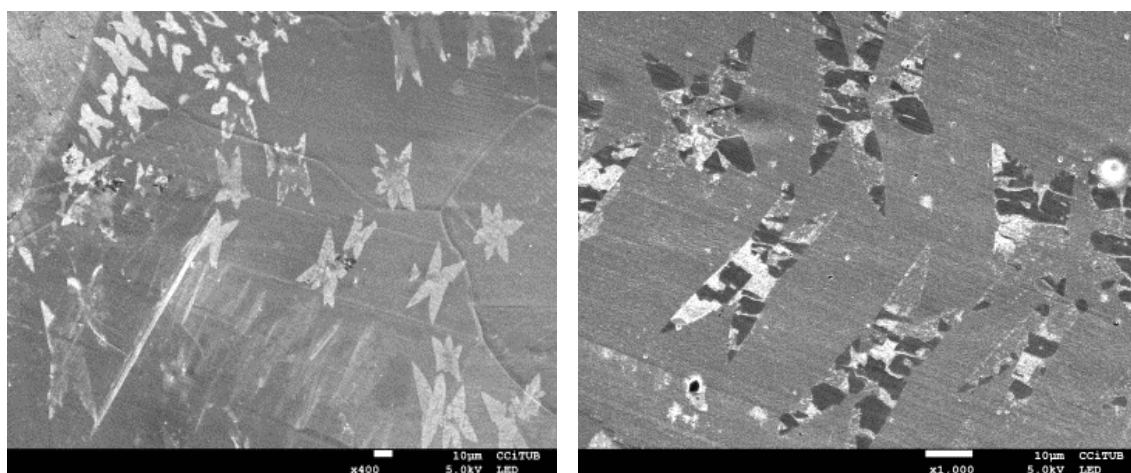
Figure 4.4-4: SEM images of a) crystals partially delaminated ,appearing damaged after the process and b) graphene 'fingerprints', a result of the copper oxide formation.

2015], during the storage of graphene a native copper oxide layer is grown between the foil and the graphene sheet. We believe that in the parts of the foil when graphene is absent this copper oxide is reduced to copper through the reaction [Shiddiky, 2011]:

$$Cu_2O + H_2O + 2e^- \rightarrow 2\,Cu\,(s) + 2\,OH^-$$
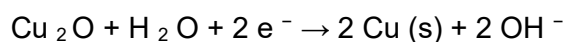
In the areas covered with graphene the copper oxide layer remains. The enhanced oxidation of the copper in the areas that it is covered with graphene has been reported in the work of Shriver et al. [Shriver, 2013]

After the complete delamination of the graphene/PMMA the stacking had to be 'fished' by a SiO$_2$/c-Si substrate. The PMMA was cleared by acetone. The SEM image reveals that the transferred crystals have maintained their morphology (Figure 4.4-5). The clearer image in this figure corresponds to the metallic contact of Au, deposited by vacuum metallization through a photolithographic mask on top of the SiO$_2$.
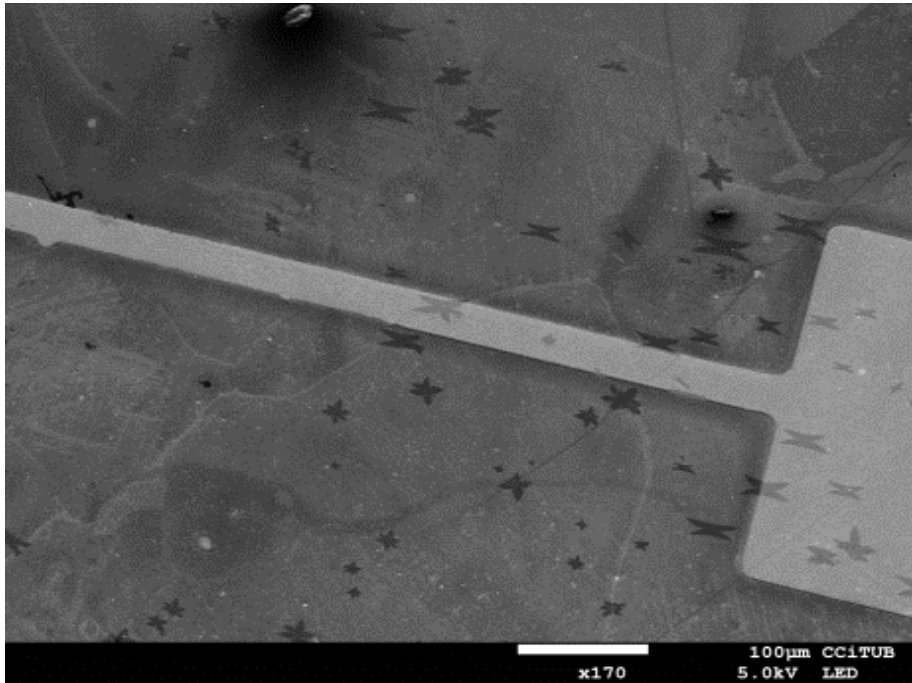
Figure 4.4-5: SEM image of the graphene crystals after the transfer on top of SiO$_2$.

4.4-2 Graphene Transfer with PMMA in FEMAN, UB

To further characterize the graphene samples, they were transferred with the support of PMMA in top of SiO$_2$/c-Si substrates. In the case of the Raman spectroscopy, the copper foil can introduce a lot of 'noise' in the spectra of the graphene. The less intense characteristic peaks, like the D+D'', are very difficult to be distinguished from the background noise. To obtain good graphene spectra, where all the information is easy to get extracted, is recommended a previous transfer to highly plan surfaces like polished silicon wafers or glass substrates. The graphene was grown on top of copper foil (see growth details in the relevant section 4.2). The transfer process starts spreading PMMA resist (MicroResist technology, Ref. Number 37071000) by spin coating on the graphene/copper foil at 3000 rpm for 60 s. Then, the copper is removed away by introducing the stacking PMMA/graphene/copper foil into a FeCl$_3$ etching solution, 0.1M. The graphene stays attached to the PMMA, floating on the surface of the solution. After being transferred to the SiO$_2$/c-Si, the stacking is heated to 90°C for 60 minutes to acquire

a better adhesion of the graphene to the substrate. The PMMA can be removed by solving with acetone. In Figure 4.4-6 we see a SEM image of the graphene as grown on top of the copper foil and on 4.4-7 an optical image of the crystals after their transfer on top of SiO_2/c-Si. This optical microscope is adapted to the Raman spectrometer in order to provide an image of the area where the spectra is obtained. The light pink color of the optical image is because of the PMMA residues that were not efficiently removed. These residues help although to achieve a better contrast in the image between the graphene and the substrate, since monolayer graphene is difficult to be distinguished by optical microscopes, even on top of SiO_2. The Raman spectra acquired by these samples are shown on the right of Figures 4.4-6 and 4.4-7. The spectra were acquired by a 532nm laser, operating with an acquisition time of 30 s. Comparing both spectra, we can see that on Figure 4.4-7 there is a low background noise although the 2D/G ratio remains approximately the same (~1.9). The D+D" peak of Raman spectrum of Figure 4.4-7 is also visible at ~2450cm^{-1}.
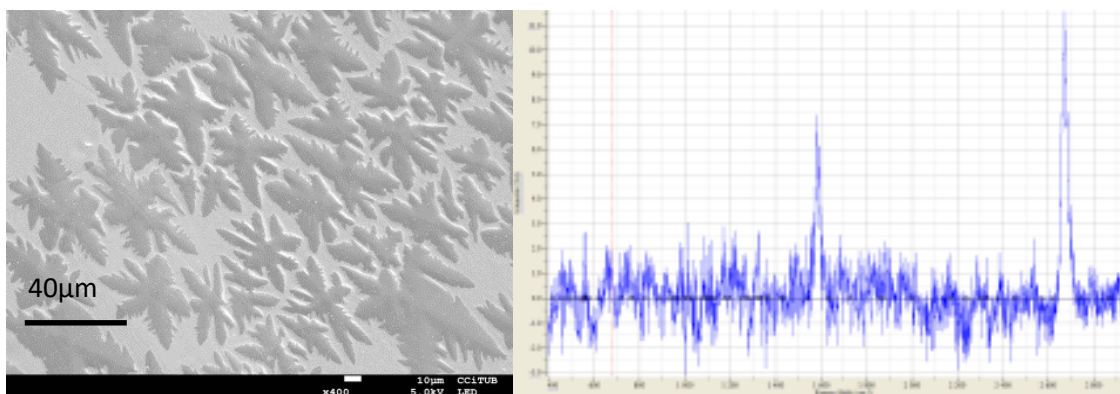
Figure 4.4-6: SEM image of the graphene crystals as grown on copper foil. Right plot corresponds to the Raman spectra of each sample. For this transfer was used sample 15C2001
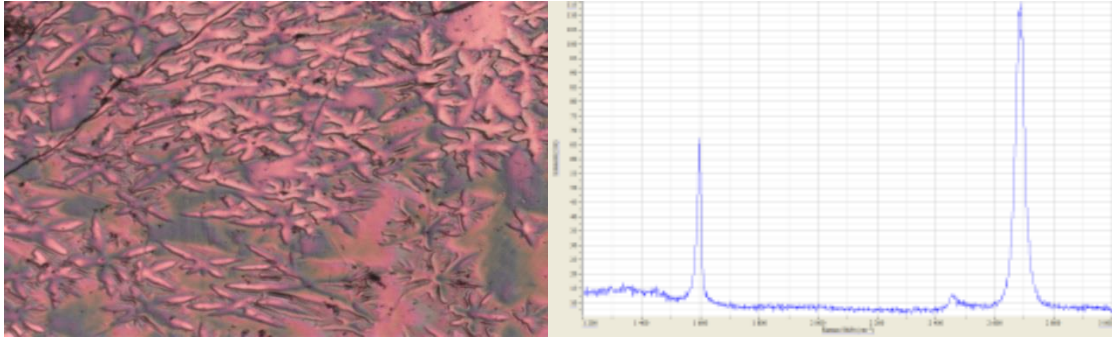
Figure 4.4-7: Optical image of the graphene crystals after transferring them on top of SiO$_2$ with the support of PMMA. Right plot corresponds to its Raman spectrum. This transfer corresponds to the sample 15C2001

4.4-3 Electrochemical Delamination Transfer in LTFN, AUTh

This work has been executed during my staying in the Laboratory of Thin Films and Nanometrology of the Aristotle University of Thessaloniki, Greece. This happened since May until July, 2015. The motivation was the optimization of the graphene transfer technique. The highest quality graphene becomes necessary in view of real life applications. The goal was to use the graphene as electrode in a cell for application in organic photovoltaics. My supervisor during my stay in LTFN was Prof. S. Logothetidis. I had the luck to collaborate with Dr. E.M. Pechlivani and Mr. D. Papas.

The set up used for these experiments was similar to the one presented in Figure 4.4-8a. During the experiments we used a modified electrochemical delamination process. From our previous experience we know that in an ordinary electrochemical delamination (spin coating PMMA on top of graphene/copper foil, delaminate the PMMA/graphene, transfer it to preferable substrate, clean the PMMA) appears one difficulty in the execution of the process that can potentially prevent the smooth delamination of the graphene. The PMMA sheet can stay attached to the copper foil in some parts, even only in one part, while it delaminates from the rest of the surface. This results in the wrapping of the sheet before its complete delamination, introducing cracks in the graphene as well. This is a process whose result is not always the desired.

To prevent this, we introduced the use of a thermal release tape (TRT) on top of the PMMA. The TRT in this case does not act as the medium for transferring the graphene but as a support substrate that maintains flat the PMMA film/graphene stacking. Even when immersed inside the aqueous solution, the TRT applies a small force to the PMMA that prevents it from wrapping or crumpling. Moreover, the TRT permits the easy handle of the PMMA/graphene, avoiding the step of 'fishing' it from the solution with the transfer

substrate. This often appears to be a complicate process that can lead to loss of the sample. A similar method has been introduced previously in the work of *Gupta et al* [Gupta, 2014]. In this work, they use a kapton tape instead as the support film and the delamination is not electrochemical. Only by immersing the stack inside deionized water and heating to 90 °C leads to the penetration of the water in the graphene-copper interface. After a period of time the stack of the graphene/PMMA/Kapton tape can be peeled away leaving the metal catalyst behind.

4.4-4 Graphene on copper foil

In these experiments was used graphene grown in polycrystalline copper foil, 75μm thick. The graphene film was continuous, following the required growing process (as described in the relative chapter considering the graphene growth). The graphene samples were prepared in FEMAN group, UB. (Samples with code 15D2201, 15D2401, 15C2601, 15D3002, 15B1101, 15B1101, 15B1201, 15B1301, details available in Annex 1). In
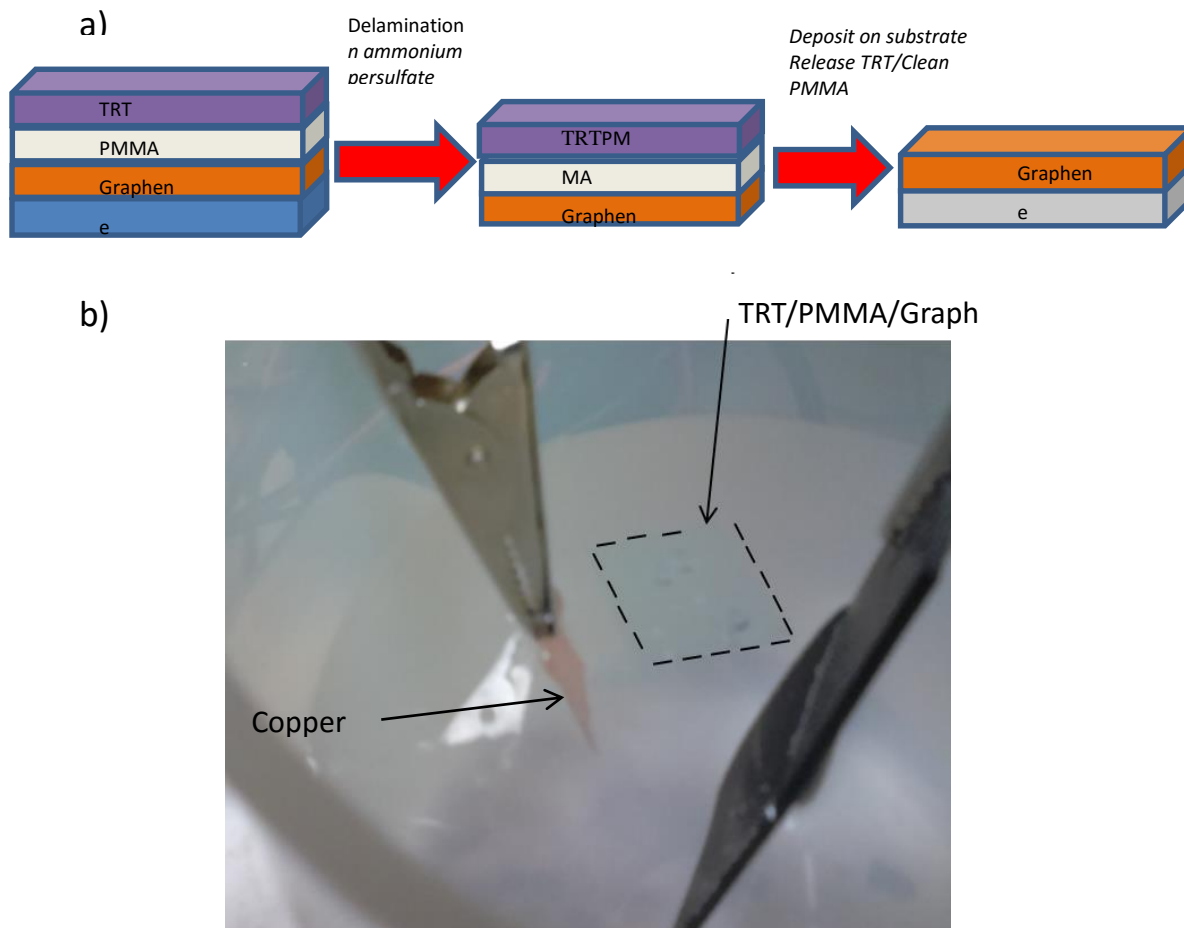
Figure 4.4-8: a) A scheme with the steps followed for the electrochemical delamination process. First PMMA is spin coated and then TRT is placed on top of graphene on copper foil. By the electrochemical delamination process the TRT/PMMA/graphene is delaminated. The stack is transferred to the desired substrate and the TRT and PMMA are removed by heating and acetone cleaning respectively. b) Image of the TRT/PMMA/graphene stack floating on the surface of the aqueous solution after completely delaminated.

Figure 4.4-8a we have a scheme of the steps of the electrochemical delamination process followed. In these processes was used a ammonium persulfate solution

$((NH_4)_2S_2O_8)$ in very low concentration of 0,2 mM. A higher concentration could accelerate the process but as ammonium persulfate can act as an etchant for the copper, could damage our sample. Depending on the applied voltage, the total delamination lasted from some minutes to one hour. On Figure 4.4-8b we see an image of the graphene/PMMA/TRT stack floating in the surface of the aqueous solution after the delamination.

The applying voltage in all the experiments was in the range of 4-24 V. The distance between the anode and the cathode was around 2-3 cm. The current passing through was measured between 1 and 3 mA, on a straight dependence to the applied voltage.

The TRT/PMMA/graphene stack was transferred then in the desired substrate. Heating to about 110 °C causes the almost instantaneous release of the TRT. Then the sample was immersed on acetone to remove the PMMA. The complete removal of the PMMA can also become a difficult task, althoughit is necessary to fabricate high efficiency devises. The acetone is heated to 50 °C. To remove the PMMA more efficiently is suggested the combination of acetone with heating up to 400 °C in an argon environment, but in that moment we did not have this facility available.

The substrates used to transfer the graphene were glass and SiO_2/c-Si. First we performed the transfer on top of glass to observe the samples in the optical microscope. The optical microscope was an optical transmission microscope (Axio Vert. A1) so the substrate had to be transparent.

Figure 4.4-9 shows an image of the graphene film on top of the glass substrate. On a first view is difficult to distinguish the graphene. The red lines indicate the edge of the film. On the right part is the film. On the left part is only the glass substrate. If we look carefully in the edge we can observe that the part with the graphene has a slightly darker color. The graphene in this image is around ~600×600 µm. No voids or wrinkles are visible at first, although electron microscopy is more suitable for characterization in the microscale. Raman spectrum of Figure 4.4-9 corresponds to graphene single layer. This estimation is based both on the I_{2D}/I_G intensity ratio as well as in the 2D peak shape (low FWHM and symmetrical shape of the peak).
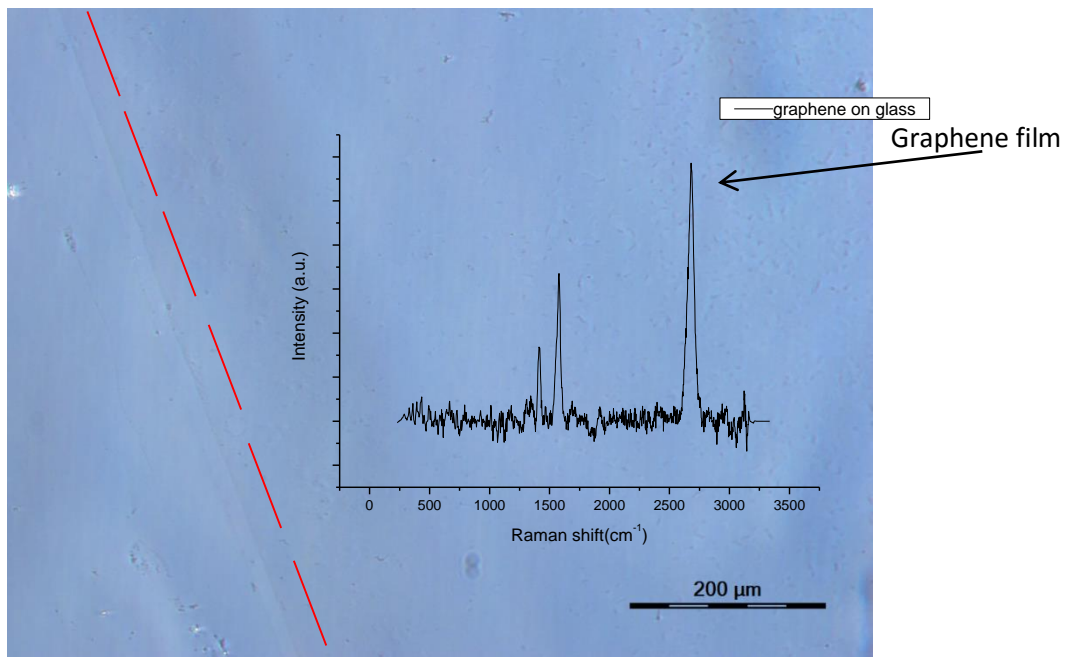
Figure 4.4-9: Optical image of graphene film after transferring on top of glass substrate. The transferring has been executed by electrochemical delamination with the support of TRT. On the inside, the Raman spectrum of graphene film on glass corresponding to single layer graphene (SLG).

4.4-5 Graphene on copper sputtered on SiO_2/c-Si

There have been also transfer processes performed with graphene grown on silicon wafers. The growths took place in a Black Magic system by Aixtron witch permits the load and growth in wafers of 6 inches diameter. The wafers have a 300nm intermediate SiO_2 layer followed by a 600nm copper film on top (Figure 4.4-10a).The silicon oxide layer is of crucial importance as it prevents the diffusion of the copper into the silicon during the CVD process [Ismach, 2010]. The growth by CVD is taking place up to 960°C, temperature in which the evaporation and diffusion of copper film is very high. The whole process has to be carried out in extremely optimized conditions to avoid the dewetting and evaporation of the copper. When we run the same growth process in wafers with 150 nm SiO_2, the dewetting of the copper was very high, forbidding the growth of graphene in many parts of the wafer area. The thickness of the copper film is important in order to avoid its dewetting. In the work of *Ismach et al* [Ismach, 2010] is compared the dewetting evolution with the time for copper films of 100 and 450nm, in temperatures up to 1000°C. The samples with a 100 nm thick copper film are completely dewetted when long growth processes are followed. In other works [Levendorf, 2009] 500nm thick

copper is used, we have not found any reference where thinner copper film is used.

The growth is taking place in 25 mbar in a mixture of CH_4/H_2/Ar gases. The flows of the gases, the growth temperature and the growth time are variables that affect the growth of the graphene.

A typical growth process consists of the annealing and the growth part.

The annealing takes place in an atmosphere of H_2 and Ar. It consists of brief annealing steps in different temperatures for short period of times.

During the growth a flow of methane is introduced as a carbon precursor. The growth temperature is set at 960 °C. The heat of the chamber takes place in the presence of Ar. When the chamber reaches the growth temperature (960 °C) hydrogen is introduced for a period 420 seconds to anneal and clean the wafer from possible impurities. Then the methane is introduced for the growth of the graphene. The growth lasts 1200 sec. In Figure 4.4-10b is presented a time/temperature diagram of the whole process. We can see the flows of the participant gases in each step of the process, 10 sccm of methane, 1000 sccm of argon and 40 sccm of hydrogen. After, the sample is let to cool down inside the chamber in a flow of 250 sccm Ar. This step is also very important as a high flow of Argon can possible etch away the grown graphene. We wait until the temperature falls below 150 °C before we expose the sample to the atmosphere to avoid possible oxidation.
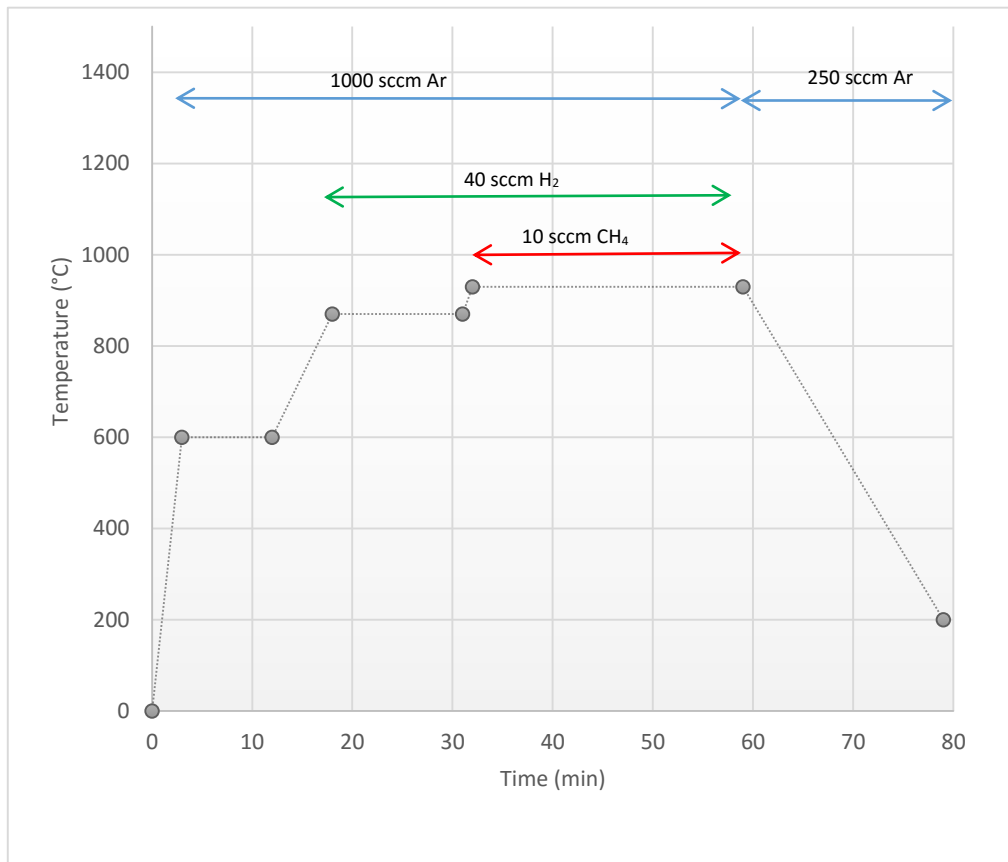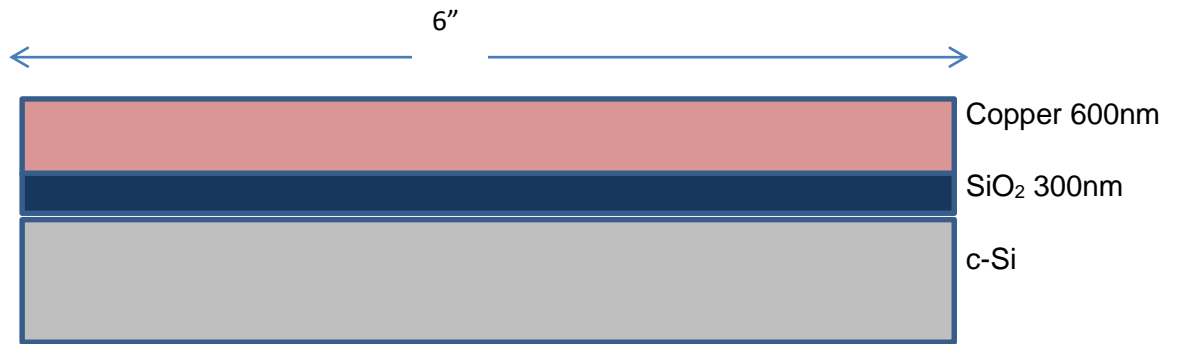
Figure 4.4-10: a) schematic illustration of the wafer used for growing graphene by CVD. b) temperature / time diagram of the whole growth process where the presence of gases (flows) in each step is presented. The pressure is stable at

To transfer the graphene grown on the Si wafers, a similar electrochemical delamination process to the one described in the case of the copper foil was followed. Both PMMA and TRT were used following the same technique explained before. Here the bubbles produced during the electrochemical process cause the delamination of the copper film, with the TRT/PMMA/graphene on top of it (Figure 4.4-11a). This happens probably because the adhesion of the copper to the SiO_2 is poor, so the bubbles can easier penetrate in the interface copper/SiO_2.

The delamination here is much quicker than in the case of the foil, in all the cases the stack delaminates after few minutes (2-10 minutes approximately). Then the metal catalyst has to be etched away. As the copper film here is much thinner than in the case of foil, the etching process is very fast. In principle the solution used for the delamination was the same as in the case of the copper (aqueous solution of ammonium persulfate, 0.1 mM). Using a much higher concentration of 0.1 M permits us to have a very quick delamination of the stack and etching of the copper at the same time, while the stack is floating on the surface of the solution. In this way we do not have to transfer the stack in another solution for the etching of the metal, and the etching does not take more than some few seconds.

After this, the TRT/PMMA/graphene stack is transferred to different substrates. Here, we present the transfer on glass and on polyethylene terephthalate polymer (PET) substrate. We prepared a sample where PMMA was spin coated on the whole surface, but TRT was applied only on the half of it. We performed the electrochemical delamination and we transfered the sample on glass. In this way, we can make a direct comparison between the two different approaches used as transfer media (PMMA or PMMA with TRT as support).

The images taken with the optical microscope reveal the effectiveness after using the TRT support (Figure 4.4-11b). In the right part of the image is the graphene film transferred with PMMA and the support of the TRT. In the left part is the part transferred only with PMMA. We can see that the film in the right part is continuous without voids or tearing, in contrast to the film in the left part that appears seriously damaged after the transfer process.
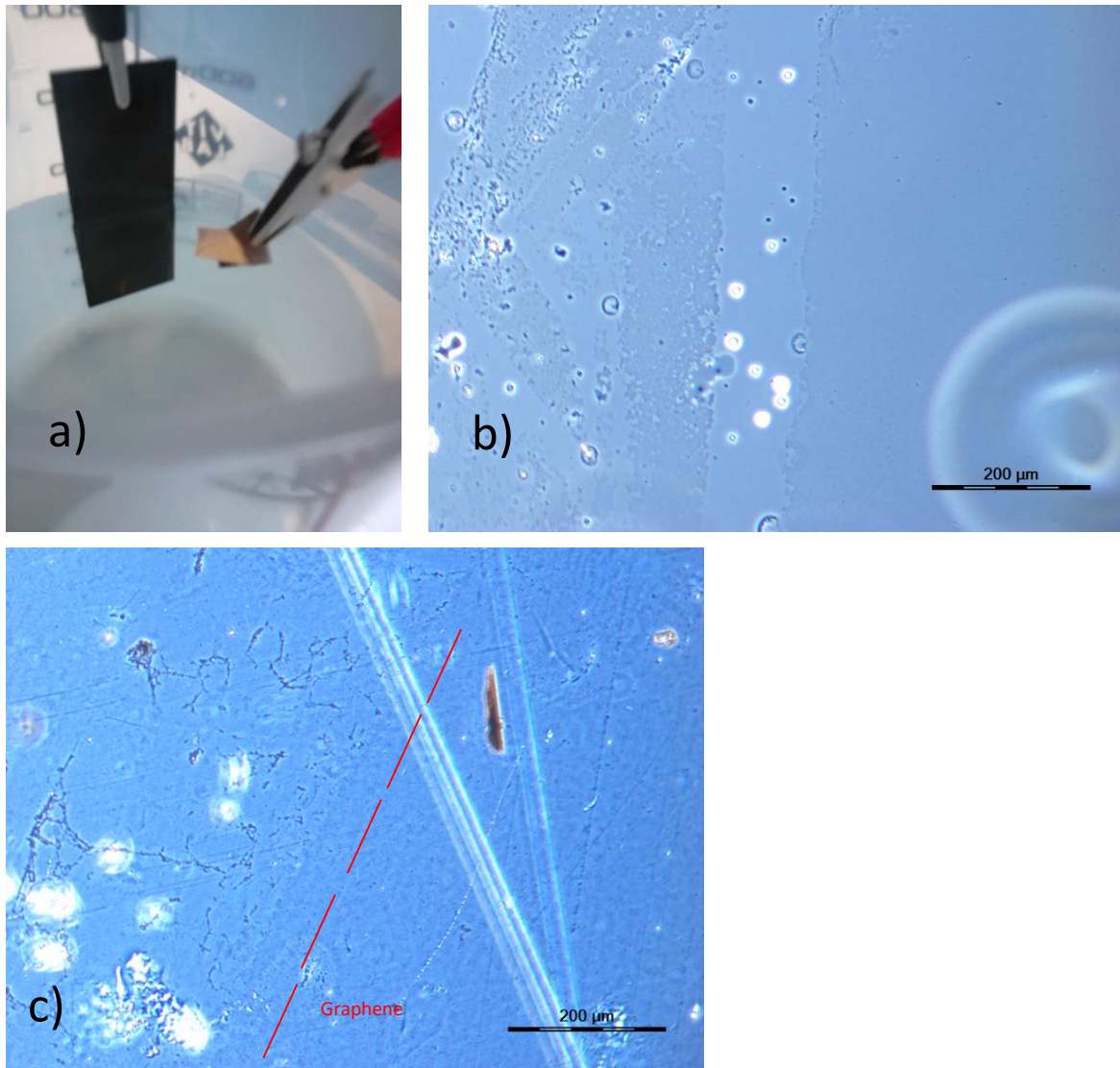
Figure 4.4-11:a) Image of the cell used for the electrochemical delamination transfer of graphene grown on silicon wafers sputtered with a thin copper film. The hydrogen bubbles cause the delamination of the stack copper/graphene/PMMA/TRT from the silicon substrate. In the image we see how the stack is floating on the surface while the silicon remains immersed inside the solution. b) Optical image of the graphene transferred on top of glass. In the left part the delamination is realized with the use of PMMA. In the left part TRT is used as an extra support film, contributing to maintain the graphene film continuous and undamaged. c) Optical image of the graphene film transferred on top of PET.

PET presents some interesting properties for applications like high glass transition
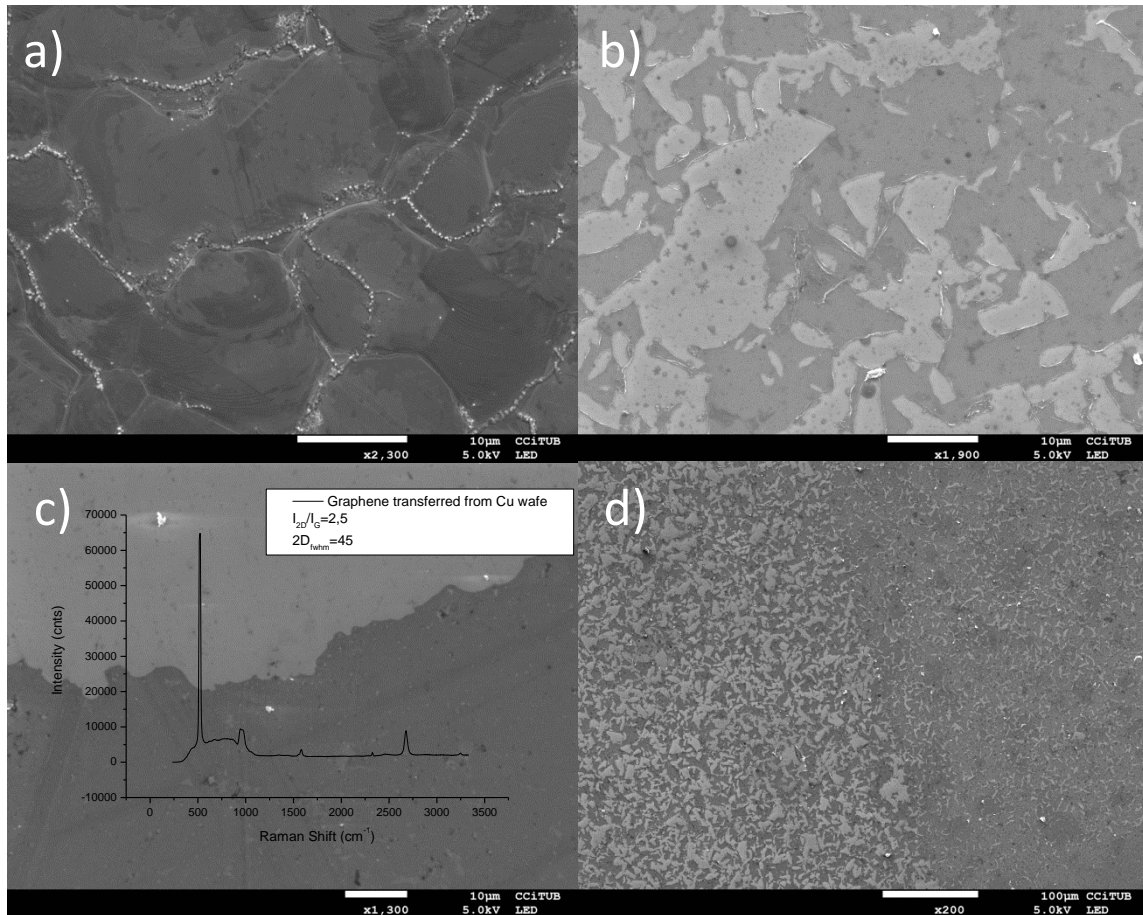
Figure 4.4-12: SEM images of a) graphene film as grown on top of the copper film, b) graphene film being delaminated only by the support of copper, c) graphene film being delaminated by the support of PMMA+TRT and d) direct comparison of the graphene film uniformity, delaminated by the support of PMMA (left region) and by the support of PMMA+TRT (right region). In images a), b) and c) the scale bar is 10μm. In image d) the scale bar is 100μm.

temperature, high chemical resistance, good mechanical properties and easy forming. When combined with graphene, PET is a potential candidate for applications in electronic devices, solar cells, touch screens, flat panel display and more as devices based on these film provide very low film sheet resistance [De Arco, 2010; Tapan, 2013]. To obtain graphene on PET, an interesting alternative in order to avoid the transfer process has been presented in the work of *Zheng et al.*, where the nanocomposites were prepared using a melt compounding method. The device presented an increased electrical conductivity with the increase in graphene content [Zheng, 2004]. In Figure 4.4-11c we present an optical image of the graphene transferred on top of PET. The film is in the right part of the red dashed line. The brown bright piece in the up part of the image is

copper that has not been etched away.

However, optical microscopy can not provide information about defects down in the scale of some tenths of micrometer. For that, scanning electron microscopy (SEM) was used to obtain information at this scale.

The same transfer methods described before were used, transferring the graphene to SiO_2/c-Si. SEM images of Figure 4.4-12 allow us to compare the uniformity of the film after the transfer with PMMA and with PMMA and TRT as a support. In Figure 4.4-12a we have a SEM image of the graphene film as grown on top of the copper film. We see that the graphene here is completely uniform without any voids. The bright particles are defective centers formed during the growth [Li, 2009]. Observing the graphene being delaminated by PMMA we see that in many parts the film is not continuous (Figure 4.4-12b). Using TRT as an extra support film contributes to the uniformity of the graphene. In Figure 4.4-12c, on the down part of the image is the continuous graphene. On the up part is the silicon oxide substrate. The Raman spectrum of this figure provides an evidence (I_{2D}/I_G = 2.5) of the single layer thickness of the graphene. Finally, the direct comparison between the two transferring techniques (Figure 4.4-12d), like the one made in the description of the optical microscopy image in Figure 4.4-11b, reveals the important role of the TRT. In the right part of figure 4.4-12d the delamination has been realized with the support of the TRT upon the PMMA. On the left part the delamination has been realized with the support of PMMA only. The difference in the uniformity of the film is clear between the two regions is clear.

4.4-6 Conclusions

The graphene transfer process is as critical as the growth of the material itself. Almost in all variety of applications, it is a necessary step in order to deposit the graphene film in the desired substrate. The process should be designed ensuring that it will introduce no defects to the graphene film. This task appears to be complicated in most of the cases. The different materials used for the transfer (polymers, TRT, support substrates) introduce impurities in the surface of the film, which are difficult to be completely removed. Trying to solute this, there have been introduced methods that there is no need of an additional transfer means. Although, in these are introduced surface tensions that cause tears and voids in the film surface. In other cases, the method is designed to transfer the graphene in a specific substrate, so it can not be a candidate solution for all different application.

From our experience, we consider that the idea of using the PMMA as a transfer media and the TRT as an extra support film in an electrochemical delamination process is the ideal candidate solution for an effective graphene transfer. The method is designed to take advantage of the characteristics of every means. The PMMA is ideal for the transfer of continuous graphene film. With the use of the TRT as a support layer, the film is protected from bending that can cause tears. The electrochemical delamination from the metal catalyst saves the graphene from the impurities that the metal etchant inputs. Both optical and electron microscopy ensure us the uniformity of the transfer film. Electrical measurements at large scale should be made as well.

5. WO3/graphene and CeO2/graphene films based supercapacitors

Electrochemical energy storage devices like supercapacitors and batteries are recently being very popular for use as power supplies in a wide variety of applications, from portable electronic devices, such as cell phones and laptops, to hybrid electric vehicles [Hall, 2008]. Supercapacitors can exhibit a higher power density and a superior life cycle, but exhibit lower energy density, when compared to conventional batteries [Hall, 2010]. To meet the demands for a possible commercialization, supercapacitors should consist of low-cost electrode materials that can be used to provide powerful electrochemical devices, devices based on the high charge storage capacitance. They should present excellent stability, fast charge, and discharge rates, as well as high energy and power density combined with light weight, high flexibility and optical transparency.

The latest research around the design and optimization of new electrodes has promoted the combination of graphene with different metal oxide films [Yang, 2015; Lake, 2012] to build hybrid supercapacitors. Graphene has been shown to be an effective material for constructing supercapacitor electrodes due to its large surface area, high mechanical stability, and electrical conductivity. Only graphene electrodes allow double layer specific capacitances of up to 135 F/g, while when combined with other metal oxide composites like Fe_2O_3/graphene and MnO_2/graphene, they have demonstrated capacitances up to 380 F/g. [Zhang, 2010].

In our work, single and layer-by-layer graphene stackings (with metal oxides sputtered on top) have been fabricated combining graphene transfer techniques and magnetron sputtering. On top of the graphene were sputtered different metal oxide particles (WO_3 and CeO_2). Compared to monolayer graphene, multilayer graphene films have more electrode/electrolyte interfaces, which are beneficial to the absorption/desorption of electrolyte ions and provide more electrical pathway for electrolyte ions during the charging and discharging. The introduction of metallic particles enhances the specific capacitance of ultrathin layer at a relative low mass loading [Zhang, 2014]. In previous works CeO_2 particles have demonstrated high capacitance, in the order of 119 mF/cm^2, when combined with nickel foam [Hu, 2012]. Considering the WO_3 films, recent work reports electrodes made by WO_3 rods presenting a capacitance of 266 F/g [Shinde, 2015].

The electrochemical properties of the samples were analyzed using a Swagelok cell and organic (1 M $LiClO_4$ dissolved in ethylene carbonate (EC) and diethyl carbonate (DEC) mixed in 1:1 volumetric proportions) and aqueous (1 M $NaSO_4$ solution) electrolytes.

Continuous graphene films were grown by chemical vapor deposition in GRAPHMAN reactor, following the growth recipes presented in the relative chapter of this Thesis.

The electrodes were cut in pieces ~0.7 cm^2. The metal oxide particles were deposited in
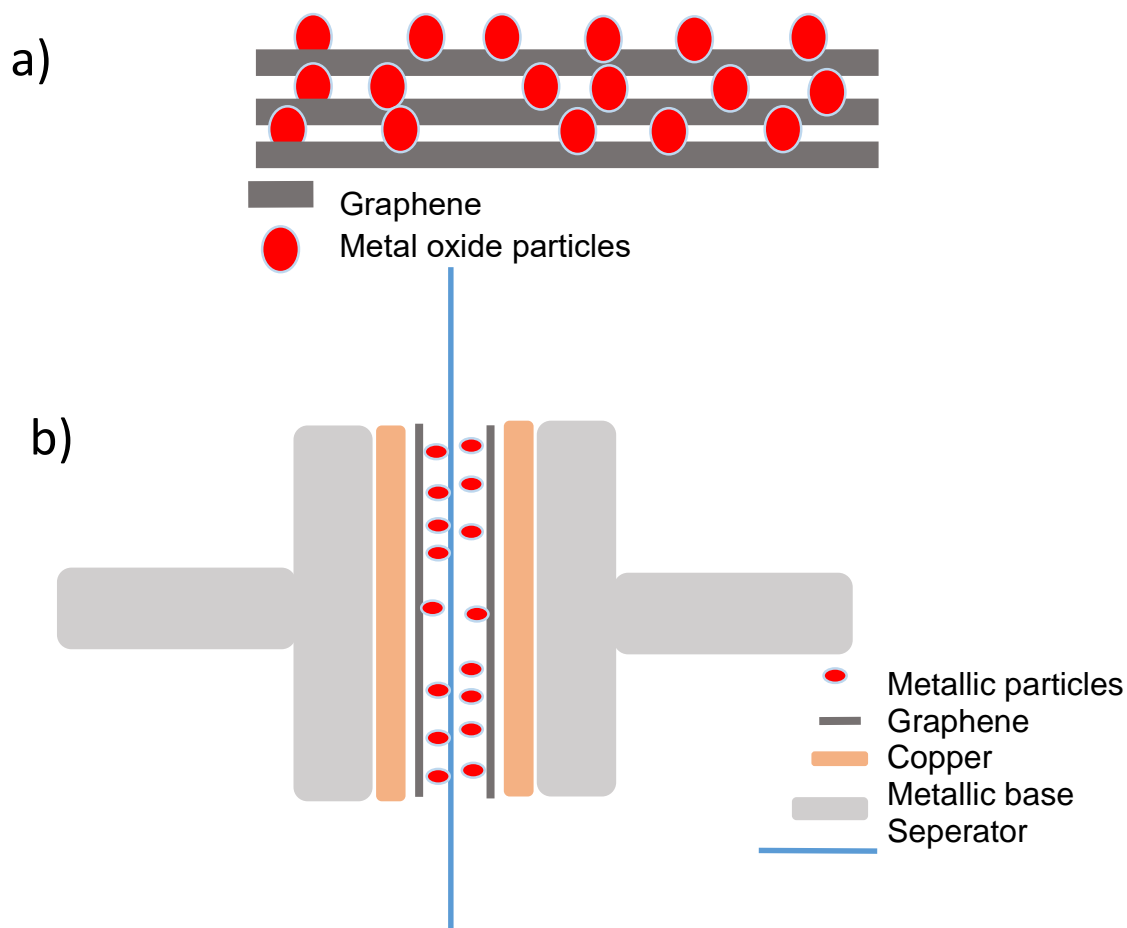
Figure 1: a) Scheme of the stacking of 3 layers graphene/metal oxide particles, b) Scheme of the design of the cell. The separator (glass fiber flter) is soaked with 1 M LiClO4 dissolved in ethylene carbonate (EC) and diethyl carbonate (DEC) mixed in 1:1 volumetric proportions.

the graphene by pulsed magnetron sputtering (1 Pa of total pressure, 13/7 sccm/sccm of Ar/O$_2$ flow rates and 60 W of pulsed-DC power). To prepare the 3-layers stackings of metal-oxide/graphene, the copper was etched away by FeCl$_3$ and the remaining metal-oxide/graphene was transferred over another layer of metal-oxide/graphene. PMMA was used as support scaffold. The final 3 layer stack had a geometry similar to Figure 5-1a. In Figure 5-1b we can see the scheme of the as used cell (with one layer of graphene/metal oxide particles on each electrode).

To study the supercapacitance behavior of the devices we first made cyclic voltammetry (CV) measurements in different scan rates. The capacitance *C* was calculated by the equation,

$$C = \frac{I}{\frac{dV}{dt}}$$

where *I* is the average current in ampere and *dV/dt* is the voltage scanning rate.

The interfacial capacitance C_i was calculated using the relation,

$$C_i = \frac{C}{A}$$

where *A* is the area of active material dipped in the electrolyte. Figure 5-2 presents the CV measurements of the different electrodes.

The application of Ar/O_2 plasma to oxidize the graphene film increases its capacitance when compared to the as grown graphene film. The as grown graphene film presents a capacitance of 8 mF/cm^2 at 10 mV/s, which increases to 14 mF/cm^2 after the O_2 plasma application. Graphene films sputtered with WO_3 particles present a better capacitance (10 mF/cm^2) than those sputtered with W particles (4 mF/cm^2). The increase in the number of layers increase slightly the capacitance of the devices.
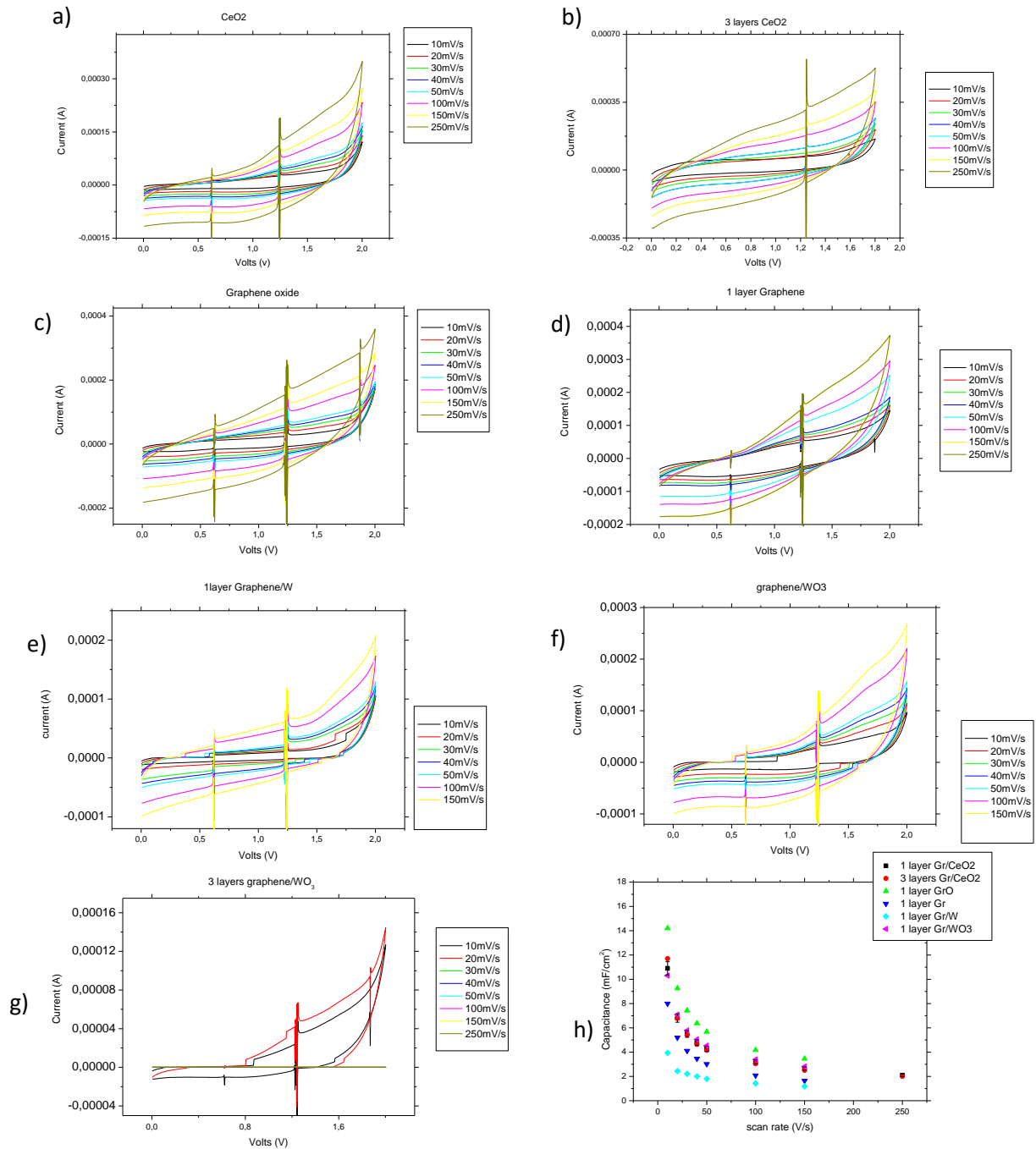
Figure 2: a-g) CV measurements of the different hybrid electrodes at different scan rates. a) 1 layer CeO₂/Gr, b) 3 layers CeO₂/Gr, c) 1 layer GrO, d) 1 layer Gr, e) 1 layer W/Gr, f) 1 layer WO₃/Gr, g) 3 layers WO₃/Gr, h) capacitance (per area) of the different hybrid electrodes at different scan rates. All devices present the higher capacitance at the lower scan rates.

In summary, the electrodes made of 1 layer of CeO_2/Gr have a capacitance of 10.8 mF/cm^2, which increase to 11.8 mF/cm^2 when two more layers of CeO_2/Gr are added. Similar behavior is observed to the WO_3/Gr electrodes. Their capacity increases from 10.2 mF/cm^2 to 11.8 mF/cm^2 when two more layers of WO_3/Gr are added over the first layer. The peaks appearing to all measurements in 0.62 V and 1.24 V have their origin in some artefact, oblivious to samples.

Considering their stability, the electrodes based on WO_3/Gr appear to present a better retention of their capacitance in comparation to the ones based on CeO_2/Gr. The first ones were stable during the first ~850 cycles while the second ones exceed the 1000 cycles as we can see in Figure 5-3a. The principal decay in the capacitance during the first cycles can be attributed to the pulverization of original metal oxide and *in situ* formed metal nanoparticles during Li insertion and extraction process, which lead to loss of electrical connectivity between neighbouring particles [Liu, 2015]. The electrodes consisted of CeO_2/Gr present a better charge/discharge efficiency during more cycles as seen in Figure 5-3b. The performance of all devices is between 60-70%.

The galvanostatic charge/discharge curves reveal that when more layers of metal oxide/graphene are added, more time is necessary for the charging and discharging process. This is visualized in Figure 5-4a. 1 layer CeO_2/Gr needs 2 s approximately for a charge/discharge cycle when charged by 400 mA/cm^2. When 2 more layers are added over the first one, this time increases to ~5.5 s. The 3 layers WO_3/Gr charge faster in compare to these of CeO_3, as we see in Figure 5-4b. In all measurements we take into consideration the second cycle.

a)
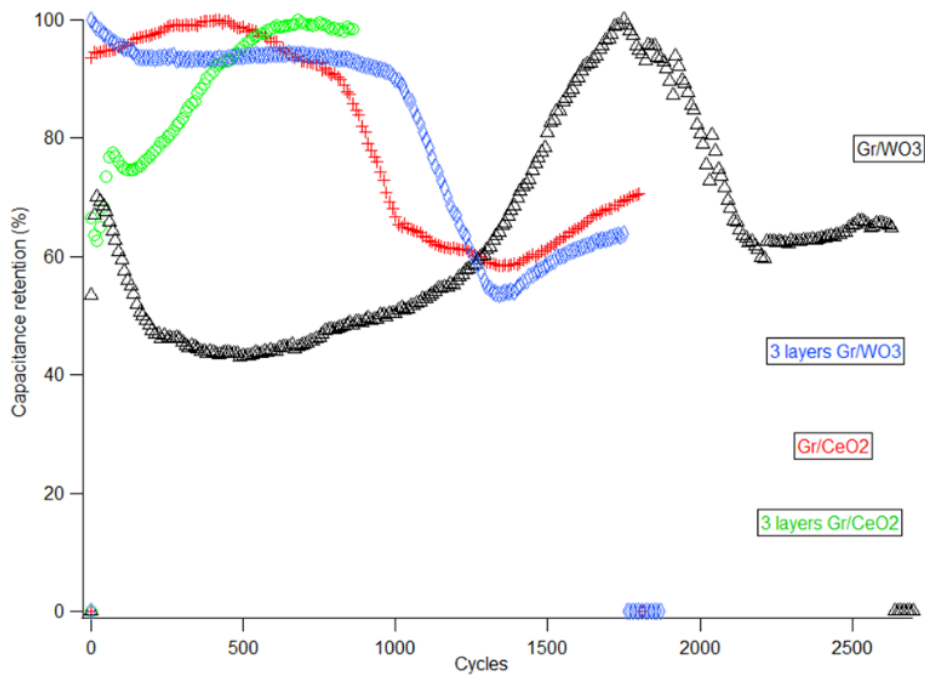
b)
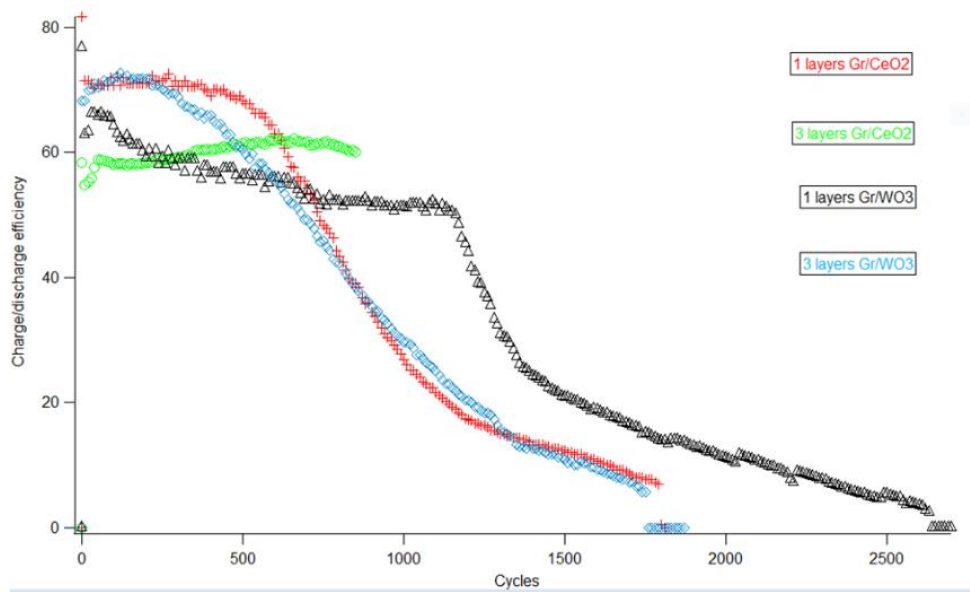
Figure 5-3: a) Capacity retention of the different electrodes and b) charge/discharge efficiency.
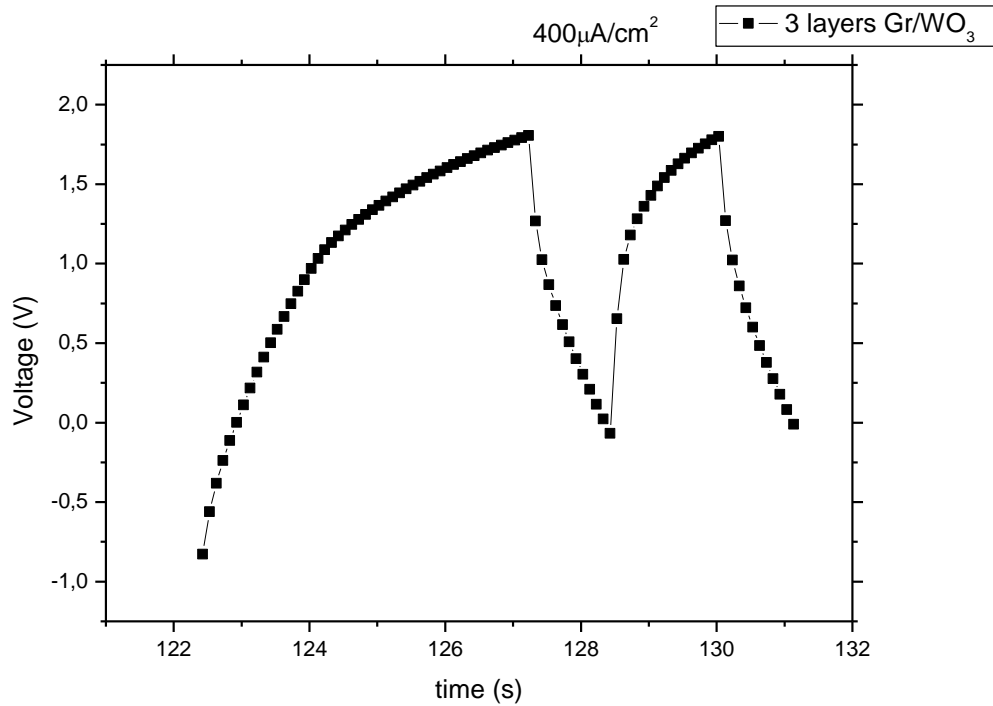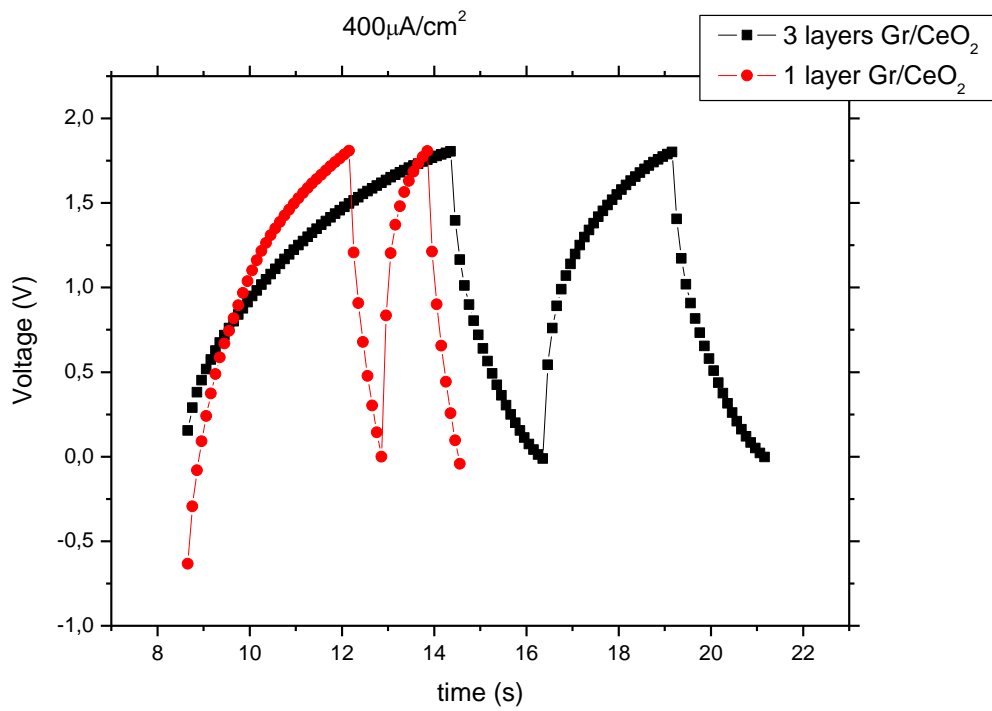
Figure 5-4: a) Charge-discharge cycle of 1 and 3 layers Gr/CeO₂ and b) the same for 3 layers Gr/WO₃

5.1 Conclusions

Layer by layer evaluation of graphene electrodes combined with different metal oxides was performed. The results reveal that all devices present a higher capacity in the smallest scan rate (10 mV/s). The oxidation of the graphene film increases its capacitance. The same happens when more layers of metal-oxide/Gr are added over the first layer. The devices where Gr was combined with CeO_2 are presenting a slightly higher capacity than those where Gr was combined with WO_3. Considering their stability all devices maintain their initial performance for more than 800 cycles. The charge-discharge period increases with the addition of more layers. The deposition of the metal oxide particles by oxyen plasma sputtering proably results in the etching of the graphene film [Mumen, 2014]. Different deposition techniques should be taken into consideration like chemical polymerization, ultrasound sonication [Raj, 2015] and more. Moreover, a structural characterizationof the electrodes should be performed, with X-ray diffraction and Transmission electrode microscopy, before and after the realization of the measurements in order to obtain information about the deposition of the particles.

6. Fabrication and evaluation of Graphene Field effect Transistor

Graphene is among the main candidate materials for use in post silicon electronics. Between other applications, a lot of attention has attracted the potential use of graphene as an electrode in field effect transistor.

FET is one of the most successful device concept in electronics, therefore scientists from the field rapidly get involved to incorporate graphene in it. We can not neglect to mention the groundbreaking work of Prof. Novoselov and Prof. Geim, [Electric Field effect in Atomically Thin Carbon Films,Novoselov, 2004], where they experimentally study the electrical properties of graphene for first time. Thanks to its ballistic transport properties, very large carrier mobilities can be achieved. Since very early, it has been reported the fabrication of transistors which exceed 200.000 cm^2/V s by use suspended graphene as a channel [Bolotin, 2008]. As graphene is a gap less semiconductor, it shows an ambipolar behaviour,i.e., both charge carrier types contribute to its conductivity [Ochedowski, 2013]. Because of the absence of bandgap, graphene can´t be used in application requiring any digital switching. Today a lot of research is made in this direction, trying to figure out ways to open and tune the band gap of graphene. Different methods have been proposed, including dopings, substrate effects patternings, hydrogenations, adatoms [Park, 2015].

A simple FET device was fabricated in order to extract information about the electrical properties of the graphene. First, single layer graphene grown on copper foil (see relative chapter) was transferred onto 90 nm SiO_2 on a Si wafer (in this case <100> p-doped boron, ρ= 0.001-0.005 Ω·cm, and 525 µm thick).

The transfer was made by the use of PMMA as support layer (see relative chapter for more information into transfer processes). Then, the source-drain contacts have been placed on top by vacuum evaporation. For this process it has been used the evaporation chamber placed in the clean room of the Physics Faculty, in University of Barcelona (Figure 6.1).

Figure 6.1: Base holders inside the vapor deposition chamber, where the different metals are placed for evaporation. From left to right the holder for Au, Cr and Al.

To achieve a good adhesion of the contacts we first deposit 20 nm of Cr, followed by 150 nm of Al and finally 20 nm of Au, to prevent the oxidation of the contacts. The evaporation shadow mask used for the deposition of the contacts was provided by Ossila (product code item E329). The channel has a width W=4mm and a length L=0,02mm. In Figure 6.2a we see a scheme of the transistor devise, helping to understand it´s geometry. In Figure 6.2b is provided microscopy some optical microscopy images of the devise where we can see more in detail the geometry of the channel.

a
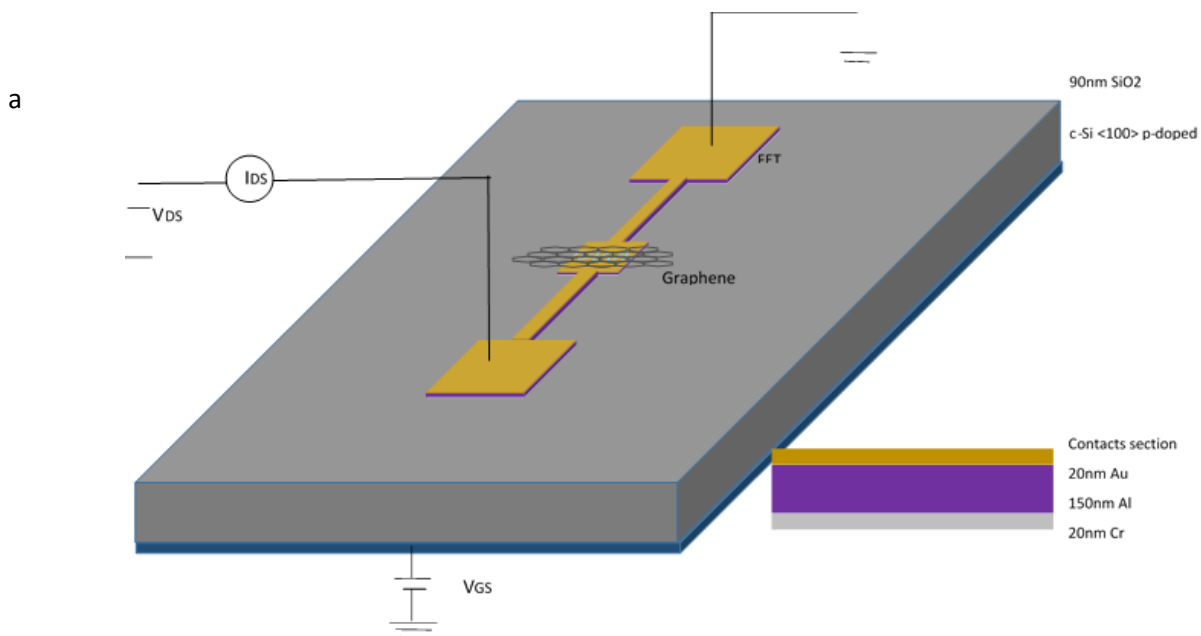
b
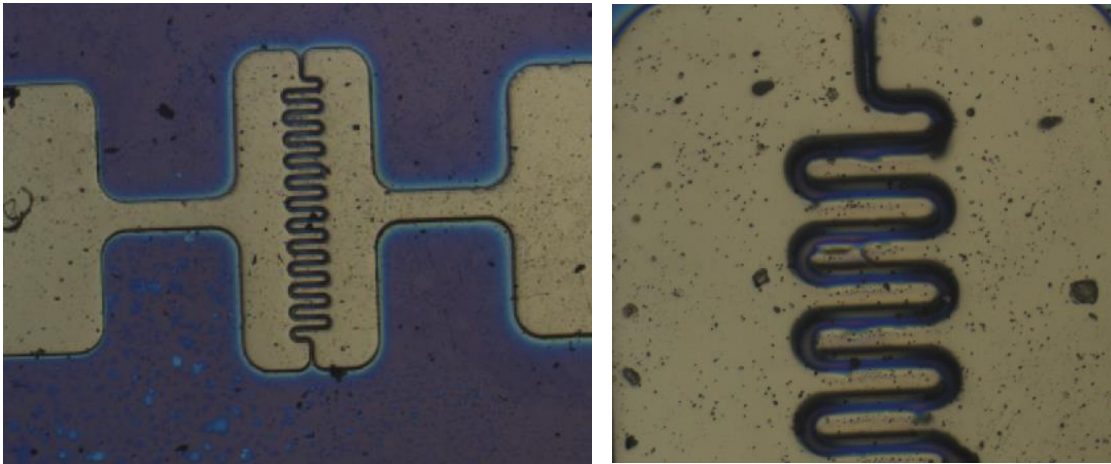
Figure 6.2: a) Scheme of the electrical set up of the FET based on graphene. Cr is used to achieve a good adhesion of the contact and cold to prevent the oxidation of it. The Si substrate is used as a back gate and the SiO_2 as dielectric. b) Optical images of the FET device. On the zoomed image we can see the geometry of the channel, designed to have a long width and a short length.

First, the SiO_2 was deposited over the Si substrate by magnetron sputtering. As we observed from the devices fabricated later, this is not an adequate method to obtain a homogeneous film. The SiO_2 was conducting carriers, proof of being inhomogeneous. This can be seen in the first measurements that had been performed. In Figure 6.3 we see that the I_{DS} is obtaining negative values for negative V_{GS}, during a positive V_{DS}, a behavior that is not normal when the dielectric functions properly.
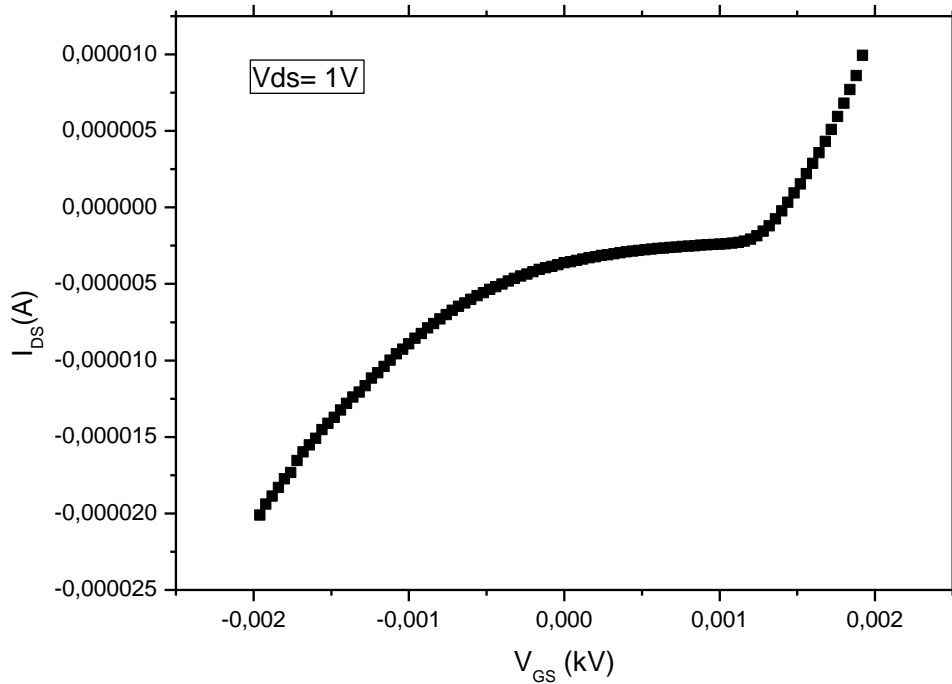
Figure 6.3: Transfer characteristic curve of the field effect transistor device fabricated over sputtered SiO$_2$.

We then grow the SiO$_2$ film by thermal oxidation of the Si substrate. This process requires the remove of the SiO$_2$ from the one face of the substrate which will function as the back-gate of the transistor later. Step-by-step the process is described in Figure 6.4. First 300nm of SiO$_2$ are grown by heating of the Si substrate in atmospheric pressure, on both faces of it. Then, the one face of the substrate is covered with an apiezon wax compound (dissolved in Trichloroethylene) to be protected. HF (20% in distilled water) is used to etch away the SiO$_2$ from the other face (etching rate, 40nm/min). Then, a Cr 50nm film is sputtered in the SiO$_2$ free face to ensure the good conductivity in the back-gate. The substrate is then washed with trichloroethylene, acetone and D.I. to remove the apiezon from the other face. Finally, the deposition of the FET contacts is taking place as described above.
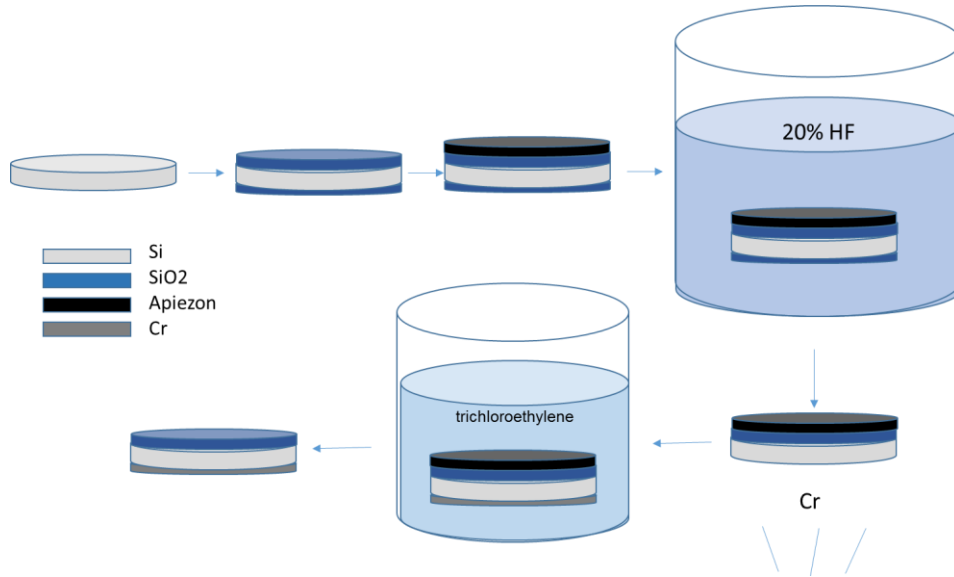
Figure 6.4: Step by step thermal growth of the SiO₂

Then, we proceed to extract the electrical properties of the device we fabricated, with respect to its output ($I_{DS}(V_{DS})$) and transfer ($I_{DS}(V_{GS})$) characteristics. I_{DS} is the current between the source and the drain, V_{DS} is the voltage between the drain and the source and V_{GS} is the voltage between the back gate and the source. The voltage between the source and the drain remain stable. From the plot $I_{DS}(V_{GS})$ we can obtain information regarding the carrier mobility μ and conductivity σ.

$$\mu = \frac{dI_D}{dV_{GS}} \cdot \frac{L}{WC_iU_{DS}} \; (1) \; \text{ and } \; \sigma = \frac{dI_D}{dV_{DS}} \; (2)$$

$C_i = \varepsilon \cdot \varepsilon_r / d = 3.837 \; 10^{-4}$ F/m^2, is the capacitance between the channel and the back gate per unit area, where ε and ε_r are the dielectric constants of air and the dielectric (SiO2: $\varepsilon_r = 3.9$), respectively, and d is the thickness of the oxide layer (90 nm).

In the plots in Figure 6.5a and 6.5b we can see the electrical behavior of our device. The linear amplification of the current starts above 5V. By fitting the linear regime into a linear polynomial ($y = a + bx$) in the range 5-10V, we obtain the slope of the curve which corresponds to the dI_{DS}/dV_{GS}.

y= -1.26226x10^{-4}+ 1.0873x10^{-4}x

For a source drain $V_{DS}=0.02V$ the $dI_{DS}/dV_{GS}=1.0873 \times 10^{-4}$.

a

b
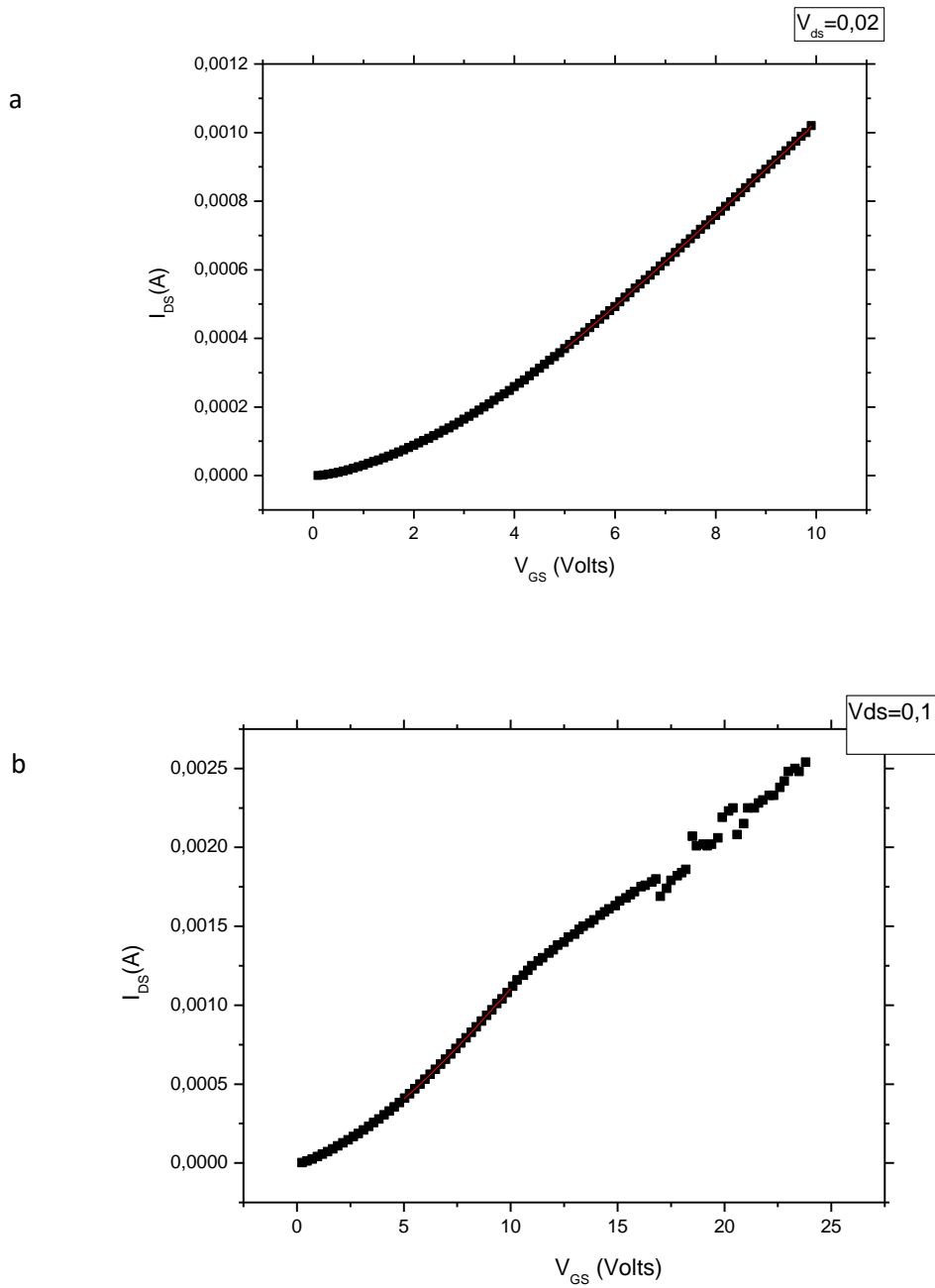
Figure 6.5: a) Transfer characteristics of the graphene-based FET device with a drain-source voltage of 0.02 V. b) the same for a drain source voltage of 0.1V. The linear fit is visible with a red line in both plots.

Knowing the dI_{DS}/dV_{GS} value and replacing it in the equation (1), we can extract the value of the mobility $\mu=708$ cm^2/V s.

The surface conductivity σ_s can be derived from the equation (2) at V_{GS}= 10V, using the data of Figure 2a and 2b.

σ_s=1.25x10^{-3} S.

The charge carrier surface density can be derived from the equation

$$n_s = \frac{\sigma_s}{e\,\mu_n} \text{ (3)}$$

n_s=9.06x10^{12} /cm^2,

All values obtained are typical ones that can be found in the literature for cvd graphene, taking under consideration the defects introduced by the grain boundaries [Song, 2012].In the work of Song et al has been explored the increase in the field effect mobility when devices with narrower channel are used. This minimize the effect of the polycrystalline nature of the graphene film to the performance of the device.

6. 2. Graphene FET with different contacts geometry
Apart from the measurements described above, we fabricated another graphene device to carry out field effect measurements. The contacts and the measurements regarding this device were carried out with collaborators of the Institut of Microelectronics of Barcelona.

In this case, continuous single layer CVD graphene was transferred over 300 nm SiO$_2$/Si wafer. Then, metal contacts were deposited by e-beam lithography over the graphene. This time the contacts consisted of 20nm of Cr/ 20nm of Au, with the Cr in contact with the silicon oxide (Figure 6.6). We deposited different contacts, varying both the width a (values=0,5/1/5/10µm) and the length b (values=5/10/20µm). In the back-gate we deposited 20 nm of Cr by evaporation.
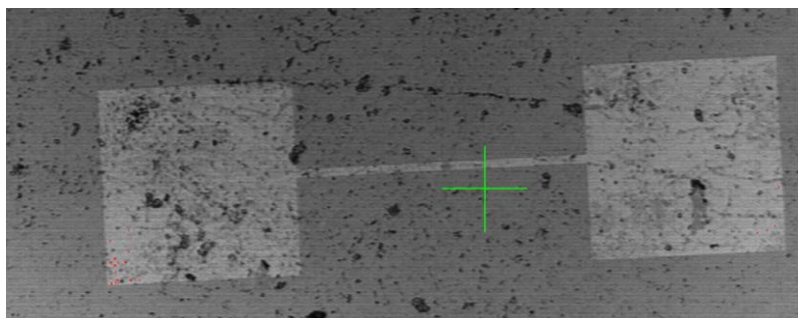
Figure 6.6: Optical microscopy image of the graphene FET.

In the measurements that with this devise we could not observe any field effect. A possible reason is the bad contact of the back-gate. The other critical parts of the device seemed to work well, since we could measure the current between the source and the drain and the current between the source and the gate was many orders of magnitude lower than this between the source-drain.

Then, we measure the resistivity of the graphene by 2 probes for the various values of canal´s length and width (Figure 6.7).
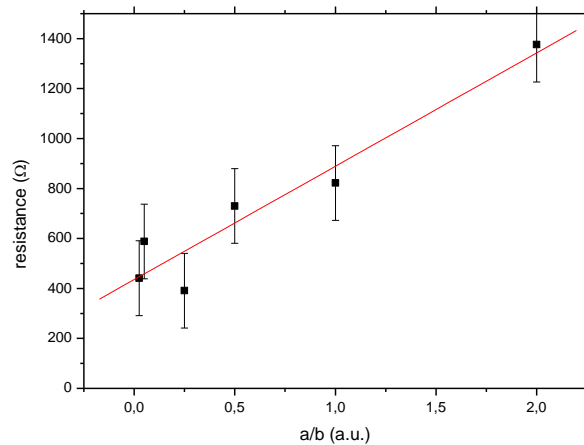
Figure 6.7: Resistivity dependence on canal´s dimensions.

In the above measurements, apart from graphene´s resistance, there is also a resistance introduced by the contacts. Then

$R_T = R_G + R_C$

, where R_T is the total resistance (that we measure), R_G is the resistance of the graphene and R_C the resistance introduced by the contacts. The resistance of the canal depends on its dimensions through the equation

$$R_G = \frac{1}{\sigma_s} \frac{a}{b}$$

Where σ is the conductivity. The linear fitting of the experimental points of Figure 6.7 gives the equation

y=435.44 +453.68 x

, where R_C= 435.44 Ω is the resistivity of the contacts and $\frac{1}{\sigma_s} = 453.68$. Then, we calculate the conductivity σ_s=0.0022 Ω^{-1}

In addition, we obtain the characteristic I_{DS}-V_{DS} of the two terminal configuration (Figure 6.8). We use Ohm´s law to extract the conductivity of the sheet

$$\sigma_s = L/RW$$

,where R= 628.9 Ω extracted by Figure 6.8 [Mojarad, 2009].
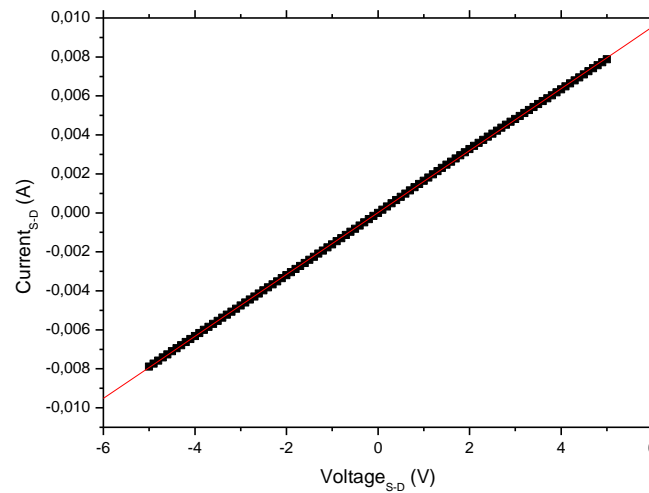
Figure 6.8: Characteristic I_{DS}-V_{DS} of the 2 terminal configuration with the graphene in the channel.

The dimensions of this device channel is L=W=10 µm, therefore σ_s=0.00159 Ω^{-1}. The above values of conductance extracted both measuring the resistivity as well as the I_{DS}-V_{DS} characteristic come in agreement in the order of magnitude with bibliographic references [Miao, 2007].

6.1 Conclusions

CVD graphene is used for the fabrication of a field effect transistor. The objective is the electrical characterization of the graphene regarding characteristics like the conductivity, carrier density and carrier mobility. Apart from the field effect measurements, similar conductivity was measured in the graphene films when measuring the characteristic IDS-VDS in a two contacts configuration. The agreement in the measurements (made in different apparatus), ensure us about the preciseness of them. CVD graphene may present a less qualitative behavior compared to other ones, like exfoliated. This is a result

of the presence of grain boundaries as well as of other defects in its atomic structure. Although, CVD graphene present the advantage of large scale synthesis and high homogeneity in its quality. Other source of impurities can be the ionized charged impurities at the graphene-oxide interface. It has been demonstrated in other works how these impurities can limit the electric properties of the device [Hwang, 2007]. In this work the graphene has been transferred on the substrate by the use of PMMA. It would be interesting to see how different transfer processes (described in the relative chapter of this Thesis),or the selection of a different substrate for the fabrication of the device [Sachs, 2014], could improve the characteristics of the device. The values obtained are standard values that can be found in the literature.

7. Conclusions

- GRAPHMAN reactor consist a sufficient and economic system for the growth of high quality monolayer graphene in large scale, moreover when compared with other commercialized systems that exceed it´s cost hundreds of times.

- The study reveals the sufficiency of hydrogen plasma to reduce the copper oxide layer that is formed on top of the copper foil. The technique is quite faster than the usual thermal annealing that is applied in this case.

- The optical emission spectroscopy is proved to be a very sufficient tool to obtain information about the reduction of the copper oxide.

- Electron back scattered diffraction provide as with usefull information about the crystallinity of the copper surface. Longer thermal annealing or longer growth processes do not affect result in farther growth of the copper domains. The copper domains reach in all cases no more thatn about 8000µm^2.

- Graphene crystals were grown by CVD in both sides of copper foil in low pressure at 1040 °C. Two parameters are being examined, the total pressure and the hydrogen flow. We studied the two parameters individually to know the effect each one has in the graphene growth. The SEM characterization indicates that small variations in these parameters can affect the morphology, nucleation density and size of the graphene crystals.

- In concrete, the hydrogen flow appears to have an important role to the morphology of the crystals but not in the size of them. Concrete quantity of hydrogen can perform strong etching to the graphene. In our results the etching effect appears to be inversely proportional to the hydrogen flow.

- In the parts of the substrate that the graphene is not being etched away we see that the domains maintain the same size independently of the hydrogen flow. The total graphene covered area is varying a lot, depending on the nucleation density and the hydrogen etching effect. Increasing the hydrogen flow in a stable chamber pressure resulted in the growth of a continuous film. In slightly lower hydrogen flows the film was being etched anisotropically and appeared seriously damaged.

- The chamber pressure appears to affect the nucleation density as well as the size of the graphene crystals in stable gases flows. A big increase in the ΔPH/ΔPch4 ration during the growth, in a stable pressure, appears to decrease the nucleation density. A smaller nucleation density gives more surface space to each crystal to growth, resulting in the formation of graphene films with less grain

boundaries.

- The nucleation density appears to follow a linear dependence in relation to the % total coverage, when the second is normalized with the lobe´s length.

- In addition, we observed that the nucleation density is remarkably higher, the double or more, in the facet (310) in compare to the (221). This conclusion is fundamental. Selecting etching of the copper facets could permit the abidance of the (221) facet in the foil surface would allow the growth of graphene from a small number of nucleus.

- Outside the range of pressures that we studied here, between 10 to 25 Pa, the graphene nucleation is not being performed or the film obtained is seriously damaged, as a result of the anisotropic etching. The above information can be useful in the design of experiments that target to grow low density graphene crystals.

- We underline the importance of the exponential increase of the hydrogen concentration which is not usually taken into consideration when the hydrogen flow is constant. In addition, we highlight that the relative pressure $<P_{H2}>/<P_{CH4}>$ ratio diagram follows the same variation as the % coverage diagram, proving that the partial pressure can be a more efficient evidence than the flow when we want to characterize the effect of the hydrogen, as it takes under consideration the evacuation efficiency of the pumping system.

- The Raman characterization ensures that all the surface of the foil is covered with monolayer graphene. The presence of the D peak can be due to defects on the film. After the transfer of the film to SiO_2 we notice a significant contraction of the 2D peak. On the other hand, the I_G/I_{2D} ratio appears unaffected of the substrate.

- Considering the experiments done to establish a balanced concentration of hydrogen, the ability of more sufficient control in the growth of graphene is being explored. The hydrogen flow appears to perform an etching in the graphene domains which affects their morphology and uniformity. The results reveal that a sufficient graphene growth is possible when we optimize the switching of the carbon precursor/ hydrogen flow ratio during the process. This reduces the etching effect that the hydrogen is performing, allowing the growth of graphene and the full cover of the substrate by it. Large area graphene is necessary when it comes to large scale applications followed by a careful transfer, to avoid the damaging of the graphene film.

- The Raman spectroscopy ensures us about the single layer thickness of the

graphene film. Performing the Raman measurements on top of different substrates, (copper foil, glass, SiO2) does not affect significantly the shape and ratio of the characteristic graphene peaks.

- Considering the pulsed injection of methane, the ability of growing graphene through a different synthetic route is explored. Based on the concept of the monolayer formation time, we propose the injection of pulses of methane instead of a continuous flow. By this mean the growth is much faster. The results reveal the growth of domains of single layer graphene of 400µm^2.

- Considering the use of different carbon precursors, alternative carbon sources are used, benzene and toluene, to promote the growth of graphene in lower temperatures, at 500 ˚C and 600˚C respectively. Single layer graphene is grown over copper foil. The domains have a size of 25µm^2.

- Raman spectroscopy is proved to be a direct, fast and trustworthy mean in order to characterize the graphene samples. The only ´disadvantage´ is the necessary post treatment of the data in order to remove the photoluminescence background signal. By a careful observation in the characteristic of the graphene peaks we confirm the monolayer thickness of the samples.

- The shift of the 2D peak with respect to its position when it is relaxed, allows us to calculate the strain of the graphene. This is a result of the ripples that are formed in the copper foil during the cooling step. The ripples increase the surface area, introducing a strain $\varepsilon=0,052\%$ in the graphene. When transferred over SiO2 , the graphene relaxes. This is translated in a decrease in the shift of the 2D peak and a strain relaxation of $\varepsilon=0,0026\%$.

- In addition, we report the small but noticeable decrease in the FWHM of the 2D peak when the graphene is transferred over SiO2.

- Finally, the Raman mapping performed in different samples can provide useful information about the homogeneity of the graphene domains. An interesting observation is the decrease in both the 2D peak intensity as well as in the 2D/G area ration in the very edge of the crystal.

- Our results indicate the capability to control the strain in cvd single layer graphene by a careful control of the hydrogen flow. Through the control on the flow, the ripple´s density is regulated. An increase in the flow of hydrogen can reduce the compressive strain, as a result of the levitation of the graphene from copper substrate in the concave regions. Although, the introduced hydrogen flow should be selected with care, as high flows can lead to the anisotropic etching of the graphene film.

- The graphene transfer process is as critical as the growth of the material itself. Almost in all variety of applications, it is a necessary step in order deposit the graphene film in the desired substrate. The process should be designed ensuring that it will introduce no defects to the graphene film. This task appears to be complicated in most of the cases. The different materials used for the transfer (polymers, TRT, support substrates) introduce impurities in the surface of the film that is hard to get completely removed.

- From our experience, we consider that the idea of using the PMMA as a transfer media and the TRT as an extra support film in an electrochemical delamination process is the ideal candidate solution for an effective graphene transfer. The method is designed to take advantage of the characteristics of every mean. The PMMA is ideal for the transfer of continuous graphene film. With the use of the TRT as a support layer the film is protected from bending that can cause tears. The electrochemical delamination from the metal catalyst saves the graphene from the impurities that the metal etchant inputs. Both optical and electron microscopy ensure us about the uniformity of the transfer film.

- Layer by layer evaluation of graphene electrodes combined with different metal oxides is performed to explore the posibilty for use I supercapasitors applications. The results reveal that all devices present a higher capacity in the smallest scan rate (10mV/s).

- The oxidation of the graphene film increases its capacitance. The same happens when more layers of Gr/metal oxide are added over the first layer. The devices where Gr is combined with CeO_2 are performing slightly higher than those where Gr is combined with WO_3.

- Considering their stability all devices maintain their initial performance for more than 800 cycles. The charge-discharge period increases with the addition of more layers. The deposition of the metal oxide particles by plasma sputtering results in the etching of the graphene film.

- Different deposition techniques should be taken into consideration. Moreover, a structural characterization of the electrodes should be performed before and after the realization of the measurements in order to obtain information about the deposition of the particles.

- CVD graphene is used for the fabrication of a field effect transistor. The objective is the electrical characterization of the graphene regarding characteristics like the conductivity, carrier density and carrier mobility. Apart from the field effect measurements, similar conductivity was measured in the graphene films when

measuring the characteristic IDS-VDS in a two contacts configuration. The agreement in the measurements (made in different apparatus), ensure us about the preciseness of them. CVD graphene may present a less qualitative behavior compared to other ones, like exfoliated. This is a result of the presence of grain boundaries as well as of other defects in its atomic structure. Although, CVD graphene present the advantage of large scale synthesis and high homogeneity in its quality. The values obtained are standard values that can be found in the literature. $\sigma=1,25*10^{-3}\ \Omega^{/1}$ and $\mu=861 cm^2/V\ s$.

8. References

V. Adamyan and V. Zavalniuk, "Phonons in graphene with point defects,"Journal of Physics Condensed Matter, 23(2011)015402

Ch. Androulidakis , G. Tsoukleri , N. Koutroumanis , G. Gkikas b, P. Pappas ,J.Parthenios , K. Papagelis , C. Galiotis," Experimentally derived axial stress–strain relations for two-dimensional materials such as monolayer graphene", CARBON, 81(2015)322 – 328

J. Anthony, R. Bideaux, K. Bladh and M. Nichols, "Graphite". Handbook of Mineralogy, 1990

S. Bae, H. Kim, Y. Lee, X. Xu, J.-S. Park, Y. Zheng, J. Balakrishnan, T. Lei, H. R. Kim, Y. I. Song, Y.-J. Kim, K. S. Kim, B. Ozyilmaz, J.-H. Ahn, B. H. Hong and S. Iijima," Roll-to-roll production of 30-inch graphene films for transparent electrodes",Nat. Nanotechnol., 5(2010)574–578

A. Balandin, S. Ghosh, W. Bao et al., "Superior thermal conductivity of single-layer graphene,"Nano Letters, 8(2008)902–907

P. Bampoulis,L. Zhang, A. Safaei, R. van Gastel, B. Poelsema, H.J. Zandvliet, "Germanene termination of Ge2Pt crystals on Ge(110)". Journal of Physics: Condensed Matter, 26(2014)442001

D.M. Basko, S. Piscanec and A. Ferrari, ''Electron-electron interactions and doping dependence of the two-phonon Raman intensity in graphene.'', Phys. Rev. B, 80(2009)165413

D.M. Basko,``Boundary problems for Dirac electrons and edge-assisted Raman scattering in graphene.´´, Phys. Rev. B, 79(2009)205428

E. Bertran, V.-M. Freire, A. Ramírez, E. Pascual, J.-L. Andújar, Process for the controlled production of graphene at very low pressure and device to carry out the process (Procedimiento para la producción controlada de grafeno a muy baja presión y dispositivo para llevar a cabo el procedimiento). ES201330585 (OEPM), PCT/ES2014/070295 (PCT) and AVCRI189 (FBG).

V. Blank, M. Popov, G.Pivovarov, N.Lvova, K.Gogolinsky, V. Reshetov,"Ultrahard and superhard phases of fullerite C60: Comparison with diamond on hardness and wear". Diamond and Related Materials, 7(1998)427

F. Bonaccorso, Z. Sun, T. Hasan, and A. C. Ferrari, "Graphene photonics and optoelectronics,"Nature Photonics, 4(2010)611–622

D.A. Boyd, W.-H. Lin, C.-C. Hsu, M.L. Teague, C.-C. Chen, Y.-Y. Lo, W.-Y. Chan, W.-B. Su, T.-C. Cheng,C.-S. Chang, C.-I. Wu & N.-C. Yeh.," Single-step deposition of high-mobility graphene at reduced temperatures". Nat. Commun. ,6(2015)6620

.L. Brown, E. B. Lochocki, J. Avila, C.-J. Kim, Y. Ogawa,R. W. Havener, D.-K. Kim, E. J. Monkman, D. E. Shai, H. I. Wei, M. P. Levendorf, M. Asensio, K. M. Shen and J. Park," Polycrystalline graphene with single crystalline electronic structure.", Nano Lett., 14(2014)5706.

A. Buchsteiner, A. Lerf and J. Pieper, '' Water Dynamics in Graphite Oxide Investigated with Neutron Scattering'', J. Phys. Chem. B,110(2006)22328–22338.

D. Caldwell, T. J. Anderson, J. C. Culbertson, G. G. Jernigan, K. D. Hobart, F. J. Kub, M. J. Tadjer, J. L. Tedesco, J. K. Hite and M. A. Mastro, "Technique for the Dry Transfer of Epitaxial Graphene onto Arbitrary Substrate",ACS Nano, 4(2010)1108–1114

J. Carlsson, "Graphene: Buckle or break". Nature Materials, 6(2007)801–2

A. Castro Neto,F. Guinea,N. M. R. Peres,K. S. Novoselov and A. K. Geim," The electronic properties of graphene", REVIEWS OF MODERN PHYSICS, 81 (2009)

C. Casiraghi, S. Pisana, K. S. Novoselov, A. K. Geim, and A. C. Ferrari, "Raman fingerprint of charged impurities in graphene,"Applied Physics Letters, 91 (2007)Article ID 233108

C. Casiraghi, A. Hartschuh, H. Qian, S. Piscanec, C. Georgi, A. Fasoli, K. S. Novoselov, D. M. Basko,| and A. C. Ferrari,´´ Raman Spectroscopy of Graphene Edges´´, NANOLETTERS,9(2009)1433-1441

S. Chaitoglou, E. Pascual, E. Bertran, and J. L. Andujar, ´´Effect of a Balanced Concentration of Hydrogen on Graphene CVD Growth´´, Journal of Nanomaterials,(2016)9640935

Y.M. Chang, J. Leu, B.H. Lin, Y.L. Wang, Y.L. Cheng," Comparison of H2 and NH3 treatments for copper interconnects", Adv. Mater. Sci. Eng., (2013) 825195

S. Chen, L. Brown , M. Levendorf , W. Cai , S. Ju , J. Edgeworth , X. Li , C. W. Magnuson , A. Velamakanni , R. D. Piner, J. Kang , J. Park and R. S. Ruoff ,''Oxidation Resistance of Graphene-Coated Cu and Cu/Ni Alloy'', ACS Nano, 5(2011)1321–1327

J. Chen , C. Jang, S. Xiao, M. Ishigami, & M. S. Fuhrer,'' Intrinsic and extrinsic performance limits of graphene devices on SiO2'', Nature Nanotechnology, 3(2008)206 – 209

J. Cheng, S. Kim, H. Choi, D. Kim, S. Jang,M. Jin, J. Park, J. Choi and H. Jung, '' Ultraclean transfer of CVD-grown graphene and its application to flexible organic photovoltaic cells'', J. Mater. Chem. A, 2(2014)20474

S. Cheng, M. Chen, ´´ Fabrication, characterization, and kinetic study of vertical single-crystalline CuO nanowires on Si substrates´´, Nanoscale Res Lett.,7(2012)119

C. Cherian, F. Giustiniano , I. M.Fernandez , H. Andersen ,J. Balakrishnan , and B. Özyilmaz ,'''Bubble-Free' Electrochemical Delamination of CVD Graphene Films '',Small ,11(2015)189–194

S. Cho, K. Kikuchi and A. Kawasaki,'' Radial followed by longitudinal unzipping of multiwalled carbon nanotubes'', Carbon, 49(2011)3865–3872

J. Choi, Z. Li, P. Cui, X. Fan, H. Zhang, C. Zeng and Z. Zhang,´´ Drastic reduction in the growth temperature of graphene on copper via enhanced London dispersion force´´,. Sci. Rep., 3(2013)1925

M. Choucair, P. Thordarson and J. A. Stride,'' Gram-scale production of graphene based on solvothermal synthesis and sonication'',Nat. Nanotechnol., 4(2009)30–33

D. Chung, ''Exfoliation of graphite'', J. Mater. Sci., 22(1987)4190–4198

D. Cooper , B. D'Anjou, N. Ghattamaneni, B. Harack, M. Hilke, A. Horth, N. Majlis, M. Massicotte, L. Vandsburger, E. Whiteway, and V.,'' Experimental Review of Graphene'', International Scholarly Research Network ISRN Condensed Matter Physics,(2012)Article ID 501686

P. Coutsoukis, "The Diamond Industry". photius.com. Retrieved July 7, 2009

S. Da Costa, A. Righi, C. Fantini, Y. Hao, C. Magnuson, L. Colombo, R. S. Ruoff, M. A. Pimenta,''Resonant Raman spectroscopy of graphene grown on copper substrates'', Solid State Communications, 152(2012)1317–1320

S.A. Da Silva, A. D. S. Cortes, M. H. Oliveira, Jr., E. F. Motta, G. A. Viana, P. R. Mei, and F. C. Marques,'' Application of amorphous carbon based materials as antireflective coatings on crystalline silicon solar cells'', J. Oof Apl.- Phys., 110(2011)043510

A. Das, B. Chakraborty and A K Sood,'' Raman spectroscopy of graphene on different substrates and influence of defects'', Bull. Mater. Sci. ,31(2008)579–584

T. K. Das and S. Prusty,'' Graphene-Based Polymer Composites and Their Applications'', Polymer-Plastics Technology and Engineering, 52(2013)319–331

A. Das, B. Chakraborty and A K Sood,'' Raman spectroscopy of graphene on different substrates and influence of defects'', Bull. Mater. Sci., 31(2008)579–584

S. Das Sarma, S. Adam, E. H. Hwang, and E. Rossi, "Electronic transport in two-dimensional graphene," Reviews of Modern Physics, 83,(2011)407–470

A. Dato, V. Radmilovic, Z. Lee, J. Phillips and M. Frenklach,'' Substrate-Free Gas-Phase Synthesis of Graphene Sheets'', Nano Lett., 8(2008)2012–2016

G. De Arco Y. Zhang, C. Schlenker,K. Ryu,M. Thompson, C. Zhou ,´´Continuous, highly flexible, and transparent graphene films by chemical vapor deposition for organic photovoltaics´´, ACS Nano., 25(2010)2865–2873

P. Delhaes, . , Graphite and Precursors. CRC Press. 2001,ISBN 90-5699-228-7.

V.E. Dorgan, M. H. Bae, and E. Pop, "Mobility and saturation velocity in graphene on SiO2," Applied Physics Letters, 97(2010)Article ID 082112

X. Du, I. Skachko, A. Barker, and E. Y. Andrei, "Approaching ballistic transport in suspended graphene,"Nature Nanotechnology, 3(2008)491–495

R.S. Edwards and K. S. Coleman,'' Graphene synthesis: relationship to applications'', Nanoscale, 5(2013)38

R.S. Edwards and K. S. Coleman, '' Graphene Film Growth on Polycrystalline Metals'', ACCOUNTS OF CHEMICAL RESEARCH, 46(2013)23-30

K.V. Emtsev, A. Bostwick, K. Horn, J. Jobst, G. L. Kellogg, L. Ley, J. L. McChesney, T. Ohta, S. A. Reshanov, J. Rohrl, E. Rotenberg, A. K. Schmid, D. Waldmann, H. B. Weber and T. Seyller,'' Towards wafer-size graphene layers by atmospheric pressure graphitization of silicon carbide'', Nat. Mater., 8(2009)203–207

J.M. Englert, J. Rohrl, C. D. Schmidt, R. Graupner, M. Hundhausen, F. Hauke and A. Hirsch,'' Soluble Graphene: Generation of Aqueous Graphene Solutions Aided by a Perylenebisimide-Based Bolaamphiphile'', Adv. Mater., 21(2009)4265–4269

G.Eres , M. Regmi , C. M. Rouleau , J. Chen , I. N. Ivanov , A. A. Puretzky and D. B. Geohegan "Cooperative Island Growth of Large Area Single-Crystal Graphene by Chemical Vapor Deposition on Cu." ,ACS Nano,8(2014)5657-5669

G. Faggio , A. Capasso, G. Messina , S. Santangelo , Th. Dikonimos , S. Gagliardi, R. Giorgi , V. Morandi , L. Ortolani , and N. Lisi ,''High-Temperature Growth of Graphene Films on Copper Foils by Ethanol Chemical Vapor Deposition'',J. Phys. Chem. C, 117(2013)21569–21576

A. C. Ferrari, J. C. Meyer, V. Scardaci, C. Casiraghi, M. Lazzeri, F. Mauri, S. Piscanec, D. Jiang, K. S. Novoselov, S. Roth, and A. K. Geim, ''Raman Spectrum of Graphene and Graphene Layers'', Phys. Rev. Lett., 97(2006)187401

A.C. Ferrariet al, '' Science and technology roadmap for graphene, related two-dimensional crystals, and hybrid systems'', Nanoscale, 7(2015)4598

A. Ferrari and J. Robertson, ´´Interpretation of Raman spectra of disordered and amorphous carbon.´´, Phys. Rev. B, 61(2000)14095–14107

A. Ferrari and J. Robertson,,´´Resonant Raman spectroscopy of disordered, morphous, and diamondlike carbon.´´, Phys. Rev. B, 64(2001)075414

A. Ferrari and J. Robertson,''(eds) Raman spectroscopy in carbons: from nanotubes to diamond, Theme Issue'', Phil. Trans. R. Soc. A, 362(2004)2267–2565

A. Ferrari,'' Raman spectroscopy of graphene and graphite: Disorder, electron-phonon coupling, doping and nonadiabatic effects.'', Solid State Comm., 143(2007)47–57

A. Ferrari and D. M. Basko,'' Raman spectroscopy as a versatile tool for studying the properties of graphene'', NATURE NANOTECHNOLOGY ,8 (2013)235-246

I. W. Frank, D.M. Tanenbaum, A.M. Van Der Zande, P.L.McEuen,, "Mechanical properties of suspended graphene sheets" , J. Vac. Sci. Technol. B, 25(2007)2558–2561

V.M. Freire,"Fabrication and Characterization of Macroscopic Graphene Layers on Metallic Substrates", PhD Thesis, Universitat de Barcelona, (2014)117-119

L. Gan and Z. Luo,'' Turning off Hydrogen To Realize Seeded Growth of Subcentimeter Single-Crystal Graphene Grains on Copper'',ACS Nano, 7(2013) 9480

D.J. Gardiner,´´Practical Raman spectroscopy´´, Springer-Verlag(1989)

A. Geim and K. S. Novoselov, ''The rise of graphene'', Nature Materials, 6(2007)183-191

A. Geim,'' Random Walk to Graphene (Nobel Lecture)'', Angew. Chem. Int. Ed., 50(2011)6967 – 6985

D. Geng, B. Wu, Y. Guo, B. Luo, Y. Xue, J. Chen, G. Yu and Y. Liu, ''Controllable Synthesis of Submillimeter Single-Crystal Monolayer Graphene Domains on Copper Foils by Suppressing Nucleation'',J. Am. Chem. Soc., 135(2013)6431–6434.

D. Geng, B. Wu, Y. Guo, L. Huang, Y. Xue, J. Chen, G. Yu, L. Jiang, W. Hu, Y. Liu,,''Uniform Hexagonal Graphene Flakes and Films Grown on Liquid Copper Surface'', Proc.Natl. Acad. Sci. U.S.A., 109 (2012)7992–7996

J. Getty, March Plasma Systems, Concord, Calif,''How plasma-enhanced surface modification improves the production of microelectronics and optoelectronics'', Chip Scale Rev.,(2002)72–75

E. Gibney, ''The super materials that could trump graphene'', Nature, 522(2015)274–276

S. Goler, C. Coletti, V. Tozzini, V. Piazza, T. Mashoff, F. Beltram, V. Pellegrini, and S. Heun,´´ Influence of Graphene Curvature on Hydrogen Adsorption: Toward Hydrogen Storage Devices´´, J. Phys. Chem. C , 117(2013)11506−11513

R. Golizadeh-Mojarad and S. Datta, ´´ Effect of contact induced states on minimum conductivity in graphene´´, Phys. Rev. B, 79(2009)085410

S. Gottardi, K. Müller, L. Bignardi, J. C. Moreno-Lopez,́ T. A. Pham,O. Ivashenko,M. Yablonskikh, A. Barinov, J. Björk, P. Rudolf,and M. Stöhr,'' Comparing Graphene Growth on Cu(111) versus Oxidized Cu(111)'', Nano Lett., 15(2015) 917−922

R. Gran Table , V. Shenoy and R.S. Ruoff , ''Anomalous strength characteristics of tilt grain boundaries in graphene'' ,Science,330(2010)946–8

L.Greenemeier,http://www.scientificamerican.com/article/carbon-nanotube-danger, (22008)

P. Gupta, P. D. Dongare, S. Grover, S. Dubey, H. Mamgain, A. Bhattacharya and M. M.

Deshmukha," A facile process for soak-and-peel delamination of CVD graphene from substrates using water", Sci Rep. ,4(2014)3882

P.J. Hall, E. Bain,´´Energy-Storage Technologies and Electricity Generation. Energy Policy´´, 36(2008)4352−4355

P.J. Hall, M. Mirzaeian, S.I. Fletcher, F.B. Sillars, A.J.R. Rennie, G.O. Shitta-Bey, G. Wilson, A. Cruden, R. Carter,´´ Energy Storage in Electrochemical Capacitors: Designing Functional Materials to Improve Performance. ´´, Energy Environ. Sci., 3(2010)1238−1251

G. Han,H. Shin,; E. Kim ,S. Chae ,J. Choi, Y. Lee, ''Poly(ethylene co- vinyl acetate)-assisted one-step transfer of ultra-large graphene'', NANO, 6(2011)59

Y. Hao, M. S. Bharathi, L. Wang, Y. Liu, H. Chen, S. Nie, X. Wang, H. Chou, C. Tan, B. Fallahazad, H. Ramanarayan, C. W. Magnuson, E. Tutuc, B. I. Yakobson, K. F. McCarty, Y.-W. Zhang, P. Kim, J. Hone, L. Colombo and R. S. Ruoff,''The Role of Surface Oxygen in the Growth of Large Single-Crystal Graphene on Copper'', Science, 342(2013)720.

C. R. Herron, K. S. Coleman, R. S. Edwards and B. G. Mendis,'' Simple and scalable route for the 'bottom-up' synthesis of few-layer graphene platelets and thin films'', J. Mater. Chem., 21(2011)3378–3383

S. Hong, S. M. Song, O. Sul and B. J. Cho,"Carboxylic Group as the Origin of Electrical Performance Degradation during the Transfer Process of CVD Growth Graphene " ,J. Electrochem. Soc., 159(2012)107–K109

J. Hong, M. Park, E. J. Lee, D. Lee, D. Hwang and S. Ryu,´´ Origin of New Broad Raman D and G Peaks in Annealed Graphene´´,Scient Repots, 3(2013)2700

Q. Huang, X. Chen, J. Liu, W. Wang, G. Wang, W. Wang, R. Yang, Y. Liu and L. Guo,'' Epitaxial graphene on 4H-SiC by pulsed electron irradiation'', Chem. Commun., 46(2010)4917–4919

S. Hussain, R. Amade, H. Moreno, Enric Bertran,'' RF-PECVD growth and nitrogen plasma functionalization of CNTs on copper foil for electrochemical applications'', Diamond & Related Materials, 49(2014)55–61

Y. Hu, T.T. Shi, J. Ni ,H. Jin, M. Zhu, Y. Li, Q. Bai, ´´Super-Capacitive Performances of Nickel Foam Supported CeO2 Nanoparticles´´, J. Shanghai Jiaotong Univ. (Sci.), 17(2012)513-516

A. Ismach, C. Druzgaski, S. Penwell, A. Schwartzberg, M. Zheng, A. Javey, J. Bokorand Y. Zhang,"Direct Chemical Vapor Deposition of Graphene on Dielectric Surfaces", Nano Lett., 10(2010)1542– 1548

S. Iijima,, "Helical microtubules of graphitic carbon". Nature, 354(1991)56–58

Y. Jin, B. Hu,,Z. Wei, Z. Luo, D. Wei, Y. Xi, Y. Zhang and Y. Liu, ´´Roles of H2 in annealing and growth times of graphene CVD synthesis over copper foil´´,J. Mater. Chem. A,2(2014)16208

X. Jia, J. Campos-Delgado, M. Terrones, V. Meunier and M. S. Dresselhaus, '' Graphene edges: a review of their fabrication and characterization'', Nanoscale, 86 (2011) 86–95

Z.Y. Juang, C.-Y. Wu, C.-W. Lo, W.-Y. Chen, C.-F. Huang, J.-C. Hwang, F.-R. Chen, K.-C. Leou and C.-H. Tsai,'' Synthesis of graphene on silicon carbide substrates at low temperature'', Carbon, 47(2009)2026–2031

Y.R.Kang, Y.-L. Li and M.-Y. Deng,'' Precise unzipping of flattened carbon nanotubes to regular graphene nanoribbons by acid cutting along the folded edges'',J. Mater. Chem., 22(2012)16283–16287

J. Kang, D. Shin, S. Bae and B.Hong," Graphene transfer: key for applications", Nanoscale, 4(2012)5527

S. Kang, B. Kim, K. S. Kim, Y. Zhao, Z. Chen, G. H. Lee, J. Hone, P. Kim and C. Nuckolls, "Inking Elastomeric Stamps with Micro-Patterned, Single Layer Graphene to Create High-Performance OFETs",Adv. Mater., 23(2011)531–3535

J. Kang, S. Hwang, J. Kim, M. Kim, J. Ryu, S. J. Seo, B. Hong, M. Kim, and J. Choi,"Efficient Transfer of Large-Area Graphene Films onto Rigid Substrates by Hot Pressing", ACS Nano, 6(2012)5360–5365

S. Kasap, H. Khaksaran, S. Çelik, H. Ozkaya, C. Yanık and I. Kaya,'' Controlled growth of large area multilayer graphene on copper by chemical vapour deposition'', Phys. Chem. Chem. Phys.,17(2015)23081

A. Kasry., M. A. Kuroda, G. J. Martyna, G. S. Tulevski and A. A. Bol,"Chemical Doping of

Large-Area Stacked Graphene Films for Use as Transparent, Conducting Electrodes", ACS Nano, 4(2010)3839–3844.

M. Katsnelson, K. S. Novoselov, and A. K. Geim, "C hiral tunnelling and the Klein paradox in graphene," Nature Physics, 2(2006)620–625

S. Kim, A. Hsu, Y. Lee, M. Dresselhaus, T. Palacios, K. Kim and J. Kong ''The effect of copper pre-cleaning on graphene synthesis'',NANOTECHNOLOGY , 24 (2013)365602

K.S.Kim, Y. Zhao, H. Jang, S. Y. Lee, J. M. Kim, K. S. Kim, J.-H. Ahn, P. Kim, J.-Y. Choi and B. H. Hong,"Large-scale pattern growth of graphene films for stretchable transparent electrodes ", Nature, 457(2009)706–710

 S. Kim, A. Hsu, Y. Lee, M. Dresselhaus, T. Palacios, K. K. Kim and J. Kong ''The effect of copper pre-cleaning on graphene synthesis'',NANOTECHNOLOGY , 24(2013)36

K. Kim , V. Artyukhov ,W. Regan ,Y. Liu ,M. Crommie,B. Yakobson and A.Zettl , ''Ripping Graphene: Preferred Directions '',NanoLett,(2012)12293–7

N. T. Kirkland,, T. Schiller,, N. Medhekar, N. Birbilis,,'' Exploring graphene as a corrosion protection barrier'', Corrosion Sci., 56(2011)1–4

K. Kostarelos, A. Bianco, M.Prato,''Promises, facts and challenges for carbon nanotubes in imaging and therapeutics'', Nature Nanotech., 4(2009)627–633

S.B.Kumar and J. Guo, ''Strain-Induced Conductance Modulation in Graphene Grain Boundary'', Nano Lett.,12(2012)1362–6

J. R. Lake, A. Cheng, S. Selverston, Z. Tanaka, J. Koehne, M. Meyyappan and B. Chen,´´ Graphene metal oxide composite supercapacitor electrodes´´, Journal of Vacuum Science & Technology B, 30(2012)03D118

J. Lee, C. Park andG.M.Whitesides,"Solvent Compatibility of Poly(dimethylsiloxane)-Based Microfluidic Devices",Anal. Chem., 75(2003)6544–6554

J. Lee , G. Ahn , J. Shim , Y. S. Lee and S. Ryu, ´´ Optical separation of mechanical strain from charge doping in graphene´´, nature communications , 3(2012)1024

C.Lee, X. Wei, J.W.Kysar, J.Hone, "Measurement of the Elastic Properties and Intrinsic Strength of Monolayer Graphene". Science 321, (2008)385–8

M.P. Levendorf, C.S. Ruiz-Vargas, S. Garg, J. Park, ''Transfer-Free Batch Fabrication of Single Layer Graphene Transistors'', Nano Lett., 9(2009)4479- 4483

J. Li, X. Wang, X. Liu, Z. Jin, D. Wang and L. Wan,''Facile growth of centimeter-sized single-crystal graphene on copper foil at atmospheric pressure'', J. Mater. Chem. C, 3(2015)3530

X. Li,L. Wang,K. Chen and Y. Luo ,'' Effects of interface roughness on electronic transport properties of nanotube-molecule-nanotube junctions'' ,J.Phys.Chem.C,115(2010)12616–24

X. Li, C.Magnuson, A. Venugopal, R. Tromp, J. Hannon, E. Vogel, L. Colombo, R. Ruoff,''Large-Area Graphene Single Crystals Grown by Low-Pressure Chemical Vapor Deposition of Methane on Copper'', J. Am. Chem. Soc.,133(2011)2816– 2819

X.S. Li, W.W. Cai, L. Colombo, R.S. Ruoff,''Evolution of Graphene Growth on Ni and Cu by Carbon Isotope Labeling'', Nano Letters,9(2009)4268-4272

Z.Li, Y. Wang, A. Kozbial, G. Shenoy, F. Zhou, R. McGinley, P. Ireland, B. Morganstein, A. Kunkel, S. P. Surwade, L. Li and H. Liu, "Effect of airborne contaminants on the wettability of supported graphene and graphite", NATURE MATERIALS , 12(2013)925-931

X. Li, C.W. Magnuson, A. Venugopal, J. An, J.W. Suk, B. Han, M. Borysiak, W. Cai, A. Velamakanni, Y. Zhu, L. Fu, E.M. Vogel, E. Voelkl, L. Colombo, R.S.Ruoff,'' Graphene Films with Large Domain Size by a Two-Step Chemical Vapor Deposition Process'', Nano Lett., 10(2010)4328–4334

Y. Li, H. Yuan, A. von dem Bussche, M. Creighton, R. H. Hurt,A. B. Kane and H. Gao,'' Graphene microsheets enter cells through spontaneous membrane penetration at edge asperities and corner sites'', PNAS ,110(2013)12295–12300

X. Li, Y. W. Zhu, W. W. Cai, M. Borysiak, B. Y. Han, D. Chen, R. D. Piner, L. Colombo and R. S. Ruoff,"Transfer of large-area graphene films for high-performance transparent conductive electrodes",Nano Lett., 9(2009)4359–4363

X. Li, W. Cai, J. An, S. Kim, J. Nah, D. Yang, R. Piner, A. Velamakanni, I. Jung, E. Tutuc, S. K. Banerjee, L. Colombo and R. S. Ruoff,"Large-Area Synthesis of High-Quality and Uniform Graphene Films on Copper Foils", Science, 324(2009)1312–1314

N. Liu, Z. Pan, L. Fu, C. Zhang, B. Dai, and Z. Liu, ´´The Origin of Wrinkles on Transferred Graphene´´, Nano Res. ,4(2011)996–1004

C. Lui, Leandro M. Malard, SukHyun Kim, Gabriel Lantz, François E. Laverge, Riichiro Saito, and Tony F. Heinz. ,"Observation of layer-breathing mode vibrations in few-layer graphene through combination Raman scattering.", Nano Lett., 12(2012)5539–5544

X. Liang, B. A. Sperling, I. Calizo, G. J. Cheng, C. A. Hacker, Q. Zhang, Y. Obeng, K. Yan, H. L. Peng, Q. L. Li, X. X. Zhu, H. Yuan, A. R. Hight Walker, Z. F. Liu, L. M. Peng and C. A. Richter,"Toward Clean and Crackless Transfer of Graphene", ACS Nano, 5(2011)9144–9153.

J. Lin, W. Fang, W. Zhou, A. R. Lupini, J. C. Idrobo, J. Kong, S. J. Pennycook, and S. T. Pantelides," AC/AB Stacking Boundaries in Bilayer Graphene", Nano Lett. , 13(2013)3262−326

Z. Liu, L. Song, S. Zhao, J. Huang, L. Ma, J. Zhang, J. Lou and P. M. Ajayan, '' Direct Growth of Graphene/Hexagonal Boron Nitride Stacked Layers", Nano Lett., 11(2011)2032–2037

L. Liu, M. An, P. Yang and J. Zhang,´´ Superior cycle performance and high reversible capacity of SnO2/graphene composite as an anode material for lithium-ion batteries´´, SCIENTIFIC REPORTS ,5(2015) 9055

E. Lock, M. Baraket, M. Laskoski, S. P. Mulvaney, W. K. Lee, P. E. Sheehan, D. R. Hines, J. T. Robinson, J. Tosado, M. S. Fuhrer, S. C. Hernandez and S. G. Walton,"High-quality uniform dry transfer of graphene to polymers.", Nano Lett., 12(2012)102–107.

T. Ma, W. Ren, X. Zhang, Z. Liu, Y. Gao, L. C. Yin, X. L. Ma, F. Ding and H. M. Cheng, '' Edge-controlled growth and kinetics of single-crystal graphene domains by chemical vapor deposition",Proc. Natl. Acad. Sci. U. S. A., 110(2013)20386–20391

D.L. Mafra, G. Samsonidze, L. M. Malard, D. C. Elias, J. C. Brant, F. Plentz, E. S. Alves, and M. A. Pimenta,´´ Determination of LA and TO phonon dispersion relations of

graphene near the Dirac point by double resonance Raman scattering.´´, Phys. Rev. B, 76(2007)233407

C. Mattevi , H Kima and M. Chhowalla, ''A review of chemical vapour deposition of graphene on copper'', J.Mater. Chem.,21(2011) 3324-3334

J. Maultzsch, S. Reich, and C. Thomsen,´´ Double-resonant Raman scattering in graphite: Interference effects, selection rules, and phonon dispersion.´´, Phys. Rev. B, 70(2004)155403

A.D. McNaught, A. Wilkinson, "Amorphous carbon". IUPAC Compendium of Chemical Terminology: the "Gold Book" (2nd ed.). Oxford: Blackwell Scientific Publications.,(1997)

J. Meija, "Goldberg Variations Challenge" (PDF). Analytical and Bioanalytical Chemistry, 385(2006)6–7

E.J. Mele,´´ Interlayer coupling in rotationally faulted multilayer graphenes'',J. Phys. D: Appl. Phys., 45(2012)154004

E. Meca , J. Lowengrub , H. Kim , C. Mattevi and V. B. Shenoy, '' Epitaxial Graphene Growth and Shape Dynamics on Copper: Phase-Field Modeling and Experiments'',NANOLETTERS, 13(2013)5692–5697

J.C. Meyer, A. K. Geim, M. I. Katsnelson, K. S. Novoselov, T. J. Booth and S. Roth," The structure of suspended graphene sheets",Nature, 446(2007)60–63
Mindat. "Diamond",(2009)

F. Miao, S. Wijeratne, Y. Zhang, U. C. Coskun, W. Bao, C. N. Lau,´´ Phase-Coherent Transport in Graphene Quantum Billiards´´,Science, 317(2007)1530-1533

A. Michon, S. Vézian, E. Roudon, D. Lefebvre, M. Zielinski, T. Chassagne, and M. Portail , ''Effects of pressure, temperature, and hydrogen during graphene growth on SiC(0001)using propane-hydrogen chemical vapor deposition'',Journal of Applied Physics 113(2013)203501

V. Miseikis, D Convertino, N Mishra, M Gemmi, T Mashoff, S Heun, N Haghighian, F Bisio, M Canepa, V Piazza and C Coletti,''Rapid CVD growth of millimetre-sized single crystal graphene using a cold-wall reactor'', 2D Mater.,2(2015)014006

T. M. G. Mohiuddin, A. Lombardo, R. R. Nair, A. Bonetti, G. Savini, R. Jalil, N. Bonini, D. M. Basko, C. Galiotis, N. Marzari et al., "Uniaxial strain in graphene by raman

spectroscopy: G peak splitting, gr€uneisen parameters, and sample orientation," Phys. Rev. B, 79(2009) 205433

A. Mohsin, L. Liu, P. Liu, W. Deng, I. N. Ivanov, G. Li, O. E. Dyck, G. Duscher, J. R. Dunlap, K. Xiao and G. Gu, '' Synthesis of millimeter-size hexagon-shaped graphene single crystals on resolidified copper'',ACS Nano, 7(2013)8924

H. Mumen, F. Rao, W. Li, L. Dong,´´ Singular Sheet Etching of Graphene with Oxygen Plasma´´,Nano-Micro Lett. 6(2014)116-124 R. Nair, P. Blake, A. N. Grigorenko, K. S. Novoselov, T. J. Booth, T. Stauber, N. M. R. Peres, A. K. Geim, '' Fine Structure Constant Defines Visual Transparency of Graphene'',Science,320(2008)1308

R.G. Nemanich, G. Lucovsky and S.A. Solin,'' Infrared active optical vibrations of graphite.'' Solid State Comm., 23(1977)117–120

Z. Ni et al. ,``On resonant scatterers as a factor limiting carrier mobility in graphene.´´, Nano Lett., 10(2010)3868–3872

K.S. Novoselov, A. K. Geim, S. V. Morozov, D. Jiang, M. I. Katsnelson, I. V. Grigorieva, S. V. Dubbonos and A. A. Firsov,"Two-dimensional gas of massless Dirac fermions in graphene", Nature, 438(2005)197–200

K.S. Novoselov, A. K. Geim, S. V. Morozov, D. Jiang, Y. Zhang, S. V. Dubonos, I. V. Grigorieva and A. A. Firsov, "Electric Field Effect in Atomically Thin Carbon Films",Science, 306(2004)666–669

F. Otakar,J. Vejpravova, V. Holy, L. Kavan, M. Kalbac,´´ Interaction between graphene and copper substrate: The role of lattice orientation´´, Carbon, 68(2014)440–451

Y. Peng, B. Locascio, M. Zapol, P. Li, S. Mielke, S. L.Schatz, G. C. Espinosa,D. Horacio, "Measurements of near-ultimate strength for multiwalled carbon nanotubes and irradiation-induced crosslinking improvements". Nature Nanotechnology ,3(2008)626–631

T. M. Paronyan, E. M. Pigos, G. Chen, and A. R. Harutyunyan,´´ Formation of Ripples in Graphene as a Result of Interfacial Instabilities´´, Nano,5(2011) 9619–9627

S. Pei and H.-M. Cheng,'' The reduction of graphene oxide'', Carbon, 50(2012)3210–3228

A.Pirkle, J. Chan, A. Venugopal, D. Hinojos, C. W. Magnuson, S. McDonnell, L.Colombo, E. M. Vogel, R. S. Ruoff and R. M. Wallace,"The effect of chemical residues on the physical and electrical properties of chemical vapor deposited graphene transferred to SiO2 ", Appl. Phys. Lett., 99(2011)122108

L.A. Ponomarenko, R. Yang, T. M. Mohiuddin, M. I. Katsnelson, K. S. Novoselov, S. V. Morozov, A. A. Zhukov, F. Schedin, E. W. Hill and A. K. Geim,'' Effect of a high-kappa environment on charge carrier mobility in graphene.'', Phys. Rev. Lett., 102(2009)206603

V.N.Popov, "Theoretical evidence for T ½ specific heat behavior in carbon nanotube systems,"Carbon, 42(2004)991–995A. Puretzky, B. Geohegan, S. Pannala, C. M. Rouleau, M. Regmi, N. Thonnard and G. Eres,´´ Real-time optical diagnostics of graphene growth induced by pulsed chemical vapor deposition´´, Nanoscale, 5(2013)6507

Y. Qi , J. R. Eskelsen , U. Mazur and K. W. Hipps ,''Fabrication of graphene with CuO islands by chemical vapor deposition'', Langmuir, 28(2012)3489–3493

R. Qiao, A. Roberts, A. Mount, S.Klaine, . P.C. Ke , "Translocation of C60 and Its Derivatives Across a Lipid Bilayer". Nano Letters,7(2007)614

Z. Raskova, Krcma F, Klima M,J. Kousal,''Diagnostic of plasma chemical treatment of archaeological artefacts'', Czech. J. Phys., 52(2002)D927– D932

B. G. S. Raj , R. N. R. Ramprasad , A. M. Asiri , J. J Wu , S. Anandan, ´´ Ultrasound assisted synthesis of Mn3O4 nanoparticles anchored graphene nanosheets for supercapacitor applications´´, Electrochimica Acta, 156 (2015) 127–137

C.V. Raman and K.S. Krishnan, ''A new type of secondary radiation´´,. Nature, 121(1928)501–502

P. Ray ,H. Yu,P. P. Fu,'' Toxicity and Environmental Risks of Nanomaterials: Challenges and Future Needs'', J Environ Sci Health C Environ Carcinog Ecotoxicol Rev., 27(2009)1–35

W. Regan, N. Alem, B. Alemán, B. Geng, Ç. Girit, L. Maserati, F. Wang, M. Crommie and A. Zettl, ´´ A direct transfer of layer-area graphene´´, Ap. Ph. Let., 96(2010)113102

A. Reina, S. Thiele, X. Jia, S. Bhaviripudi, M. S. Dresselhaus, J. A. Schaefer and J. Kong,'' Growth of large-area single- and bi-layer graphene by controlled carbon precipitation on polycrystalline Ni surfaces'', Nano Res., 2(2009)509–516

C. Riedl, C. Coletti and U. Starke, '' Structural and electronic properties of epitaxial graphene on SiC(0 0 0 1): a review of growth, characterization, transfer doping and hydrogen intercalation'', J. Phys. D: Appl. Phys., 43(2010)374009

J. Robertson, "Amorphous carbon". Advances in Physics, 35(1986)317

K. Sasaki et al. Kohn anomalies in graphene nanoribbons. Phys. Rev. B, 80(2009)155450

M. Schriver, W. Regan, W. J. Gannett, A. M. Zaniewski, M. F. Crommie, A. Zettl, ´´Graphene as a long-term metal oxidation barrier: Worse than nothing.´´ ACS Nano, 7(2013)5763–5768

M. Shiddiky, A. P. O'Mullane , J. Zhang , L. D. Burke , A. M. Bond ,"Large Amplitude Fourier Transformed AC Voltammetric Investigation of the Active State Electrochemistry of a Copper/Aqueous Base Interface and Implications for Electrocatalysis", Langmuir, 27(2011)10302 – 10311

H. Shin, W. M. Choi, S.-M. Yoon, G. H. Han, Y. S. Woo, E. S. Kim, S. J. Chae, X.-S. Li, A. Benayad, D. D. Loc., F. Gunes, Y. H. Lee and J.-Y. Choi,"Transfer-free growth of few-layer graphene by self-assembled monolayers", Adv. Mater., 23(2011)4392–4397

N. M.Shinde, A. D. Jagadale, V. S. Kumbhar, T. Rana, J. Kim, C. D. Lokhande,´´ Wet chemical synthesis of WO_3 thin films for supercapacitor application´´, Korean Journal of Chemical Engineering, 32(2015)974-979

N. Srivastava, H. Guowei, Luxmi, P. C. Mende, R. M. Feenstra and S. Yugang,'' Graphene formed on SiC under various environments: comparison of Si-face and C-face'' ,J. Phys. D: Appl. Phys., 45(2012)154001

C.Y. Su, A. Y. Lu, C. Y. Wu, Y. T. Li, K. K. Liu, W. Zhang, S. Y. Lin, Z. Y. Juang, Y. Y. Tan, Y. Zhang, K. Bolotin et al., "Measurement of scattering rate and minimum conductivity in graphene," Physical Review Letters, 99,(2007)Article ID 246803

P.H. Tan,   W. P. Han,   W. J. Zhao,   Z. H. Wu,   K. Chang,   H. Wang, Y. F. Wang,   N. Bonini,   N. Marzari,   N. Pugno,   G. Savini,   A. Lombardo

& A. C. Ferrari. ,''The shear mode of multilayer graphene.'', Nature Mater., 11(2012)294–300

T. Tanaka, A. Ito, A. Tajima, E. Rokuta and C. Oshima,'' Heteroepitaxial film of monolayer graphene/monolayer h-BN on Ni(111)'', Surf. Rev. Lett.,10(2003)721–726

L. Tapasztó, T. Dumitrica, S. Kim, P. Nemes-Incze, C. Hwang and L. P. Biró, ´´Breakdown of continuum mechanics for nanometre-wavelength rippling of graphene´´, NATURE PHYSICS,8(739-742)2012

C. Thomsen and S. Reich,''Double resonant Raman scattering in graphite.'', Phys. Rev. Lett., 85(2000)5214–5217

G. V. Troppenz, Marc A. Gluba, Marco Kraft, Jörg Rappich and Norbert H. Nickel,´´ Strain relaxation in graphene grown by chemical vapor deposition´´, J. Appl. Phys., 114(2013)214312

F. Tuinstra and J.L. Koenig, ,''Raman spectrum of graphite'', J. Chem. Phys., 53(1970)1126–1130

S. Unarunotai, Y. Murata, C. E. Chialvo, H. S. Kim, S. MacLaren, N.Mason, I. Petrov and J. A. Rogers,"Transfer of graphene layers grown on SiC wafers to other substrates and their integration into field effect transistors ",Appl. Phys. Lett., 95(2009)202101

I. Vlassiouk , P. Fulvio, H. Meyer, N. Lavrik, S. Dai, P. Datskos, S. Smirnov,'' Large scale atmospheric pressure chemical vapor deposition of graphene'', CARBON, 54(2013)58 –67

I. Vlassiouk, M. Regmi, P. Fulvio, S. Dai, P. Datskos, G. Eres and S. Smirnov,'' Role of Hydrogen in Chemical Vapor Deposition Growth of Large Single-Crystal Graphen''ACS NANO, 5(2011)6069–6076

I.Vlassiouk , S. Smirnov , M.Regmi , S. P. Surwade , N.Srivastava , R. Feenstra , G. Eres , C. Parish , N. Lavrik , P. Datskos , S. Dai , and P. Fulvio, ''Graphene Nucleation Density on Copper: Fundamental Role of Background Pressure'', J. Phys. Chem. C, 117(2013)18919– 18926

J.A. Venables, G. D. T. Spiller,& M. Hanbucken,'' Nucleation and growth of thin films'', Rep. Prog. Phys., 47 (1984)399–459

Wall, ´´ The Raman Spectroscopy of Graphene and the Determination of Layer Thickness´´ Application Note: 52252, Thermo Fisher Scientific

H. Wang, G. Wang, P. Bao, S. Yang, X. Xie, W. Zhang,,''Controllable Synthesis of Submillimeter Single-Crystal Monolayer Graphene Domains on Copper Foils by Suppressing Nucleation'', J. Am. Chem. Soc., 134 (2012)3627–3630

P.R. Wallace, ,''The band theory of graphite'', Phys. Rev., 71(1947) 622–634

H. Wang,G. Wang, P. Bao, S. Yang, W. Zhu, X. Xie, W. Zhang,, ''Controllable Synthesis of Submillimeter Single-Crystal Monolayer Graphene Domains on Copper Foils by Suppressing Nucleation.'', J. Am. Chem. Soc. ,134(2012)3627–3630.

J. Wang, K. K. Manga, Q. Bao and K. P. Loh,´´ High-Yield Synthesis of Few-Layer Graphene Flakes through Electrochemical Expansion of Graphite in Propylene Carbonate Electrolyte'', J. Am. Chem. Soc.,133(2011) 8888–8891

X. Wang, X. Li, X. Qunqing, Jing Jin, Z: Wang, J: Li, J. Yan, S. Kaili Fan, "Fabrication of Ultralong and Electrically Uniform Single-Walled Carbon Nanotubes on Clean Substrates". Nano Letters, 9(2009)3137–3141

Y.Wang , Y. Zheng , X. Xu , E. Dubuisson , Q. Bao , J. Lu , and K. Loh '' Electrochemical Delamination of CVD Grown Graphene Film: Toward the Recyclable Use of Copper Catalyst´´,ACS NANO,5(2011)9927–9933

X. Wang,L.Zhi,N.Tsao, Z. Tomovic, J. Li and K. Mullen Angew,'' Transparent Carbon Films as Electrodes in Organic Solar Cells'', Chem.Int.Ed., 47(2008) 2990– 2992

J.M. Wofford, S. Nie, K. F. McCarty, N. C. Bartelt and O. D. Dubon,''Graphene Islands on Cu Foils: The Interplay between Shape, Orientation, and Defects. '',Nano Lett. 10 (2010) 4890-4896

J. Wood W. Scott . A. Schmucker, S. Lyons, E. Pop and J. W. Lyding. ''Effects of Polycrystalline Cu Substrate on Graphene Growth by Chemical Vapor Deposition'',Nano Lett. 11(2011) 4547–4554

P. Wu, X. Zhai, Z. Li and J. Yang, ´´Bilayer Graphene Growth via a Penetration Mechanism´´, J. Phys. Chem. C, 118(2014) 6201–6206

Y.A. Wu,Y. Fan,S. Speller, G.L. Greeth, J.T. Sadowski, K. He, A.W. Robertson, C.S. Allen, J.H. Warner, , ´´Large SingleCrystals of Graphene on Melted Copper Using ChemicalVapor Deposition'', ACS Nano , 6 (2012)5010–5017

W. Wu, L.A Jauregui, Z. Su, Z. Liu, J. Bao, Y.P. Chen, Q. Yu, ,''Growth of Single Crystal Graphene Arrays by Locally Controlling Nucleation on Polycrystalline Cu Using Chemical Vapor Deposition'', Adv. Mater. , 23(2013) 4898–4903

T. Wu, G. Ding, H. Shen, H. Wang, L. Sun, D. Jiang, X. Xie,M. Jiang,''Triggering the Continuous Growth of Graphene Toward Millimeter-Sized Grains'', Adv. Funct. Mater. ,23(2013)198– 203

B. Wu, D. Geng, Z. Xu, Y. Guo, L. Huang, Y. Xue, J. Chen, G. Yu and Y. Liu,'' Self-organized graphene crystal patterns'', NPG Asia Mater., 5(2013)36.

Y. Xu, B. Yan, H.-J: Zhang, J. Wang, G. Xu, P. Tang, W. Duan, S.-C. Zhang,´´ Large-gap quantum spin Hall insulators in tin films'', Phys. Rev. Lett., 1112013)136804

M. H. Yang, K. G. Lee, S. J. Lee, S. B. Lee, Y.K. Han and B. G. Choi,´´ Three-Dimensional Expanded Graphene−Metal Oxide Film via SolidState Microwave Irradiation for Aqueous Asymmetric Supercapacitors´´,ACS Appl. Mater. Interfaces, 7(2015)22364−22371

Z.Yan, J. Lin, Z. Peng, Z. Sun, Y. Zhu, L. Li, C. Xiang, E. Loιc Samuel, C. Kittrell, and J. M. Tour,'' Toward the Synthesis of Wafer-Scale Single-Crystal Graphene on Copper Foils'',ACS NANO,12(2012)9110-9117

O. Yazyev and S. Louie , 'Topological defects in graphene: Dislocations and grain boundaries'' ,Phys. Rev. B,81(2010)195420

O. Yazyev and S. Louie , ''Electronic transport in polycrystalline graphene'', Nature Mater.,9(2010)806–9

T. Yoon, W. C. Shin, T. Y. Kim, J. H. Mun, T. Kim and B. J. Cho,"Direct Measurement of Adhesion Energy of Monolayer Graphene As-Grown on Copper and Its Application to Renewable Transfer Process", Nano Lett., 12(2012)1448–1452

Q. Yu, L.A. Jauregui, W. Wu, R. Colby, J. Tian, Z. Su, H. Cao, Z. Liu, D. Pandey, D. Wei, et al.,'' Control and Characterization of Individual Grains and Grain Boundaries in Graphene Grown by Chemical Vapor Deposition'',Nature Materials, 10 (2011)443–449

W. Yu, Y. Zheng,X. Xu, E. Dubuisson, Q. Bao, J. Lu and K. P. Loh,"Electrochemical Delamination of CVDGrown Graphene Film: Toward the Recyclable Use of Copper Catalyst,"ACS Nano , 5(2011)9927–9933

X. Zang, P. Li, Q. Chen, K. Wang, J. Wei, D. Wu and H. Zhu, ´´ Evaluation of layer-by-layer graphene structures as supercapacitor electrode materials´´, Journal of Applied Physics, 115(2014) 024305

L. L. Zhang, R. Zhou and X. S. Zhao.,´´ Graphene-based materials as supercapacitor electrodes´´, J. Mater. Chem., 20(2010)5983

Y. Zhang , Z. Li,P.. Kim , L. Zhang and C. Zhou , '' AnisotropicHydrogen Etching of Chemical Vapor Deposited Graphene'', ACS NANO, 6(2012)126–132

B. Zhang,W. H. Lee, R. Piner, I. Kholmanov, Y. Wu, H. Li, H. Ji, and R. S Ruoff, ´´Low-Temperature Chemical Vapor Deposition Growth of Graphene from Toluene on Electropolished Copper Foils´´, ACS Nano, 6(2012)2471–2476

X. Zhang,   J. Ning,   X. Li,   B. Wang,   L. Hao,   M. Liang,   M. Jin and   L. Zhi '' Hydrogen-induced effects on the CVD growth of high-quality graphene structures'', Nanoscale, 5(2013) 8363

W. Zhang, P. Wu, Z. Li, J. Yang,,'' First-Principles Thermodynamics of Graphene Growth on Cu Surfaces'',J. Phys. Chem. C 115,(2011) 17782–17787

Y. Zhang, L: Zhang,and C. Zhou, '' Review of Chemical Vapor Deposition of Graphene and Related Applications'', Accounts of Chemical Research, 46(2013) 2329–2339

Z. Zhan, J. Sun,L. Liu, E. Wang, Y. Cao,N. Lindvall, G. Skoblin and A. Yurgens,"Pore-free bubbling delamination of chemical vapor deposited graphene from copper foils ",J. Mater. Chem. C, 3(2015)8634

Y. Zhang, J. P. Small, W. V. Pontius and P. Kim,"Fabrication and Electric Field Dependent Transport Measurements of Mesoscopic Graphite Devices", Appl. Phys. Lett., 86(2005)073104

W. Zheng, X. Lu, S.C. Wong,'' Electrical and mechanical properties of expanded graphite-reinforced high-density polyethylene'', J. Appl. Polym. Sci.,91(2004) 2781–2788
L. Zhong, F. R. Chen and L. J. Li,"Direct Formation of Wafer Scale Graphene Thin Layers on Insulating Substrates by Chemical Vapor Deposition", Nano Lett., 11(2011)3612–3616

Acoording to **FED-STD-209 E,** *Airborne Particulate Cleanliness Classes in Cleanrooms and Cleanzones,* canceled on November 29, 2001 by the United States General Services Administration(GSA)

https://en.wikipedia.org/wiki/Graphite

https://en.wikipedia.org/wiki/Fullerene

https://en.wikipedia.org/wiki/Fullerene

http://www.ncnr.nist.gov/staff/taner/nanotube/types.html

http://www.shimadzu.com/an/elemental/oes/oes.html

"2010 Nobel Physics Laureates'', nobelprize.org

www.fbg.ub.edu/images/AVCRI189_Flyer_Physical-materialsnanotechnology.pdf, (2013).

''Things you could do with graphene'', Nature Nanotechnology,9(2014) 737-747,

https://en.wikipedia.org/wiki/Graphene#

http://graphene-flagship.eu

http://www.graphene.manchester.ac.uk/explore/the-story-of   graphene/discovery-at-manchester//

"GRAPHENITE™ – GRAPHENE INFUSED 3D PRINTER POWDER – noble3dprinters.com. Noble3DPrinters.

http://www.graphene-info.com/new-security-tags-built-using-vorbecks-graphene-based-inks-start-shipping-q1-2012

http://www.graphene-info.com/graphene-products

https://graphene-supermarket.com/Graphene-Transfer-Guide.html
galaxycapitalcorp.com. ,"Electric Graphite Growing Demand From Electric Vehicles & Mobile Electronics" (PDF),(2011)

IUPAC, Compendium of Chemical Terminology, 2nd ed. (the "Gold Book") (1997)

USGS. ,"Graphite Statistics and Information". Retrieved 2009-09-09.

Publications

S. Chaitoglou, E. Pascual, E. Bertran, and J. L. Andujar '' Effect of a balanced concentration of hydrogen on graphene CVD growth", Journal of Nanomaterials, Volume 2016, 2016, Article ID 9640935, 10 pages

S. Chaitoglou, M. Reza Sanaee, N. Aguiló-Aguayo, and E. Bertran, "Arc-Discharge Synthesis of Iron Encapsulated in Carbon Nanoparticles for Biomedical Applications," Journal of Nanomaterials, vol. 2014, Article ID 178524, 8 pages, 2014. doi:10.1155/2014/178524

S. Chaitoglou and E. Bertran, '' Effect of pressure and hydrogen flow in nucleation density and morphology of graphene bidimensional crystals.",accepted in Material Research Express, 2016

S. Chaitoglou and E. Bertran, ´´ Control of the strain in CVD grown Graphene via the H2 flow´´, Submitted in New Journal of Physics, 2016

Communications in Conferences

2016

´´Evaluating layer-by-layer structures of different graphene/metal and graphene/metal oxide as electrodes for supercapacitors´´, Graphene2016, Genova, S. Chaitoglou, R. Amade, E. Bertran

2015

´´Kinetics in CVD graphene growth.The effect of pressure and gases flows´´,Nanotexnology 2015, Thessaloniki, Greece, S. Chaitoglou*, S. Logothetidis, E. Pascual , J.L. Andújar and E. Bertran

"Efficient transfer of graphene grown on copper substrates using electrochemical delamination",Nanotexnology   2015,Thessaloniki,Greece,   D.   Papas,   S.

Chaitoglou, A. Zachariadis, E. M. Pechlivani, A. Papamichail, A. Laskarakis, S. Logothetidis

´´ Effect of a balanced concentration of hydrogen on a high quality graphene CVD growth´´,ImagineNano2015, Bilbao,Spain,S. Chaitoglou*,E. Bertran J.L. Andújar and E. Pascual

2014

''Effect of the gas mixture and flow on the growth of graphene layers at low pressure'', Oral presentation, XXX Trobades de la Mediterrània 2014 (GRAPHENE), S. Chaitoglou, V.Freire, E.Pascual, J.L.Andújar and E.Bertran

'' The hidden influence of the flux of gas on the growth of graphene layers by low pressure chemical vapor deposition'', poster contribution, TNT 2014, Barcelona, Spain, S. Chaitoglou, A. Musheghyan, V-M Freire, E. Pascual, J-L Andújar and E.Bertran

 "RamanDay: Workshop on Advanced Applied Raman Spectroscopy",Attendance in workshop held by the Centres Cientifics i Tecnologics of the University of Barcelona

 "Synthesis of fullerene on the surface of carbon nanoparticle by arc discharge method" in Proceedings of the International Conference on Trends in Nanotechnology, Phantoms Foundation, Barcelona, Spain, October 27-31, 2014,M. Reza Sanaee, S. Chaitoglou and Enric Bertran

"Poster: Investigation of monolayer-formation time for the synthesis of graphene on copper/nickel/silicon using very-low pressure pulses of methane",VI Jornada IN2UB. Universitat de Barcelona, 2014,Barcelona (Spain) ,V.-M. Freire, A. Ramírez, S. Chaitoglou, E. Bertran, E. Pascual, J.-L. Andújar

2013

''Arc-Discharge Synthesis of Fe@C Nanoparticles for General Applications'', Oral presentation in JIPI (Jornada d'Investigadors Predoctorals Interdisciplinària) S. Chaitoglou*, M. Reza-Sannae, N. Aguiló-Aguayo, E. Bertran

''Graphene grown on Silicon by a modified chemical vapor deposition technology at very low pressure pulses of methane'', Attendance and Poster contribution in „ALBA Synchrotron, new instrumentation for Nanoscience and molecular materials characterization" Workshop in ALBA synchrotron light source, Barcelona, S. Chaitoglou, V.-M. Freire, A. Diaz, E. Pascual, J.-L. Andújar and E. Bertran

''Modified chemical vapor deposition technology to produce graphene with very low pressure pulses of methane'',poster contribution,TNT 2013, Sevilla,Spain , S. Chaitoglou, V.-M. Freire, A. Diaz, E. Pascual, J.-L. Andújar and E. Bertran

''Exploring new ways of chemical vapor deposition technology to produce graphene'' ,oral presentation, Imaginenano 2013,Bilbao,Spain , Victor-Manuel Freire,S. Chaitoglou,A. Ramírez,M. Reza Sanaee,E. Pascual,J.-L. Andújar and E. Bertran

"Design and synthesis of carbon encapsulated iron nanoparticle for drug delivery",poster contribution, Imaginenano 2013,Bilbao,Spain , M. Reza Sanaee, S. Chaitoglou, V.-M. Freire, N. Aguiló-Aguayo, E. Bertran

"Study of carbon encapsulated iron nanoparticles produced by a modified arc discharge by applying nitrogen, argon and helium",poster contribution, Imaginenano 2013 ,Bilbao,Spain , M. Reza Sanaee, S. Chaitoglou, V.-M. Freire, N. Aguiló-Aguayo, E. Bertran,

"Arc-Discharge Synthesis of Fe@C Nanoparticles for General Applications",poster contribution, ImagineNano 2013, Bilbao, Spain, S. Chaitoglou*, M. Reza Sanaee, N. Aguiló-Aguayo, E. Bertran

2012

"Influences of argon-helium mixtures on the carbon-coated iron nanoparticles produced by amodified arc discharge," in Proceedings of the 9th International Conference on Nanoscience and Nanotechnologies, p. 12,Artion, 2012,Thessaloniki, Greece,M.R. Sanaee, S. Chaitoglou, N. Aguil´o-Aguayo, and E. Bertran,

Research Stay

Research stay of 3 months (1st May-31st July, 2015) in Aristotle Univeristy of Thessaloniki (AUTH), Greece. Host research group was the Laboratory of Thin Films and Nanostructures (LTFN). Director of the group is Prof. Dr. S. Logothetidis of the Physics faculty. My work consisted on the transfer of graphene samples by a modified electrochemical delamination technique and the characterization of them by means of spectroscopy and microscopy. Results were presented in the NN 2015 conference.

In addition, I participated in the training as an operator of the Aixtron Black Magic CVD reactor as well as in the preliminary studies of the samples prepared there.

External collaborations

- Collaboration with the Institute of Microelectronics of Barcelona. The objective of the collaboration was the deposition of metallic contacts by means of electron beam lithography on top of Graphene/SiO_2/Si, targeting in the fabrication of a field-effect transistor. Electrical measurements of the device were transacted with an HP4155B analyzer. We collaborate with Dr. Xavier Borisse and Dr. Sergi Sanchez for this project.
- Collaboration with the Nanotechnology Platform of the Institute of Bioengeeniring of Cataluña for the fabrication of a quartz photomask. Mettalic contacts were deposited over quartz in a pattern designed by our group. The photomask permits the reproduction of its pattern in different patterns by photolithography. We collaborated with Dr. Mateu Pla for this project.
- All measurement of Raman spectroscopy (Jobin-Yvon LabRam HR 800), atomic force microscopy (AFM Multimode 8) and scanning electron microscopy (JEOL JSM 7100F) presented in this Thesis were made in collaboration with the Centres Científics i Tecnològics de la Universitat de Barcelona. The author has obtained the expertise to operate the above instruments.

Annex I

Samples List

Table 1: Samples grown with continuous flow of gases using methane as carbon precursor.

sample name	Type	Pre-Treatment		Comments	Pre-annealing		Growth	Time(minutes)	Temperature (°C)	H2 flow(sccm)	CH4 flow (sccm)
		Acid Treatment	H2 Plasma		H2 flow (sccm)	Ar flow (sccm)	Total Pressure (Pascal)				
14k1301	Cu foil	yes	no		no	no	20	20	1040	20	5
14k1901	Cu foil	yes	yes		no	no	20	40	1040	20 first 20'/0 after	5
14k1902	Cu foil	yes	no		no	no	20	20	1040	20	5
14k1401	Cu foil	yes	yes		no	no	20	40	1040	20	5
14k2001	Cu foil	yes	yes		no	no	20	60	1040	20 first 20'/5 after	5
14l0201	Cu foil	yes	yes		no	no	20	5	1040	20	5
14l1901	Cu foil	yes	yes		no	no	20	20	1040	20	5
14l2301	mask	no	no		no	no	20	15	400		benzene vapors
15a0901	100nm SiO2	no	no		10 for 10'	no	20	15	500		benzene vapors
15a1301	Cu foil	yes	yes		no	no	20	25	1040	20	5
15a1401	Cu foil	yes	yes		no	no	10	25	1040	20	5
15a1402	Cu foil	yes	yes		no	no	30	20	1040	20	5
15a1501	Cu foil	yes	yes		no	no	5	20	1040	10	5
15a1502	Cu foil	yes	yes		no	no	20	20	1040	20	5
15a1601	400nm Cu/Si	yes	yes		no	no	20	5	1040	20	5
15a1901	600nm Cu/Si	yes	yes		no	no	20	5	1040	20	5
15a2001	600nm Cu/Si	no	yes		no	no	20	5	500	20	benzene vapors
15a2202	Cu foil	yes	yes		no	no	15	20	1040	20	5
15a2601	Cu foil	yes	yes		no	no	12,5	20	1040	20	5
15a2602	Cu foil	yes	yes		no	no	17,5	20	1040	20	5
15a2702	125nm Ruthenium/Si	no	yes		no	no	20	20	1040	20	5
15a2703	125nm Ruthenium/Si	no	no		no	no	20	20	1040	20	5

15b0 201	Cu foil	yes	yes		no	no	15	20	1040	0	5
15b0 202	Cu foil	yes	yes		no	no	15	20	1040	20	3
15b0 401	200nm Ni/Si	no	yes		no	no	15	20	1040	20	5
15b0 601	Cu foil	yes	yes		no	no	5	10	1040	5	0
15b1 101	Cu foil	yes	yes		no	no	15	20	1040	10	5
15b1 201	Cu foil	yes	yes		no	no	23	20	1040	30	5
15b1 301	Cu foil	yes	yes		no	no	15	20	1040	25	5
15b1 602	Cu foil	yes	yes		no	no	15	20	1040	15	5
15c0 101	Cu foil	yes	yes		no	no	20	20	1040	10	5
15c0 102	Cu foil	yes	yes		no	no	10	20	1040	10	5
15c0 501	Cu foil	yes	yes		no	no	17,5	20	1040	10	5
15c0 502	Cu foil	yes	yes		no	no	15	20	1040	20	5
15c0 601	Cu foil	yes	yes		no	no	12,5	20	1040	15	5
15c1 601	Cu foil	yes	yes		no	no	15	30	1040	20	5
15c1 602	Cu foil	yes	yes		no	no	15	20	1040	20 Ar	5
15c1 901	Cu foil	yes	yes		no	no	15	20	700	20	5
15c1 902	Cu foil	yes	yes		no	no	15	20	900	20	5
15c2 001	Cu foil	yes	yes		no	no	15	30	1040	20	5
15c2 302	Cu foil	yes	yes		no	no	15	10	1040	20	5
15c2 601	Cu foil	yes	yes		no	no	15	50	1040	20	5
15c3 001	Cu foil	yes	yes		no	no	15	40	1040	20	5
15c3 002	Cu foil	yes	yes	tube	no	no	15	20	1040	20	5
15d0 801	Cu foil <111>	yes	yes		no	no	20	20	1040	20	5
15d1 301	Cu foil	yes	yes		no	no	20	7	1040	20	5
15d1 601	Cu foil	yes	yes		no	no	15	10	1040	20	5
15d2 001	Cu foil	yes	yes	outside oven zone	no	no	15	50	1040	20	5
15d2 101	Cu foil	yes	yes		no	no	15	20	1040	20	5
15d2 102	Cu foil	yes	yes	send to Victor	no	no	15	10	1040	20	5
15d2 301	Cu foil	yes	yes		no	no	20	20	1040	20	5
15d2 401	Cu foil	yes	yes	send to Victor	no	no	20	20	1040	20	5
15j09 01	Cu foil	yes	yes		no	no	30	20	1040	10	5
15j09 02	Cu foil	yes	yes		no	no	20	20	1040	10	5
15j13 01	600nm Cu/Si	no	yes		no	no	20	20	1040	10	5
15j14 01	Cu foil	yes	yes		no	no	20	20	1040	20	5

16j16 01	Cu foil	no	yes		no	no	20	50	1040	20	5
15j19 01	Cu foil	yes	yes		no	no	20	20	1040	20	20
15j22 01	Cu foil	no	yes		no	no	20	50	1040	20	5
15j23 01	Cu foil	yes	yes		no	no	50	10	1040	20	10
15j29 01	Cu foil	no	yes		no	no	20	50	1040	20	5

Table 2: Samples grown with continuous flow of gases using methane as carbon precursor, without use of hydrogen plasma for the copper reduction.

Sample Name	Type	Pre-Treatment		Pre-annealing			Growth				
		Acid Treatment	Comments	H2 flow (sccm)	Ar flow (sccm)	Temperature (°C)	Total Pressure (Pascal)	Time(minutes)	Temperature (°C)	H2 flow(sccm)	CH4 flow (sccm)
14g0901	foil 75um	extra pre cleaning		22		1000	60Pa	40	1000	22	11
14g1001	foil 75um	extra pre cleaning		22		1000	60Pa	40	1000	22	6
14g1101	foil 75um	extra pre cleaning		22		1000	60Pa	40	1000	11	6
14g1401	foil 75um	extra pre cleaning		22		1000	60Pa	40	1000	44	11
14g2501	foil 75um	extra pre cleaning		11	50	950	110 Pa	10	950	6	
14g2801	foil 75um	extra pre cleaning		44	50	1000	60 Pa	10	1000	0	
14g2901	foil 75um	extra pre cleaning		11	50	950	60 Pa	10	950		6
14g2902	foil 75um	extra pre cleaning		11	50	950	60 Pa	10	550		24
14g3001	foil 75um	extra pre cleaning		44	50	950	60 Pa	40	950		6
14i1501	foil 75um	extra pre cleaning		44	50	950	60 Pa	40	950		6
14i1601	foil 75um	extra pre cleaning		44	50	950	60 Pa	10	550		6
14i1701	foil 75um	extra pre cleaning		11	50	950	110 Pa	10	550		24
14i1901	foil 75um	extra pre cleaning		11	50	950	35 Pa	40	950		24
14i2201	foil 75um	extra pre cleaning		44	50	1000	60 Pa	20	1000	44	24
14i2301	foil 75um	extra pre cleaning		44	50	1000	60 Pa	20	1000	22	6

14i2302	foil 75um	extra pre cleaning		44	50	1000	60 Pa	20	1000		6
14i2901	foil 75um	extra pre cleaning		44	50	1000	60 Pa	20	1000	22	6
14i3001	foil 75um	extra pre cleaning		22	50	1000	53 Pa	15	1000	22	1
14j0101	foil 75um	extra pre cleaning		11	50	1040	40 Pa	20	1040	11	3
14j0201	foil 75um	extra pre cleaning		22	50	1040	40 Pa	20	1040	22	3
14j0601	foil 75um	extra pre cleaning	with NPs as seeds	11	50	1040	40 Pa	20	1040	11	3
14j1301	100 nm Cu	extra pre cleaning		5	50	1040	32 Pa	30	1040	5	3
14j1401	100 nm Cu	extra pre cleaning		30	50	1040	70 Pa	30	1040	30	3
14j1001	Si sub.	extra pre cleaning	with NPs as seeds				36 Pa	20	750	10	3
14j2901	foil 75um	extra pre cleaning	with NPs as seeds	5	30	1040	4 Pa	5	1040	5	40

Table 3: Samples grown with pulses of gases using methane as carbon precursor.

sample name	Type	Pre-Treatment			Pre-annealing		Growth			
		Acid Treatment	H2 Plasma	Comments	H2 flow (sccm)	Ar flow (sccm)	Total Pressure (Pascal)	Time(minutes)	Temperature (°C)	pulses
14k2101	Cu foil	yes	yes		no	no	6×10^{-2}		1040	1
14k2102	Cu foil	yes	yes		no	no	0,41		1040	1
15b0901	Cu foil	yes	yes		no	no	10^{-4}		1040	10
15b1601	Cu foil	yes	yes		no	no	10^{-4}		1040	50
15c0901	Cu foil	yes	yes		no	no	2		1040	100
15c1801	Cu foil	yes	yes		no	no	10^{-4}		950	1
15c2002	Cu foil	yes	yes		no	no	10^{-4}		1040	30
15c2701	Cu foil	yes	yes		no	no	10^{-4}		1040	70

S. Chaitoglou

Table 4: Samples grown with pulses of gases using methane as carbon precursor, without use of hydrogen plasma for the copper reduction.

Sample Name	Type	Pre-Treatment			Pre-annealing			Growth		
		Acid Treatment	H2 Plasma	Comments	H2 flow (sccm)	Ar flow (sccm)	Temperature (°C)	Total Pressure (Pascal)	Time(minutes)	Temperature (°C)
14g2102	foil 75um	extra pre cleaning					1000	10^-4 Pa		1000
14j2101	foil 75um	extra pre cleaning						7X10^-4 Pa		1040
14j2201	foil 75um	extra pre cleaning			5	10	1040	7X10^-4 Pa		1040
14j2301	foil 75um	extra pre cleaning			5	10	1040	10^-4 Pa		1040

Table 5: Samples grown with the use of pulses of benzene as carbon precursor.

Sample Name	Type	comments	Pre-annealing	temperature(°C)	pressure	pulses	hydrogen
14b0301	foil 125um		15' in 550 C	550	5X10^-4	5	no
14a2901	300 nm		15' in 550 C	550	5X10^-4	3	no
14a3101	300 nm		15' in 550 C	510	5X10^-4	3	no
14a2801	300 nm		15' in 550 C	550	5X10^-4	3	no
14b1701	foil 125um	H2 annealing	20' in 970 C	500	50 Pa	30	
14b2001	foil 125um		20' in 950 C	550	25 Pa	40	
14b2002	foil 125um		20' in 950 C	550	20 Pa	100	
14b2102	foil 125um		20' in 950 C	400	20 Pa	40	
14b2501	300 nm		25' in 950 C	700	20 Pa	40	
14b2602	foil 75um		20' in 1000 C	700	1 Pa	40	
14c0701	foil 75um		20' in 1000 C	600	30 Pa	30	
14c0702	foil 75um		20' in 1000 C	600	30 Pa	60	
14c1301	foil 75um		15' in 1000 C	550	3 Pa	8	
14c1302	foil 75um		15' in 1000 C	550	3 Pa	4	
14c1303	foil 75um		15' in 1000 C	550	3 Pa	1	

14c2101	foil 75um	extra pre eaching with nitric acid	15' in 1000 C	550	2 Pa	6	
14c2102	150 nm		15' in 900 C	550	2 Pa	8	
14c2103	60 nm		15' in 900 C	600	8 Pa	16	
14c2501	20 nm		15' in 900 C	350	8 Pa	10	
14c2601	20 nm		15' in 900 C	350	8 Pa	8	
14c3101	120 nm		15' in 900 C	900	10^{-4} Pa	2	
14c3102	120 nm		15' in 900 C	650	10^{-4} Pa	2	
14d0101	180 nm		10' in 900 C	650	10^{-4} Pa	4	
14d0102	180 nm		10' in 900 C	650	10^{-4} Pa	8	
14d0401	120nm Ni/ 240 nm Cu		no	650	10^{-4} Pa	10	
1,40E+202	224 nm Ni		no	1000	10^{-4} Pa	6	
14e0501	224 nm Ni/100 nm Cu		no	1000	10^{-4} Pa	6	
14e1602	foil 75um		no	500	10^{-4} Pa	5	
14e2001	50nm		no	500	10^{-4} Pa	1	
14e1602	foil 75um		no	500	10^{-4} Pa	5	
14e2801	224nm Ni/ 30 nm Cu			550	10^{-4} Pa	4	
14e2901	foil 75um			550	10^{-4} Pa	1	
14g0101	foil 75um		20' to 800 C	600	1 Pa	20	

Table 6: Samples grown with the use of pulses of toluene as carbon precursor.

Sample Name	Type	comments	Pre-annealing	temperature(°C)	pressure	pulses
14b2702	foil 75um		20' in 1000 C	600	30 Pa	60
14c0601	foil 75um		20' in 1000 C	600	30 Pa	30
14c0602	foil 75um		20' in 1000 C	600	30 Pa	15
14c1401	foil 75um		15' in 1000 C	550	3 Pa	8
14c1402	foil 75um		15' in 1000 C	550	3 Pa	4
14c1403	foil 75um		15' in 1000 C	550	3 Pa	1
14c1801	foil 75um	extra preeaching with nitric acid	15' in 1000 C	550	3 Pa	8

Table 7: Samples grown with the use of vapors of benzene/toluene/methane (indicated in each case) as carbon precursor.

Sample Name	Type	comments	Pre-annealing	temperature	pressure	vapors	gas
13l0901	foil 125um			1000	3x10^-4	10 sec cond flow	*methane*
13l1001	foil 125um			1000	3x10^-4	20sec cond flow	*methane*
13l1301	100 nm			950	3x10^-4	180 sec cond flow	*methane*
13l1601	100 nm			1000	3x10^-4	300 sec cond flow	*methane*
13l1701	100 nm			1000	3x10^-4	600 sec cond flow	*methane*
14g0201	foil 75um			1000	100 Pa	300 sec cont flow vapors	*methane*
14g0701	foil 75um			1000	66 Pa	1800 sec cont flow vapors	*methane*
14g0702	foil 75um	etching with nitric acid	with acetyline	1000	66 Pa	1800 sec cont flow vapors	*methane*
14b0603	foil 125um		20' in 1000C	500	1-5 Pa	480sec cont flow vapors	*benzene*
14b0701	100 nm		10' in 500 C	600	3-7 Pa	300 sec cont flow vapor	*benzene*
14b0702	100 nm		10' in 500 C	550	3-7 Pa	300 cont flow	*benzene*
14b0703	foil 125um		20' in 1000C	550	3-7 Pa	480 sec cont flow	*benzene*
14b1101	100 nm		20' in 1000C	500	2-7 Pa	1200 sec cont flow	*benzene*
14b1402	foil 125um	extra annealing after	20' in 950 C	500	25 Pa	900 sec cont flow vapors	*benzene*
14b1901	foil 125um		20' in 950 C	550	20 Pa	2400 sec cont flow vapors	*benzene*
14b1902	foil 125um		20' in 950 C	550	25 Pa	60 sec cont flow vapors	*benzene*
14b2101	foil 125um		20' in 950 C	550	25 Pa	2400 sec cont flow vapors	*benzene*
14b2601	foil 75um		20' in 1000 C	700	1 Pa	2400 sec cont flow vapors	*benzene*
14bc0302	foil 75um		20' in 1000 C	650	3 Pa	750 sec cont flow vapors	*benzene*
14e1601	45nm Cu		no	600	atm pressure	900 " cont flow vapors	*benzene*
14e2301	foil 75um		60' to 1000 C	1000	100	1800 sec cont flow vapors	*benzene*
14c0401	foil 75um		20' in 1000 C	600	0.5 mbar	2400 sec cont flow vapors	*toluene*
14b2701	foil 75um		20' in 1000 C	600	50 Pa	3600 sec cont flow vapors	*toluene*
14b2801	foil 75um		20' in 1000 C	600	100 Pa	2400 sec cont flow vapors	*toluene*
14b1301	foil 125um		20' in 1000'	500	3-5 Pa	900 sec cont flow vapors	*toluene*

14b1302	foil 125um		20' in 1000'	500	50 Pa	900 sec cont flow vapors	*toluene*
14b1401	foil 125um	extra annealing after	20' in 1000'	500	50 Pa	900 sec cont flow vapors	*toluene*

Annex II

Fabrication of a quartz photomask

A 2 inches photomask were fabricated in collaboration with the Nanotechnology Platform of the Institute for Bioengineering of Cataluna (IBEC).

The mask was designed to serve in two different purposes.

- The one part of the mask consists of a table of ordered squares with dimensions down to the microscale. The purpose of this table was the easy observation of the graphene crystals after their transfer on top of it. As the graphene crystals grown by chemical vapor deposition in our reactor (GRAPHMAN, UB) have a size varying from some up to 40-50μm, we need a table that enables us to locate the same crystal in different microscopic instruments. Knowing the exact position, indicated by rows and columns, permits a more accurate characterization.

- The other part of the mask consists of various metallic contacts. The geometry of them permits the performance of electrical measurements of the graphene film. We can perform both Van der Pauw measurements (using the four contacts geometry) [1]to obtain the graphene sheet resistance, as well as carrier mobility measurements (field effect transistor fabrication)[2]

Mask Characteristics

The mask was designed by FEMAN group and the fabrication of it was executed by the Nanotechnology Platform of IBEC. A quartz glass was sputtered with 100nm of a Cr layer. On top of it was applied a 1µm resist (AS1512HS). After the exposure using a DWL mask plotter the mask with the desired design was obtained. In Figure 1 we can see an image of the quartz photomask as well as various optical microscopy images of it. All the dimensions can be distinguished, both of the tables as of the contacts.
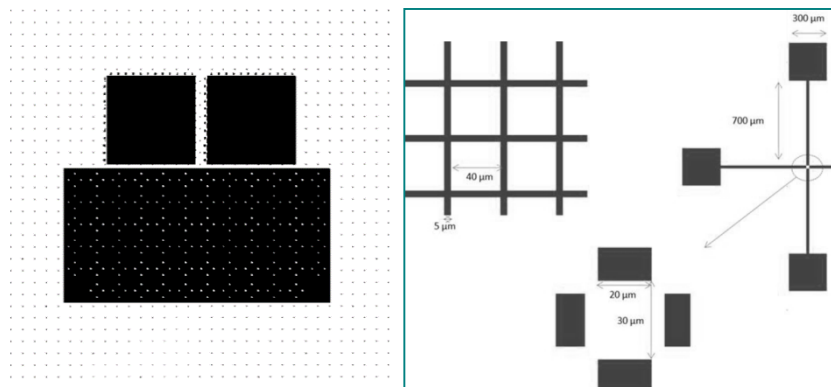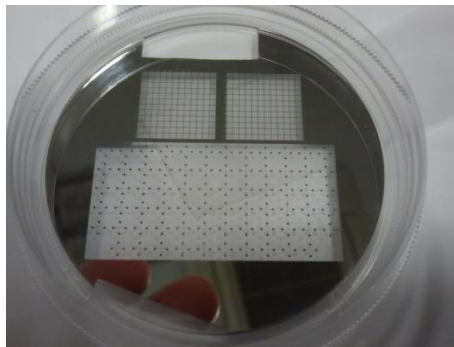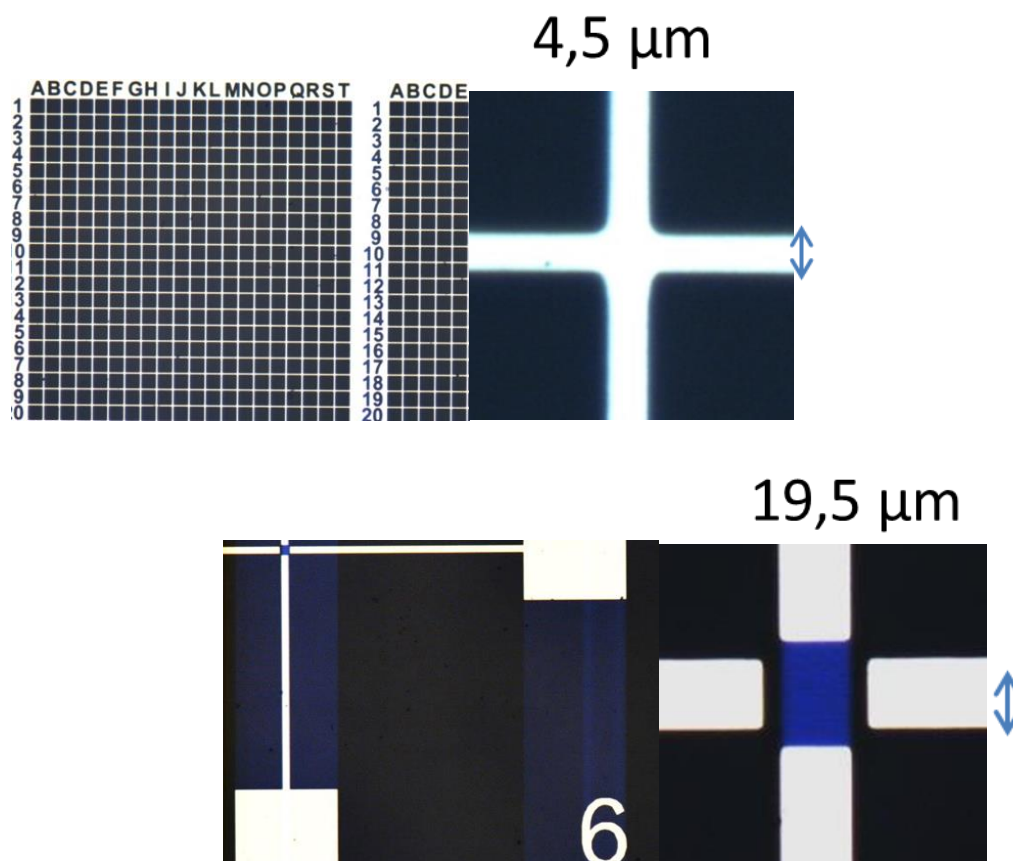
Figure 1: Images and schemes of the quartz photomask. All the important dimensions are being presented.

This mask is being used as a pattern. The re production of it is being made by a simple photolithography technique on top of Si/SiO$_2$. We use 90 nm SiO$_2$ on top of p-doped silicon wafer. The thickness of silicon oxide is important as it provides the best optical contrast with the graphene lying on top of it [3]. The steps of the photolithography process are being explained below[4].

- The wafer is being cleaned carefully in ultrasound bath of acetone and isopropanol, ten minutes each, to remove all the impurities. Rinse with DI water between every step.
- Drying of the substrate by heating to hot plate for 5 minutes in 120°C.

- The photoresist AZ5214E is being mixed with acetone in proportion 1:1. This allow us to obtain the thinner film possible while spin coating. The photoresist is deposited drop by drop on top of the wafer and being spin coated at 5000RPM for 60''. The film obtained is about 1μm thick.

- A soft bake is performed for the cure of the resist. The bake is taking place in 90°C for 60''. Then the sample is being let to cool down.

- The photomask is being placed in top of the resist/wafer and is being exposure in UV light for 5 seconds.

- Revealing of the wafer for 30'' in a AZ400K revelator (mixed with DI in proportion 1:4, revelator : DI). Then the wafer is being rinsed with DI. The unexposed areas are not removed, leaving on the top of the wafer the desired pattern.

- 100nm of metal (Cr or Ni) are being sputtered on top of the wafer by pulsed magnetron sputtering. Then the wafer is being washed in acetone bath. The parts that have the resist are being washed away, leaving behind the pattern of the metal contacts in the parts that were not covered with photoresist in the first place. (Figure 2)
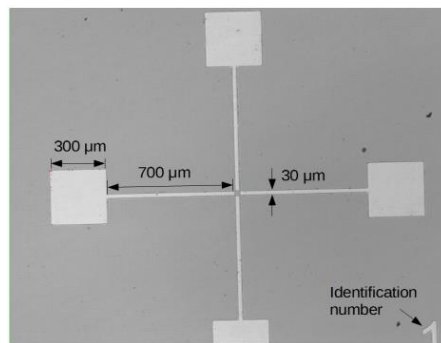
Figrue 2: Metallic contacts of Ni on top of Si wafer

References

https://en.wikipedia.org/wiki/Van_der_Pauw_method

F.Schwierz,''Graphene transistors'',Nature Nanotechnology,2010, 5, 487–496

P. Blake, E. W. Hill,A. H. Castro Neto,K. S. Novoselov, D. Jiang, R. Yang, T. J. Booth, A. K. Geim,''Making graphene visible'', Appl. Phys. Lett., 91(2007)063124

http://www.ece.gatech.edu/research/labs/vc/theory/photolith.html

References

https://en.wikipedia.org/wiki/Van_der_Pauw_method

F.Schwierz,''Graphene transistors'',Nature Nanotechnology,2010, 5, 487–496

P. Blake, E. W. Hill,A. H. Castro Neto,K. S. Novoselov, D. Jiang, R. Yang, T. J. Booth,

Annex III

Comments on graphene surface coverage calculation

We consider that the coverage *C* (the ratio of the area covered with graphene) is given by the equation

$$C = \frac{S_*^t}{S_T} = \frac{S_* \, N}{S_T} = S_* \langle n \rangle \qquad (1)$$

where $\langle n \rangle = \frac{N}{S_T}$ is the averaged density of nucleation, S_*^t is the total area covered with graphene, S_* is the surface of one graphene domain, S_T is the total area and *N* is the number of graphene nuclei.

In the case that the graphene domains would grow in an hexagonal morphology:
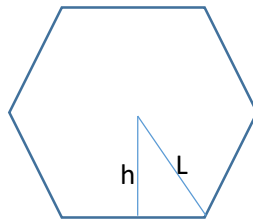
where *L = a* is the lobe's length, the area of an hexagonal domain would be $S_\bigcirc = 6\frac{ha}{2}$, and $h = a\cos 30° = \frac{\sqrt{3}}{2}a$

$$S_\bigcirc = \frac{3\sqrt{3}}{2}a^2 \qquad (2)$$

The increase in crystal's area is then calculated by derivation respect to the time

$$\frac{dS_\bigcirc}{dt} = 3\sqrt{3}\, a\, \frac{da}{dt}$$

$$dS_\bigcirc = 3\sqrt{3}\, a\, da \qquad (3)$$

The total covered area $S_\bigcirc^t$ is calculated by multiplying eq. 3 with the total number of nuclei *N*.

$$dS_\bigcirc^t = N3\sqrt{3}a\, da \qquad (4)$$

By integration of eq.4 we obtain

$$\int_0^{S_\bigcirc^t} dS = \int_0^L N3\sqrt{3}a\, da$$

$$S_\bigcirc^t = N\frac{3\sqrt{3}}{2}L^2$$

Where *L* corresponds to the lobe's length. Then, we divide with the total surface S_T to obtain the coverage ratio, *C*:

$$C = \frac{S_\bigcirc^t}{S_T} = \frac{N}{S_T}\frac{3\sqrt{3}}{2}L^2$$

,where $\langle n \rangle = \dfrac{N}{S_T}$, is the averaged nucleation density, above defined. Therefore,

$$C = \langle n \rangle \frac{3\sqrt{3}}{2} L^2$$

$$\frac{C}{L^2} = \frac{3\sqrt{3}}{2} \langle n \rangle \qquad\qquad (5)$$

In our case the graphene domains present a pseudo-hexagonal symmetry with 4 or 6 lobes (depending on the copper facet). Their area depends as well in the length *L* of the lobe, multiplied with a constant *depending of the geometry*. Then, we introduce a constant k_{geom} in order to relate the areas of the two different crystal shapes, "specific" star shape S_* and hexagonal shape $S_\circ$, as considered above:

$$S_* = k_{geom} S_\circ = kL^2 \qquad\qquad (6)$$

The coverage *C* as ratio of the total area covered with graphene will be

$$C = S_* \langle n \rangle = k\,L^2\,\langle n \rangle$$

$$\frac{C}{L^2} = k\,\langle n \rangle \qquad\qquad (7)$$

Therefore, we return to normalize the coverage ratio with respect to lobe´s length squared and plot it with the averaged nucleation density $\langle n \rangle$. As expected by eq. 7, our experimental data fit linearly (Figure 4a in manuscript).

Annex IV

Electrical measurements realized in the Institute of Microelectronics of Barcelona.
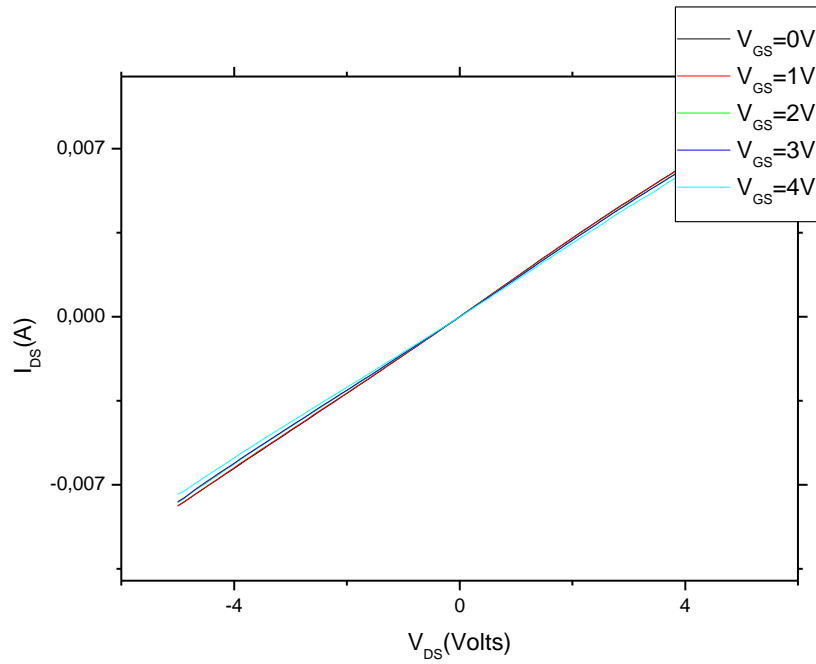
Figure 1: I_{DS}- V_{DS} characteristics in different Gate voltages.
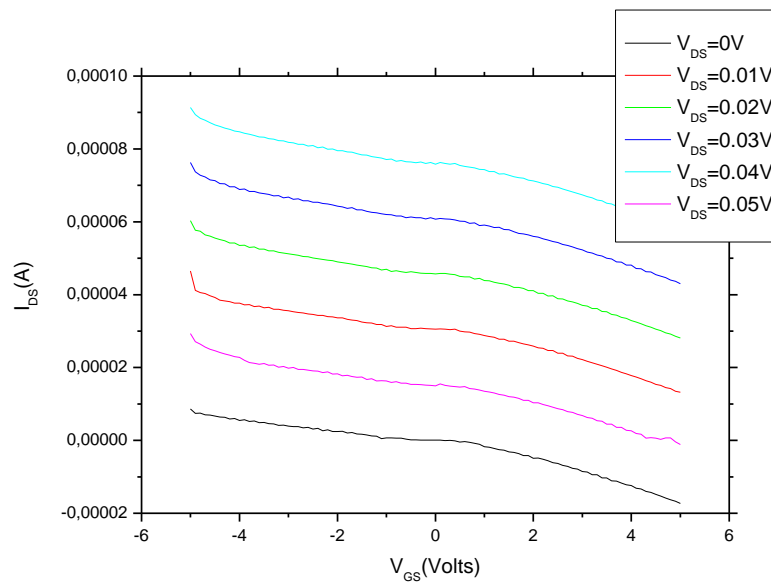
Figure 2: I_{DS}- V_{GS} characteristics in different Source-Drain voltages.

S. Chaitoglou

Stefanos Chaitoglou, 2016

S. Chaitoglou